Exploring Interactions Between The Sleep Homeostatic Process And Cortical Neuronal Dynamics



Christopher William Thomas

Exeter College

Department of Physiology, Anatomy & Genetics

University of Oxford

A thesis submitted for the degree of
Doctor of Philosophy

Hilary 2020

Contents

Acknowledgements 1

Abstract 3

Abbreviations 5

1 Background **7**

1.1 Sleep & Sleep Homeostasis 8

1.1.1 Wake, Non-REM & REM sleep 8

1.1.2 Subcortical Sleep-Wake Control 10

1.1.3 Circadian Sleep Regulation 11

1.1.4 Homeostatic Sleep Regulation 12

1.1.5 The Sleep Slow Oscillation 13

1.1.6 Local & Activity-Dependent Origins of Sleep Homeostasis 15

1.1.7 Cellular Signalling of Sleep Homeostasis 16

1.1.8 Sleep & Metabolic Homeostasis 17

1.1.9 Sleep & Synaptic Homeostasis 18

1.1.10 Sleep & Neuronal Firing Rate Homeostasis 19

1.2 Critical Dynamics in the Brain 20

1.2.1 Criticality Theory 20

1.2.2 Criticality in Neural Systems 22

1.2.3 Self-Organised Criticality 24

1.2.4 Criticality & Sleep 26

1.3 Neuropharmacology of Serotonergic Psychedelics 27

1.3.1 Sleep Homeostasis & Depression 27

1.3.2 The Therapeutic Potential of Serotonergic Psychedelics 28

1.3.3 Psychedelics are Agonists of the 5-HT_{2A} Receptor 30

1.3.4 The Distribution of the 5-HT_{2A} Receptor . . . 31
1.3.5 The Head Twitch Response . . . 32
1.3.6 Serotonergic Psychedelics & Neuronal Activity *In Vitro* . . . 34
1.3.7 Serotonergic Psychedelics & Neuronal Activity *In Vivo* . . . 36
1.3.8 Serotonergic Psychedelics & Human Brain Activity . . . 37
1.3.9 Serotonergic Psychedelics, Learning, Memory & Synaptic Plasticity 39
1.3.10 Serotonergic Psychedelics & Sleep . . . 40
1.4 Aims . . . 41

2 General Methods for Chronic Electrophysiological Recordings 43
2.1 Animals . . . 44
2.2 Surgical Procedures . . . 44
2.3 Animal Husbandry . . . 47
2.4 Sleep Deprivation . . . 48
2.5 Perfusion, Microlesion & Histology . . . 49
2.6 Data Acquisition . . . 50
2.7 Statistics . . . 51

3 Sleep Homeostasis Reflects Integrated Cortical Neuronal Activity 53
3.1 Introduction . . . 54
3.2 Methods . . . 56
3.2.1 Dataset . . . 56
3.2.2 Slow Wave Activity . . . 57
3.2.3 Off Periods Detection & Definition of "Off Occupancy" . . . 57
3.2.4 Model Fitting & Parameter Optimisation . . . 59
3.2.5 Statistics . . . 60
3.3 Results . . . 61
3.3.1 Wake and sleep are characterised by differing neuronal dynamics . . 61
3.3.2 Process S can be described as a function of vigilance state history . 61
3.3.3 Neuronal firing rates are associated with Process S dynamics and vigilance state distributions . . . 63

3.3.4 Process S dynamics can be described as a function of neuronal firing rates . . . 65
3.3.5 Process S can be defined in terms of neuronal off periods . . . 71
3.3.6 Process S dynamics, defined using off periods, can be described as a function of vigilance states or neuronal firing rates . . . 73
3.3.7 Global Process S resembles an average of local Processes S . . . 77
3.4 Discussion . . . 78

4 Cortical Critical Dynamics Vary Across the Sleep-Wake Cycle 85
4.1 Introduction . . . 86
4.2 Methods . . . 88
4.2.1 Data . . . 88
4.2.2 Neuronal Avalanches . . . 89
4.2.3 Avalanche Distributions and Power Law Fits . . . 93
4.2.4 Correlation with Slow Wave Activity . . . 95
4.3 Results . . . 95
4.3.1 Various methods fail to detect avalanches in the LFP . . . 95
4.3.2 LFP-derived avalanches indicate subcritical wake, critical NREM sleep, & supercritical REM sleep dynamics . . . 99
4.3.3 Spike-derived avalanches suggest dynamics are universally nearer criticality . . . 101
4.3.4 Proximity to criticality changes across wake & sleep in association with slow wave activity . . . 104
4.4 Discussion . . . 109

5 The Effects of Psilocin on Sleep & Cortical Neuronal Activity 113
5.1 Introduction . . . 114
5.2 Methods . . . 116
5.2.1 Preparation of Psilocin . . . 116
5.2.2 Preliminary Behavioural Observation Studies . . . 118
5.2.3 Experimental Design for Electrophysiological Recording . . . 119
5.2.4 The Head Twitch Response . . . 120
5.2.5 Time Windows for Analysis . . . 120

5.2.6 Spectral Analysis . . . 122
5.2.7 Firing Rates Analysis . . . 123
5.2.8 Process S Modelling . . . 123
5.3 Results . . . 124
5.3.1 Head twitches & transiently disturbed sleep are seen in response to psilocin . . . 124
5.3.2 Electrophysiological recordings were obtained under psilocin . . . 127
5.3.3 Sleep is acutely destabilised & fragmented after psilocin . . . 129
5.3.4 Long-term sleep-wake architecture is unaffected by psilocin . . . 133
5.3.5 Psilocin acutely enhances 3 - 5 Hz field potential power . . . 134
5.3.6 Multi-unit firing rates are acutely reduced by psilocin during undisturbed wakefulness . . . 140
5.3.7 Psilocin does not influence the sleep homeostatic process . . . 140
5.4 Discussion . . . 148

6 Conclusions **153**

6.1 Overview . . . 154
6.2 Homeostasis of Sleep & Neuronal Activity . . . 156
6.3 Limitations & Future Work . . . 161
6.4 Summary . . . 165

Bibliography **167**

Acknowledgements

First and foremost, I must express my sincerest thanks to my supervisor, Professor Vladyslav Vyazovskiy, for guiding me through this process. I have grown and learnt a great deal from working with you and am extremely grateful for the insights and encouragement you have provided me. I wish to extend my regards to all my colleagues in the Vyazovskiy group. I am particularly indebted to Laura McKillop, Cristina Blanco Duque, Lukas Krone and Tomoko Yamagata for all the teaching and demonstration needed for my in vivo work. I would further like to thank Mathilde Guillaumin, Professor Peter Achermann, Professor Trevor Sharp and Professor David Bannerman for the useful discussions and ideas which shaped my project.

I wish to thank my parents for their unwavering love and support, which I am so very grateful for. I also thank both Exeter College and the Doctoral Training Program for the opportunity to bond with so many wonderful people who have made my experience in Oxford a happy one. Most of all, I am grateful for all the friendships that sustained me over the last 5 years. A special mention goes to Charlotte Pain (and the mountain of empty wine bottles we left behind). I could not have made it without you.

Abstract

The need for sleep increases during wakefulness and decreases during sleep. This process, termed Process S, homeostatically regulates vigilance states, ensuring that individuals obtain a relatively constant daily quantity of sleep. Process S is thought to reflect the regulation of core functional properties of neurones, but many fundamental questions remain. In this thesis, a combination of electrophysiological, pharmacological and mathematical techniques are applied to better characterise interactions between the sleep homeostatic process and cortical neuronal dynamics. The local and activity-dependent origin of Process S was explored through novel computational models, demonstrating that variability in local neuronal firing rates in mouse motor cortex can predict the dynamics Process S measured both in the slow oscillation and also in population off periods. It was concluded that Process S at the local level reflects an integration of cortical activity over time, and at the global level reflects an integration over space. Multi-scale statistical properties of neuronal dynamics were then explored across the sleep-wake cycle, using the theory of criticality. It was found that neuronal avalanches indicative of criticality did not change as a function of Process S during wake, however, did so across vigilance states in association with slow wave activity. The results demonstrate one way in which the control of global brain dynamics might be intrinsically interlinked with the regulation of arousal and sleep. Neuronal dynamics in the waking brain state were then perturbed in mice using the serotonergic psychedelic, psilocin. Although the drug briefly disturbed sleep, no enduring changes were observed in sleep-wake architecture or in the dynamics of Process S, despite perturbation to ongoing neuronal dynamics. Finally, it is argued that these results support the possibility that sleep homeostasis does not serve the active homeostatic regulation of any one specific neuronal variable, but that Process S fundamentally corresponds to an intrinsic time-keeping mechanism, precisely tracking the passage of time in each state and thereby enabling only that a daily sleep quota is obtained. This perspective reconciles the global level of sleep need's dissipation from the local level of its accumulation and offers new insights into understanding both why each individual sleeps every day and why sleep duration shows dramatic differences across the animal kingdom.

Abbreviations

5-HT	-	5-hydroxytryptamine (serotonin)
AMPA	-	Alpha-amino-3-hydroxy-5-methyl-4-isoxazolepropionic acid
ANOVA	-	Analysis of variance
ATP	-	Adenosine triphosphate
DAPI	-	4,6-diamidino-2-phenylindole
DMSO	-	Dimethylsulphoxide
DMT	-	Dimethyltryptamine
DOI	-	2-5-dimethoxy-4-iodoamphetamine
EEG	-	Electroencephalography
EMG	-	Electromyography
EPSC	-	Excitatory post-synaptic current
FFT	-	Fast Fourier transform
fMRI	-	Functional magnetic resonance imaging
GABA	-	Gamma-aminobutyric acid
HTR	-	Head twitch response
ISI	-	Inter-spike interval
LFP	-	Local field potential
LSD	-	Lysergic acid diethylamide
LTP	-	Long-term potentiation
M1	-	Primary motor cortex
MEG	-	Magnetoencephalography
mPFC	-	Medial prefrontal cortex
MUA	-	Multi-unit activity
NREM	-	Non rapid eye movement
NMDA	-	N-methyl-D-aspartate
PBS	-	Phosphate buffered saline
PFA	-	Paraformaldehyde
REM	-	Rapid eye movement
SCN	-	Suprachiasmatic nucleus
SOC	-	Self-organised criticality
SWA	-	Slow wave activity
VLPO	-	Ventrolateral preoptic nucleus

1

Background

Contents

1.1 Sleep & Sleep Homeostasis 8

1.2 Critical Dynamics in the Brain 20

1.3 Neuropharmacology of Serotonergic Psychedelics 27

1.4 Aims 41

1.1 Sleep & Sleep Homeostasis

1.1.1 Wake, Non-REM & REM sleep

Sleep is a familiar and important behaviour which we all perform daily and to which we dedicate approximately one third of our lives. Despite decades of research and substantial progress in understanding the neurobiology of sleep, many fundamental scientific questions remain about its essential nature and functional roles.

In the broadest sense, sleep can be considered to be a reversible state of disconnection from the environment, with defining behavioural characteristics including reduced motor activity and a decreased responsiveness to stimuli (or conversely an increased arousal threshold). Defined in this way, sleep has been identified in some form in all animal species studied (Cirelli and Tononi 2008). Sleep is most readily identifiable in mammals and in birds, but can be found in lower model organisms such as zebrafish (Yokogowa et al., 2007), *Drosophila melanogaster* (Shaw et al. 2000) and *Caenorhabditis elegans* (Raizen et al. 2008). This universality of sleep supports the validity of the use of animal models in its scientific study, as relevant to humans. However, despite universality of its essential defining features, sleep impacts many aspects of an organism's physiology and, therefore unsurprisingly, its specific features and properties are highly heterogeneous across the animal kingdom.

The behavioural features indicative of the sleep state have well-described neural correlates conserved across species. These are readily visible in field potential signals from the brain, obtainable by placing electrodes onto the scalp for the recording of electroencephalography (EEG). Specifically, whereas the waking EEG is relatively low amplitude and irregular, sleep is associated with the appearance of a prominent high amplitude and low frequency oscillation in the slow/delta (0.5 - 4 Hz) range, termed slow wave activity (SWA). The slow wave stage of sleep is common to all animals from which an EEG can be measured and is an essential defining feature of sleep (Cirelli and Tononi 2008).

A second sleep state exists during which the EEG returns to more closely resemble that of wakefulness, including notable oscillatory power at theta (4 - 9 Hz) frequencies, while the behavioural characteristics of sleep persist. Indeed, this sleep stage is associated with further generalised motor inhibition and muscle atonia, and can therefore be easily distinguished from waking by electrical activity recorded from muscles (electromyography, EMG). Exceptionally, the extraocular muscles increase their activity in this state, resulting in spontaneous saccades, a feature which led this sleep stage to be named rapid eye-movement (REM) sleep and, by analogy, slow-wave sleep is termed non-REM (NREM) sleep. REM sleep is prominent in mammals and birds, but it remains unclear whether lower vertebrates might possess a stage of sleep analogous to REM sleep (Blumberg et al. 2020).

The temporal dynamics of sleep and wake can be uncovered by continuous monitoring of EEG and EMG. Sleep-wake architecture is variable between animal species and changes across an individual's life cycle, however, while idiosyncrasies exist, sleep-wake architecture is relatively consistent among conspecifics and from one day to the next. Human sleep is usually monophasic, occurring in one continuous approximately 8 hour period during the night. In humans, sleep passes between three differentiable NREM stages (N1-N3) of increasing depth, associated with successively increasing slow wave activity and reduced behavioural responsiveness, before eventually reaching REM sleep. A NREM-REM cycle typically repeats every 90 - 120 minutes with several occurring throughout one night of sleep and REM sleep episodes become longer and more abundant towards the end of the night.

Rodents are vital model organisms for the study of neuronal processes involved in sleep. However, there are important differences between sleep in humans and rodents. In addition to being predominantly nocturnal, laboratory mice display polyphasic sleep, have a shorter NREM-REM cycle (lasting 10 - 20 minutes), and NREM sleep is typically considered to be a single homogenous state without clear subdivisions.

1.1.2 Subcortical Sleep-Wake Control

The expression of wake and sleep states is controlled by a complex network of subcortical brain regions, which each provide specific neuromodulatory influences to the cortex. There exists a group of monoaminergic arousal-promoting centres in the brainstem and posterior hypothalamus, comprising serotoninergic raphe nuclei, dopaminergic ventral periaqueductal grey matter, noradrenergic locus coeruleus, and histaminergic tuberomammillary nucleus. These project directly to the cortex, but also to the basal forebrain and the lateral hypothalamus, which, respectively, provides the waking cortex with cholinergic inputs and orexinergic inputs. Another arousal-promoting pathway provides cholinergic stimulation to the thalamus from the brainstem. The neurones in these ascending arousal pathways are most active during wakefulness, and show reduced activity during sleep. While all monoaminergic and also orexinergic neurones are almost silent during REM sleep, the cholinergic neurones, both originating from brainstem and basal forebrain, are uniquely active in REM sleep (Lee and Dan 2012; Brown et al. 2012).

A major sleep-promoting area in the brain has been identified to be the ventral lateral preoptic nucleus (VLPO) of the anterior hypothalamus. The VLPO is active during sleep and inhibits the arousal-promoting nuclei in the brain stem and hypothalamus. Together these systems are commonly conceptualised as the brain's primary sleep switch (Saper et al. 2010). However, the exact circuit mechanisms coordinating wake-NREM-REM transitions remain incompletely defined, and other subcortical areas across the brain have been implicated in the promotion of sleep and initiation of its autonomic-regulatory and motor-suppressive functions (Liu and Dan 2019).

1.1.3 Circadian Sleep Regulation

One of the most striking regulatory influences on the occurrence of sleep is an organism's circadian rhythm. Circadian rhythms enable animals to adaptively time their activity and physiology according to predictable daily patterns in their environment. In particular, circadian rhythms powerfully bias the expression of wake and sleep to specific phases of the Earth's light-dark cycle, which varies across species according to ecological advantage. The circadian regulation of sleep depends on the existence of an oscillatory mechanism with a period of 24 hours. Such mechanisms have been found at the molecular level in highly conserved gene expression processes (Bell-Pedersen et al. 2005).

In mammals, the molecular circadian clock centres around a core transcriptional-translational feedback loop, comprising clock genes CLOCK & BMAL1, which act together as transcription factors to promote the synthesis of PER & CRY, which then inhibits CLOCK:BMAL1 activity through negative feedback. Additionally, CLOCK:BMAL1 promotes synthesis of REV-ERBα, which inhibits *Bmal1* transcription, causing this protein to oscillate in anti-phase with PER & CRY. The net effect is a circadian oscillation in CLOCK:BMAL1 activity, which additionally influences many downstream effector genes, allowing the clock to modulate myriad cellular processes (Reppert and Weaver 2002; Lowrey and Takahashi 2011; Edgar et al. 2012).

This molecular circadian mechanism is not localised to only one brain region, but is present throughout the body, in almost all individual mammalian cells (Zylka et al. 1998; Dibner et al. 2010; Mohawk et al. 2012). However, the peripheral intracellular circadian oscillators are coordinated by the "master clock" located in the suprachiasmatic nucleus (SCN) of the anterior hypothalamus (Ralph et al. 1990; Welsh et al. 2010; Hastings et al. 2014). External environmental cues, termed zeitgebers, input to the SCN in order to entrain circadian rhythms. For example, the SCN receives input from a subpopulation of photosensitive retinal ganglion cells expressing the photo-pigment melanopsin (Gooley et al.

2001; Lucas et al. 2001), whose light-induced activation increases SCN firing, increases PER transcription and thereby modulates clock phase (Hughes et al. 2015). The SCN outputs to multiple hypothalamic and brainstem areas allowing centralised autonomic and neuroendocrine coordination of peripheral circadian oscillators, and importantly also enabling modulation of neural circuits controlling sleep (Morin 2013).

1.1.4 Homeostatic Sleep Regulation

Alongside the circadian rhythm, which controls the timing of sleep, another fundamental regulatory process determines its relative quantity. This is evidenced by the phenomenon that extended wakefulness (or, equivalently, a deficit of sleep) leads to a compensatory increase in subsequent sleep. This is evident not only in terms of sleep's duration, but crucially also in its depth, as reflected in the amplitude of NREM sleep slow wave activity (Dijk et al. 1987a; Werth et al. 1996b; Vyazovskiy et al. 2007). Similarly, prolonged sleep reduces the drive for more sleep and favours wakefulness. This principle of sleep homeostasis ensures that animals tend to maintain a relative constancy of sleep's daily amount, balancing the ratio of wake and sleep states and ensuring that neither wake nor sleep continues indefinitely. Homeostatic regulation is another of sleep's defining properties, and is highly conserved across species (Tobler 1995; Cirelli and Tononi 2008). Importantly, however, the sleep-wake ratio, and therefore the parameters of this process, are highly variable. For example, total average sleep time can range from up to 19 hours per day in some species of bats to 4 hours per day in elephants (Zepelin et al. 1989; Savage and West 2007).

Homeostatic regulation of sleep implies the existence of some physiological mechanism which senses integrated sleep-wake history. This mechanism, often termed "Process S", should accumulate during wakefulness, dissipate during sleep, and also signal the need for sleep. Indeed, the levels of Process S are observable during NREM sleep in the average magnitude of slow wave activity (Dijk et al. 1987b; Borbély and Achermann 1999;

Rattenborg et al. 2009). The timing and depth of sleep is well described by the interaction between circadian and homeostatic processes, and this relationship has been captured in the classical "two process model" of sleep regulation. The central idea is that Process S is maintained within some range of values by triggering sleep when Process S levels near some upper boundary, and similarly inducing wake when it reaches a lower boundary. Importantly, these boundaries act as thresholds for sleep-wake transition and exhibit an oscillatory modulation in amplitude determined by circadian phase, termed Process C (Borbély 1982; Daan et al. 1984). Although there exists some level of interaction at the level of the SCN, these two processes are largely separate (Borbély et al. 2016).

Homeostatic regulation supports the intuitive idea that sleep's primary function is broadly restorative, counteracting some form of harmful side-effect or physiological challenge imposed by extended wakefulness. The identity of the precise mechanisms of Process S might therefore be expected to relate directly to sleep's fundamental purpose. While the cellular and molecular mechanisms which underpin circadian rhythms are relatively well characterised, many uncertainties surround basic aspects of the sleep homeostatic process.

1.1.5 The Sleep Slow Oscillation

The cortical slow oscillation is implicated as a core mechanism underlying the primary functions of sleep, as this is what defines sleep depth and increases when sleep is deprived. In addition to the scalp EEG, slow waves are visible in the local field potential (LFP) derived from electrodes implanted deep within cortical tissue. Field potentials reflect the summation of ionic currents across neuronal cellular membranes, particularly currents associated with synaptic activity and dendritic integration (Buzsáki et al. 2012; Ness et al. 2016). Oscillations therefore arise when neural activity is broadly synchronised at particular frequencies, and the sleep slow wave is no exception. During the positive phase of a recorded slow wave, intracellular recordings reveal that nearby neurones become

hyperpolarised, cease action potential firing and receive little synaptic input, termed a down state. In contrast, the negative phase of the slow wave is associated with neuronal depolarisation and high frequency firing, driven by a barrage of both excitatory and inhibitory synaptic activity, called the up state (Steriade et al. 1993b; Amzica and Steriade 1998; Steriade et al. 2001). Synchronised oscillating up and down states at the neuronal level translate into alternating on and off periods of recurrent activity at the network level and this produces measurable slow waves.

The neuronal slow oscillation (< 1 Hz) comprising alternation between up and down states can be viewed as the default dynamic mode of activity in the cortex (Sanchez-Vives and Mattia 2014). These dynamics appear whenever the cortex is functionally or anatomically disconnected from its inputs, such as with *in vitro* cortical slices (Sanchez-Vives and McCormick 2000), deafferented cortical slabs (Timofeev et al. 2000) and *in vivo* networks under anaesthesia as well as natural NREM sleep. Mechanistically, it depends on recurrent corticocortical activity, both locally and long-range (Steriade et al. 1993a; Amzica and Steriade 1995), and on the presence of activity-dependent inhibition (Mattia and Sanchez-Vives 2012).

During natural *in vivo* NREM sleep, slow waves spread widely across the brain, notably including corticothalamic loops (Timofeev and Steriade 1996), and such thalamic involvement in the cortical slow oscillation increases its frequency from the slow (< 1Hz) into the delta (1-4 Hz) range (Steriade 2003; David et al. 2013), corresponding to cortical up and down states lasting a few hundred milliseconds. Importantly, *in vivo* NREM sleep slow waves are dynamic and idiosyncratic; each successive wave, which comprises a pattern of spreading down states, may have a unique site of initiation and path of propagation (Massimini et al. 2004 Nir et al. 2011), and include only a specific subset of brain regions or networks (Riedner et al. 2011 Vyazovskiy and Delogu 2014).

The frequency, amplitude and spatial coordination of slow waves are modulated by the sleep homeostatic process, and this is reflected in the underlying neuronal activity.

When sleep drive and slow wave activity is increased, such as after sleep deprivation, off periods are longer in duration and display greater spatial extent, while a reduction in slow wave activity and accompanying down state duration and synchrony occurs throughout the course of sleep (Riedner et al. 2007; Esser et al. 2007; Vyazovskiy et al. 2009b; Nir et al. 2011; Saberi-Moghadam et al. 2018).

1.1.6 Local & Activity-Dependent Origins of Sleep Homeostasis

Despite the global level at which wake and sleep states are typically expressed, the ultimate origin of the slow oscillation which defines sleep exists at the level of local neuronal activity. Local origins permit local differences in sleep depth and associated neural dynamics. In the most extreme case, aquatic mammals and some birds can perform unihemispheric sleep, in which one brain hemisphere remains awake while the other sleeps (Mukhametov et al. 1977; Mascetti 2016), illustrating that both states can coexist in the brain simultaneously. In human parasomnias, such as sleep walking, waking function returns to some parts of the brain while the patient is unconscious and apparently asleep (Mahowald and Schenck 2005). Even in healthy terrestrial mammals incapable of full unihemispheric sleep, local slow waves associated with neuronal down states can be observed during active wakefulness (Vyazovskiy et al. 2011) and REM sleep (Funk et al. 2016) and, similarly, wake-like activity appears locally during global sleep (Nobili et al. 2011).

The local origins of sleep related dynamics are reflected also in regional differences in SWA. For example, SWA is notably higher in frontal compared to posterior cortical EEG derivations in humans and rodents, particularly after sleep deprivation (Werth et al. 1996a; Cajochen et al. 1999; Huber et al. 2000b). Importantly, these differences can be described by associating locally variable parameters to the underlying dynamics of Process S, reflecting differences in the rate of change of the sleep homeostatic process (Zavada et al. 2009; Rusterholz and Achermann 2011; Guillaumin et al. 2018). Regional

differences in Process S dynamics have also been linked to their functional properties and the behavioural content of waking, beyond just its duration. For example, repetitive task performance predicted to selectively engage specific functional areas, such as lateralised motor or specific sensory cortices, result in enhancements of local slow wave activity in these regions during subsequent NREM sleep (Kattler et al. 1994; Huber et al. 2004; Vyazovskiy and Tobler 2008; Rector et al. 2009; Murphy et al. 2011). For example, prolonged vibration of the hand in human subjects increases interhemispheric asymmetry in the EEG delta frequency power in the first hour of subsequent NREM sleep selectively in the central derivation, corresponding to an increased SWA in somatosensory cortex contralateral to the vibratory stimulation (Kattler et al. 1994). Together these results demonstrate that, while coordinated on a global level, sleep is fundamentally a property of local cortical circuits (Rattenborg et al. 2012).

1.1.7 Cellular Signalling of Sleep Homeostasis

The cellular mechanisms through which the sleep homeostatic process is locally regulated are known to involve several sleep-regulatory signalling molecules, such as adenosine, nitric oxide, prostaglandins and cytokines (Krueger et al. 2008). These molecules accumulate during wakefulness, and their production is mechanistically associated with cortical neuronal activity. In particular, adenosine triphosphate (ATP) is released alongside neurotransmitters at active synapses, and this stimulates local production of myriad sleep-regulatory signalling molecules through downstream intracellular and intercellular signalling pathways (Krueger et al. 2008). Glia play an essential role in these signalling dynamics, notably by integrating, amplifying and spreading such signals over a large cortical area (Fellin et al. 2012). During sleep, key signalling molecules are removed from the brain by exchange into the cerebrospinal fluid, resetting the sleep homeostatic signal (Xie et al. 2013).

Many of these substances act directly on hypothalamic neurones to promote the

initiation of global sleep, while several act on cortical neurones to promote local slow wave activity (Obal and Krueger 2003). Their mechanism of action in cortical neurones is to alter electrophysiological response properties through regulation of specific ion channels or expression levels of receptors for other neuromodulators (Clinton et al. 2011). For example, adenosine promotes the upregulation of the adenosine A1 receptor (Jajoo et al. 2006), which has a K^+-channel-mediated hyperpolarising effect on cortical neurones, such that adenosine sensitivity increases during wakefulness (Elmenhorst et al. 2009) and this is one possible mechanism contributing to the homeostatic regulation of local slow wave propensity (Krueger et al. 2008; Bjorness et al. 2009). The involvement of transcription and translation enables these signalling processes to unfold on a time scale of hours, and thereby plausibly reflect integrated sleep-wake history.

1.1.8 Sleep & Metabolic Homeostasis

Consistent with the intuitive function of sleep as restorative, sleep is strongly interlinked with metabolic regulation. The brain's metabolic rate is implicated as the principle determining factor in scaling relationships for the total amount and cycling time of NREM and REM sleep across mammals (Savage and West 2007). All cells, neurones included, have a limited metabolic capacity and can experience stress as a result of sustained metabolic activity, such as that associated with the continuous processing of synaptic inputs and generation of action potentials (Attwell and Laughlin 2001). Neurones are susceptible to cellular stresses that can result from sustained metabolic load, such as depletion of energy reserves (Scharf et al. 2008) or accumulation of oxidative damage (Wang and Michaelis 2010; Cobley et al. 2018). Extended wakefulness does not necessarily involve neuronal damage (Cirelli et al. 1999), however, extreme cases reveal the potential harm of sleep deprivation, the most dramatic being that a complete absence of sleep eventually leads to death. Neurodegeneration can also occur if sleep disruption is sufficiently prolonged, for example in chronic insomnia (Dauvilliers 2007). Additionally, when signalling pathways related to

cellular maintenance are impaired as a result of genetic manipulation, the damaging effects of relatively short-term sleep deprivation on the brain are revealed (Shaw et al. 2002).

Indeed, compensatory processes exist within neurones to oppose cellular stress and related metabolic homeostatic challenges by restoring energy reserves and repairing or replacing damaged cell components (Kültz 2005), and these are upregulated in sleep and after prolonged wakefulness (Cirelli and Tononi 2000; Terao et al. 2003; Naidoo et al. 2005; Cirelli et al. 2006; Mackiewicz et al. 2007; Bellesi et al. 2016). Notably, cellular homeostasis cannot be achieved by a prolonged total shutdown of metabolism, since some neuronal activity is required to prevent the destabilisation of synapses and balanced excitability (Kilman et al. 2002; Reig and Sanchez-Vives 2007; Sanchez-Vives and Mattia 2014) and this also enables the to brain to maintain some capacity for responsivity. However, neuronal down states associated with the NREM slow oscillation could provide the opportunity for neurones to prioritise such homeostatic prophylactic cellular maintenance processes, therefore mediating the fundamental cellular restorative benefits of sleep (Vyazovskiy and Harris 2013).

1.1.9 Sleep & Synaptic Homeostasis

Of all the cellular maintenance functions ascribed to sleep, the most well characterised mechanisms relate to the homeostatic regulation of synapses. The synaptic homeostasis hypothesis posits that wake is associated with a net potentiation of synapses, as a result of the ongoing plasticity which supports learning and memory, and that this must be offset by a global downscaling of synaptic strengths during sleep (Tononi and Cirelli 2003). Expression and regulation of AMPA receptors, *in vivo* electrical-evoked responses *ex vivo* excitatory postsynaptic currents and synaptic ultrastructure are consistent with increasing synaptic strength in the cortex during wake and decreasing during sleep, in a manner independent of circadian time (Vyazovskiy et al. 2008; Liu et al. 2010; de

Vivo et al. 2017). Similar evidence of increasing cortical excitability over wakefulness indicative of increased synaptic strength has also been found in humans (Huber et al. 2013). Total synaptic strength received by a neurone is therefore hypothesised to directly represent the level of its homeostatic sleep need. Indeed, increasing synaptic weights is one mechanism to increase network synchronisation and resultant slow wave activity (Esser et al. 2007). Furthermore, this process has been linked to sleep's memory functions, notably with respect to the integration and consolidation of memories (Lewis and Durrant 2011; Rasch and Born 2013; Tononi and Cirelli 2014).

1.1.10 Sleep & Neuronal Firing Rate Homeostasis

The activity-dependent regulation of sleep in the brain is further complicated by the finding that neuronal firing rates are themselves variably regulated by wake, NREM and REM sleep. The overall mean firing rate of recorded putative single neurones remains constant within a specific vigilance state over multiple days of observation, and this set point is even remembered following dramatic network activity perturbations, such as total sensory deprivation (Hengen et al. 2013). Myriad homeostatic regulatory mechanisms control synaptic weights, intrinsic excitabilities, and network excitatory-inhibitory balance to produce a variety of individual cellular response properties (Turrigiano 2011; O'Leary et al. 2014). Firing rate set points are characteristic for individual neurones and between cells vary over several orders of magnitude (Hengen et al. 2016; Watson et al. 2016). Small drift in a neurone's mean firing rate has been reported, typically as an increase during extended wakefulness and decrease during sleep (Vyazovskiy et al. 2009b; Grosmark et al. 2012). However, changes in neuronal firing rate are modulated by ongoing behaviour, for example, wheel running in mice is accompanied by a prevention of the usual firing rate increase during prolonged wake and also by an increase in voluntary wakefulness (Fisher et al. 2016). Furthermore, the magnitude and direction of state-dependent mean firing rate drift is different for neurones with a high and low intrinsic firing rate, and in different

brain regions (Watson et al. 2016; Miyawaki and Diba 2016; Miyawaki et al. 2019). These results overall indicate that homeostatic regulation of firing rates by sleep may actually occur above the individual cell level (Slomowitz et al. 2015), constraining and shaping the distribution of intrinsic firing rates within a networked population (Levenstein et al. 2017). Mechanistically, firing rate homeostasis is linked also with cellular energetics and metabolism (Styr et al. 2019; Vergara et al. 2019).

In summary, many mechanisms have been established to link the regulation of global brain dynamical states with cellular and synaptic regulatory processes occurring in single neurones and local networks. Many specific mechanisms have been implicated to correspond to the sleep homeostatic process, such as synaptic strength, levels of cellular stress, or the accumulation of adenosine, cytokines and related signalling molecules. However, it remains uncertain which, if any, of these processes are fundamentally equivalent to Process S, rather than correlated with or regulated by it. It is therefore still unknown precisely why every animal must spent a significant portion of its life asleep, and why sleep patterns should demonstrate such variation across the animal kingdom. These issues are further inexorably linked to wider problems in modern neuroscience related to understanding how complex regulatory mechanisms are orchestrated over multiple spatial and temporal scales to regulate behaviours and global body states.

1.2 Critical Dynamics in the Brain

1.2.1 Criticality Theory

Mechanisms in the brain which underpin behaviour, including but not limited to the regulation of sleep and wakefulness, have been identified over a multitude of spatial and temporal scales. A fundamental challenge in neuroscience remains to understand how these

processes which span across molecular, single cellular, local circuit and global network levels are integrated and interrelated. Multi-scale dynamics has been described mathematically in many diverse natural systems using the concept of "criticality". The hypothesis that brain activity might exhibit critical dynamics has accumulated experimental and theoretical support over the last two decades (Beggs and Timme 2012; Cocchi et al. 2017).

Criticality refers to a particular form of non-equilibrium dynamics occurring in a system where fluctuations are scale-free. Consider a system which comprises a large number of generic interacting elements. Perturbations to the system, whether due to intrinsic noise or external stimuli, may cause elements to become activated. Such an activation may spread through the system or it may decay, depending on the nature of the interactions between elements. Importantly, in a critical state the rates at which activity spreads or decays are precisely equal, and, as a consequence of this, perturbations to the system have the potential to induce changes at any scale, from a single element to the whole system. Such spreading activations are known as avalanches. The presence of critical avalanches depends on the precise setting of a control parameter, such as the interaction strength between elements. If interactions are too weak, then activity will tend to decay rather than spread; perturbations are limited to effecting the system only at the micro-scale. Such dynamics are described as subcritical; the system shows stable low levels of activity and perturbations are "absorbed". Conversely, if interactions are too strong, activations tend to spread and rapidly engulf the whole system. Such a dynamic phase is termed supercritical; activity is present but such dynamics are nonetheless stable. This illustrates how dynamical systems may exhibit very different forms of global dynamics, termed phases, depending on the setting of a number of relevant control parameters, and that critical points appear at the boundary of (continuous) phase transitions.

Despite the apparently random and chaotic nature of critical avalanches, they nonetheless obey well-characterised statistical laws which are common between very different systems. Specifically, the scale of avalanches are described by power laws; the probability

of observing an avalanche of a particular size or duration is proportional to that value raised to a characteristic negative exponent. Avalanche-like fluctuations derived from a subcritical system will have properties characterised by exponential family distributions, which decay more steeply than a power law. In contrast, supercritical processes yield bimodal distributions, as larger values become more likely than intermediate. Such differences are easily visible when distributions are plotted in log-log coordinates; power law distributions indicative of criticality display as linear, whereas distributions produced by subcritical processes are concave and supercritical processes convex. Typically, empirically derived power laws from a variety of avalanches have the same characteristic exponent, equal to -1.5 for avalanche size. Another important hallmark of criticality is that scale-free events imply fractal self-similarity and consequently signals from critical systems display increased autocorrelations, both in the spatial and temporal domains.

1.2.2 Criticality in Neural Systems

The theory is then, that communication across neural systems might organise as scale-free avalanches, and that single avalanches might reflect computationally relevant interactions, such as the transient formation of cell assemblies (Plenz and Thiagarajan 2007). Neural dynamics might therefore exist at the boundary of a phase transition between ordered vs. disordered, or synchronous vs. independent, dynamic states. The simplicity and universality of criticality makes it an attractive theory, as does evidence that the critical state is associated with a number of computational advantages which may be functionally significant to the brain (Bertschinger and Natschlager 2004; Shew and Plenz 2013). These advantages emerge owing to the increased variability in the responses of critical systems to perturbation. At criticality, local micro-scale fluctuations erratically percolate throughout a system, transporting disorder and increasing the information content across all scales. While entropy may be higher at the micro-scale in a subcritical system (or higher in the macro-scale in a supercritical one), the presence of meaningful variability in a critical

system at multiple scales outweighs this factor. As a result, the information transmission (quantified as the stimulus-response mutual information) and storage (quantified as response entropy) have been shown both theoretically and experimentally to be maximised at criticality (Haldeman and Beggs 2005; Tanaka et al. 2008; Shew et al. 2011). Similarly, this maximisation of response variability by critical avalanches maximises the dynamic range and representational diversity of neuronal networks (Kinouchi and Copelli 2006; Shew et al. 2009; Gautam et al. 2015). The increased variability at criticality extends also to properties such as synchrony (Yang et al. 2012).

While the precise nature of the phase transitions which describe neural activity remain unclear, avalanche dynamics have been repeatedly demonstrated in a number of neural systems and this remains the strongest evidence for some form of critical dynamics in the brain. The first report of neuronal avalanches came from *in vitro* cortical cultures grown onto multi-electrode arrays, which exhibited spontaneous high-amplitude LFP fluctuations (Beggs and Plenz 2003) whose spatial (number of synchronous active electrodes) and temporal (duration of avalanche) extent were well described by power laws. Neuronal avalanches with power law properties were additionally found in the LFP of anaesthetised animals *in vivo* in juvenile rat somatosensory cortex (Gireesh and Plenz 2008) and cat primary visual cortex (Hahn et al. 2010). Avalanches have been demonstrated in field potential data during wakefulness, notably in the LFP recorded from primary motor and premotor cortex of macaques (Petermann et al. 2009), and also in human whole brain EEG and magnetoencephalography (MEG) (Palva et al. 2013; Meisel et al. 2013; Shriki et al. 2013). Furthermore, spatial correlations consistent with critical avalanches have been observed in resting state fMRI (Tagliazucchi et al. 2012) and simulated critical avalanches imposed on models of the human brain connectome reproduce activity patterns in resting-state networks (Haimovici et al. 2013). Deviations from critical dynamics have been linked to pathological brain states, notably epileptic seizures appear to correspond to supercritical dynamics (Meisel et al. 2012).

Importantly, power laws are not definitive evidence for criticality, since power law distributions can be produced through non-critical processes, such as summation of exponentials or multiplicative noise (Reed and Hughes 2002; Beggs and Timme 2012). However, more rigorous evidence for criticality has been found in a few systems by demonstrating the existence of mathematical relationships between different power law exponents and fractal self-similarity in avalanche shape (Ribeiro et al. 2010; Friedman et al. 2012). Additionally, manipulations of excitatory-inhibitory balance using glutamatergic and GABAergic antagonists has been demonstrated to perturb critical avalanches towards subcritical or supercritical dynamics (Shew et al. 2009; Shew et al. 2011), further suggesting that neural avalanche power laws are associated with a continuous phase transition boundary, and hence criticality.

Crucially, however, the evidence for neuronal avalanches in spiking data is somewhat contradictory. Avalanches have indeed been reported based on individual spikes from *in vitro* cultured cortical neurones (Pasquale et al. 2008; Friedman et al. 2012). However, under anaesthesia *in vivo*, only a subset of recordings evidenced power laws and these were less robust to the setting of methodological parameters compared to avalanches derived from LFP fluctuations (Hahn et al. 2010). Power laws are additionally not found in spiking activity, analysed separately during wakefulness, NREM sleep and REM sleep, *in vivo* from rat visual and somatosensory cortex (Ribeiro et al. 2010), nor from cat or monkey primary motor cortex (Dehghani et al. 2012).

1.2.3 Self-Organised Criticality

An important aspect of criticality theory is that these unique dynamics emerge only at the critical point, which should require the fine tuning of specific control parameters. In the brain this might include any cellular variable that affects excitability and synaptic transmission. However, critical dynamics emerge in natural systems (such as earthquakes,

forest fires and solar flares) apparently without any active control process. In such systems, criticality may intrinsically be the only stable dynamic regime to which the system inevitably evolves, a phenomenon termed self-organised criticality (SOC). Many model systems have been described which show SOC. A classic example is the sand pile model (Bak et al. 1987), which comprises a two-dimensional array of sand piles, each represented by an integer number of sand grains. If the number of grains on one pile exceeds some threshold the pile collapses; sand grains are removed from the collapsed pile and redistributed to neighbouring piles. In a simulation, sand grains are added at random to the array until a collapse event occurs. This collapse and redistribution of sand may cause another pile to become unstable. In this way collapse events propagate throughout the system, corresponding to scale-free avalanches. Initially the sand piles are subcritical; sand grains are absorbed without consequence. As the energy levels increase the system moves towards a supercritical state, where collapse events occur. However, collapses reduce system energy, moving the system back toward the subcritical state, rendering the critical point in between stable.

In general, SOC can appear in systems where the energy levels of its elements increase slowly over time and dissipate quickly in the form of avalanches; there is a separation of timescales between the drive and dissipation of energy. Clearly, however, brain dynamics do not comprise isolated avalanches separated by periods of total silence. If activity is critical, it must represent many avalanches simultaneously initiating, evolving and interacting. This form of activity can be reproduced in SOC models by assuming that the system is internally slightly subcritical, but is driven also by an external excitatory input (Priesemann et al. 2014), perhaps analogous to sensory input drives to the brain.

More generally, SOC is considered to require dynamic plasticity in the interaction strength between elements. Indeed, numerous models of SOC in the brain have highlighted the important role of different synaptic plasticity processes, including Hebbian (de Arcangelis et al. 2006; Kessenich et al. 2016), and spike-timing-dependent plasticity

mechanisms at both excitatory (Rubinov et al. 2011) and inhibitory synapses (Stepp et al. 2015). Others have argued that avalanche dynamics in the brain might emerge due to its complex and heterogeneous structure, dominated by hierarchical and modular connectivity patterns, and that critical-like dynamics are actually inevitable over a wide region of parameter space (Moretti and Munoz 2013).

1.2.4 Criticality & Sleep

Despite an established role for critical (or near-critical) dynamics in the brain, and a role for synaptic plasticity in maintaining this, it is unclear whether such dynamics are an inevitable emergent property of brain networks or whether they are actively regulated by homeostatic plasticity processes. Indeed, it has been suggested that this might be the fundamental purpose of sleep and the substrate of Process S (Pearlmutter and Houghton 2009). According to this theory, net synaptic potentiation during waking (Tononi and Cirelli 2003) might drive the system towards the supercritical regime where runaway excitation might occur. The intrusion of local down states on ongoing waking activity, which increases over sleep deprivation, might be one mechanism which protects the brain from this (Pearlmutter and Houghton 2009). Homeostatic synaptic downscaling in sleep might then fundamentally act to restore critical or subcritical dynamics. Indeed, firing rate homeostasis may be sufficient to maintain criticality (Hsu and Beggs 2006).

Some experimental support was reported in humans, where a deviation from critical to supercritical dynamics was observed in avalanches of whole-brain EEG activity following 40 hours of sleep deprivation (Meisel et al. 2013). Additionally, long-range temporal correlations, another hallmark of criticality, were observed to reduce over the course of sleep deprivation in human EEG (Meisel et al. 2017a) and rodent LFP data (Meisel et al. 2017b), indicating a deviation from critical-like dynamics. Homeostatic regulation of criticality was studied in the visual cortex in response to visual deprivation over the

course of several days, finding that this induced a deviation from criticality which was restored over the subsequent two days, preceding the recovery of firing rates (Ma et al. 2019).

In summary, critical dynamics provides a powerful theoretical framework for explaining neuronal computation and offers important insights as to how brain mechanisms might operate over multiple spatial and temporal scales. However, the precise nature of the critical phase transitions that describe neuronal dynamics remain unclear, as does their relationship with the striking global dynamic transitions that occur between the states of wake and sleep. How are critical avalanches compatible with up and down states and the cortical slow oscillation, which have characteristic time scales? Furthermore, it is unknown how adherence to critical dynamics, which is a global system property, might vary locally and relate to other localised homeostatic needs, such as those associated with Process S.

1.3 Neuropharmacology of Serotonergic Psychedelics

1.3.1 Sleep Homeostasis & Depression

Sleep has a fundamental role in regulating neuronal homeostasis and plasticity, and it is therefore unsurprising that sleep dysregulation is linked to many common psychological disorders, such as depression. More than just a symptom, persistent sleep disturbance is causally implicated in the development and maintenance of depressive disorders (Baglioni et al. 2011; Meerlo et al. 2015). Interestingly, it has been hypothesised that depression may be characterised by an impairment in Process S dynamics and its interaction with the circadian rhythm (Wirz-Justice and Hoofdakker 1999). A reduced rate of Process S increase during wakefulness would account for many typical features of sleep in depression (Borbély and Wirz-Justice 1982), such as lighter NREM sleep and increased REM sleep. This may explain why, somewhat paradoxically, acute sleep deprivation exerts a rapid anti-

depressive effect; one night total of sleep deprivation successfully alleviates symptoms of low mood in approximately 60% of depressed patients, an effect attributed to an elevation of Process S (Wirz-Justice et al. 2005). Furthermore, without additional treatments, a relapse in depressive symptoms typically occurs after subsequent sleep, which would correspond to a return to low Process S.

Mechanistically, chronic sleep disturbance is associated with altered neuroendocrine stress responses (Meerlo et al. 2008), and elevated or sensitised stress responses are implicated in the aetiology of depression, through a reduction in serotonergic signalling and impairment of synaptic plasticity processes (Meerlo et al. 2015). Broadly, similar mechanisms have been linked to the anti-depressant action of sleep deprivation, as an enhancement in serotonin signalling and synaptic plasticity are implicated (Dallaspezia and Benedetti 2015), alongside a resetting of the circadian rhythm (Bunney and Bunney 2013). Importantly, serotonin signalling is also the target of classical anti-depressants, such as selective serotonin reuptake inhibitors.

1.3.2 The Therapeutic Potential of Serotonergic Psychedelics

Serotonin is a wake-promoting neurotransmitter, linked strongly to mood regulation and targeted by a range of pharmacological treatments for mental disorders. Recently, a resurgence of clinical interest has occurred towards a particular class of serotonergic agonists; activators of the 5-HT_{2A} receptor which function as classical psychedelics, such as lysergic acid diethylamide (LSD) and psilocybin.

Early clinical trials suggest that a single dose of psilocybin, when taken under the appropriate conditions and in combination with more traditional psychotherapy, can exert long-lasting improvements in mood for patients with treatment-resistant unipolar depression (Carhart-Harris et al. 2016), as well as depression and existential anxiety related to terminal illness (Grob et al. 2011; Ross et al. 2016; Griffiths et al. 2016). Psilocybin

use has also been associated with reduced psychological distress and suicidality in the wider adult population (Hendricks et al. 2015) and is effective at reducing depressive-like behaviours in rodent models of depression (Hibicke et al. 2020). Importantly, despite the acute psychotropic effects which profoundly alter perception, cognition and mood, psilocybin appears to be remarkably safe, having low toxicity and little potential for the development of physical or psychological dependence (Passie et al. 2002; Amsterdam et al. 2011). The clinical applications of psilocybin have even been considered in relation to treating obsessive compulsive disorder (Moreno et al. 2006), alcohol dependence (Bogenschutz et al. 2015), tobacco addiction (Johnson et al. 2014) and even disorders of consciousness (Scott and Carhart-Harris 2019). While all these preliminary studies have so far been small, imperfectly designed, and concerned primarily with psilocybin's safety and tolerability in patient groups (Santos et al. 2016; Carhart-Harris and Goodwin 2017), all have reported significant improvement effects.

While the clinical and scientific significance of this class of drugs has been appreciated since the discovery of LSD in the 1940s, progress in this field was effectively shut down following the development of societal stigmatisation in the 1960s and subsequent imposed legal restrictions in the 1970s. Scientific interest in the mechanisms of action of serotonergic psychedelic drugs has since recovered (Belouin and Henningfield 2018) and many essential questions remain as to their basic functioning. Importantly, the possibility of an interaction between the action of psychedelics and the regulation of sleep remains untested, a result with clear relevance for both specific clinical application and wider fundamental neuroscience. The existence of some relationship might be expected, given that both involve differential alteration of global brain dynamics, with relevance for mood regulation and psychological well-being, sharing noteworthy similarities between dreaming and psychedelic experience, and involving mechanisms such as serotonin signalling and brain plasticity.

1.3.3 Psychedelics are Agonists of the 5-HT$_{2A}$ Receptor

A range of compounds have been found to elicit psychedelic effects in humans. These include structural analogues of serotonin, the indolamines such as dimethyltryptamine (DMT), as well as the structurally-related ergolines (rigidified tryptamines) of which lysergic acid diethylamide (LSD) is archetypal. Other notable serotonergic psychedelics include the phenylethylamine mescaline, and the substituted amphetamine 2-5-dimethoxy-4-iodoamphetamine (DOI).

Of these, psilocybin has attracted the most clinical interest, largely owing to the relatively short time course of its acute psychotropic effects in humans (approximately 3 hours, compared to, for example, about 8 hours for LSD), which is more practical for clinicians. Psilocybin is a prodrug produced by the genus of fungi *Psilocybe*, which upon ingestion is rapidly converted to the pharmacologically active indolamine 4-hydroxy-dimethyltryptamine, also known as psilocin.

While different psychedelic substances induce idiosyncratic psychotropic effects in humans owing to their unique pharmacological activity profiles, all are agonists of the 5-HT$_{2A}$ receptor. Early work identified a strong correlation between the 5-HT$_{2A}$ receptor affinity of a large range of psychoactive substances and their reported hallucinogenic action (Glennon et al. 1984). Furthermore, the psychotomimetic and psychotropic effects of psilocybin in humans can be completely abolished by antagonists of the 5-HT$_{2A}$ receptor, such as ketanserin and risperidone (Vollenweider et al. 1998). Notably, psilocin acts also as an agonist of 5-HT$_{2C}$ receptors and 5-HT$_{1A}$ receptors, but has little dopaminergic or noradrenergic activity.

1.3.4 The Distribution of the 5-HT$_{2A}$ Receptor

The 5-HT$_{2A}$ receptor is distributed widely across the mammalian central nervous system. In the rat brain, immuno-labelling studies identify neocortex, hippocampus, striatum, amygdala and the olfactory bulb as the primary sites of 5-HT$_{2A}$ receptor expression (Xu and Pandey 2000; Cornea-Hébert et al. 1999). A widespread neocortical abundance of 5-HT$_{2A}$ receptor is reported also in humans, based on autoradiography and *in situ* hybridisation evidence (Pazos et al. 1987; Burnet et al. 1995). Notably, 5-HT$_{2A}$ receptor levels are low in cerebellum, thalamus and brain stem. The highest cortical density in humans has been reported to be in posterior cingulate cortex (Erritzoe et al. 2009). Within the cortex, variation in the exact laminar distribution of 5-HT$_{2A}$ receptor is reported using different species and methodologies, however, high expression levels are unanimously reported in layer 5 pyramidal neurones (Pazos et al. 1987; Burnet et al. 1995; Jakab and Goldman-Rakic 1998; Xu and Pandey 2000; Weber and Andrade 2010). The receptors are mostly located postsynaptically on the soma and dendrites of layer 5 pyramidal neurones, particularly on the apical dendrite proximal to the soma, although a minority of receptors are located on presynaptic axons of monoaminergic neurones (Jakab and Goldman-Rakic 1998; Miner et al. 2003). Furthermore, one study has emphasised the relative abundance of the 5-HT$_{2A}$ receptor in the cytoplasm, suggesting that membrane trafficking plays and important role in this receptor's regulation and function (Cornea-Hébert et al. 1999). Importantly, the 5-HT$_{2A}$ receptor is also repeatedly found to be expressed on GABAergic interneurones (Willins et al. 1997; Burnet et al. 1995; Weber and Andrade 2010). In rat prefrontal cortex, the receptor's relative abundance was precisely quantified, where 55% of pyramidal and 25% of interneurones were found to express the 5-HT$_{2A}$ receptor (Santana et al. 2004). There is also evidence for 5-HT$_{2A}$ receptor expression on astrocytes (Xu and Pandey 2000) and microglia (Glebov et al. 2015), although it is unclear what functional roles these might play.

1.3.5 The Head Twitch Response

Animal models are essential in order to study the pharmacological and molecular mechanisms which underpin the psychedelic phenomenon, yet the inherent subjectivity of this state poses a significant potential barrier for translation into animals. Fortunately, a well-characterised behavioural correlate of the activity of psychotropic 5-HT_{2A} receptor agonists is present in many mammals; the head twitch response (HTR).

The HTR was first identified in the 1950s, separately in mice (Keller and Umbreit 1956) and in rats (Winter and Flataker 1956) treated with LSD. Subsequently, the mouse HTR has been studied extensively and most thoroughly characterised in response to DOI (Canal and Morgan 2012). However, the HTR has been identified as a prominent behavioural response to a range of psychotropic 5-HT_{2A} receptor agonists, notably including psilocin, as well as many structurally modified ergolines, tryptamines and phenethylamines (Halberstadt and Geyer 2018).

In the mouse, the observed head twitch corresponds to a sudden rotational shaking movement of the head comprising around 5 - 11 side-to-side twists of the neck at around 90 Hz, each lasting approximately 10 ms (Halberstadt and Geyer 2013). The HTR strongly resembles the reflex response to tactile irritation of the pinna. Head twitches in mice occur at a low spontaneous rate which increases in frequency following treatment with serotonergic psychedelics in a dose-dependent manner up to a peak response level, after which higher doses result in lower HTR. The peak HTR that can be evoked by psilocin is reported to be around 1.5 - 2 per min, using doses between 0.5 – 3 mg/kg (Halberstadt et al. 2011; Zhuk et al. 2015; Halberstadt et al. 2020) whereas the peak head twitch frequency evoked by DOI is around 1 - 3 per min and occurs with a range doses between 1 – 5 mg/kg (Schreiber et al. 1995; Canal et al. 2010; Canal and Morgan 2012). The large range of HTR peak responses observed with DOI has been attributed to a greater potency of the (-)-DOI enantiomer compared to (+)-DOI (Darmani et al. 1990), and to

differences in mouse strain (Canal and Morgan 2012), although it is unknown whether strain differences generalise to other substances such as psilocin.

Head twitch responses to psychedelics in rats, are typically accompanied by a larger shake of the whole body, a movement which is often compared to that of a wet dog shaking in order to dry itself. Comparable shakes of the head or body induced by 5-HT_{2A} receptor agonists have also been described in shrews (Darmani et al. 1994), rabbits (Dave et al. 2002), cats (Jacobs et al. 1976), pigs and macaques (Schlemmer and Davis 1986).

The full functional significance of the HTR, and its possible relationship to hallucinatory perception, remains unclear. Despite this lack of construct validity, the utility of the HTR as a marker for psychedelic action is evidenced by its impressive predictive validity, which manifests as a strong positive correlation between the frequency of head twitches in mice and the expected psychotropic effects in humans (Corne and Pickering 1967; Halberstadt et al. 2020). The psychedelic-induced HTR is dependent on the 5-HT_{2A} receptor, as it is attenuated by 5-HT_{2A} receptor antagonists by a magnitude correlated with their receptor affinity (Leysen et al. 1982; Schreiber et al. 1995), and is completely abolished by highly selective antagonists (Fox et al. 2010). Furthermore, the HTR is absent in 5-HT_{2A} receptor KO mice but can be rescued in these animals by viral expression of the receptor in the forebrain (González-Maeso et al. 2007; Halberstadt et al. 2011). Importantly, the HTR is absent when mice are treated with 5-HT_{2A} receptor agonists which do not have hallucinogenic properties in humans, such as lisuride and ergotamine (González-Maeso et al. 2007). This property distinguishes the head twitch response from other behavioural models of psychotropic activity, such as drug discrimination (Appel et al. 1982).

The 5-HT_{2C} receptor has a complex modulatory effect on the HTR, since as both agonists and antagonists appear to attenuate it (Schreiber et al. 1995; Vickers et al. 2001; Canal et al. 2010; Canal et al. 2013). The 5-HT_{2C} receptor is not necessary for the HTR since head twitches are present in 5-HT_{2C} knockout mice, albeit at an approximately halved rate (Canal et al. 2010) and are evoked by selective psychotropic 5-HT_{2A} agonists

with no 5-HT_{2C} affinity (Fox et al. 2010; Fantegrossi et al. 2015). Increased activation of 5-HT_{2C} is a possible mechanism by which high doses of DOI result in fewer head twitches (Fantegrossi et al. 2010), however it is not the only mechanism, as reduced head twitches are seen for high doses of psychedelics selective for 5-HT_{2A} (Fantegrossi et al. 2015). Agonists of the 5-HT_{1A} receptor additionally attenuate the HTR, suggesting an inhibitory effect of this receptor (Darmani et al. 1990).

1.3.6 Serotonergic Psychedelics & Neuronal Activity *In Vitro*

Serotonin exerts a 5-HT_{2A}-receptor-mediated net excitatory influence on the neocortex *in vitro*, though a facilitation of glutamatergic transmission. It was observed that bath application of 5-HT to prefrontal cortical slices increases the frequency of spontaneous sub-threshold excitatory postsynaptic currents (EPSCs) in layer 5 pyramidal neurones. This phenomenon was sensitive to antagonists of both AMPA and 5-HT_{2A} receptors, and additionally could be mimicked by focal application of 5-HT to the apical dendritic field of identified pyramidal neurones (Aghajanian and Marek 1997). Further *in vitro* experiments found that pre-treatment of prefrontal cortical slices with the serotonergic psychedelics LSD or DOI enhances the effects of subsequent cortical electrical stimulation; stimulations that would evoke only a transient excitatory current were now sufficient to promote persistent recurrent network activity (Aghajanian and Marek 1999). Importantly, this increased excitability includes also activation of inhibitory interneurones (Zhou and Hablitz 1999), which also express 5-HT_{2A} receptors, such that the resulting persistent recurrent network activity resembles a cortical up state (Lambe and Aghajanian 2007).

Agonists of the 5-HT_{2A} receptor have been observed to increase the concentration of glutamate in the extracellular space (Scruggs et al. 2003) and treatments which interfere with the diffusion of synaptic glutamate abolish the enhancement of network activity by 5-HT_{2A} agonists, as do selective antagonists of the NMDA receptor subtype NR2B (Lambe

and Aghajanian 2006), a glutamate-dependent excitatory channel which is primarily expressed outside of synapses (Charton et al. 1999). These results are suggestive of a mechanism by which 5-HT_{2A} receptor agonists promote an increase in glutamate release from presynaptic terminals in the apical dendritic field of pyramidal neurones, leading to spill over from the synaptic clefts into the extracellular space. This mechanism has been suggested to enable the propagation of excitation between neurones which are synaptically unconnected, and this has been speculated to be one mechanism by which psychedelics produce atypical perceptions (Aghajanian 2009).

The glutamatergic inputs targeted by psychedelics were suggested to be mainly thalamocortical afferents, since lesions of the thalamus significantly reduced serotonin-induced EPSCs in layer 5 prefrontal neurones (Marek et al. 2001). However, it was found that in the 5-HT_{2A} receptor knockout mouse, viral re-expression of receptor in the cortex, but not the thalamus, was sufficient to rescue the head twitch response to LSD (González-Maeso et al. 2007), suggesting that enhanced intra-cortical glutamate transmission may be the more relevant mechanism. Indeed, an important local contribution has been identified, in the form of a small subpopulation of prefrontal layer 5 pyramidal neurones which themselves are sufficiently depolarised by 5-HT_{2A} receptor activation to induce tonic spiking (Béïque et al. 2007). Interestingly, many neurones which are directly depolarised in this way by serotonin via 5-HT_{2A}-receptor-mediated mechanisms are commissural projection neurones, highlighting that the facilitation of glutamatergic transmission is long-range as well as local (Avesar and Gulledge 2012).

One unresolved issue with this proposed mechanism stems from receptor localisation data which suggest that 5-HT_{2A} receptors are predominantly expressed postsynaptically (Xu and Pandey 2000) and that presynaptic expression is restricted to the axons of monoaminergic neurones (Miner et al. 2003). One study has investigated this issue by inducing viral expression of 5-HT_{2A} receptors in the thalamus of 5-HT_{2A} knockout mice, in order to restrict the presence of prefrontal cortical 5-HT_{2A} receptors to thalamocortical affer-

ents. This procedure was sufficient to rescue the ability of DOI, lost in receptor knockouts, to potentiate NMDA-dependent excitatory currents, and also to rescue performance on a spatial associative learning task (Barre et al. 2016), providing evidence that presynaptic 5-HT_{2A} receptors on thalamocortical afferents can indeed have physiological relevance.

The effects of myriad neuromodulatory receptors have been assayed using this paradigm of induction of recurrent activation in prefrontal slices as a model for psychedelic activity. The enhancement of network activity by 5-HT_{2A} receptor agonists can be prevented by a range of glutamate release inhibitors, including agonists of the metabotropic glutamate receptor mGlu2, the adenosine receptor A1, the dopamine receptors D1 and D5, the μ-type opioid receptor, and noradrenaline receptor β2 (Marek 2018). Intriguingly, there exists a strong correlation between the effects of drugs on this *in vitro* assay and their effects on the head twitch response, as inhibitors of 5-HT-induced EPSCs also suppress head twitches *in vivo* (Canal and Morgan 2012). There is even evidence from both human clinical studies and behavioural paradigms in rodents that inhibitors of 5-HT-induced EPSCs have an anti-depressant effect (Marek 2018).

1.3.7 Serotonergic Psychedelics & Neuronal Activity *In Vivo*

A limited number of studies have explored the effects of serotonergic psychedelics on cortical neuronal spiking *in vivo*. Two studies on anaesthetised rats found that very low DOI doses (0.05 – 0.3 mg/kg) have an overall excitatory effect on the firing rates of prefrontal pyramidal neurones (Puig et al. 2003; Celada et al. 2008). Within recorded neural populations, subgroups of roughly equal size were identified whose firing rates were increased, decreased, or unchanged by DOI. However, the observed percentage increase in firing was of approximately 50-fold greater magnitude than the percentage decrease (Puig et al. 2003). In contrast to equivalent *in vitro* studies (Marek et al. 2001), thalamic lesions did not alter the neural response to DOI, however, both these excitatory and inhibitory

effects were sensitive to 5-HT_{2A} receptor antagonists, and the inhibitory effect could additionally be abolished by a GABA antagonist (Puig et al. 2003; Celada et al. 2008). This suggests that DOI's effects have an intracortical origin, and that its inhibitory effects are mediated by inhibitory interneurones, themselves excited by 5-HT_{2A} receptor activation.

Another study which investigated the effects of DOI on prefrontal pyramidal firing treated awake rats with higher doses of DOI, finding no significant change in firing with 1 mg/kg and a reduction in firing with 3 or 5 mg/kg DOI (Wood et al. 2012). Dose dependency of DOI's effects on prefrontal cortex had been shown in earlier work (Ashby et al. 1989) and if the predictive validity of head twitch data is believed, dosages which induce inhibition may be more representative of the psychedelic response. However, it is alternatively possible that the differences in these studies are due to the use of anaesthetised vs. awake animals, or on the differing recording location (prelimbic cortex in the former two and orbitofrontal/anterior cingulate cortex in the latter).

While the directional change in firing rate may be dose dependent, a disruption in the relationship between spike timing and gamma oscillations has been more consistently found. DOI has been shown, dependent on 5-HT_{2A} receptor activation, to reduce the locking of spikes to the active phase of LFP oscillations (Celada et al. 2008), to decrease overall gamma oscillatory power, and also to decrease the correlation between gamma power and spike rate (Wood et al. 2012).

1.3.8 Serotonergic Psychedelics & Human Brain Activity

In contrast with the relatively sparse and conflicting results obtained from animal studies, the human neuroimaging literature reveals a more comprehensive picture of how neuronal dynamics are altered on a global scale by serotonergic psychedelics. The effects of these drugs are characterised by a generalised desynchronisation of neuronal activity, originating from a suppression of regulation by higher default mode network structures,

such as medial prefrontal and posterior cingulate cortex. Psilocybin decreases fMRI blood-oxygen-level dependent signal in these regions and is accompanied by a decrease in measures of functional connectivity between prefrontal and cingulate cortex, and also between these regions and the hippocampus and parahippocampal gyrus (Carhart-Harris et al. 2012; Carhart-Harris et al. 2014; Lord et al. 2019). Similar results have been reported using the DMT-containing drink ayahuasca (Palhano-Fontes et al. 2015). Consistent with this finding, the oscillatory power of field potentials broadband decreases, generally focussed over posterior association cortical areas, in individuals given psilocybin (Muthukumaraswamy et al. 2013) or ayahuasca (Riba et al. 2004). Reduced oscillatory power in the alpha band over occipital and parietal cortex in particular has been specifically linked to visual-stimulus-evoked responses and putatively may account for the alterations in visual perception associated with the psychedelic experience (Kometer et al. 2013). Furthermore, dynamic causal modelling using a simplified canonical cortical circuit suggests that increased excitability of deep pyramidal neurones by 5-HT_{2A} receptor activation, as has been found *in vitro*, could account for the decreased power in the theta and alpha range (Muthukumaraswamy et al. 2013).

Recently, more abstract measures of neuronal dynamics have been applied to understand the effects of this apparent decoupling of the brain from the default mode network. A prominent theory identifies an increase in the entropy of neuronal dynamics, particularly with respect to the repertoire of functional connectivity motifs that the brain may express (Carhart-Harris et al. 2014). Indeed, a number of fMRI studies have found increases in measures of entropy of patterned functional connectivity states during resting induced by serotonergic psychedelics, including psilocybin (Tagliazucchi et al. 2014), LSD (Lebedev et al. 2016; Atasoy et al. 2017) and ayahusaca (Viol et al. 2017). Similarly, there is reportedly increased MEG Lempel-Ziv complexity in response to a range of psychedelics, particularly in the single-channel temporal domain (Schartner et al. 2017). This result is interpreted in the context that measures of complexity and entropy form reliable indices of

the level of consciousness, and can be used to discriminate wakefulness from sleeping and unconscious brain states (Casali et al. 2013; Abasolo et al. 2015). It is argued that the psychedelic state may represent one of enhanced conscious content (Carhart-Harris et al. 2014; Carhart-Harris 2018). Furthermore, one study identified near power laws in the frequency distribution of brain states, finding that LSD slightly increased the power law fit (Atasoy et al. 2017), supporting the idea that the psychedelic state may increase the closeness to criticality of wakefulness, which is normally sub-critical (Carhart-Harris 2018).

1.3.9 Serotonergic Psychedelics, Learning, Memory & Synaptic Plasticity

While the acute effects of psychedelic 5-HT_{2A} receptor agonists on neuronal activity have been relatively well-characterised, it remains unclear how these dynamics effect neuronal plasticity and what are the long-term consequences for brain function. One study has reported that sustained DOI exposure causes long-term depression of AMPA synapses in layer 5 pyramidal neurones from mouse prefrontal cortical slices (Berthoux et al. 2019). However, another study found that the *in vivo* administration of a range of 5-HT_{2A} receptor agonists, including DOI, to rats promotes synaptogenesis, increases the complexity of dendritic arbours, and enhances spontaneous EPSC frequency and amplitude, measured *ex vivo* hours after the drug has left the body (Ly et al. 2018). A combination of the depression of existing synapses and an enhancement of the formation of new synapses is entirely consistent with descriptions of the psychological benefits of the psychedelic state. The initial breakdown of the functional integrity of networks during the experience, notably in the default mode network, is reportedly followed by a recovery of these networks, at least in depressed patients (Carhart-Harris et al. 2017). This has been likened to a "resetting" or "annealing" like mechanism.

A number of learning paradigms in both humans and animals have been used in an

attempt to characterise which forms of learning might be enhanced by 5-HT_{2A} agonists. Notably, a range of 5-HT_{2A} receptor agonists, including psilocybin and DMT, have been demonstrated to enhance fear extinction learning in rodents (Catlow et al. 2013; Zhang et al. 2013; Cameron et al. 2018), which is notably relevant in the context of mental health. This form of learning depends on a well-characterised neural circuit linking the hippocampus, amygdala and prelimbic and infralimbic cortices (Tovote et al. 2015). Activation of 5-HT_{2A} receptors has been associated with an enhancement of NMDA-dependent plasticity in both the rodent medial prefrontal cortex (Arvanov et al. 1999) and basolateral amygdala (Chen et al. 2003). In addition, increased hippocampal neurogenesis has also been implicated as a possible mechanism of the 5-HT_{2A}-receptor-mediated enhancement of fear extinction learning (Catlow et al. 2013).

Psychedelic 5-HT_{2A} receptor agonists have been associated with the enhancement of memory consolidation in other paradigms, such as object recognition memory (Zhang and Stackman 2015) and, arguably, spatial memory in the Morris water maze (Rambousek et al. 2014; Froese et al. 2018). The mechanisms remain unclear, and in particular, the degree to which these effects are dependent on sleep, the importance of which in memory consolidation is well established, is unknown (Froese et al. 2018).

1.3.10 Serotonergic Psychedelics & Sleep

A few older studies have reported on the acute effects of classical psychedelics on sleep-wake architecture. In all cases wakefulness was reported to increase, suppressing both NREM and REM sleep, for 1 - 3 hours after drug administration, and this was found using mescaline in rats (Colasanti and Khazan 1975), LSD in cats (Kay and Martin 1978) and DOI in rats (Monti and Jantos 2006). Notably, animals were reportedly more drowsy during this wakefulness (Colasanti and Khazan 1975) and one study also reported an increase specifically in light NREM sleep as opposed to slow wave sleep (Monti and Jantos

2006). One study in humans reported the quality of one night's sleep 11 hours after ingestion of ayahuasca (Barbanoj et al. 2008). Interestingly, higher slow wave activity was reported in initial NREM sleep, obtained by averaging power over all channels across the scalp, suggesting a generalised increase in sleep pressure (Barbanoj et al. 2008). This study also found a significant suppression of REM sleep. However, the ayahusaca preparation also contains monoamine oxidase inhibitors, which are known to powerfully suppress REM sleep, confounding the interpretation of this result (Wyatt et al., 1971). Indeed, the suppression of REM sleep by DOI in rats was not found to depend on the 5-HT_{2A} receptor (nor the 5-HT_{2C} receptor), unlike the changes to wake and NREM sleep (Monti and Jantos 2006).

In summary, psychedelic 5-HT_{2A} receptor agonists exert powerful and complex effects on neurophysiology, from the level of local neuronal firing rates and network excitatory-inhibitory balance up to the level of global dynamical complexity. They are capable of promoting lasting synaptic plasticity and changes to global functional connectivity which have generally positive influences on psychological well-being. However, the consequences of such effects for sleep-wake regulation are unknown, despite some similarity in aspects of the underlying mechanisms.

1.4 Aims

In this thesis, I aim to explore a number of possible links between the dynamics of cortical neuronal activity and the sleep homeostatic process, both at local and global levels. I aim to achieve this through the analysis of chronic *in vivo* electrophysiological data sets obtained from freely behaving mice, comprising LFP and multi-unit spiking data from either motor or medial prefrontal cortex, alongside EEG, including both spontaneous sleep-wake cycling and also experimentally-induced sleep deprivation.

In chapter 3, I aimed to develop novel alternative measures and quantitative models of Process S in mice, in order to test the prediction that its temporal dynamics can be derived entirely from local neuronal activity, without any reference to the animal's sleep and wake states. I further aimed to compare Process S dynamics on both local (LFP-derived) and global (EEG-derived) scales, in order to understand how the apparently local-scale origin of Process S might be reconciled with the global-scale of its regulation.

In chapter 4, I aimed to explore whether measures of critical dynamics based on neuronal avalanches, obtained both from LFP and spiking data, vary consistently between wake, NREM and REM sleep, or as a function of Process S.

In chapter 5, I aimed to collect electrophysiological recordings from the prefrontal cortex of mice while exposed to the serotonergic psychedelic psilocin, in both an undisturbed condition and when combined with sleep deprivation. I further aimed to determine whether psilocin alters sleep-wake architecture, sleep-related neuronal activity, or the dynamics of local or global Process S, and on what timescale do any observed effects unfold.

2

General Methods for Chronic Electrophysiological Recordings

Contents

2.1 Animals **44**

2.2 Surgical Procedures **44**

2.3 Animal Husbandry **47**

2.4 Sleep Deprivation **48**

2.5 Perfusion, Microlesion & Histology **49**

2.6 Data Acquisition **50**

2.7 Statistics **51**

2.1 Animals

Two electrophysiological datasets were analysed in the work documented within this thesis. The first, analysed in chapters 3 & 4, was obtained by my colleague Laura McKillop as part of a previous study (McKillop et al. 2018), and comprised recordings from 6 animals from frontal cortex over 48 hours including baseline and sleep deprivation. The second dataset, analysed in chapter 5, was obtained myself, and comprised 8 animals. These were implanted with either a microwire array or single-shank electrode in medial prefrontal cortex, and recorded for 11 days including baseline, sleep deprivation and injection of psilocin. The methodology used for obtaining both data sets was very similar and so is described primarily with focus on the second data set (my own work), although important methodological differences are highlighted where relevant. All animals used for electrophysiology in both datasets were young adult male C57BL/6J mice, ages ranging from 20 - 24 weeks (M1 dataset) and 14 - 20 weeks (mPFC dataset). The animals were surgically implanted with electrodes for the continuous recording of electroencephalography (EEG), electromyography (EMG) and cortical neuronal activity. All procedures were performed under a UK Home Office Project License and conformed to the Animals (Scientific Procedures) Act 1986.

2.2 Surgical Procedures

Surgeries were performed under isoflurane anaesthesia (4% induction, 1 - 2% maintenance). Anaesthetic depth was monitored frequently by estimating the rate of respiration, and isoflurane concentration adjusted to maintain a rate of 40 - 80 breaths per minute. Thermal support was provided and temperature was recorded using a rectal probe, maintaining the animal at 36°C. Liquid gel (Viscotears, Alcon Laboratories Ltd, UK) was regularly applied to the animal's eyes to keep them hydrated.

Analgesics were administered immediately before surgery (5 mg/kg metacam and 0.1

mg/kg vetergesic, subcutaneous) and for at least three days following surgery (metacam, oral). In addition, immunosuppressant was given both the day before surgery (0.2 mg/kg dexamethasone, intraperitoneal) and immediately before surgery (0.2 mg/kg dexamethasone, subcutaneous). Saline was administered at the end of surgery (0.1 ml per 20 g body weight per hour of surgery, subcutaneous) to replace lost fluids.

Once anaesthetised, the fur covering the head and neck was shaved and the skin cleaned using iodine and alcohol wipes. Subsequent work was performed under sterile conditions. The animal was mounted onto a stereotaxic frame (David Kopf Instruments, California, USA), and an incision was made exposing the skull. To stabilise the attachment of the implant to the skull, all connective tissue was carefully removed, the bone was scored by gentle scratching with the scalpel blade and then treated with phosphoric acid etching gel (Henry Schein, New York, USA) applied for 2 minutes. The position of lambda and bregma were measured and marked onto the skull. The head tilt of the mouse was adjusted within the stereotaxic frame to ensure a level dorsoventral plane (lambda and bregma coordinates within ± 0.3 mm). The coordinates of all implanted electrodes as detailed below are relative to bregma and these were marked onto the skull.

A head stage was constructed in advance of each surgery which comprised three EEG bone screws and two stainless steel EMG wires, soldered to an 8-pin surface mount connector (Pinnacle Technologies Inc., Kansas, USA). The EEG screw electrodes were inserted into holes drilled into the skull (0.7 mm drill bit, InterFocus Ltd., Cambridge, UK). One EEG screw was located above the right frontal cortex (primary motor area: anteroposterior 2 mm, mediolateral 2 mm), one above the right occipital cortex (primary visual area: anteroposterior 3.5 mm, mediolateral 2.5 mm), and one above the left cerebellum, which served as the reference signal. The two EMG wires were inserted into left and right nuchal muscle. An additional screw was inserted above left occipital cortex, which served as a ground for the intracortical electrodes (Figure 2.1).

Four animals were implanted with a single-shank probe targeting left medial prefrontal

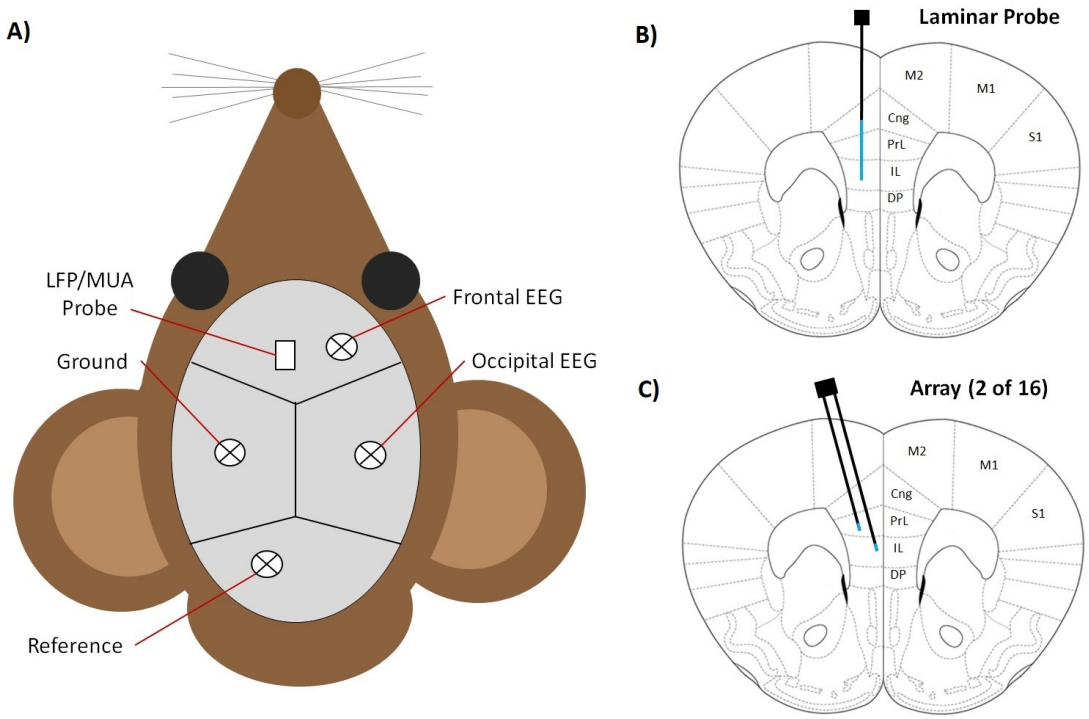


Figure 2.1: A) A cartoon schematic of the locations of surgically implanted EEG and intracortical probes relative to the skull. Anatomical atlas illustrating the intended target sites of **B)** the laminar probe and **C)** multi electrode array. Blue probe termini indicate the location of electrode contact sites, where in **B)** all 16 are together on the single shank and in **C)** one site is located on each of 16 shanks. Only 2 of the 16 multielectrode array shanks are shown, others targeting more anterior and posterior medial prefrontal cortical regions. S1: Somatosensory cortex. M1: Primary motor cortex. M2: Secondary motor cortex. Cng: Cingulate cortex. PrL: Prelimbic cortex. IL: Infralimbic cortex. DP: Dorsal peduncular cortex. Coronal sections correspond to 1.7 mm anterior of bregma and are adapted from Paxinos and Franklin 2013.

cortex (anteroposterior 1.7 mm, mediolateral 0.25 mm, depth 2 mm). The probe comprised a 5 mm shank containing 16 iridium electrode sites of 30 µm diameter, regularly spaced 50 µm apart and extending up to 800 µm from the probe's tip (A1x16-5mm-50-703, NeuroNexus, Michigan, USA). The remaining four animals were implanted with a custom-designed polyimide-insulated tungsten microwire array (Tucker-Davis Technologies Inc., Florida, USA), spanning a larger area of medial prefrontal cortex (centred anteroposterior 2.23 mm, mediolateral 0.75 mm, depth 2.2 mm, rotation 10 degrees). The array comprised 16 wire channels of 33 µm diameter arranged in 2 rows of 8, with row separation 375 µm, columnar separation 250 µm, and tip angle 45 degrees. Each wire was a custom-specified

length for precise targeting of prefrontal regions (lateral row from anterior to posterior: 3.2 mm, 3.5 mm, 3.5 mm, 3.8 mm, 3.8 mm, 4 mm, 4 mm, 4 mm; medial row from anterior to posterior: 2.5 mm, 2.8 mm, 3 mm, 3.2 mm, 3.2 mm, 3.5 mm, 3.5 mm, 3.5 mm). The six animals of the first dataset were implanted with very similar arrays, however these were targeted into the left frontal cortex (primary motor area: anteroposterior 2 mm, mediolateral 2 mm). Wire lengths were identical within a row, but one row of wires was 250 µm longer than the other to account for cortical curvature.

For the single-shank probe, a hole was made similarly as for the insertion of EEG screws but slightly larger. For the arrays, a 1 × 2.25 mm craniotomy window was drilled into the skull. Before insertion of either probe type, the dura was carefully removed from the exposed brain using a 25 gauge needle. Saline was frequently applied to keep the exposed brain moist. Once the array/probe was implanted, a silicone gel (KwikSil, World Precision Instruments, Florida, USA) was applied to seal the craniotomy and protect exposed brain. Dental acrylic cements were used to stabilise all the implanted electrodes (Super Bond, Prestige Dental, Bradford, UK) and to protect the exposed wires (Simplex Rapid, Kemdent, Swindon, UK).

2.3 Animal Husbandry

Following surgery, mice were housed in separate individually ventilated cages and their recovery was closely monitored. The weight, spontaneous behaviour, provoked behaviour, respiration rate and grimace of each mouse was scored daily, until the mice reached baseline level for three consecutive days. The second dataset was collected in two batches, each of four mice. Within a batch, all surgeries were performed in the same week and ten days after the final surgery all mice were judged to have fully recovered. They were then rehoused in individual custom-made transparent plexiglass cages (20.3 × 32 × 35 cm), and placed in pairs inside ventilated sound-attenuated Faraday chambers (Campden

Instruments, Loughborough, UK). A camera was mounted inside each chamber and video was recorded continuously during the light period. EEG and EMG head stages were connected to the recording equipment using custom-made cables, and both LFP probe types were connected using spring-wrapped Zif-clip head stages (Tucker-Davis Technologies Inc., Florida, USA). Mice were habituated to their cables for three days before the first baseline recording began. The recording room was kept on a 12 - 12 hour light-dark cycle (lights on at 9 am), at 22 $\pm$ 1 ^{o}C and 50 $\pm$ 20 % humidity. Food and water were provided *ad libitum* throughout. In the first dataset of animals (implanted in motor cortex), a two week recovery period was used, video was not recorded and mice were additionally provided with a running wheel (Campden Instruments).

2.4 Sleep Deprivation

Sleep deprivation was performed using the well-established gentle handling procedure (Fisher et al. 2016). During this period, experimenters constantly monitored both the behaviour and ongoing neurophysiological recordings of the mice. As soon as any animal showed signs of sleepiness (such as immobility, or slow waves in the EEG), novel objects were introduced to the cage (such as cardboard, colourful plastic, sponge, tin foil, wooden blocks and plastic wrap) in order to encourage wakefulness. In some cases, towards the end of the sleep deprivation period, the mice stopped responding to novel objects and were awakened instead by gentle physical stimulation (brushing with tissue paper or disturbance of their nest). Sleep deprivation lasted 6 hours in the first (M1) dataset, and 4 hours in the second (mPFC) dataset.

2.5 Perfusion, Microlesion & Histology

When all experimental recordings were complete the animals were euthanised by intraperitoneal injection of pentobarbital (Euthatal, 40 mg in 0.2 ml). Their brains were prepared for histological analysis of the location of inserted probes. A microlesion protocol was applied immediately after death (confirmed by an absent pedal and corneal reflex), aiming to scar the cortical tissue in contact with specific probe channels and thereby aid their visualisation. The microlesioning was performed using a NanoZ stimulation device (White Matter LLC, Seattle, USA). Four channels (chosen to be as equally spaced across the area covered by the probe as possible) were sequentially stimulated with 10 µA of current for 20 seconds. Furthermore, the device was used to check the electrical impedance of each channel before and after applying current. A reduction in impedance was evidence that the electrical lesioning was successful.

Next, a transcardial perfusion protocol was performed to achieve fixation of the brain. Cuts were made around the ribcage and through the diaphragm in order to expose the heart. A butterfly needle attached to a pump was inserted into the left ventricle of the heart and the right atrium was cut in order to drain the venous system. The mouse was first perfused with phosphate-buffered saline (PBS) until exsanguinated, and then with paraformaldehyde (PFA, 4% in PBS) until the body was fully rigidified. Finally, the head was removed and suspended in PFA for 24 - 48 hours, before being stored in PBS (with sodium azide).

When sectioning was ready to be performed, the brains were removed from the skull and suspended in a 30% sucrose PBS solution, which acts as a cryoprotectant. The brains were sectioned into 50 µm coronal slices using a freezing microtome across a region of interest spanning 1.3 - 3.2 mm anterior of bregma. These were mounted onto glass slides and stained with DAPI, a DNA binding fluorophore. The slices were imaged using an Olympus FV1000 confocal microscope and compared with an anatomical atlas (Paxinos and Franklin 2013) to aid localisation of probes. Histology was only completed

for 4 prefrontal electrodes, as interruptions necessitated by the COVID-19 pandemic unfortunately led to a loss of sample quality. Histological confirmation for the motor cortex implants is published elsewhere (McKillop et al. 2018).

2.6 Data Acquisition

Electrophysiological signals were acquired using a multichannel neurophysiology recording system (Tucker-Davis Technologies Inc., Florida, USA). EEG signals were obtained from frontal and occipital derivations, LFP from each channel of the array/probe, and all were referenced against cerebellar EEG. EMG was obtained as the differential of the two wire signals.

Signals were managed and processed online using the software package Synapse (Tucker-Davis Technologies Inc., Florida, USA). All signals were amplified (PZ5 NeuroDigitizer preamplifier, Tucker-Davis Technologies Inc., Florida, USA), filtered online (0.1 – 128 Hz) and stored with a sampling rate of 305 Hz. In addition, the raw LFP signal was processed to extract extracellular multi-unit spiking. The signal was filtered (300 Hz – 1 kHz) and an amplitude threshold was manually selected for each channel to detect the occurrence of spikes. When threshold crossing occurred the time stamp and signal snippets (46 samples at 25 kHz, 0.48 ms before and 1.36 ms after threshold crossing) were stored.

Data were pre-processed offline using custom written Matlab scripts. Signals were read from tank formats into Matlab (using the software package *TDTMatlabSDK*) and amplified by a factor of 10^6. The signals were filtered with a zero-phase 4^{th} order Butterworth filter (using Matlab functions `butter` and `filtfilt`) between 0.5 - 100 Hz for EEG and LFP signals and between 10 – 45 Hz for EMG, then resampled at 256 Hz (using the Matlab function `resample`). All signals were cut into 12 hour segments, corresponding to the light or dark period of one day.

Spiking activity from each channel was first cleaned offline for artefacts using the Matlab spike sorting software *Wave_clus* (Quiroga et al. 2004). Although this software outputs putative sorted single units, very few separable clusters were typically found (often only one) and these were not of high quality (many inter-spike intervals below 3 ms refractory period), so unit clusters were merged and treated as multi-unit activity. However, the software was very useful for identifying waveforms which were not spike-like, and were therefore discarded as electrical artefacts. Cleaned multi-unit spiking data were stored separately for each channel as both a binary signal with 1 ms resolution and as a total firing rate, in Hz, calculated in epochs of 4 seconds. As with the other signals, these were trimmed into separate 12 hour segments corresponding to the light or dark period of one day.

Vigilance states were scored manually by visual inspection at a resolution of 4 seconds using the software SleepSign (Kissei Comtec, Nagano, Japan), after conversion to European Data Format using open source Neurotraces software. Vigilance states were classified as waking (low amplitude but high frequency EEG with high or phasic EMG activity), NREM sleep (presence of EEG slow waves, a signal of a high amplitude and low frequency, and a low level of EMG activity) or REM sleep (low amplitude, high frequency EEG, and low EMG). In order to identify time periods with large amplitude artefactual deflections in all LFP channels simultaneously, a hybrid LFP signal was created comprising the maximum absolute value of any one LFP at each time point, and plotted alongside EEG. Artefacts were then scored whenever they appeared in any of these signals.

2.7 Statistics

Statistical tests were all performed using Matlab. Paired samples t-tests were conducted using Matlab function `ttest` and analysis of variance with `anova1` (one-way) and `anovan` (two-way with unequal group size). The effect size (η^2) was calculated for a factor as its sum of squares divided by the total sum of squares in the ANOVA and reflects the fraction

of the variance accounted for by that factor. Data were first confirmed to pass a Lillie's test for normality (using the function `lilliestest`). In some cases, where indicated, tests were run after applying a log transform to improve data normality.

To summarise the results in figures throughout this thesis, boxplots were included alongside individual data points. These indicate the median, 25^{th} and 75^{th} percentiles, with whiskers extending to the most extreme value which falls within 150% of the interquartile range of the box. In some cases, where indicated, results from individual channels are pooled across animals, whereas in others channels from the same animal were presented as separate populations.

3

Sleep Homeostasis Reflects Integrated Cortical Neuronal Activity

Contents

3.1 Introduction **54**

3.2 Methods **56**

3.3 Results **61**

3.4 Discussion **78**

3.1 Introduction

The need for sleep accumulates during wakefulness and dissipates during sleep. The earliest theoretical descriptions of sleep homeostasis supposed the existence of a single variable, termed Process S, which describes sleep drive at the global level (Borbély 1982). This variable is assumed to always increase during wakefulness, independently of its content, and to determine the depth of subsequent sleep, which is reflected in the slow wave activity (SWA, 0.5 - 4 Hz spectral power) observable during NREM sleep in neurophysiological field potentials, such as electroencephalogram (EEG) or local field potential (LFP). As sleep progresses, it is assumed that this variable always declines, and the maximum depth of sleep reached within each successive episode of NREM sleep declines in parallel. These dynamics were shown to be well captured in mathematical models, which accurately accounted for sleep and slow wave activity data from both humans and rodents, despite their differing sleep-wake architecture (Daan et al. 1984; Franken et al. 1991b; Achermann et al. 1993; Guillaumin et al. 2018).

Current views on the mechanistic origins of Process S emphasise its local and activity-dependent component (Krueger and Tononi 2011; Rattenborg et al. 2012; Tononi and Cirelli 2014). It was shown that SWA is far from uniform across the brain, and that the behavioural and cognitive content of waking, beyond its mere duration, influences subsequent sleep and SWA (Kattler et al. 1994; Huber et al. 2004; Vyazovskiy and Tobler 2008; Rector et al. 2009; Murphy et al. 2011; Fisher et al. 2016). Indeed, many candidate mechanisms for the substrate of sleep homeostasis implicate processes occurring at a cellular and network level. These include the maintenance of cellular homeostasis (Reimund 1994; Mackiewicz et al. 2007; Vyazovskiy and Harris 2013; Bellesi et al. 2016), the replenishment of energy stores (Scharf et al. 2008), the influence of sleep-related signalling molecules such as adenosine or cytokines (Krueger et al. 2008), and the renormalisation of imbalanced synaptic strength (Tononi and Cirelli 2003; Vyazovskiy et al. 2008; Liu et al. 2010; Vivo et al.

2017). Although the equivalence of these processes with Process S has not been conclusively demonstrated (Frank and Heller 2019), the existing evidence supports the relevance of sleep-wake-dependent differences in neuronal activity for understanding the regulation of sleep.

Cortical neuronal activity is generally higher during waking compared to sleep (Vyazovskiy et al. 2009b; Niethard et al. 2016; McKillop et al. 2018). Lower spike firing typical of sleep is due, at least in part, to regular periods of widespread synchronous network silence, termed off periods, intruding on ongoing activity (Steriade et al. 1993b; Steriade et al. 2001; Sanchez-Vives and Mattia 2014). Importantly, off periods in neural populations are thought to underpin slow wave dynamics at the level of the field potential (Steriade et al. 1993c; Massimini et al. 2004; Buzsáki et al. 2012) and their properties reflect homeostatic sleep need (Vyazovskiy et al. 2009b; McKillop et al. 2018; Saberi-Moghadam et al. 2018).

Neuronal firing rates typically fluctuate around a homeostatic set point, which is characteristic for individual cells and variable across the population (Turrigiano 2011; Hengen et al. 2013; O'Leary et al. 2014; Styr et al. 2019). The homeostatic regulation of firing rates may depend on processes occurring specifically in sleep and wakefulness (Grosmark et al. 2012; Hengen et al. 2016) and evidence suggests that firing rates change as a function of time spent awake, conditional on the behaviour (Vyazovskiy et al. 2009b; Fisher et al. 2016). Additionally, the magnitude and direction of state-dependent changes in firing rate differs between neurons, depending on the brain region and their individual firing rate set point (Miyawaki and Diba 2016; Watson et al. 2016; Miyawaki et al. 2019). Firing rate homeostasis may occur above the individual cell level (Slomowitz et al. 2015), possibly through synaptic plasticity induced by the sleep slow oscillation which may act to narrow the population firing rate distribution (Levenstein et al. 2017).

Overall, the evidence suggests that the homeostatic regulation of sleep and of neuronal firing rates may be intrinsically related, however, this functional link remains incompletely defined. Mathematical modelling approaches present an opportunity to address this problem. To this end, Process S dynamics were explored, at multiple levels and using

different models, in a dataset of electrophysiological recordings from the motor cortex of 6 mice over 48 hours, including sleep deprivation. Specifically, the aims were to:

- Determine to what degree local neuronal multi-unit firing rates carry sufficient predictive information to describe local Process S dynamics, through the development of novel mathematical models.
- Derive a measure of Process S dependent on local neuronal spiking off periods rather than slow wave activity.
- Compare the agreement to empirical data obtained from novel activity-dependent Process S models with the classical vigilance-state-dependent model.
- Compare the parameters and time course of Process S dynamics at multiple levels, from local off periods to global EEG.

3.2 Methods

3.2.1 Dataset

This study analysed data from chronic electrophysiological recordings from six young adult (4.8 – 5.7 months old, mean 5.2 months) male C57BL/6J mice. This data set is derived from a previous study (McKillop et al. 2018). The animals were surgically implanted with electrodes for the continuous recording of electroencephalography, electromyography and neuronal activity from frontal cortex. All the data analysed here were collected over 48 hours, corresponding to two days of a standard 12 - 12 hour light-dark cycle. The first day served as a baseline, while the animals were completely undisturbed. A sleep deprivation protocol was enforced at light onset on the second day, immediately after the baseline day, and lasted 6 hours. More detailed description of the animal husbandry, surgical procedures and electrophysiological data acquisition process is given in chapter 2.

For this analysis, over the six mice, a total of 78 out of 96 channels were analysed (minimum 10 out of 16 from one mouse). The excluded channels were characterised by poor signal to noise ratio, frequent artefacts, unsystematic rapid fluctuations in firing rates, or major drifts in spiking which could not be related to ongoing state. For the off occupancy models described below, 75 out of 96 channels were used; a further 3 channels were excluded because multi-unit firing rates, while stable, were too low to yield a reasonable estimate of the occurrence of off periods.

3.2.2 Slow Wave Activity

Each EEG and LFP signal was processed to extract a measure of the slow wave activity (SWA). Signal segments were extracted within windows of 4-second duration and 1-second spacing (giving 3-second overlap), and Hann tapered. A Fourier transform was applied to each signal segment and the mean power in the slow wave range (frequencies from 0.5 to 4 Hz) was calculated. This measure was smoothed by finding the median over five temporally adjacent overlapping segments, yielding a SWA measurement for each sequential epoch of 4 second. For normalisation within each channel, SWA values were then expressed as a percentage of the mean SWA calculated over all artefact-free epochs scored as NREM sleep in the baseline 24 hours. The median value of the SWA during each continuous NREM sleep episode served as an estimate of Process S. NREM sleep episodes shorter than 1 min were excluded, as in a previous study modelling Process S in mice (Guillaumin et al. 2018). Brief awakenings (short arousals accompanied by movement, lasting $\leq$ 20 seconds) were excluded from analysis but were not considered to be the ending of a NREM sleep episode.

3.2.3 Off Periods Detection & Definition of "Off Occupancy"

One aim of this study was to develop measures of Process S independent of the EEG with more local origins, and so neuronal spiking off periods were investigated. Off periods refer

to brief interruptions of spiking activity which occur synchronously across many recording sites, last approximately 70 - 100 ms, and are coincident with the positive deflection of LFP slow waves. In previous studies, off periods were detected by pooling spikes over all channels and identifying inter-spike intervals (ISIs) that exceed a threshold duration (Vyazovskiy et al. 2009b; McKillop et al. 2018). However, pooling spikes removes the ability to compare local differences, and if an off period does not involve all channels it will go undetected. To overcome this limitation, off periods were defined separately for each channel by looking at the co-occurrence of local slow waves and spiking silence.

There is no universally accepted method for slow wave detection, and a recent comparison suggests that a simple amplitude-threshold-based approach, while in theory adequate, may underperform due to channel differences in overall LFP amplitude and large amplitude fluctuations of higher frequencies (Bukhtiyarova et al. 2019). For this reason, the LFP was first filtered from 0.5 to 6 Hz (4^{th} order Butterworth filter), and a threshold was defined individually for each channel, using the median plus one median absolute deviation of the peak amplitude of all positive half waves (including all vigilance states, but excluding epochs with artefacts). All positive half waves with peak amplitude above threshold were then considered to be slow waves.

Next, for each LFP slow wave, the multi-unit spike preceding and following the slow wave peak was identified and the corresponding ISI determined. The distribution of these ISIs which coincide with slow waves was often (in 64 out of 75 channels) unambiguously bimodal, allowing the threshold to be selected at the local minimum between these two modes. When there was no evidence of bimodality a value of 120 ms was chosen, corresponding to the maximum value selected for the other channels. All inter-spike intervals aligned to slow wave peaks with duration exceeding the threshold were considered off periods. Finally, the metric termed off occupancy was defined, for each epoch of 4 seconds, as the percentage of time spent in a detected off period during that epoch. Just as with SWA (see above), the median value of off occupancy over NREM sleep

episodes was used to represent the level of Process S.

3.2.4 Model Fitting & Parameter Optimisation

Three theoretical models were used to describe the time course of Process S. The model equations were solved using a discrete time approximation, iteratively updating the value of modelled Process S in time steps of 4 seconds (Euler method). The fitting of various models to a particular channel of data is equivalent to finding the optimal choice of parameters to achieve the closest match between simulation and empirical SWA/off occupancy. In all models, the initial value of Process S was included as an additional free parameter. The selection of parameter values for model fitting was achieved using a semi-automated approach. First, an algorithmic methodology was established, which depends primarily on the definition of an error metric to assess fit quality between modelled Process S and empirical data. For each animal, NREM sleep episodes were identified with a duration of at least 1 minute. For each NREM sleep episode ($n = 1 : N$), the median empirical SWA/off occupancy (X_n), and similarly the median modelled value of Process S (S_n), were computed. The error metric (E) is defined as the sum of absolute differences between model and data, weighted by the relative episode duration (w_n). This weight was defined as the absolute duration (d_n) of the NREM sleep episode, normalised by the total duration of all episodes.

$$E = \sum_{n=1:N} w_n |X_n - S_n|$$

$$w_n = {}^{d_n}/_{\sum_{n=1:N} d_n}$$

Algorithmic parameter optimisation was performed separately for each channel, aiming to minimise this error metric. This was achieved using the Matlab function `fminsearch`, which uses the Nelder-Mead simplex algorithm (Lagarias et al. 1998). Many parameter combinations produce very similar dynamics, and many possible optimal (or near-optimal) parameter regimes exist, therefore algorithmic optimisation is sensitive to initial values.

For this reason, initial values for the parameters were first set manually, aided with the use of a custom-made Matlab graphical user interface. Manually selected values were then fed into the algorithmic optimisation. Final parameter values were visually inspected to ensure that this optimisation produced an improvement of fit.

The final fit quality of a model to the data was expressed as the median percent error (E^*). This is calculated by finding the absolute difference between median empirical (X_n) and simulated (S_n) SWA/off occupancy for each NREM sleep episode, expressed as a percentage of the empirical SWA/off occupancy in that episode. E^* is then defined as the median over all NREM sleep episodes of these difference values. This alternative error metric is used for presentation of results because it has more comprehensible units (percentage of empirical SWA/off occupancy) compared to the original error metric, with arbitrary units.

$$E^* = \underset{n=1:N}{\text{median}} \left[\frac{|X_n - S_n|}{X_n} \right] .100\%$$

3.2.5 Statistics

The correlation between wake duration, wake firing rates and changes in SWA was calculated separately for each LFP channel. Episodes of NREM sleep of at least 1-minute duration were identified (exactly as for modelling) and the median SWA in each episode was obtained. Time periods between two NREM episodes comprising at least 80% wake and lasting at least 5 minutes were then identified. Pearson correlation coefficients were calculated between 1) the duration of these wake periods, 2) the mean multi-unit firing rate during these periods, and 3) the change in median SWA from preceding to the following NREM sleep episode (using the Matlab function `corrcoef`).

3.3 Results

3.3.1 Wake and sleep are characterised by differing neuronal dynamics

NREM sleep can be defined and distinguished from waking and REM sleep by the presence of high amplitude slow (0.5 - 4 Hz) waves in the EEG and LFP (Figure 3.1, Figure 3.2A). Greater average spectral power in the slow wave range (termed slow wave activity; SWA) was evident in epochs scored as NREM sleep, compared to wake or REM sleep, in every LFP recording channel and every animal in this dataset (Figure 3.2B). Slow waves are associated with spiking silence, termed "off" periods (Figure 3.1), causing firing rates to be typically much lower during NREM sleep compared to wake and REM sleep. Consistent with this assumption, the mean multi-unit firing rate averaged over all periods of wake was larger than the firing rate averaged over all periods of NREM sleep in every recording channel (Figure 3.2C).

3.3.2 Process S can be described as a function of vigilance state history

The average SWA in NREM sleep varies as a function of the animal's recent sleep-wake history, and this relationship has been captured in a classical quantitative theory using the concept of "Process S" (Borbély and Wirz-Justice 1982; Daan et al. 1984). Process S describes a variable whose magnitude can be estimated using the level of SWA during NREM sleep, reflecting the intensity of sleep, and which is interpreted as corresponding to the homeostatic component of sleep drive (Franken et al. 1991b; Achermann et al. 1993; Huber et al. 2000a; Vyazovskiy et al. 2007; Guillaumin et al. 2018). Theoretically, Process S follows simple dynamics: during wake it increases according to a saturating exponential

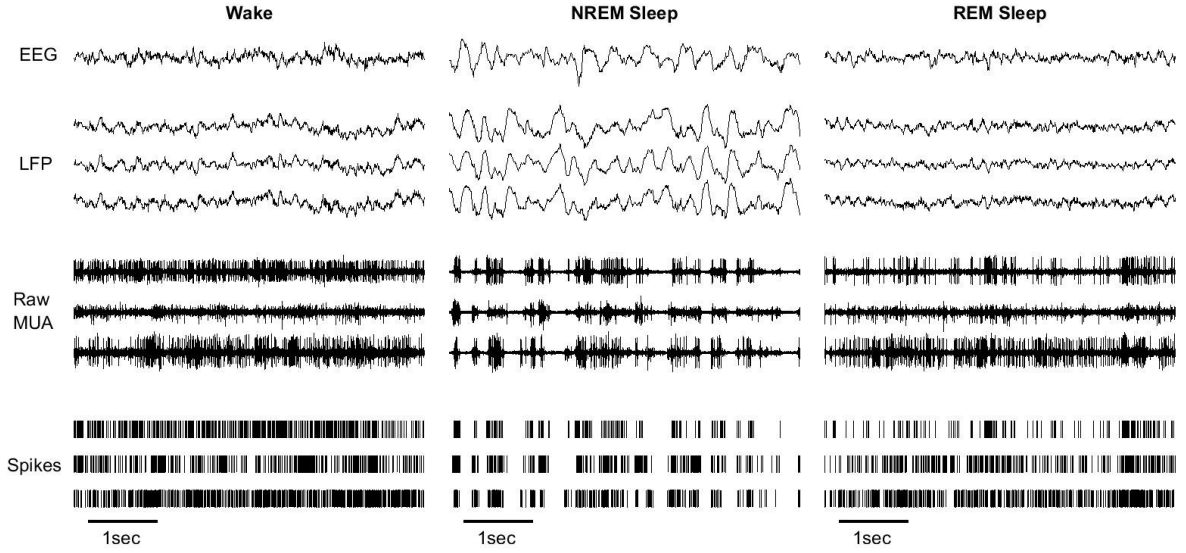


Figure 3.1: An example of frontal electroencephalogram (EEG), 3 primary motor cortical local field potentials (LFP), corresponding raw signal with multi-unit activity (MUA), and detected spikes, in representative segments of waking, NREM and REM sleep.

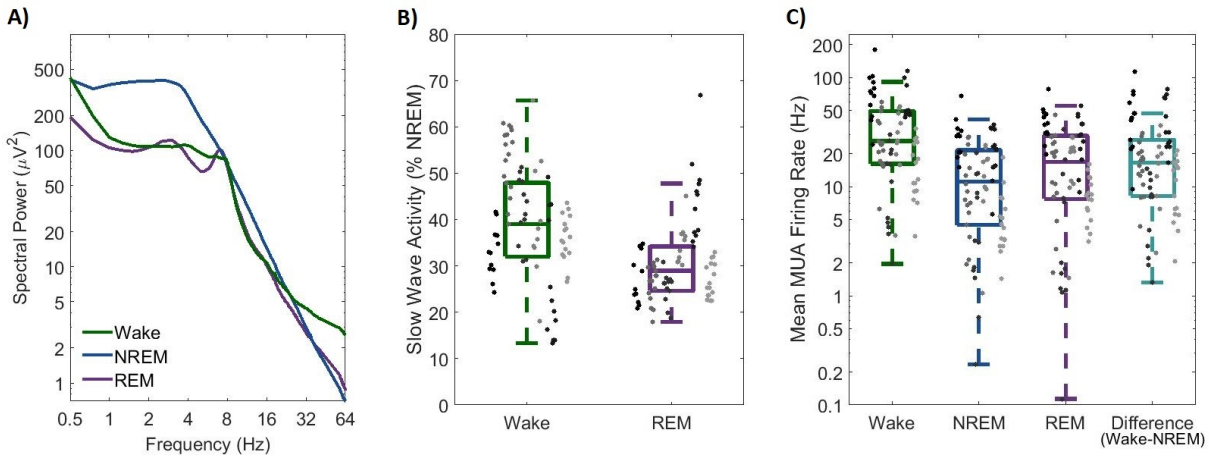


Figure 3.2: A) The average power spectra derived from wake (green), NREM sleep (blue) and REM sleep (purple) over all LFP channels from all animals. **B)** Average slow wave activity during wake and REM sleep over the whole dataset of LFP channels, expressed as a percentage of the average SWA in NREM sleep. **C)** The distribution of mean firing rates during wake, NREM and REM sleep over the whole dataset, and the difference in mean firing rates in wake compared to NREM sleep (cyan). All are positive, reflecting higher firing in wake. Points indicate channels grouped by animal (left to right), but boxplots reflect channels from all animals treated as one population.

function towards an upper asymptote, while during NREM sleep it decays exponentially towards a lower asymptote. There are many published variants of the precise equations for this model, but crucially, all these variants use the sleep-wake state history of the animal as the key predictive variable for Process S. Here, the specific equations used are:

$$\text{WAKE/REM:} \qquad \frac{dS}{dt} = \alpha(S_{max} - S(t))$$

$$\text{NREM :} \qquad \frac{dS}{dt} = -\beta(S(t) - S_{min})$$

Where S represents the level of Process S, S_{max} and S_{min} are upper and lower asymptotes, and α and β are rate parameters. The first equation is applied when the animal is scored to be awake or in REM sleep and the second equation is applied when it is scored to be in NREM sleep. Here, the typical approach is used, applying the wake dynamics equation to REM sleep (Franken et al. 1991b; Huber et al. 2000a; Vyazovskiy et al. 2007), but for simplicity separate parameters are not set for wake vs. REM sleep. For convenience, S is expressed in units equivalent to those of SWA. This classical formalism is throughout abbreviated as model Cl-SWA. Process S as described by these simple dynamics accounts for the time course of empirical SWA with high accuracy. This model was applied to SWA derived from the frontal EEG of all animals and, as expected, a high quality fit was obtained (Figure 3.3).

3.3.3 Neuronal firing rates are associated with Process S dynamics and vigilance state distributions

The slow oscillation is underpinned by local neuronal activity, and therefore can be expected to be heterogeneous across the neocortex. Regional differences in SWA dynamics have been previously described, for example between frontal and occipital EEG derivations (Werth et al. 1996a; Huber et al. 2000b), and can be accounted for within the classical

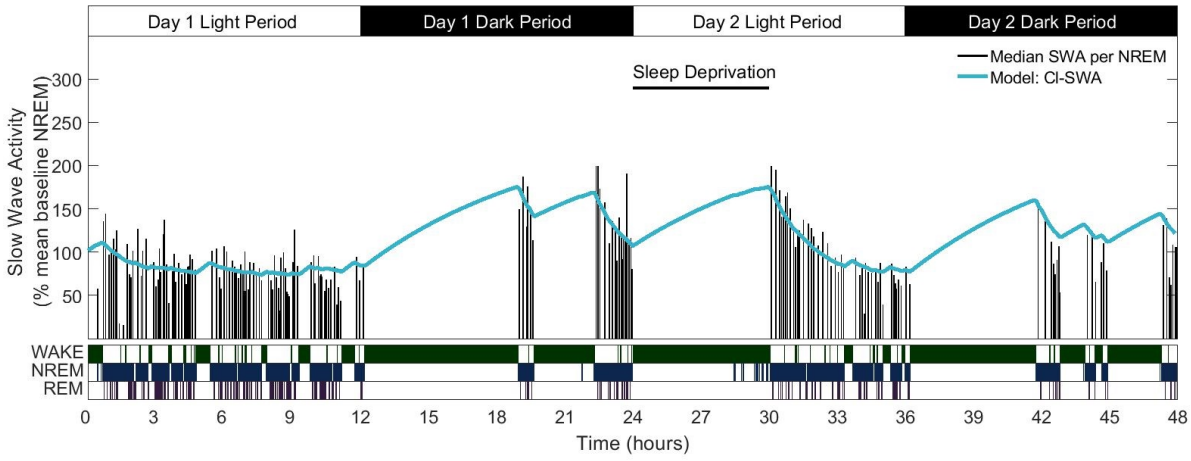


Figure 3.3: An example of the classical state-based Process S model (blue) describing the dynamics of frontal EEG SWA (median per NREM sleep episode, black bars) over 48 hours in one representative animal. Sleep deprivation occurred as indicated at light onset of the second day and lasted 6 hours. Scored vigilance states are also shown.

Process S model through the selection of locally variable values for model rate parameters (Zavada et al. 2009; Rusterholz and Achermann 2011; Guillaumin et al. 2018).

Whichever specific processes within the brain underpin these state-dependent dynamics for Process S, it was hypothesised that it is reflected in some way in neuronal spiking activity. To explore whether spike firing rates might account for some of the variation in the rate of increase of Process S, the correlation was calculated between the change in LFP SWA from one NREM sleep episode to the next (when separated by wakefulness lasting at least 5 minutes) and the mean spike firing rate during this intervening wake period, and also with the duration of that wake period. Correlation coefficients were obtained separately for each recording channel, and pooled across animals. As expected, large positive correlation coefficients were obtained between the duration of a period of wakefulness and the change in LFP SWA in all channels (mean: $r = 0.66$; Figure 3.4). Importantly however, the change in LFP SWA was on average also positively correlated with the firing rate (mean: $r = 0.27$), meaning that, generally, a higher firing rate during waking was associated with a larger increase in SWA in subsequent NREM

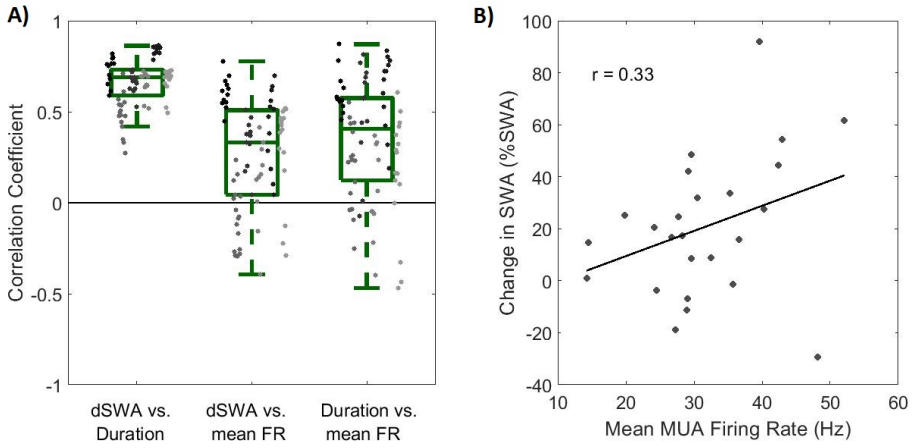


Figure 3.4: A) Distribution of correlation coefficients, calculated within each single channel, between wake episode duration (Duration), the change in slow wave activity (dSWA), and mean firing rate (mean FR). Points indicate channels grouped by animal (left to right), but boxplots reflect channels from all animals treated as one population. **B)** An example scatter plot of the correlation between the change in median SWA from one NREM episode to the next and the mean firing rate during the intervening period of wakefulness.

sleep. Interestingly, these phenomena were not independent, as a positive correlation was also found between wake episode duration and firing rate (mean: r = 0.35). These results further support the possibility that neuronal activity is associated with Process S dynamics. To test this hypothesis a quantitative modelling approach was used.

3.3.4 Process S dynamics can be described as a function of neuronal firing rates

It was first sought to determine whether a model expressing Process S dynamics solely as a function of local multi-unit neuronal firing rates might describe the levels of sleep SWA in the corresponding LFP with comparable accuracy to the classical model which is dependent on vigilance states defined at the global level. The classical Process S model was used as a starting point for the development of a novel firing-rate-dependent alternative. To do this, the equations of the classical model were adapted in two ways. Firstly, an instantaneous firing rate threshold (F_θ) was introduced as a new model parameter to

replace the wake vs. sleep criterion, assuming an increase in Process S when the threshold is exceeded and decrease when firing is below. Conceptually, this firing rate threshold resembles a set point; a target firing rate at which the dynamics are stable. Secondly, it was assumed that the rate of change of Process S is proportional to the difference between firing rate and this threshold. Introducing this change to the equations ensures that the rate of change of Process S is equal to zero exactly at the set point, and a continuous function of firing rate around this value. This version of the model is later abbreviated as Fr-SWA. The equations are:

$$F(t) < F_\theta : \qquad \frac{dS}{dt} = \alpha(S_{max} - S(t))(F(t) - F_\theta)$$

$$F(t) > F_\theta : \qquad \frac{dS}{dt} = -\beta(S(t) - S_{min})(F_\theta - F(t))$$

This novel model was applied, alongside the classical model, to describe SWA dynamics at the LFP level, by finding parameter values that would minimise the difference between empirical SWA and modelled Process S. The two models were fit to the SWA from each LFP channel separately, using the multi-unit firing rate from the same channel for the firing-rate-dependent model. The models were also fit to the SWA obtained by averaging the LFP (and firing rate) over the whole population of channels within the same mouse.

Figure 3.5 shows two examples of the fit of both models, first to SWA derived from the average LFP, and also to SWA derived from a single LFP channel (these examples are from the same animal as in Figure 3.3). The overall pattern of Process S dynamics was similar at both LFP and EEG recording levels and was well described by both the classic and novel firing-rate-based model. Throughout the dataset, this purely firing-rate-dependent model described the overall dynamics of LFP SWA during NREM sleep to a comparable accuracy as the classical model, as reflected in the median percent error deviation between modelled and empirical SWA (Figure 3.6). Both the model type and animal have a highly significant effect on the median percent error of the model fit to individual LFP channels,

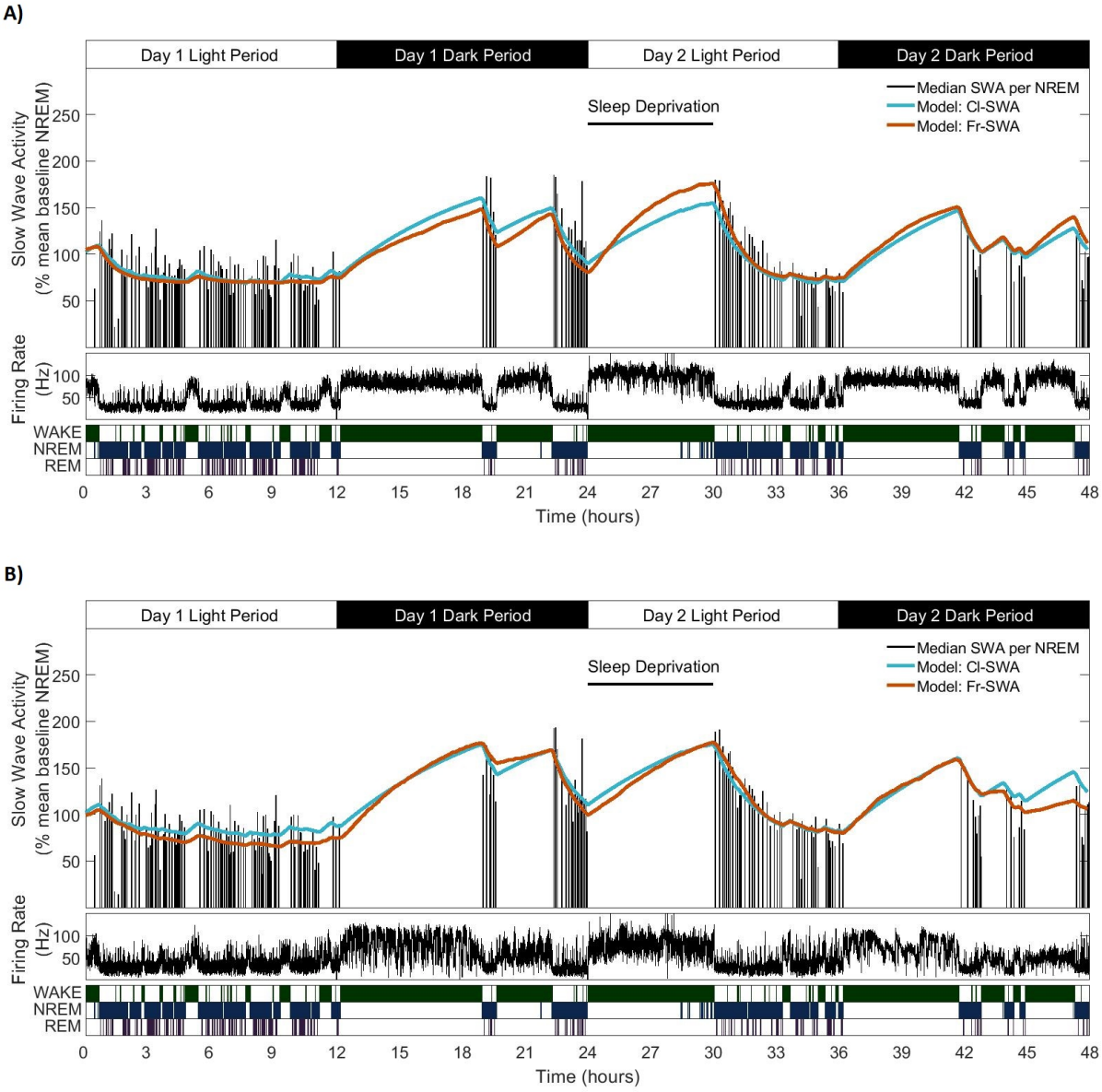


Figure 3.5: **A)** An example from one representative animal modelling the SWA averaged over all LFP channels, of both the classical model (blue) and novel firing-rate-based model (orange), calculated from the firing rate also averaged over all LFP channels. **B)** An example of both models applied to the SWA of a single LFP channel. Both figures are from the same animal.

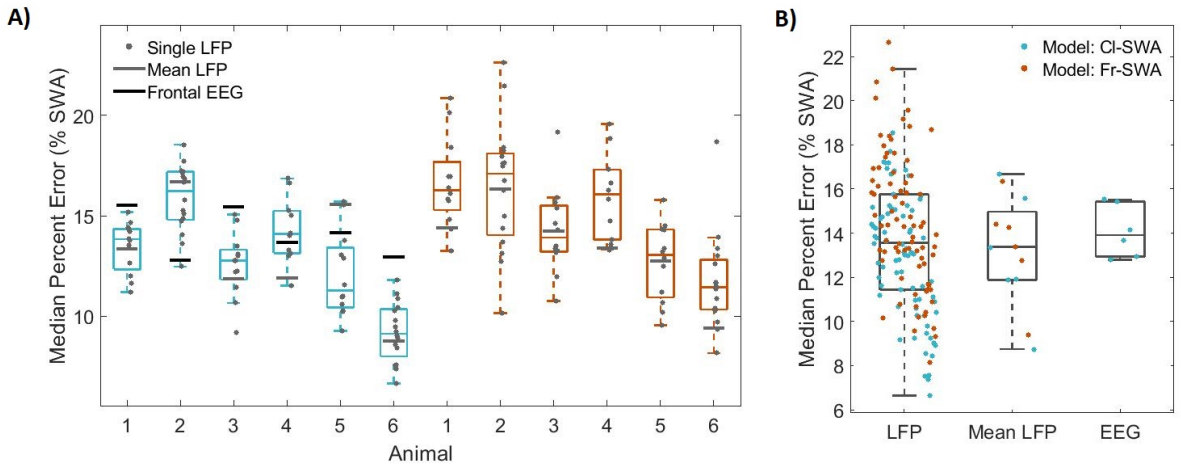


Figure 3.6: A) For each animal, the distribution over channels of the median difference between the model and empirical SWA, expressed as a percentage of empirical SWA, for both classic (blue) and firing-rate-based (orange) models. Points correspond to models of data from individual LFP channels, grey lines to models of using mean LFP, and black lines to frontal EEG. **B)** The same median percent error, grouped over animals and models, separately showing errors at the level of single LFP, mean LFP and EEG.

although there is no significant interaction (Model: $F_{(1,144)} = 25.9$, $p = 1.1 \times 10^{-6}$; Animal: $F_{(5,144)} = 30.2$, $p = 6.3 \times 10^{-21}$; Model $\times$ Animal: $F_{(5,144)} = 1.65$, $p = 0.15$; two-way ANOVA unequal groups). Errors were higher for the novel model, importantly however, the differences in fit quality due to the model type are small relative to the effect size of the particular animal and channel, on which fit quality depends much more strongly (Model: $\eta^2 = 0.079$; Animal: $\eta^2 = 0.459$; Model x Animal: $\eta^2 = 0.025$; Channel (residuals): $\eta^2 = 0.437$). The errors of the model fit on the averaged LFP and on the EEG (classical model only) are also shown in Figure 3.6A, but are more explicitly compared in Figure 3.6B. There is no significant effect of the field potential level (EEG, average LFP, single LFP channels) on the model error ($F_{(2,171)} = 0.2$, $p = 0.82$, one-way ANOVA).

The distributions of final optimised parameters are shown in Figure 3.7A-D for the classic model and Figure 3.7E-I for the firing-rate-based model. Most parameters in both models were significantly different between animals, with the exception of S_{min} in the firing-rate-dependent model (Cl-SWA α : $F_{(5,77)} = 4.03$, $p = 2.8 \times 10^{-3}$; Cl-SWA β : $F_{(5,77)} = 8.65$, $p = 1.9 \times 10^{-6}$; S_{max} : $F_{(5,77)} = 14.35$, $p = 9.8 \times 10^{-10}$; Cl-SWA

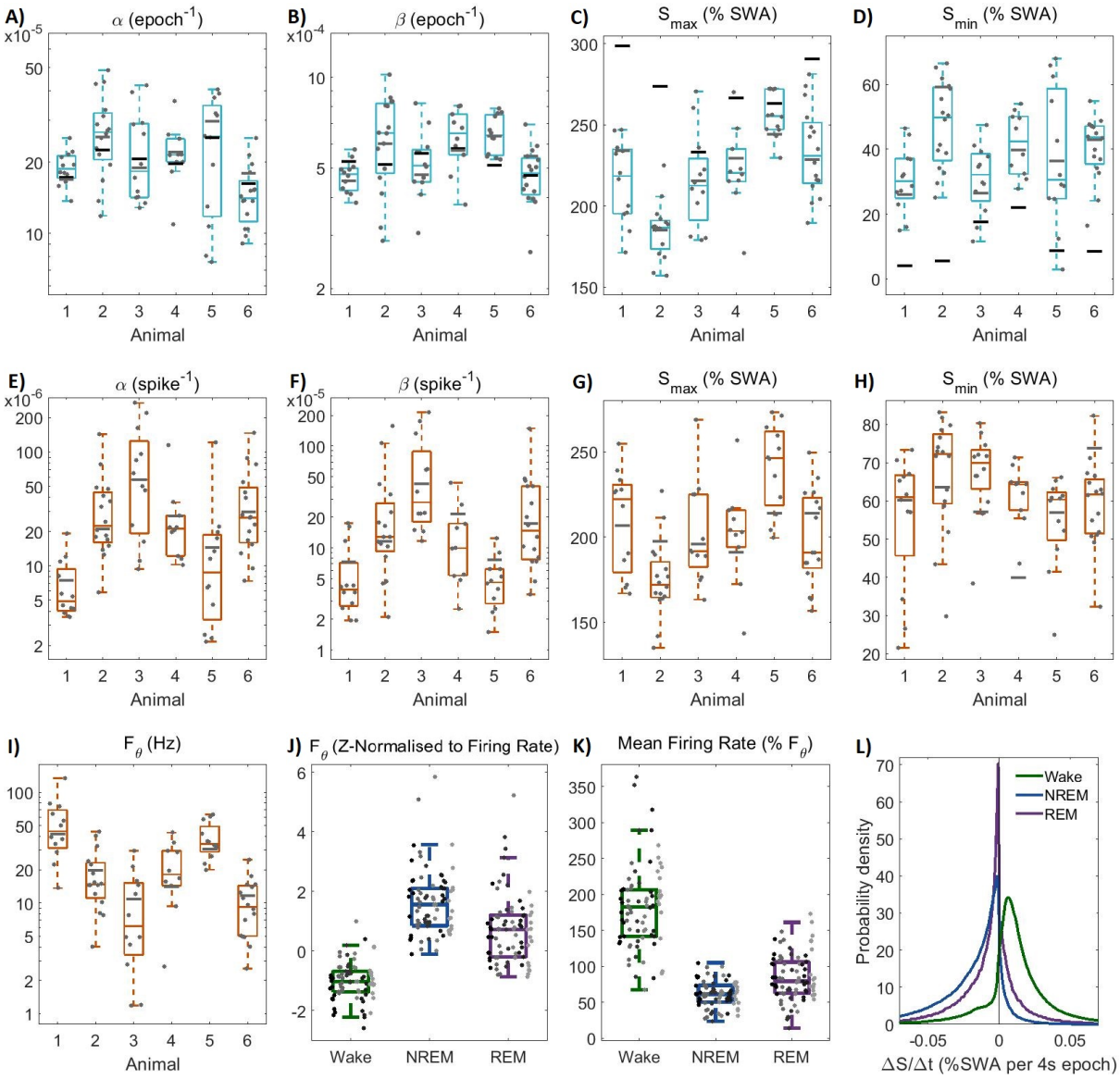


Figure 3.7: A-D) The distribution of values used for each parameter in the classic model (blue) and **E-I)** in the firing-rate-based model (orange), with boxplots plotted separately for each animal. The black lines indicate the values obtained from modelling the averaged LFP SWA and firing rate over all channels within an animal. Points correspond to models of data from individual LFP channels, grey lines to models using mean LFP, and black lines to frontal EEG. **J)** The distribution of the final optimised value for the firing rate set point parameter (F_θ) of the firing-rate-based model, z-normalised to the distribution of firing rates within wake, NREM and REM sleep. Points indicate channels grouped by animal (left to right), but boxplots reflect all channels treated as one population. **K)** The distribution of mean firing rate in wake, NREM and REM sleep, expressed as a percentage of the firing rate set point parameter (F_θ). Points indicate channels grouped and coloured by animal, but boxplots reflect all channels treated as one population. **L)** The distribution of the change in Process S ($\Delta S/\Delta t$) from one 4-second time step to the next derived from the Fr-SWA model in wake, NREM sleep and REM sleep. All mice, channels and time are pooled.

S_{min} : $F_{(5,77)} = 12.42$, $p = 1.1 \times 10^{-8}$; Fr-SWA α : $F_{(5,77)} = 8.33$, $p = 3.0 \times 10^{-6}$; Fr-SWA β : $F_{(5,77)} = 9.27$, $p = 7.5 \times 10^{-7}$; Fr-SWA F_θ : $F_{(5,77)} = 14.3$, $p = 1.0 \times 10^{-9}$; Fr-SWA S_{max} : $F_{(5,77)} = 6.64$, $p = 3.9 \times 10^{-5}$; Fr-SWA S_{min} : $F_{(5,77)} = 2.16$, $p = 0.07$; one way ANOVA). The optimised α and β rate parameters for EEG and averaged LFP data consistently fall within the range of the single channel population (Figure 3.7A-I). The relationship between the optimal firing set point and state specific firing rates is shown in Figure 3.7J. Firing rate threshold was z-normalised (subtract the mean firing rate over a given state and divide by the standard deviation) separately with respect to the distribution of firing rates in wake, NREM and REM sleep. This shows, as expected, that the set point is typically below mean firing in wake (-1.0 ± 0.6; mean ± std), well above mean firing in NREM sleep (1.6 ± 1.1), and slightly above mean firing of REM sleep (0.7 ± 1.1). These were all significantly different from zero (Wake: $p = 1.6 \times 10^{-13}$, NREM: $p = 1.9 \times 10^{-14}$, REM: $p = 3.4 \times 10^{-7}$, two-sided Wilcoxon signed rank test). Figure 3.7K further shows the state-dependent distribution of average firing rate, expressed as a percentage of the chosen firing set point parameter. Mean firing was 182 ± 57.6% of the firing rate set point during wake, 61.8 ± 17.6% during NREM sleep, and 84.2 ± 31.8% during REM sleep. Again, these distributions were all significantly different from 100% (Wake: $p = 6.7 \times 10^{-14}$, NREM: $p = 2.0 \times 10^{-14}$, REM: $p = 5.4 \times 10^{-5}$). Note that, in a few channels, the optimal firing rate threshold is actually above the mean firing rate during waking. This occurs when the waking firing rate distribution overlaps substantially with the NREM sleep firing rate distribution but has a heavier tail. REM sleep, in this dataset, is typically associated with firing below the set point, and therefore Process S decreases, albeit at a reduced rate compared to NREM sleep (Figure 3.7L). Interestingly, there are no significant correlations between the model fit error and the threshold normalisation relative to any one vigilance state (Wake: $p = 0.06$, $r = 0.21$; NREM: $p = 0.35$, $r = -0.11$; REM: $p = 0.94$, $r = -0.01$), suggesting that there is no clear relationship between the firing rate set point and firing rate distribution of any one particular state.

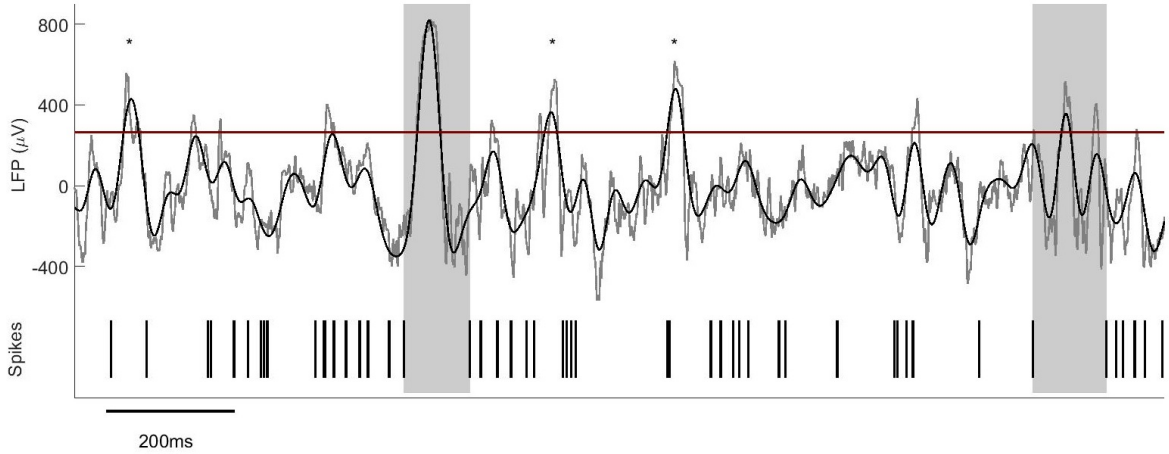


Figure 3.8: The definition of off periods and off occupancy. An example section of LFP (raw in grey, 0.5 - 6 Hz filtered in black) and simultaneous MUA spikes. During this time window, the filtered LFP crosses above the amplitude threshold (265 µV for this channel, red line) five times. The multi-unit inter-spike interval aligned to two of these peaks exceeds the duration threshold (85 ms for this channel) and so two off periods are detected (grey boxes). ISIs aligned to the other three out of five crossings (asterisks) are too short to be considered off periods.

3.3.5 Process S can be defined in terms of neuronal off periods

When considering the relationship between multi-unit firing rates and LFP slow waves, a conceptual complication arises due to the different origins of the LFP and MUA from within the same channel. While the MUA firing rate represents the activity of only a few individual neurones, factors such as volume conduction result in spatial smoothing of the LFP signal, and as such it can be influenced by the activities of neurones covering a cortical area potentially on the order of several millimetres (Kajikawa and Schroeder 2011). This means that when a slow wave is detected in the LFP, it is not guaranteed that all local neurones contributing to the MUA are necessarily silent (Todorova and Zugaro 2019). Similarly, not every long interspike interval is necessarily associated with a population off period. An estimation of the occurrence of off periods may be obtained by combining LFP and spiking data (Figure 3.8).

Slow wave detection was performed on each LFP over the whole 48 hour period,

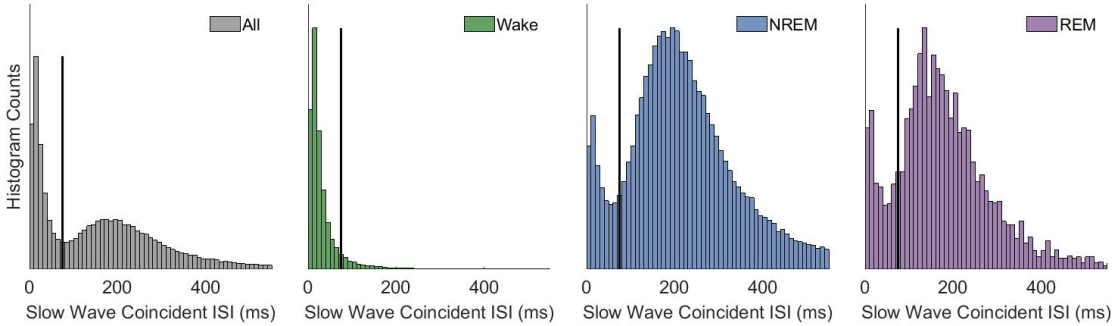


Figure 3.9: Histograms of multi-unit inter-spike intervals aligned with detected slow waves for this example channel. The four plots show, from left to right, ISIs over the whole recording (grey) and ISIs separately during wake (green), NREM (blue) and REM (purple) sleep only. The ISI duration threshold (black line) is selected using the histogram of all ISIs (leftmost) at the minimum between the two modes.

including all vigilance states (0.5 - 6 Hz filter followed by an amplitude threshold, values shown in Figure 3.10A). All multi-unit inter-spike intervals (ISIs) which coincide with the peak of detected slow waves were identified. The distribution of the duration of these ISIs was often (64 out of 75 channels) unambiguously bimodal (Figure 3.9). This could be interpreted as evidence for the existence of two spiking states occurring locally during the more widespread network slow oscillation; high frequency spiking (on period) and extended silence (off period). Note that these two distributions do not simply correspond exactly to sleep vs. wake conditions, because bimodality is often evident in the distribution of slow wave coincident ISIs from NREM sleep only, or even from REM sleep only (Figure 3.9).

The distribution of slow wave coincident ISIs (over all vigilance states) was used to define an ISI duration threshold for the detection of off periods, separately for each channel (values shown in Figure 3.10B). The average multi-unit firing rate aligned to the peak of slow waves in detected off periods reveals a clear suppression of firing, consistent with expectations (Figure 3.10C). A rebound increase in average firing is visible in this example channel immediately after the off period, a phenomenon which has been previously documented in some cortical neuronal populations (Chauvette et al. 2010). The total fraction of time each channel spends in off periods was calculated over all epochs of 4

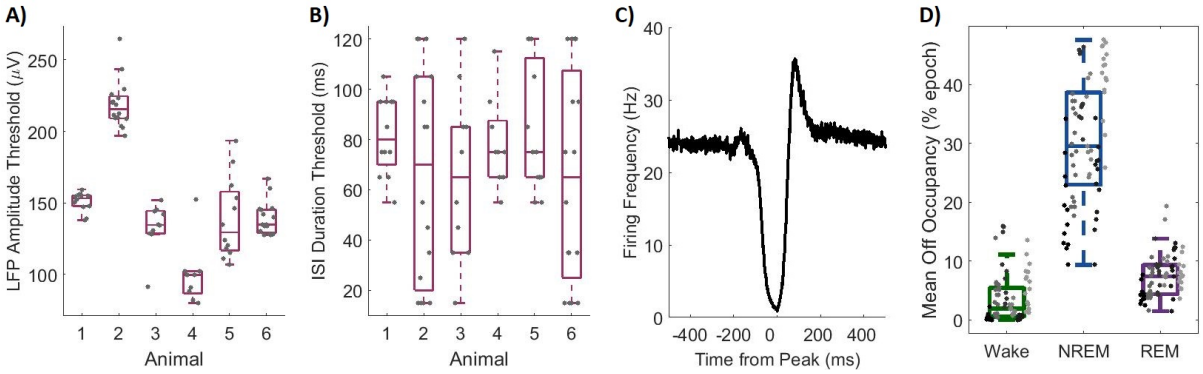


Figure 3.10: A) The distribution of LFP amplitude and **B)** ISI duration threshold values used for definition of off periods for each channel, with boxplots plotted separately for each animal. **C)** The mean multi-unit firing rate over a period of 1 second centred on the peak of detected slow waves, calculated over all slow waves within one example channel with a resolution of 1 ms. **D)** Distributions of mean off occupancy (%) for all channels averaged over wake, NREM and REM sleep. Points indicate channels grouped by animal (left to right), but boxplots reflect all channels treated as one population.

seconds, and termed the "off occupancy". Off occupancy defined in this way is high in NREM sleep and low in both wake and REM sleep (Figure 3.10D). The existence of a non-zero frequency of local cortical off periods has been previously reported during wakefulness (Vyazovskiy et al. 2011; Vyazovskiy et al. 2014; Fisher et al. 2016), and REM sleep (Funk et al. 2016). The off occupancy measure displays similar temporal dynamics to SWA, derived from either LFP or EEG, over both sleep deprivation and spontaneous sleep and wake (Figure 3.11).

3.3.6 Process S dynamics, defined using off periods, can be described as a function of vigilance states or neuronal firing rates

In order to investigate whether the off occupancy measure reflects Process S, the classical state-based model was applied to the time course of off occupancy, exactly as was done with single channel SWA. The classical model was applied with its equations unchanged, and is abbreviated as Cl-Off. Figure 3.12 shows an example of the resulting Process S time course

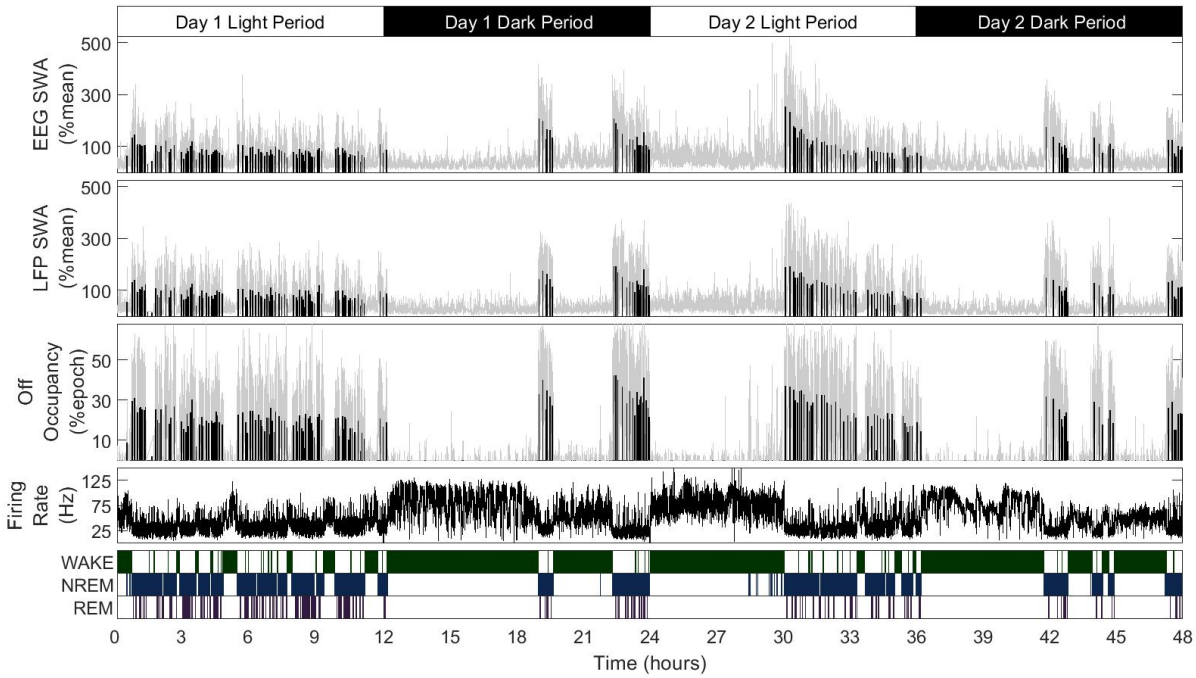


Figure 3.11: Off occupancy is shown alongside EEG and LFP SWA for an example channel over 48 hours. Traces represent these values calculated at 4-second resolution (light grey), in addition to the median value per NREM sleep episode, as used for model fitting (black bars). Firing rate and scored vigilance states are also shown.

obtained in this way with a high quality of fit. In contrast, some changes were introduced to the firing-rate-based model in order to describe off occupancy dynamics. Consider that the different dynamics above vs. below a particular firing rate set point may be due to two opponent processes simultaneously active in dynamic opposition but with differential magnitude in wake vs. NREM sleep. Specifically, consider a Process S increasing term which is proportional to instantaneous firing rate, and a Process S decreasing term which is proportional to the time spent in off periods (off occupancy). The equation used is:

$$\frac{dS}{dt} = \alpha F(t)(S_{max} - S(t)) - \beta X(t)(S(t) - S_{min})$$

In this model, one term drives S towards an upper asymptote (S_{max}) in proportion to firing rate (F), while the other drives S towards a lower asymptote (S_{min}) in proportion

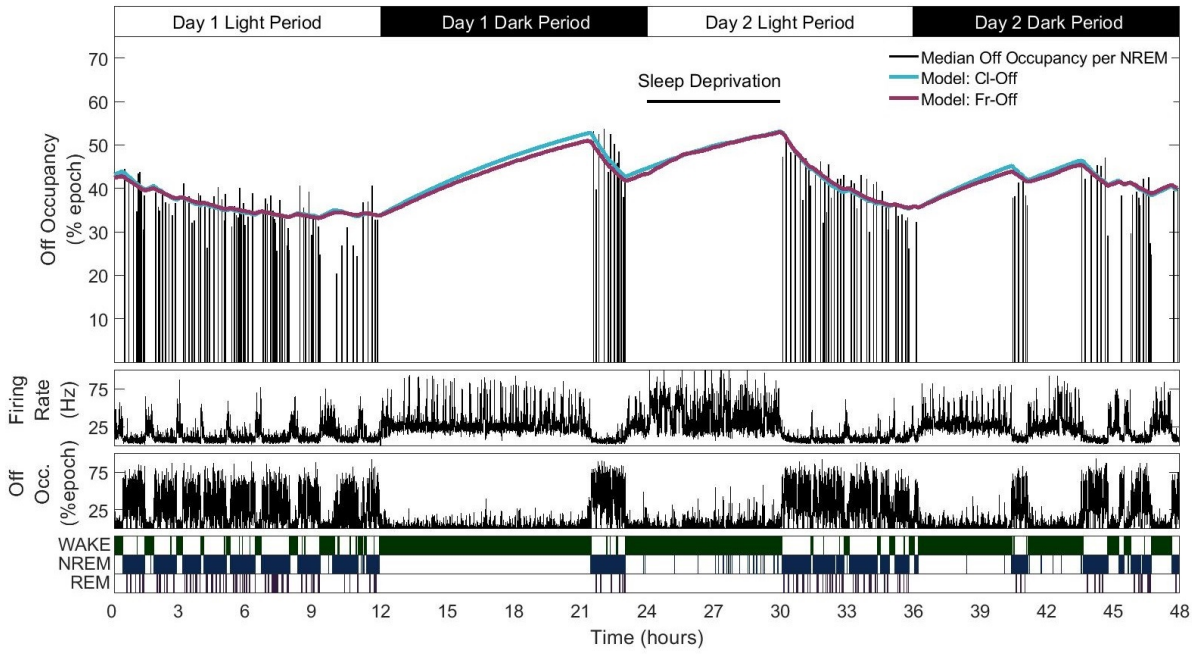


Figure 3.12: An example of the novel model based on firing rates and off occupancy (purple), and the classic state-based model (blue), with optimised parameters describing the dynamics of off occupancy (median per NREM episode, black bars) over 48 hours. Sleep deprivation occurred as indicated at light onset of the second day and lasted 6 hours. Firing rate and off occupancy per 4-second epoch and scored vigilance states are also shown.

to the off occupancy (X). Again, two rate parameters α and β are required. This model behaves similarly to previous models because firing is high in wake and low in NREM sleep, whereas off occupancy is high in NREM sleep and low in wake. This variant of the model is abbreviated as Fr-Off. Figure 3.12 also includes the fit from this model, demonstrating a high level of agreement between the two models and an accurate fit to the data.

The distribution of the median percent errors for the fits from both models over all animals and channels is shown in Figure 3.13A. As before, the model type and animal has a significant effect (Model: $F_{(1,138)} = 8.06$, $p = 5.2 \times 10^{-3}$; Animal: $F_{(5,138)} = 17.2$, $p = 3.2 \times 10^{-13}$; Model $\times$ Animal: $F_{(5,138)} = 0.52$, $p = 0.76$; two-way ANOVA with unequal groups) and the classic model achieved a slightly lower median percent error. However, this effect was again very weak compared with the variation in fit quality between animals and channels (Model: $\eta^2 = 0.034$; Animal: $\eta^2 = 0.367$; Model $\times$ Animal:

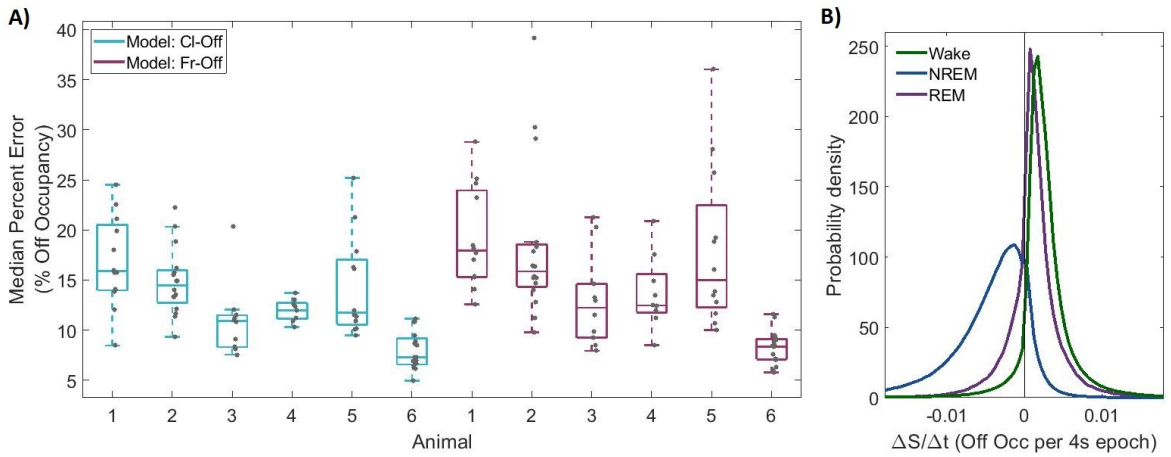


Figure 3.13: **A)** For each animal, the distribution over channels of the median difference between the model and empirical off occupancy, expressed as a percentage of the off occupancy, for both classic and firing-rate-based models. **B)** The distribution of values of the change in Process S ($\Delta S/\Delta t$) from one 4-second time step to the next derived from the Fr-SWA model in wake, NREM sleep and REM sleep. All mice, channels and time are pooled.

$\eta^2 = 0.011$; Channel (residuals): $\eta^2 = 0.588$). Figure 3.13B shows the distribution of values for the change in modelled Process S from one simulated time step to the next resulting from the firing-rate-based model (Fr-Off), in wake, NREM and REM sleep, pooling all animals, channels and time. Unlike in the previous firing-rate-based model, REM sleep is now typically associated with an increase in Process S. The distributions of final optimised parameters are shown in Figure 3.14A-D for the classic model and Figure 3.14E-H for the firing rate and off occupancy model. Most parameters in both models were different between animals to a high significance level (Cl-Off α : $F_{(5,74)} = 2.4$, $p = 0.047$; Cl-Off β : $F_{(5,74)} = 2.29$, $p = 0.055$; Cl-Off S_{max} : $F_{(5,74)} = 9.49$, $p = 6.4 \times 10^{-7}$; Cl-Off S_{min} : $F_{(5,74)} = 16.79$, $p = 8.0 \times 10^{-11}$; Fr-Off α : $F_{(5,74)} = 9.86$, $p = 3.9 \times 10^{-7}$; Fr-Off β : $F_{(5,74)} = 5.14$, $p = 4.6 \times 10^{-4}$; Fr-Off S_{max} : $F_{(5,74)} = 10.08$, $p = 2.8 \times 10^{-7}$; Fr-Off S_{min} : $F_{(5,74)} = 10.25$, $p = 2.3 \times 10^{-7}$; one way ANOVA). Notably, the weakest evidence for inter-animal differences were for α and β in the classic model.

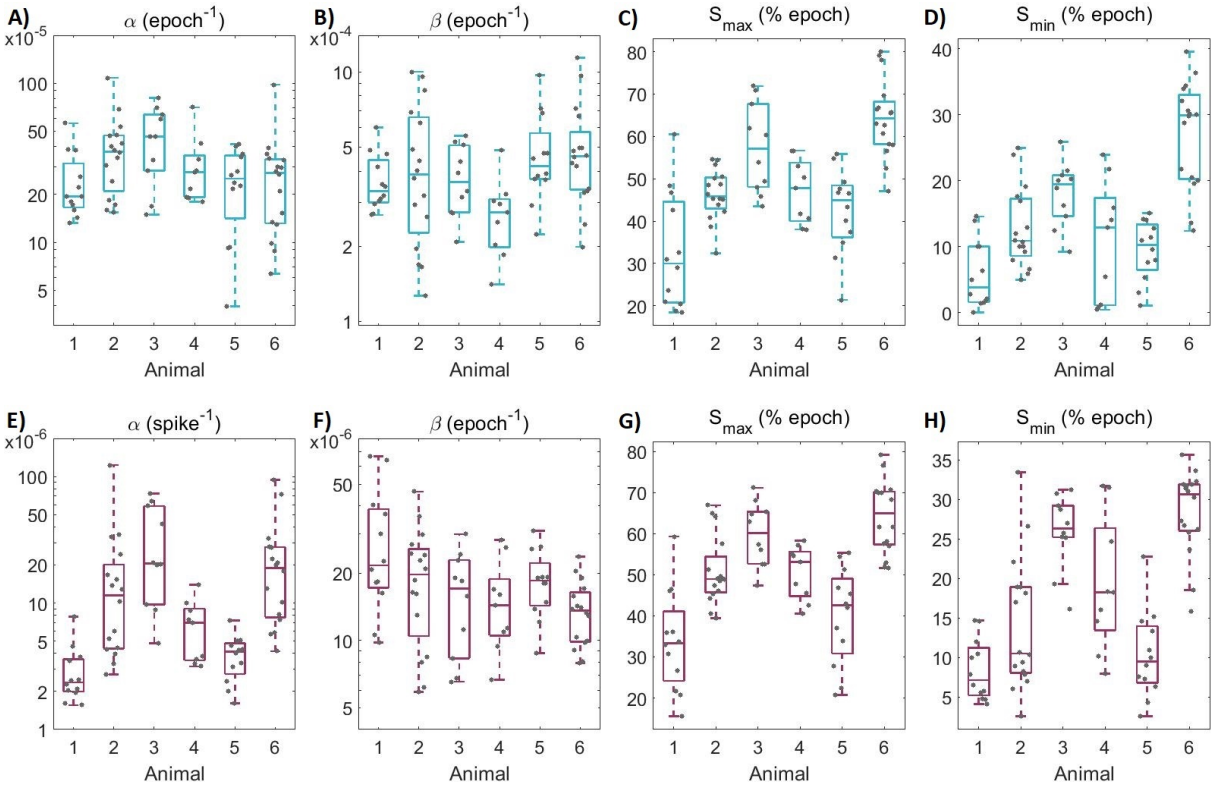


Figure 3.14: The distribution of optimised values used for each parameter in **A-D)** the classic model and **E-H)** the firing rate model, with boxplots plotted separately for each animal.

3.3.7 Global Process S resembles an average of local Processes S

The modelling approaches described here all identify variability in Process S between recording channels, indicating that a local component determines its dynamics. To understand how local and activity-dependent Processes S might relate to the global Process S which reflects sleep-wake history, their time courses derived from the various models were compared. This was done by normalising each Process S in a range from zero to one, determined by the fitted values of S_{max} and S_{min} (Figure 3.15). Importantly, the mean over individual Processes S derived from single channels closely matches the shape of Process S derived from the EEG using the classical model. This held for both SWA (Figure 3.15A) and off occupancy (Figure 3.15B) models. Indeed, over all animals the global level Process S is typically in between the average of local Processes S derived

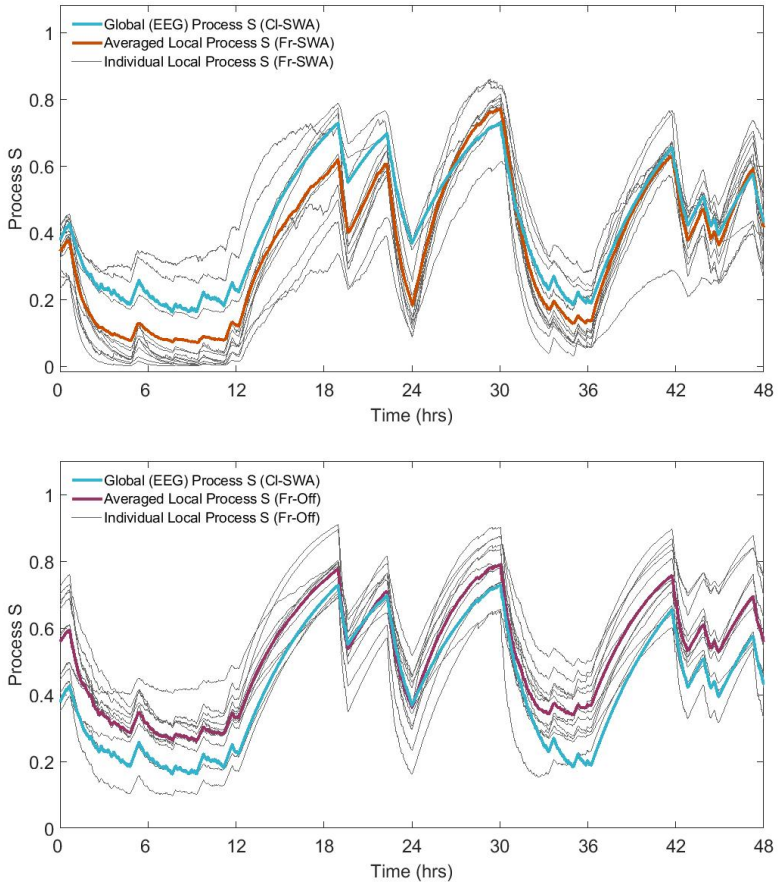


Figure 3.15: Process S derived from applying the Cl-SWA model to frontal EEG (blue) alongside Process S derived from applying **A)** Fr-SWA and **B)** Fr-Off to all individual LFP channels within one representative animal (grey) and their mean (orange/purple). All Process S time series are normalised between individual S_{min} and S_{max} values for fair comparison.

from the two activity-dependent models (Figure 3.16). This result suggests that global Process S calculated at a higher spatial scale might reflect an averaging across a manifold of local Processes S that exist on a finer spatial level.

3.4 Discussion

The aim of this study was to explore the hypothesis that patterns of cortical neuronal spiking may be sufficient to predict the dynamics of Process S, and that Process S might consequently show local variation in its dynamics which could be accounted for by local

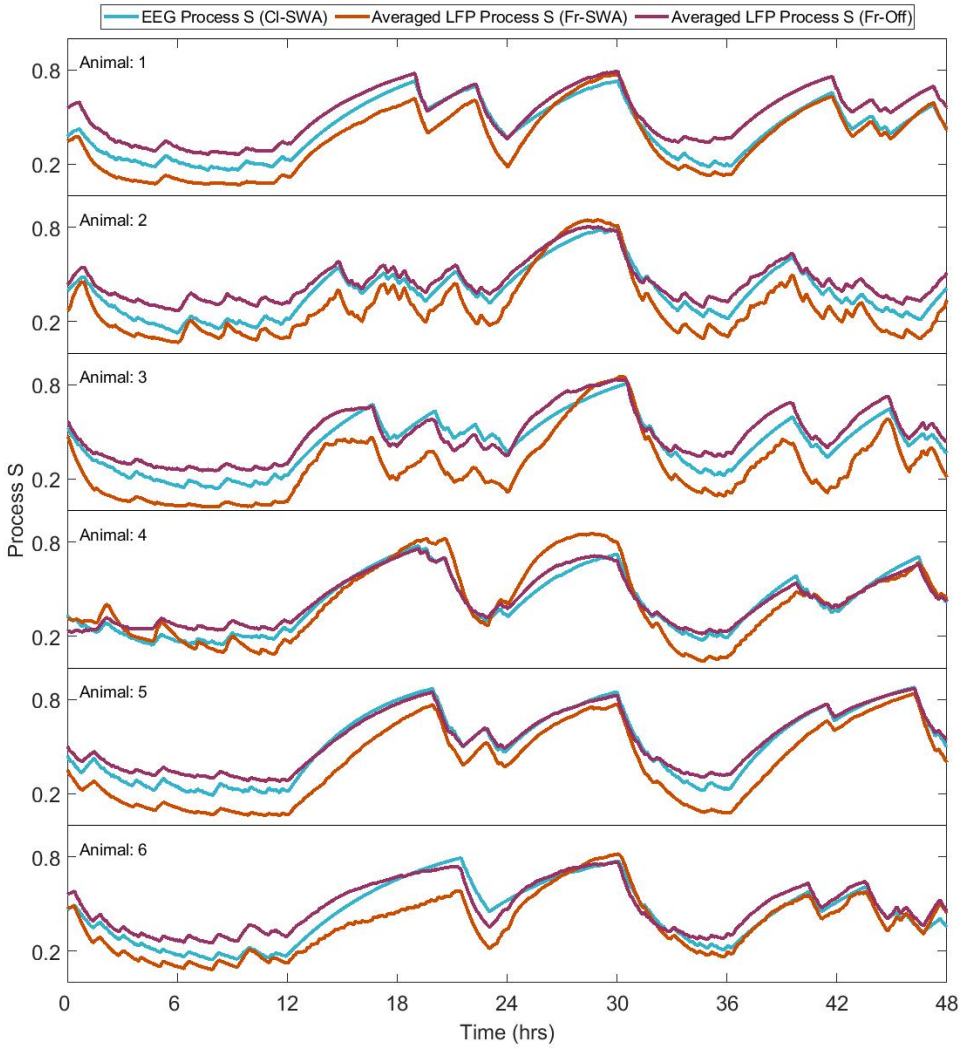


Figure 3.16: Process S derived from applying the Cl-SWA model to frontal EEG (blue) and the mean Process S derived from applying Fr-SWA (orange) and Fr-Off (purple) to all individual channels. The results are shown for each of the six animals analysed.

differences in spiking. To address this hypothesis, the classical vigilance state based model of Process S was reformulated, assuming that local Process S reflects the integrated history of local multi-unit firing rates, relative to a locally-defined firing rate set point. Indeed, this novel model was found to describe the temporal dynamics of local field potential slow wave activity during spontaneous wake, natural sleep and enforced prolonged wake, in a dataset of recordings from the primary motor cortex of 6 mice. A novel metric for Process S was then developed, aiming to further dissociate Process S from global level measures based on field potentials, and instead based on local spiking activity. The metric, termed off occupancy, measures the fraction of time a neural population spends in off periods, defined by the coincidence of LFP slow waves and multi-unit spiking silence. The modelling approach was combined with the off occupancy metric and tested on the same dataset to present a quantitative framework for understanding dynamics of Process S at a highly local level in terms of neural spiking and off periods. Finally, an exploration of the variability of the parameters and time courses of locally derived Processes S suggested that Process S at more global levels, such as the EEG, reflects an averaging of Processes S at more local levels. Therefore, in addition to a temporal integration of spiking activities, Process S appears to involve a spatial integration over many neighbouring local networks of neurones.

Central to this modelling perspective is the assumption that the generation of spikes by a neural network is in some way correlated with an increase in sleep pressure, and that this manifests in the subsequent expression of slow waves and off periods, reflecting Process S. Indeed, the energetic cost of spiking is high (Attwell and Laughlin 2001), the regulation of a neurone's firing rate set point is linked to cellular energetics (Styr et al. 2019; Vergara et al. 2019), and neurones are susceptible to cellular stresses that can result from sustained metabolic load, such as oxidative stress (Wang and Michaelis 2010; Cobley et al. 2018; Kempf et al. 2019). Furthermore, spiking activity may be mechanistically associated with synaptic plasticity, and it has been argued that firing rates are an important determinant of overall changes in synaptic strength, with higher spiking

leading to greater changes (Graupner et al. 2016; Lappalainen et al. 2019). Compensatory processes exist within neurones to oppose cellular stress and related homeostatic challenges (Kültz 2005) and off periods could provide the opportunity for neurones to prioritise such processes, therefore mediating the restorative benefits of sleep (Vyazovskiy and Harris 2013). Similarly, off periods are associated with distinct synaptic plasticity rules (González-Rueda et al. 2018), and so their prevalence and patterning is likely also related to whatever regulation of synaptic strength occurs during sleep (Tononi and Cirelli 2014; Timofeev and Chauvette 2017; Seibt and Frank 2019).

In these models, spike firing rate is chosen to represent the level of neural activity because it is convenient to record, locally variable, and directly linked to neuronal functionality. However, no strong claim is made that firing rates are necessarily causally responsible for the accumulation of homeostatic sleep pressure. Indeed, it would likely be possible to obtain a reasonable quantitative account of sleep homeostasis using any physiological variable (or set of variables) that are consistently higher in either the wake or sleep state. For example, a model assuming that Process S increases in proportion to local cortical temperature, which, in laboratory rodents, drops by approximately 2°C when falling asleep (Franken et al. 1991a; Tobler et al. 1997) and which has been mechanistically implicated in sleep regulation (Hoekstra et al., 2019), might also provide a plausible description of Process S dynamics. However, these results demonstrate that firing rates are a useful measurable correlate of the processes that directly underpin Process S, and therefore firing rate variance resulting from differences in experience and behaviour may well account for the variance in Process S accumulation in normal individuals, between waking periods and between cortical regions.

It should be noted that the activity-dependent models used here typically slightly under-perform relative to the classic model, in terms of minimising the error between simulation and empirical data. There are a number of reasons why a limit on the accuracy of the model is to be expected, related to technical restrictions rather than conceptual ones.

In this approach, each MUA channel records only a few randomly sampled nearby neurones, which may have very different spiking properties, and so grouping these as a single measure of local network activity is somewhat arbitrary. It may be valuable to explore genetic and pharmacological manipulations of firing rate in order to further test this model's validity. Unfortunately, the effects of any manipulation on the accumulation, expression and dissipation of sleep pressure, separately to the effects on firing, is unknown, and so this may be hard to interpret. For example, one study found that systemic atropine administered during behavioural wakefulness produces slow wave activity, reducing neuronal activity (as measured by c-Fos expression) yet increasing the duration of subsequent NREM sleep (Qiu et al. 2015). While this was interpreted as evidence that spiking activity is not related to sleep pressure accumulation, the direct effects of atropine on cellular homeostasis and the functional significance of the resulting induced slow oscillation are unclear. Similarly, another study found that local optogenetic activation of cortex during sleep, despite raising firing rates to waking levels, was not accompanied with increased SWA or off periods during subsequent NREM sleep (Rodriguez et al. 2016). Again, it is difficult to disentangle the direct effects of this local stimulation, which is not physiologically realistic, on the mechanisms surrounding the accumulation, expression and dissipation of sleep pressure. On the other hand, these results might be interpreted as evidence that the expression of the level of Process S involves an integration of homeostatic sleep need across neural populations and therefore local firing rate manipulations are not able to substantially influence Process S dynamics at a global level.

A potential conceptual issue with the novel models exists due to the reliance on the multi-unit activity to characterise local Process S, rather than single neurones. In particular, different neurones may behave differently with respect to their individual firing rate set points, which vary over several orders of magnitude (Watson et al. 2016). This choice is justified, however, because, neuronal activities are not independent, but necessarily highly correlated within the local network in which they are embedded. Some

neurones do exhibit activity patterns which are less coupled to population levels (Okun et al. 2015) and their exclusion might improve model fit quality. Given the high overall quality of model performance, this is a minor concern.

One noteworthy potential complication with the proposed method for defining off periods arises due to a recent report that a specific population of cortical inhibitory neurones preferentially fire during network off periods (Zucca et al. 2019). The presence or absence of such neurones in the multi-unit activity in these recordings cannot be definitely determined. However, if such neurones were contributing to the MUA, there are two possible consequences; either they fire so frequently that network off periods are completely undetectable, or they fire only occasionally so that off periods are consistently underestimated. The abundant bimodality in slow wave aligned inter-spike interval histograms is evidence that the first case is not likely; there are two different detectable states, corresponding to network on and off periods in almost all channels. In the second case, the presence of such a firing phenotype might increase the number of false negatives in off period detection, and therefore cause off occupancy to be underestimated. However, this effect would be expected to be uniform across the 48 hour period. Since model parameters are proportional to off occupancy, and Process S reflects off occupancy relative to some maximum and minimal levels, this is not a problem for estimating Process S dynamics. If off periods are severely underestimated, this would be compensated by larger values for the β decay rate parameter. The distribution of values for β did not show abnormally high variance, which is further evidence that this effect is not present. Furthermore, previous methods for detecting off periods do so by pooling spiking over many channels, a method which would only exacerbate the problem of off-period-active inhibitory neurones. The fact that off occupancy is strongly correlated with SWA, and that the off occupancy based model was successful, support that detected off periods correspond to something physiologically meaningful.

It is reasonable to assume that sleep homeostasis unfolds on multiple time scales and

Process S as defined by these models describes a relatively fast one, approaching its upper asymptote after continuous wakefulness on a time scale of hours. The inclusion of processes acting over longer or shorter time scales might explain discrepancies in all these models, however, the challenge remains to identify what these could be. Furthermore, the role of REM sleep in Process S dynamics has not been explicitly addressed or considered in the construction of these models. Depending on the model variant, REM sleep is associated either with a small increase or small decrease in Process S, because firing rates are low in REM sleep (closer to NREM sleep than waking) and yet off period occupancy is also low (closer to wake levels than NREM sleep). It is possible that REM sleep might represent a homeostatically neutral state, in which the level of Process S changes minimally, or not at all (Vyazovskiy and Delogu 2014).

4

Cortical Critical Dynamics Vary Across the Sleep-Wake Cycle

Contents

4.1 Introduction 86

4.2 Methods 88

4.3 Results 95

4.4 Discussion 109

4.1 Introduction

Sleep is essential for regulating and maintaining healthy neuronal functions. Sleep deprivation, even acutely, is associated with many deleterious consequences for cognition, including impairments in attention, memory, cognitive flexibility and information processing (Killgore, 2010). One possibility is that Process S, which accumulates during wake and dissipates during sleep, directly reflects fundamental neuronal properties or processes which must be regulated in order to maintain brain functioning at optimum levels. In this case, wake would be associated with gradual changes to particular functional properties, of individual neurones or of neuronal networks, and the resulting deviation from a homeostatic set point would explain both sleep-deprivation-dependent functional impairment and the origin of the homeostatic sleep signal.

Indeed, during wake, synaptic strengths globally increase (Tononi and Cirelli 2003; Vyazovskiy et al. 2008; de Vivo et al. 2017) and cortical firing rates diverge at the population level (Watson et al., 2016; Levenstein et al., 2017). Furthermore, prolonged wake is associated with increasing low frequency power in the field potential, corresponding to the emergence of intrusive localised periods of neuronal silence, which have been directly linked to impaired performance (Pigarev et al. 1997; Vyazovskiy et al. 2009b; Vyazovskiy et al. 2011; Van Dongen et al. 2011). However, it remains unknown what the consequences are of these phenomena for ongoing neuronal functional capabilities and to what extent they are mechanistically involved in sleep-loss-dependent cognitive impairments. Moreover, do synaptic weights, firing rates or related neuronal properties fundamentally underlie the sleep homeostatic process, or are they merely correlated with it?

One influential theory, which might possibly relate local changes in neuronal excitability to global level computational capabilities, is that cortical networks are poised at a critical state, and that activity propagation through cortical networks can be described by critical avalanche dynamics. Criticality is a concept which originated in statistical physics, and

describes dynamical systems in which fluctuations in activity are scale free, implying that distributions of activity patterns within the system obey power laws. At criticality, excitation and inhibition are balanced such that activity is precisely equally likely to spread as it is to decay. Criticality in neural systems has been shown to offer many functional advantages, such as increased dynamic range, information transmission and information capacity (Bertschinger and Natschlager 2004; Shew and Plenz 2013).

Criticality has been demonstrated in neuronal systems most commonly using neuronal avalanche analysis, which involves finding power law distributions in the size and duration of synchronous activations across distributed recording sites. Critical avalanches were first found, *in vitro* in cultured cortical tissue (Beggs and Plenz 2003), but are also reported in awake *in vivo* animals (Petermann et al. 2009) and even in humans across vigilance states (Priesemann et al. 2013; Shriki et al. 2013). Such avalanches were based on definitions of activity as large amplitude negative deflections in field potentials. In contrast, investigations of neuronal avalanches in spiking data have occasionally yielded distributions that decay faster than a power law. This result has previously been explained as a result of subsampling, which results in true critical systems producing distributions that interpolate between power law and exponential family (Priesemann et al. 2009; Ribeiro et al. 2010). However, recent modelling analysis suggests that spike avalanche distributions during wakefulness are most consistent with systems that are indeed slightly subcritical (Priesemann et al. 2014; Wilting and Priesemann 2019).

Theoretically, synaptic plasticity, such as which occurs over extended wakefulness, might challenge the stability of the critical state, and net potentiation would be expected to drive dynamics towards the supercritical regime (Pearlmutter and Houghton 2009; Meisel et al. 2013). Alternatively, the occurrence of local off periods during extended wake might prevent or disrupt the spread of activation, thereby producing dynamics which are more subcritical. It is also possible that brain criticality arises intrinsically due to homeostatic processes or global brain architecture (de Arcangelis et al. 2006; Moretti

and Munoz 2013; Rubinov et al. 2011; Kessenich et al. 2016) and consequently emerges invariably regardless of alterations in neuronal dynamics.

Importantly, despite a growing acceptance for some role of critical dynamics in cortical function, it remains unclear to what extent critical dynamics are homeostatically regulated and whether such regulation is related to the sleep homeostatic process. Criticality might ultimately offer a useful conceptual framework to characterise changes in neuronal dynamics related to Process S and sleep loss and therefore to understand how and why synapses and firing rates might be regulated by sleep. Currently, very little work has explored the temporal stability, or otherwise, of signatures of criticality in the brain across the sleep-wake cycle. To this end, various measures of criticality based on neuronal avalanche analysis were explored in a dataset of electrophysiological recordings from the motor cortex of 6 mice over 48 hours, including sleep deprivation. The aims were to:

- Find methods to measure criticality in these data and determine whether critical dynamics are differentially evident in wake, NREM and REM sleep.
- Test whether changes in criticality measures robustly occur over sleep deprivation or recovery sleep in a manner which might reflect Process S.
- Determine to what extent consistent results could be obtained by measuring criticality in the field potential vs. in spiking data.

4.2 Methods

4.2.1 Data

In this study, analyses were performed on the same dataset as described in the previous chapter, which comprised local field potential and multi-unit activity (16 channels per animal) recorded from the motor cortex in 6 mice over 48 hours, including sleep deprivation.

To compare neuronal avalanche statistics between wake, NREM and REM sleep, a 24-hour period (baseline day before sleep deprivation) was analysed for each animal. All continuous and artefact-free time periods within the same vigilance state, which were at least 1 minute duration, were identified. Avalanches were always extracted from such time periods separately, in order to avoid including artefactual activity in ongoing avalanches. All detected avalanches were then pooled within time periods of the same vigilances state to produce the overall distributions of size and duration.

To investigate whether avalanche statistics or putative deviation from criticality varied across the sleep-wake cycle in association with Process S, continuous episodes of the same vigilance state over the whole 48-hour period were identified and separately analysed. Any vigilance state episode less than 2 minutes in duration was excluded. Episodes were not split by the presence of artefacts, since this produced time series which were too short in duration for the effective estimation of avalanche distributions. Instead, any episode with more than 10% of its duration marked as artefact was additionally removed from subsequent analysis. Furthermore, all vigilance state episodes longer than 20 minutes (which all corresponded wakefulness) were split into a number of time windows for analysis of equal duration, such that these lasted 10 - 15 minutes (the number of divisions was equal to the episode duration divided by 10 minutes, rounded down to an integer). This enabled changes over extended wakefulness to be measured. Variations in this threshold for the division of long episodes were tested, and 10 minutes was chosen as a good compromise to between temporal resolution and statistical noise in avalanche distributions.

4.2.2 Neuronal Avalanches

The procedure for identifying neuronal avalanches in a given data time series has two main steps, 1) the detection of activity events and 2) their clustering into temporally continuous avalanches (Figure 4.1).

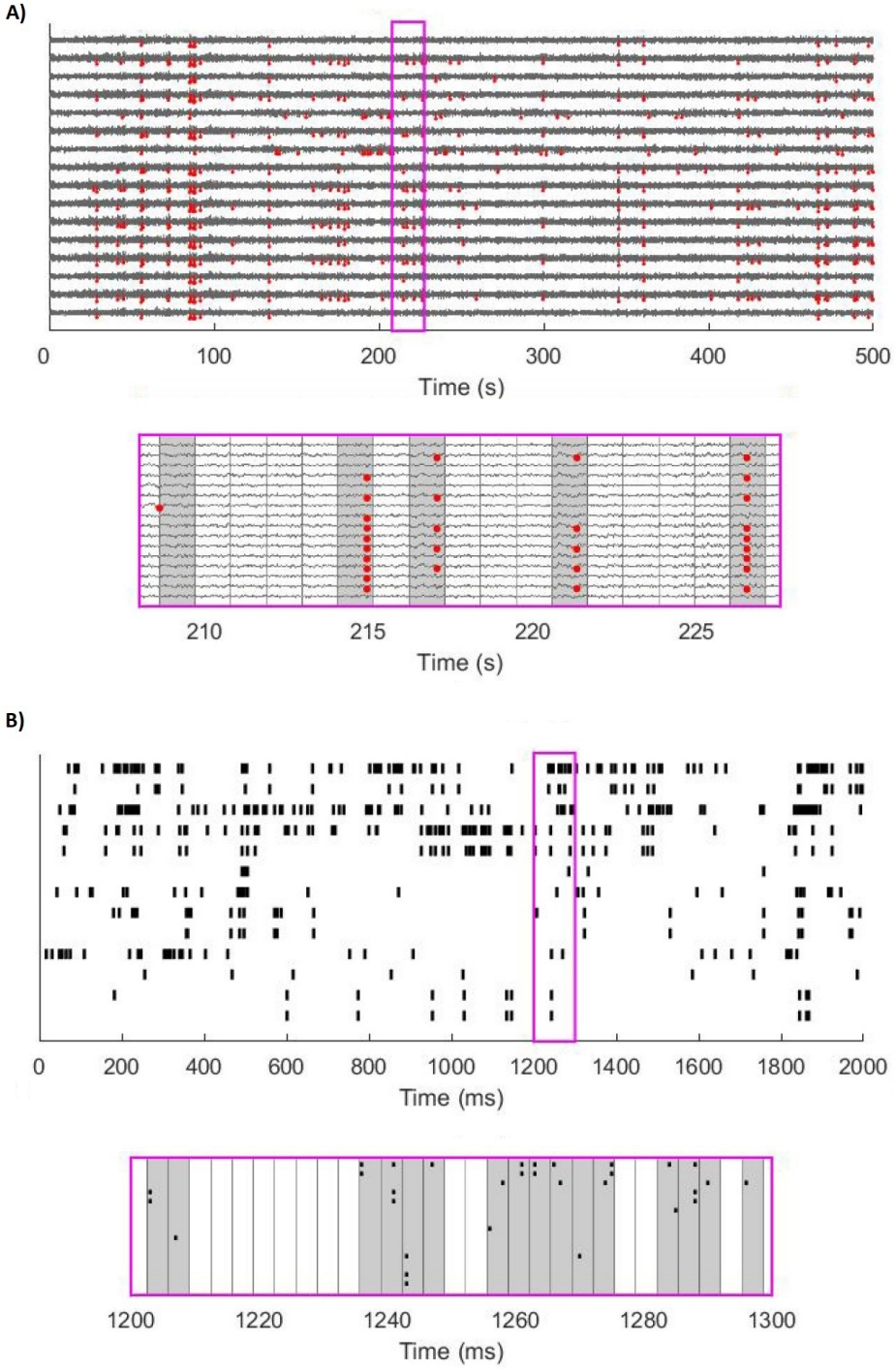


Figure 4.1: A) 500 seconds of exemplary LFP data from 16 simultaneously recorded channels. Red dots mark events identified as large amplitude negative deflections. Data in the pink window is expanded below, showing a 20 second window discretised with a bin width of 1.1 seconds. Five avalanches are found here with sizes, $s = 1$, 10, 5, 5 & 9. **B)** Two seconds of exemplary spike train data. Data in the pink window is expanded below, showing a 100 ms window discretised with a bin width of 3.3 ms. Five avalanches are found here with sizes, $s = 3$, 9, 12, 6 & 1.

For LFP data, activation corresponds to a negative deflection of the signal with a maximum absolute amplitude exceeding a pre-defined threshold, and the time of the event is taken as the time of the peak (Beggs and Plenz 2003; Petermann et al. 2009). In order to accomplish this, LFP segments were band pass filtered (1 - 30 Hz; 4^{th} order Butterworth zero-phase filtering using the Matlab functions `butter` and `filtfilt)`, and then Z-transformed by subtracting the mean and dividing by the standard deviation. A range of suitable thresholds were trialled, ranging from -1.5 to -4, and a value of -2 was used for the majority of analyses. Methodological variants for processing LFPs were tested in order to reduce the impact of shared volume conducted signal biasing the detection of avalanches and are described when used (see results). Notably, a final method was developed in which one individual LFP channel was subtracted from all others, and avalanches were detected as before over the 15 LFP difference signals. This procedure was repeated, detecting avalanches separately using the difference between one of the 16 channels and the remaining 15.

For multi-unit activity data, each activation event simply corresponds to a single spike (Hahn et al. 2010; Ribeiro et al. 2010). An alternative method was tested attempting to replicate a previous report finding power law behaviour in spike-derived avalanches (Ma et al. 2019). Spikes were binned to obtain a population firing rate and a threshold was defined, with avalanches corresponding to continuous excursions of the population firing rate above this threshold. Different parameters were explored, including bins ranging from 10 – 500 ms in duration and thresholds corresponding to the 15^{th} – 75^{th} percentile of the population firing rate.

Once activation events were identified within each channel, their times were pooled over all simultaneously recorded channels to produce a single event sequence (except where specified that avalanches were detected from single channels). In neuronal data, there exists no separation of timescales between the duration of avalanches and the inter-avalanche delay. Consequently, it is non-trivial to identify individual avalanches in a melange of

activity and the event sequence must be discretised by the application of time bins. The total frequency of events relative to the size of the time bin has an important influence on the definition of avalanches, since using a longer/shorter time bin will tend to group/split events more readily, resulting in larger/smaller avalanches. The appearance of power laws depends on the correct setting of the bin width. Fortunately, a solution exists to rate-normalise avalanche detection and thereby enable fair comparison of data collected at different times and in different brain states, by using a bin size equal to the mean inter-event interval in that time window (Beggs and Plenz 2003). This means that, by definition, there is on average one event per bin. This procedure was used for the analysis of LFP data resulting in variable time bins ranging between approximately 50 – 100 ms, giving similar values for the original method (Wake: mean = 64.9 ms; NREM: mean = 91.7 ms; REM: mean = 64.0 ms) and the pairwise LFP difference method (Wake: mean = 62.3 ms; NREM: mean = 82.3 ms; REM: mean = 73.0 ms). However, this was not practical for spiking data as the mean population inter-spike interval was close to 1 ms, the resolution at which spikes were recorded. It was therefore necessary to use a constant time bin, typically 1 ms unless otherwise stated, in all spike avalanche analyses.

In order to control for confounds in event rate, a surrogate event sequence was created for every sequence of activation times (spikes or large amplitude LFP deflections). This was achieved by keeping the inter-event intervals within a single channel and randomly reordering them. In this way, the event number and within-channel statistics are unchanged, but between-channel event synchrony is disrupted. When testing different methodological variants, comparison with the shuffled avalanches distribution was useful to identify which methods did and did not identify meaningful structure in activity.

4.2.3 Avalanche Distributions and Power Law Fits

After binning events, each continuous sequence of time bins containing an event marks the occurrence of a neuronal avalanche (Figure 4.1). For each avalanche its size (number of events, whether spikes or large amplitude negative LFP deflections) and duration (number of time bins) was recorded. Probability distributions were estimated by normalising the observed counts of avalanches. Whenever multiple avalanche detections were performed (on different combinations of individual channels or pairwise channel differences) the mean avalanche distributions were taken.

The shape of avalanche distributions can reveal putative critical dynamics, as sizes (s) and durations (d) are expected to follow a power law distribution with characteristic exponents $P(s) \propto s^{\alpha}$ and $P(d) \propto d^{\tau}$, where exponents α and τ are negative. However many practical issues complicate the detection of power law behaviour in neuronal data. Distributions derived from LFPs display clear cut-offs in power laws at sizes equal to the number of channels. This occurs due to the practical inability to detect larger events without multiple reactivations of individual units, a phenomenon hindered by neural refractory periods and, in the LFP, the wavelength of ongoing dominant oscillations. The existence of power law cut-offs are documented also in finite models of critical systems (Priesemann et al. 2009). For this reason, size distributions are only informative over a range of values less than or equal to the number of channels simultaneously recorded (16, or 15 when one signal is subtracted) and distributions over larger values were omitted from all plots.

When systems which generate avalanches deviate into subcritical or supercritical regimes, these changes can be detected most sensitively over the distribution tail. The largest avalanches decrease in frequency, relative to power law predicted levels, in a subcritical system and increase in one which is supercritical. For this reason, critical exponents were estimated from the low value end of the distribution, over sizes $s \leq 5$. This value was chosen manually by observation of a large number distributions and corresponds

to the minimum commonly observed inflection point. Exponent estimation was performed by linear regression in log-log space (using the Matlab function `polyfit`).

In contrast with LFP-derived avalanches, size distributions derived from spiking activity do not display a cut-off or similar discontinuity. This may be because each channel's multi-unit activity already represents multiple individual units, and so refractoriness is less dominant. However, spike avalanche distributions typically deviate from a power law prominently over small values. This may be due to subsampling (Priesemann et al. 2009) or the inclusion of false positive spikes (which are uncorrelated across channels and therefore disproportionately contribute small avalanches). As a result, distributions typically interpolate between power law and exponential family (Ribeiro et al. 2010). Despite this, the power law component remains detectable in the distribution tail in some cases (Hahn et al. 2010; Ma et al. 2019).

Indeed, in many animals the tail of the distribution appeared to obey a power law, particularly in NREM sleep, in agreement with LFP-derived avalanches (see Results). For this reason, the best fit power law was derived from an intermediate range of distribution values, as a compromise between avoiding the influence of non-power law behaviour at low values and remaining able to sensitively detect deviation from a power law in the highest values. By inspecting a large number of spike avalanche size distributions in different animals and vigilances states, this range was set between $5 \leq s \leq 20$.

Measures of the deviation of the empirical distribution from this power law fit reflect drift into putative sub-or-super-criticality. The chosen measure, κ, introduced in Shew et al., 2009, quantifies the mean distance between the empirically-derived cumulative probability distribution of sizes ($F(s)$) and the cumulative probability distribution function of the best fit power law ($F^*(s)$). The measure κ, is defined for avalanche sizes in the range $s = 1 : N$, with the formula:

$$\kappa = 1 + \frac{1}{N}\sum_{n=1}^{N}(F^*(s=n) - F(s=n))$$

Once a power law exponent was obtained, κ was calculated over the whole range of sizes $1 \leq s \leq 15$ for LFP analysis and all sizes $s \geq 5$ for spike analysis.

4.2.4 Correlation with Slow Wave Activity

Slow wave activity was calculated in 4-second epochs using an FFT-based approach (as previously described, see chapter 3) for every LFP difference signal across all combinations of channel pairs. The mean SWA across all channel difference signals was obtained and finally a median value taken within time windows corresponding to those used to calculate avalanches and κ. These values were correlated with corresponding κ (using the Matlab function `corrcoef`) independently for all animals and separately for episodes of wake, NREM and REM sleep.

4.3 Results

4.3.1 Various methods fail to detect avalanches in the LFP

The initial aim was to explore different methods for defining neuronal avalanches in order to determine whether *in vivo* LFP and MUA signals display hallmarks of critical dynamics during wakefulness, NREM or REM sleep. To begin, neuronal avalanches were defined in local field potentials using the most widely described method (Beggs and Plenz 2003; Petermann et al. 2009), in which neural activation is defined as large amplitude negative deflections in the LFP and avalanches as spatially distributed yet temporally sequential patterns of such activations (Figure 4.1A).

Avalanches were detected in this way over the baseline 24 hours in each animal, pooling over all epochs scored as wake, NREM and REM sleep and the resulting avalanche size distributions are shown in log-log coordinates in Figure 4.2A-C for all animals. While

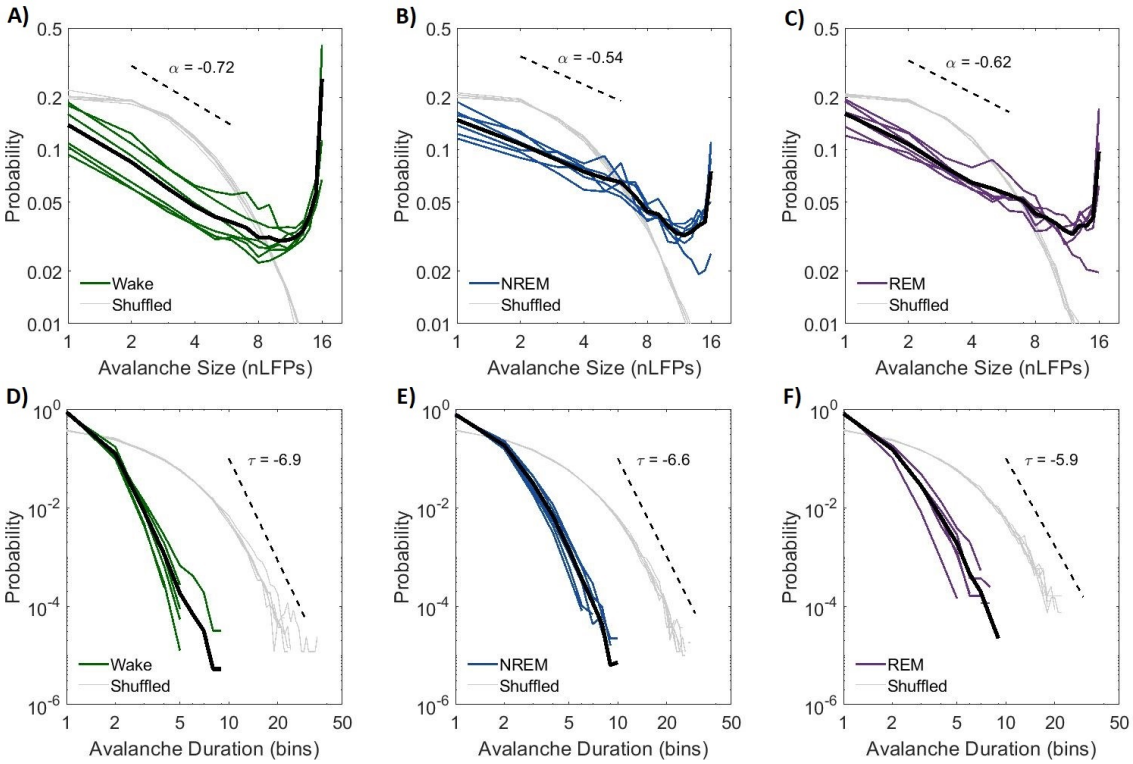


Figure 4.2: The size distributions of avalanches of negative LFP deflections plotted on a log-log scale derived from time periods scored as **A)** Wake, **B)** NREM, and **C)** REM sleep. Corresponding duration distributions are also shown separately for **D)** Wake, **E)** NREM, and **F)** REM sleep. Coloured lines correspond to individual animals and black lines to the mean distribution. Power laws were fit to sections of the mean distribution in order to estimate the exponent (α for size and τ for duration). Exponent values are shown alongside the equivalent slope (dashed line). Grey lines correspond to distributions derived from surrogate shuffled time series.

these distributions show approximate power law behaviour (log-log linear) over low values, all possess a large peak at size $s = 16$, equal to the number of LFP channels. Avalanches larger than the system size are rarely observed, due to inherent neural refractory periods, and so are not plotted. The tendency to observe frequent total synchronous activation in all LFP channels likely does not reflect local recurrent excitation (evidence of supercritical dynamics) but is more likely the result of signal shared through volume conduction. Because distributions were highly similar across animals, a single value was estimated for the slope over low values, obtaining much shallower exponent estimates than the widely reported α = -1.5 (Wake: α = -0.72; NREM: α = -0.54; REM: α = -0.62). However, shallow α has been previously explained as the result of subsampling a critical system

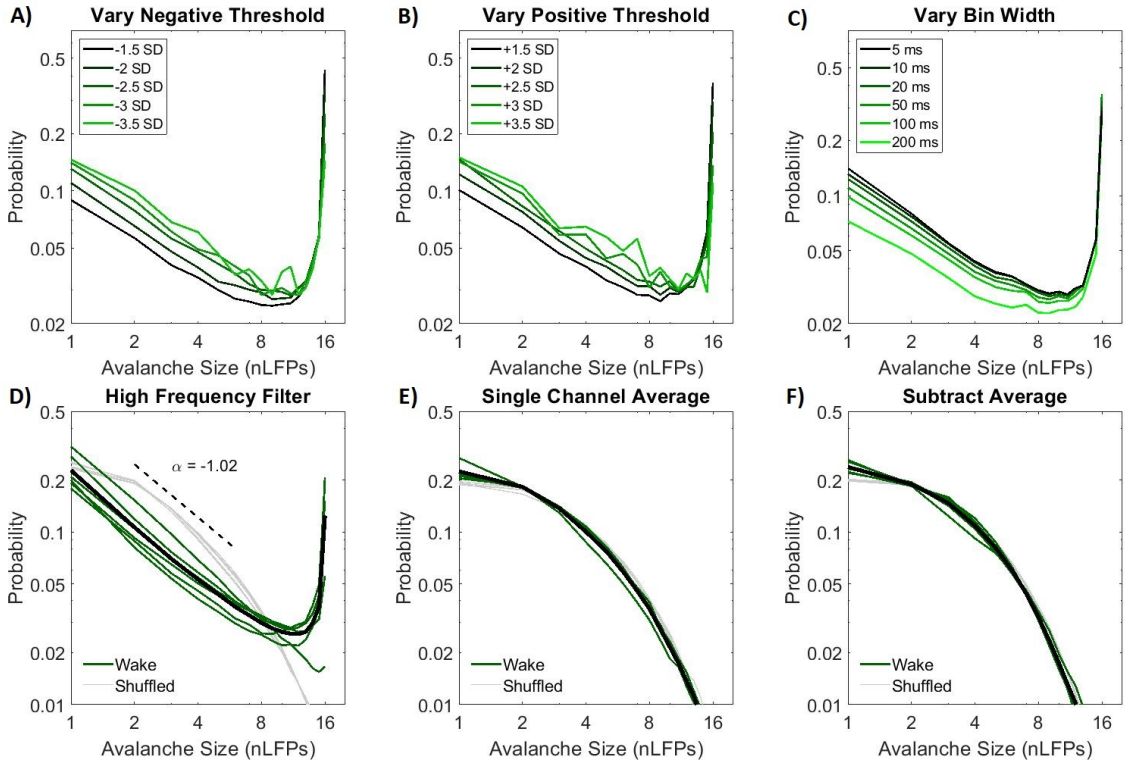


Figure 4.3: The size distributions of avalanches of negative LFP deflections obtained **A)** by varying the event detection threshold, **B)** alternatively detecting positive deflections, and **C)** by varying the avalanche bin width. These plots were derived from one representative animal, pooling over wakefulness. **D)** Avalanche size distributions derived from LFPs which were high frequency (30 - 70 Hz) band pass filtered. The best fit power law exponent α is additionally shown. **E)** Size distributions of negative LFP deflection avalanches derived from single channels, averaged over channels. **F)** Avalanche size distributions derived from LFPs after subtracting the mean LFP over all channels. Coloured lines correspond to individual animals and black lines to the mean distribution. Grey lines correspond to distributions derived from surrogate shuffled time series.

with closely spaced recording sites (Priesemann et al. 2009).

The corresponding avalanche duration distributions are shown in Figures 4.2D-F. These distributions decayed very steeply, although were not incompatible with power laws with very steep negative exponents (Wake: τ = -6.9; NREM: τ= -6.6; REM: τ= -5.9). The frequent occurrence of simultaneous activation in all 16 LFP channels will prevent the observation of very long avalanches. Distributions of both size and duration differed from the surrogate shuffled event times, which demonstrated the expected exponential decay in avalanche size.

This observation of unexpectedly high synchrony is not due to the selection of basic methodological parameters. The threshold for the detection of negative LFP deflections was varied from -1.5 to -3.5 multiples of the standard deviation of the LFP signal. Higher thresholds increased the noise in the distribution, owing to fewer avalanches detected, but did not substantially change the slope or presence of a peak at size $s = 16$ (Figure 4.3A, for one representative animal during wakefulness). Furthermore, it has been reported that avalanches with power law statistics can be observed by detecting events in positive LFP deflections, rather than negative ones, although these correspond generally to neuronal silence rather than activation (Touboul and Destexhe 2010). Using a positive threshold rather than a negative one did not change the results substantially (Figure 4.3B). In addition, using a fixed width of time bin for avalanche detection (instead of setting bin width to the average inter-event interval) somewhat reduced the distribution's initial slope, but nonetheless resulted in the appearance of a large peak at size $s = 16$ (Figure 4.3C).

A number of methods were then applied aiming to remove shared LFP signal owing to volume conduction, while retaining the signal variations which reflect local functional interactions, in order to uncover more promising evidence for critical or near-critical dynamics. Firstly, since volume conduction is stronger for lower frequencies, the LFP was filtered in the gamma range (30 - 70 Hz, rather than 1 - 30 Hz) before detecting negative LFP deflections. This procedure was not effective at removing the peak at size $s = 16$ (Figure 4.3D). Interestingly, however, the resulting avalanche size distributions did have a steeper slope, closer to the expected $\alpha = -1.5$ (Wake: α = -1.02; NREM: α = -1.02; REM: α = -1.05). After this, avalanche analysis was applied to events from individual LFP channels, in hope of exploiting the universality of critical dynamics which might extend to power laws into the exclusively temporal domain of activity. However, resulting size and duration distributions displayed exponential decay and were indistinguishable from shuffled surrogate avalanches (Figure 4.3E). Furthermore, in order to more explicitly remove shared signal components, the mean LFP was computed and subtracted from all individual LFPs

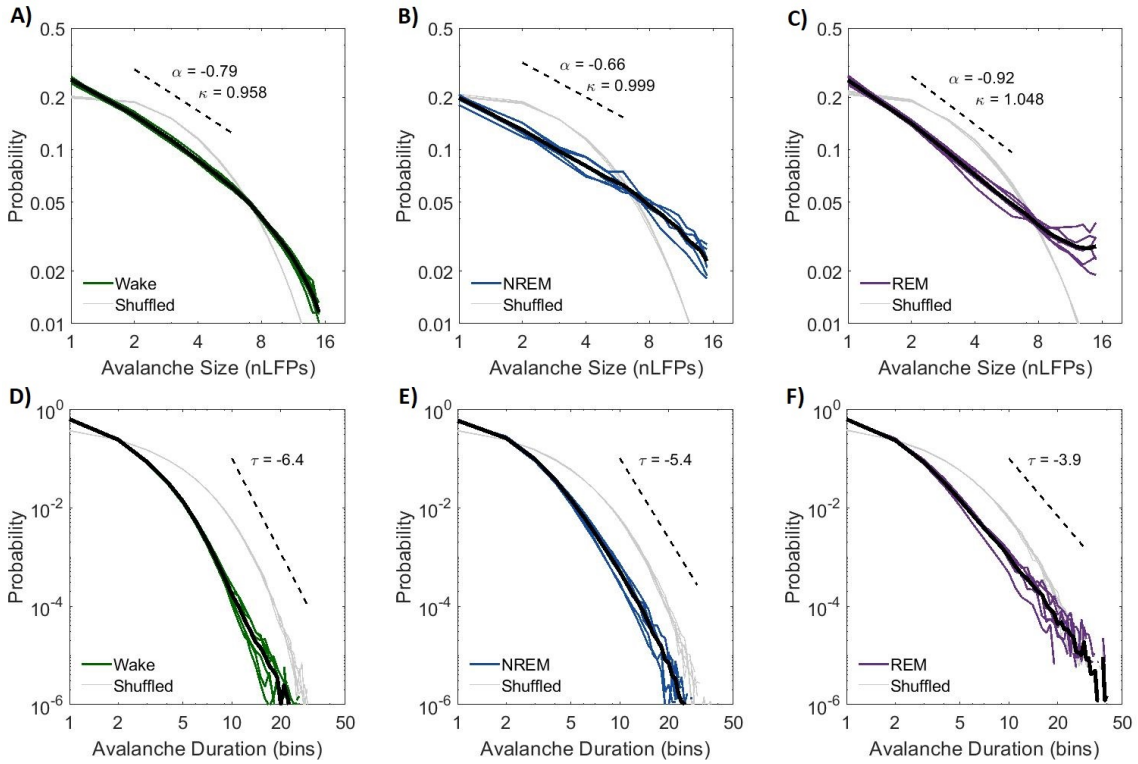


Figure 4.4: The size distributions of avalanches obtained from pairwise LFP difference signals plotted on a log-log scale derived from time periods scored as **A)** Wake, **B)** NREM, and **C)** REM sleep. Corresponding duration distributions are also shown separately for **D)** Wake, **E)** NREM, and **F)** REM sleep. Coloured lines correspond to individual animals and black lines to the mean distribution. Power laws were fit to sections of the mean distribution in order to estimate the exponent (α for size and τ for duration). Exponent values are shown alongside the equivalent slope (dashed line). Grey lines correspond to distributions derived from surrogate shuffled time series.

before detecting avalanches as before. Again, the resulting distributions of size and duration were not different from shuffled surrogates, reflecting independent signals (Figure 4.3F).

4.3.2 LFP-derived avalanches indicate subcritical wake, critical NREM sleep, & supercritical REM sleep dynamics

One final procedure was then tested to remove shared volume conducted signal without loss of meaningful local synchronisation. The signal from one single LFP channel was subtracted from all others and avalanches were subsequently detected over the resulting signals in the usual manner. This was repeated using each of the 16 channels as the

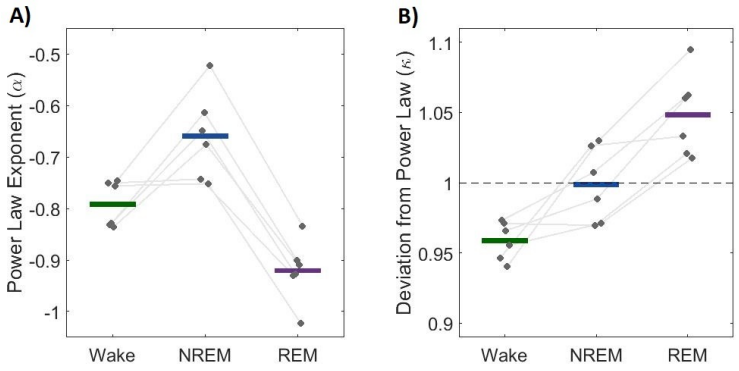


Figure 4.5: A) Best fit size distribution power law exponents α and **B)** deviation from power law measures κ from individual animals in wake (green), NREM sleep (blue) and REM sleep (purple). Grey lines link values derived from the same animal and coloured lines denote the group mean.

removed signal and the final distribution estimates were averaged. Taking the difference of two LFPs in this way reduces overall oscillatory power, but preserves state-specific oscillations, such as SWA in NREM sleep.

Interestingly, power law (or partial power law) behaviour is retained in the avalanche size distributions derived from all vigilance states and the extreme peak at the system size (now $s = 15$) is not present (Figure 4.4A-C). In wakefulness, the distribution decays faster than a power law at large values, consistent with a tendency towards subcriticality. In REM sleep, avalanche size distributions show the opposite trend, with a slight upward inflection in most animals for large values, indicative of supercriticality. In NREM sleep, avalanche size distributions appear closest to log-log linear, and the distributions derived from individual animals vary in their deviation towards apparent subcritical or supercritical regimes. Power laws were fit to individual (Figure 4.5A) and averaged size distributions (Wake: $\alpha = -0.79$; NREM: $\alpha = -0.66$; REM: $\alpha = -0.92$). Furthermore, the quality of the agreement between empirical distributions and the best fit power law was quantified using the metric κ (Shew et al., 2009), which represents the mean distance between cumulative distribution functions. A value of one represents an exact fit, whereas lower values indicate deviation into subcritical, and higher values supercritical, distributions. The resulting values agree that wake is subcritical ($\kappa = 0.958$) and REM supercritical (REM: $\kappa = 1.048$)

on average as well as in all individual animals (Figure 4.5B). Similarly, NREM sleep almost exactly matches the power law on average ($\kappa = 0.999$) but this is due to both subcritical and supercritical tendencies in distributions from individual animals, to a degree which overlaps with wake and REM sleep. The avalanche duration distributions generally resemble those obtained with the original method, displaying approximate power laws over larger values and with a less steep decay (Wake: $\tau = -6.4$; NREM: $\tau = -5.4$; REM: $\tau = -3.9$).

4.3.3 Spike-derived avalanches suggest dynamics are universally nearer criticality

Avalanche analysis was next applied to multi-unit spiking activity. In this method, the events which organise into avalanches correspond to single spikes. Avalanche size distributions were obtained for wake, NREM and REM sleep (Figure 4.6A-C). These were broadly similar to previously described distributions, characterised by approximate power laws over large values of avalanche size and a deviation from this for the smallest size values. Interestingly, there was considerably more variation between animals in distribution shape compared with those derived from the LFP.

Power law slopes were estimated, over an intermediate range of size values, for individual (Figure 4.8A) and the population average size distributions (Wake: $\alpha = -3.71$; NREM: $\alpha = -3.73$; REM: $\alpha = -3.61$). It is noteworthy that averaging the avalanche size distribution across animals, particularly in wakefulness, increased the deviation from a power law over low values, an effect which was less prominent in distributions derived from individuals. The shape of avalanche duration distributions was generally similar to their corresponding size distribution; they were also described by power laws only over intermediate to large duration values (Figure 4.6D-F). The best fit exponents were steeper than size exponents, but less variable between vigilance states compared with duration distributions derived from LFP (Wake: τ = -5.1; NREM: τ = -5.5; REM: τ = -5.0).

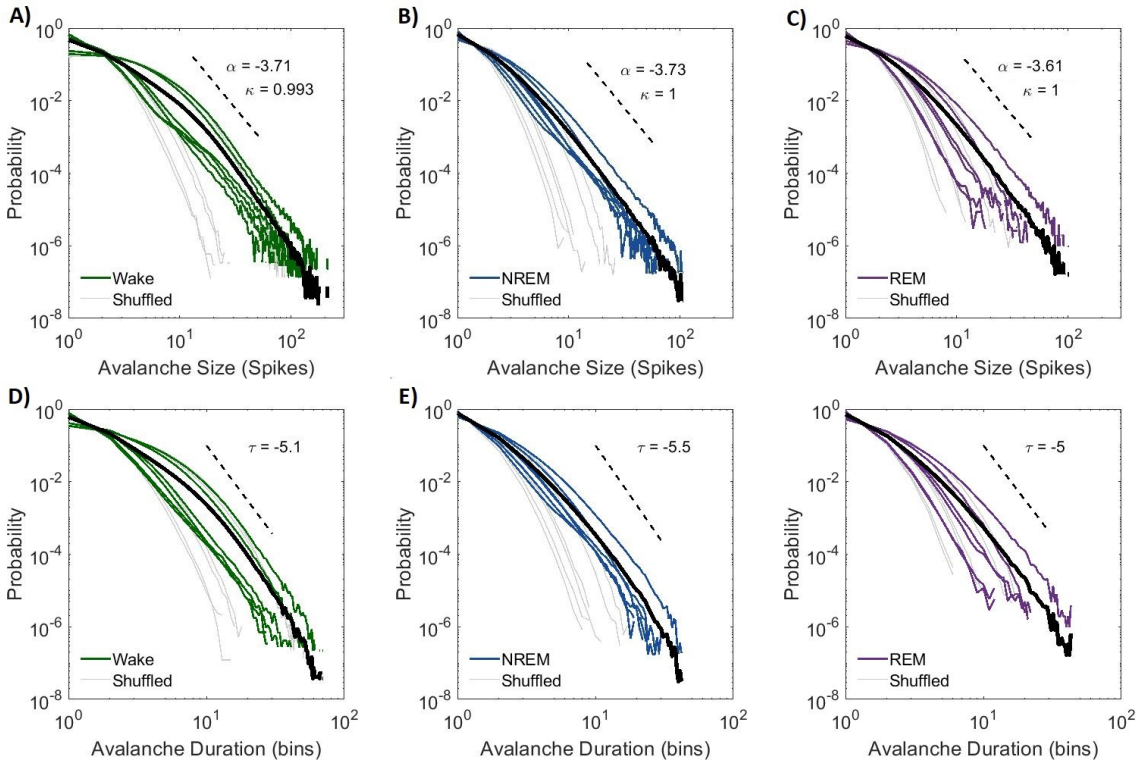


Figure 4.6: The size distributions of avalanches obtained from multi-unit spiking plotted on a log-log scale derived from time periods scored as **A)** Wake, **B)** NREM, and **C)** REM sleep. Corresponding duration distributions are also shown separately for **D)** Wake, **E)** NREM, and **F)** REM sleep. Coloured lines correspond to individual animals and black lines to the mean distribution. Power laws were fit to sections of the mean distribution in order to estimate the exponent (α for size and τ for duration). Exponent values are shown alongside the equivalent slope (dashed line). Grey lines correspond to distributions derived from surrogate shuffled time series.

The range of values which could be described by a power law was not increased by increasing the avalanche detection time bin (Figure 4.7A). Since spikes were only recorded at 1 ms precision, it was not possible to reduce the bin further. When increasing the bin width beyond 4 ms, bins with zero spikes became too rare and all spikes were lumped into single avalanches spanning the whole analysed time window. Instead, firing rates were calculated within time bins and activation events were considered to be elevations of firing rate above some threshold level, as has been done previously (Ma et al. 2019). Resulting size distributions were not well described by power laws, even when varying the time bin (Figure 4.7B) or event threshold, expressed as a percentile of the total firing rate distribution (Figure 4.7C).

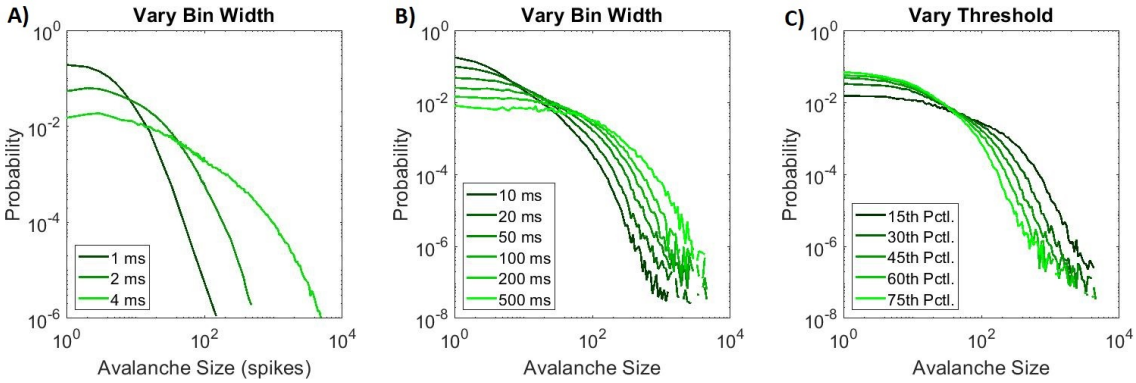


Figure 4.7: A) The size distributions of avalanches of multi-unit spikes obtained by varying the avalanche bin width. The size distributions of avalanches of large amplitude fluctuations in population firing rate obtained by varying the **B)** avalanche bin width and **C)** event detection threshold. These plots were derived from one representative animal, pooling over wakefulness.

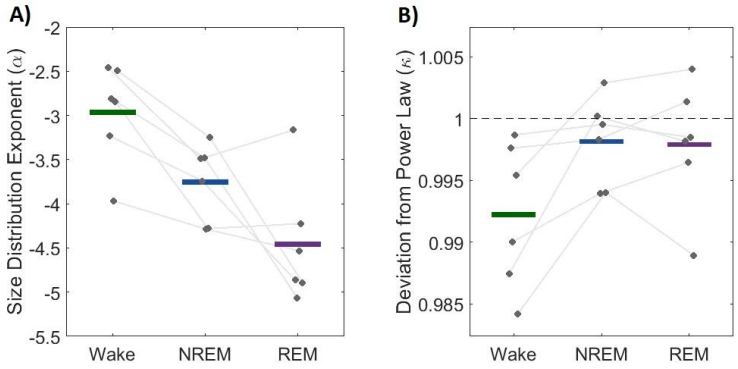


Figure 4.8: A) Best fit size distribution power law exponents α and **B)** deviation from power law measures κ from individual animals in wake (green), NREM sleep (blue) and REM sleep (purple). Grey lines link values derived from the same animal and coloured lines denote the group mean.

Deviation from power law measures were obtained for spiking avalanche size distributions, applied to the range of values $s \geq 5$. Both NREM and REM sleep were very close matches to the power law for the average distribution, yielding $\kappa = 1.000$, whereas wake was very slightly subcritical ($\kappa = 0.993$). Values of κ derived from individual animals were similar (Figure 4.8B), overall tending towards subcritical values in all vigilance states, but generally clustered closer to unity than values derived from LFP avalanches.

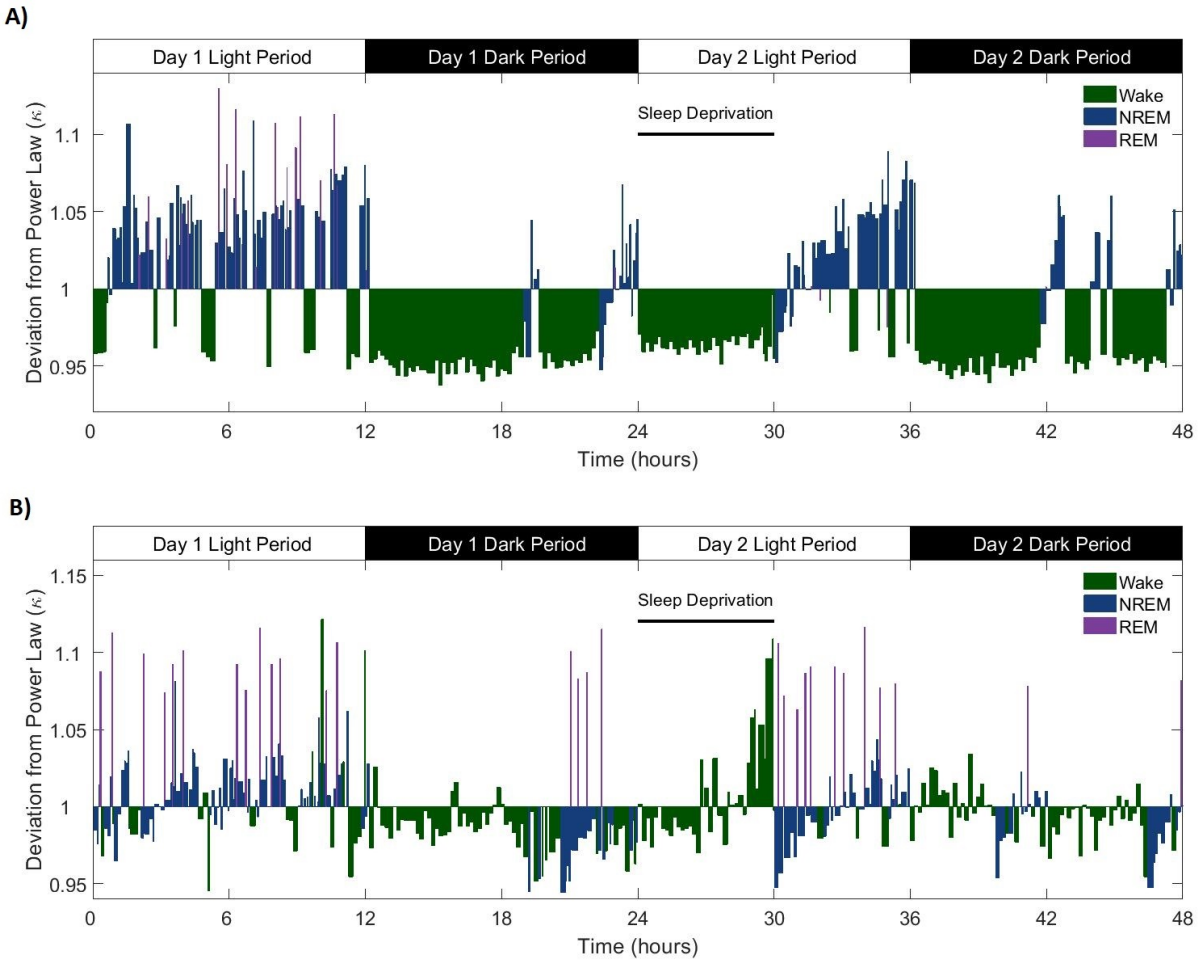


Figure 4.9: The deviation of negative LFP deflection avalanche size distributions from a power law, κ, plotted over 48 hours calculated in continuous episodes of the same vigialnce state, wake (green), NREM sleep (blue) and REM sleep (purple). The experimentally enforced sleep deprivation period at light onset of the second day is marked. Two examples are shown from representative animals.

4.3.4 Proximity to criticality changes across wake & sleep in association with slow wave activity

The temporal variability of avalanche properties was subsequently explored in order to determine whether critical dynamics might be related to Process S. Avalanches were detected and their size distributions calculated (using the previously described pairwise LFP difference method, as well as using spikes) separately within windows corresponding to continuous episodes of the same vigilance state over 48 hour periods, including sleep

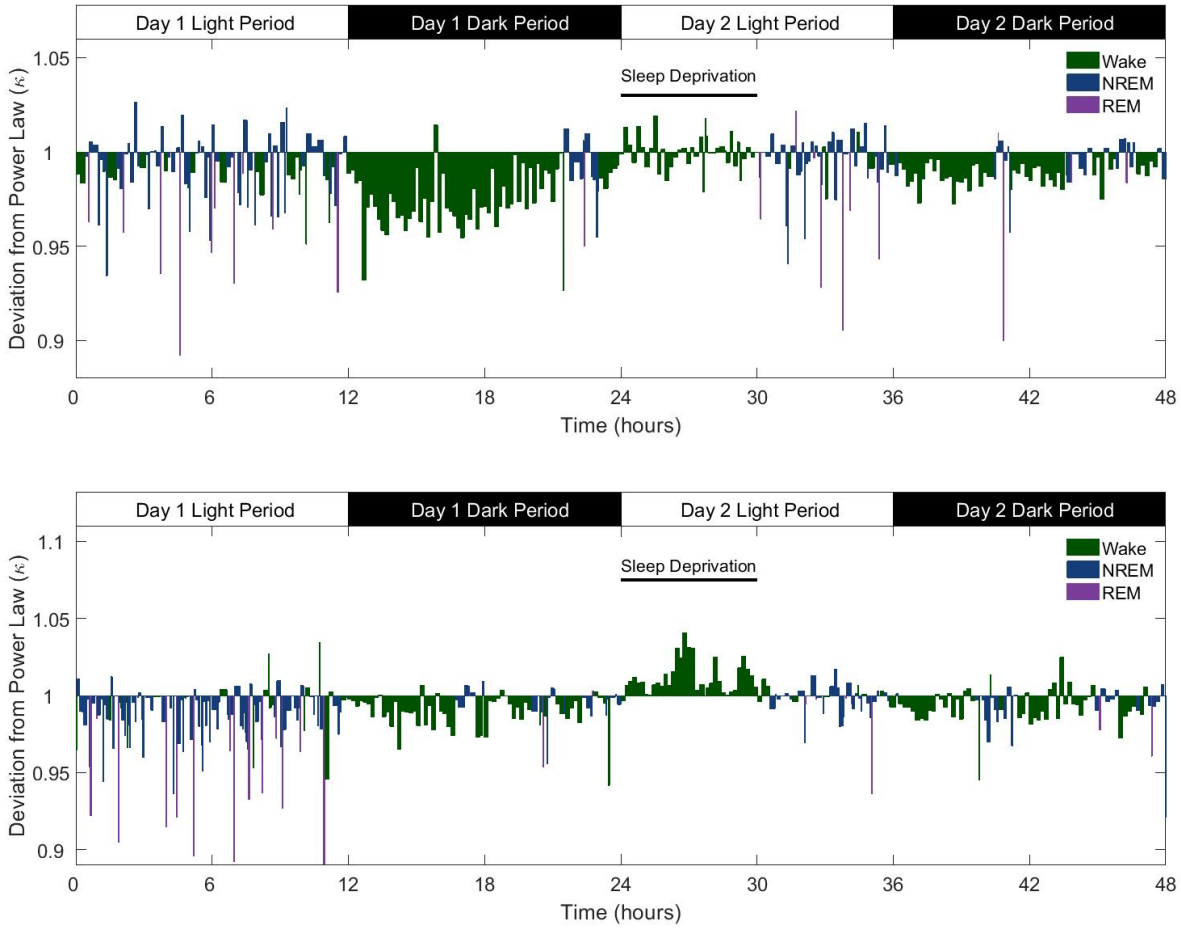


Figure 4.10: The deviation of multi-unit spiking avalanche size distributions from a power law, κ, plotted over 48 hours calculated in continuous episodes of the same vigialnce state, wake (green), NREM sleep (blue) and REM sleep (purple). The experimentally enforced sleep deprivation period at light onset of the second day is marked. Two examples are shown from representative animals.

deprivation. The deviation from power law metric, κ, was obtained for each time window.

For the LFP-derived avalanches, two exemplary time series are shown, reflecting the smallest (Figure 4.9a) and the largest (Figure 4.9B) observed variability in κ. In wake, κ values were typically consistent with stable subcriticality for the majority of time in most animals (Figure 4.9A). However, in some instances, κ values above one were found during wakefulness and this typically occurred towards the end of experimentally enforced sleep deprivation (Figure 4.9B). In NREM sleep, κ values were more variable, both between and within animals. Both net supercritical (Figure 4.9A) and subcritical

(Figure 4.9B) NREM sleep κ values were found, but all animals displayed a clear trend for increasing κ over the course of several hours of sleep, in almost all sleep episodes. REM sleep values were consistently high, above one, in all animals, with no discernible temporal pattern. However, the lack of striking patterns related to REM sleep might be due to the relatively low frequency of REM sleep episodes which were sufficiently long enough to estimate avalanche distributions.

Time series for values of κ derived from spiking was also obtained (Figure 4.10). As in the LFP, values associated with wakefulness were mostly subcritical. Higher values close to or above one were more commonly observed during the light period, particularly during sleep deprivation. Also, κ from NREM sleep showed a similar variability around unity, with no consistent tendency for supercritical or subcritical values. In contrast with the LFP-derived κ, REM sleep was not robustly supercritical and κ values displayed a similar variability between animals as in NREM sleep. Furthermore, no obvious trends associated with Process S were noticeable in any vigilance state.

The possible relationships between sleep-wake history and hallmarks of critical dynamics in LFP-derived avalanches were further investigated by comparing the average trend over animals during and after sleep deprivation. While κ values were stable for the majority of the sleep deprivation period, they were on average consistent with a change from subcritical to critical, or even supercritical, dynamics (Figure 4.11A). Importantly, this trend was not observed in every animal, nor was it linear with time, but emerged during the final hour of sleep deprivation in a minority of cases. In contrast, however, no increases in κ were found towards the end of any period of voluntary extended wakefulness (Figure 4.11B), which occurred during the dark period on the baseline day. These periods lasted between 2.7 and 9.6 hours (mean = 6.4 hours), so were of comparable duration to experimental sleep deprivation, yet differed in their circadian phase (dark vs. light period) and on behavioural content (wheel running vs. interaction with novel objects). Note that, for this analysis, the voluntary extended wake periods were normalised such that time was

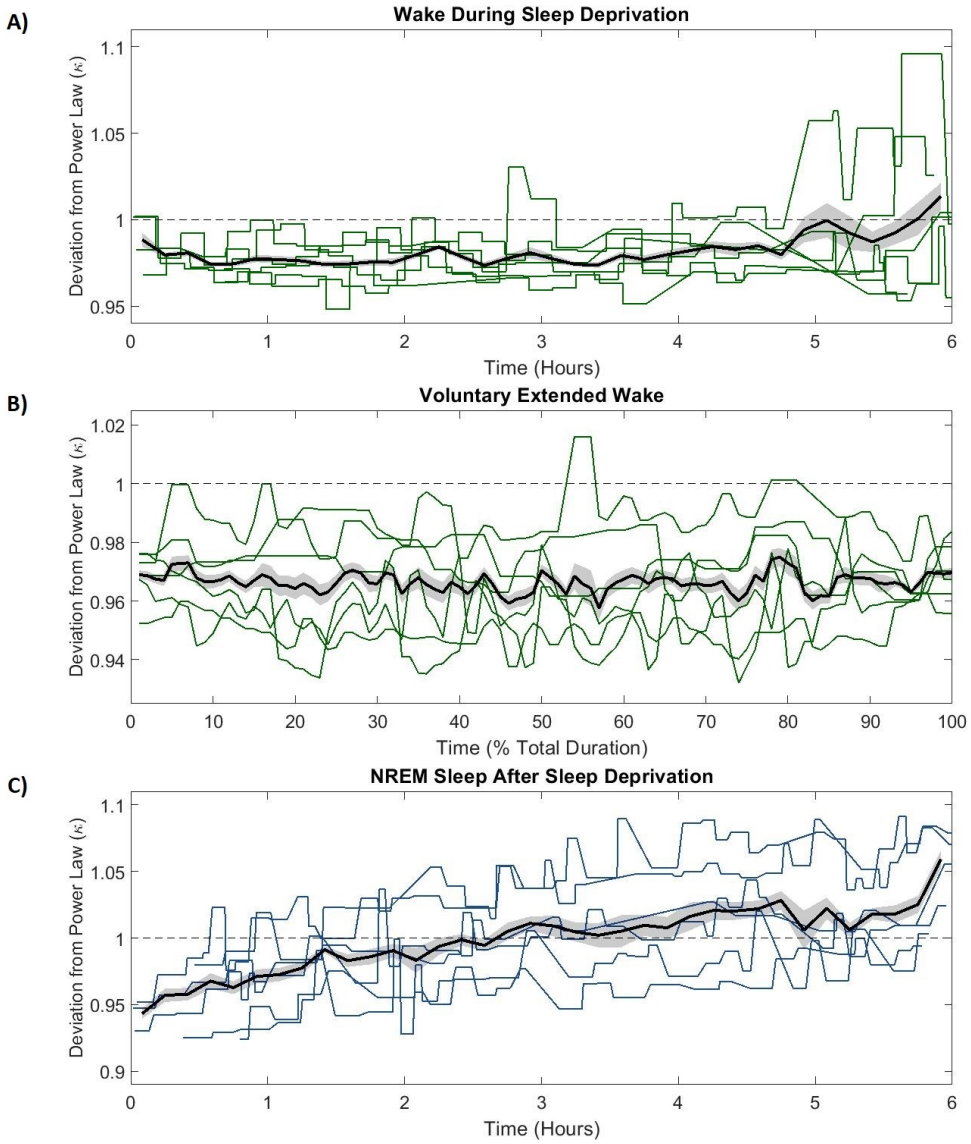


Figure 4.11: The trend in the power law fit deviation measure κ over **A)** experimentally enforced sleep deprivation on the second day lasting 6 hours, **B)** the longest episode of voluntary extended wakefulness during the baseline day (with time normalised as a percentage of the total episode duration), and **C)** NREM sleep in the 6 hours after experimental sleep deprivation. Coloured lines correspond to indiviudal animals, black to the mean and grey to the standard error of the mean. The mean traces in **A)** and **C)** are plotted with lower temporal resolution than individual traces, averaging over 10 minute intervals.

expressed as a percentage of the total duration of the period.

The time course of putative critical dynamics during 6 hours of recovery sleep after sleep deprivation is shown in Figure 4.11C. There was a consistent and approximately linear trend, observed in every individual animal, for increasing κ over time, corresponding to an average tendency to drift from subcritical into supercritical dynamics.

The trend analysis over sleep deprivation, recovery sleep and voluntary wake was repeated also for κ values derived from spike avalanches. Variation between animals was much higher in all conditions, and no overall trends were evident in average traces. Notably, the mean values were all consistently very close to $\kappa = 1$, with a weak tendency for higher κ during experimentally enforced sleep deprivation compared with voluntary extended wake.

To further determine how these changes might relate to Process S and associated neuronal dynamics, κ values in all vigilance states across all 48 hours were correlated with the median slow wave activity calculated within the same time window, averaged across all LFP differential signals. Remarkably, SWA and κ were consistently correlated (Figure 4.12A). All correlations were statistically significant ($p << 0.05$) in all animals and vigilances states, but strongest in NREM sleep. Importantly, however, the direction of the relationship was reversed in all animals from NREM sleep, in which SWA and κ were strongly negatively correlated (mean: $r = -0.88$), to positively correlations in both wake (mean: $r = 0.37$) and REM sleep (mean: $r = 0.30$) (Figure 4.12B). Intriguingly, by pooling all animals together, a relationship emerges spanning a larger range of SWA values (Figure 4.12C). This suggests that dynamics may tend to be subcritical for the lowest and highest values of SWA, but are supercritical at intermediate values, and therefore must approach criticality at two particular levels of SWA. Interestingly, the correlation between κ derived from the LFP with κ derived from spiking is highly variable between animals, and this is true whether analysis is restricted to specific vigilance states or when pooling all time together (Figure 4.12D).

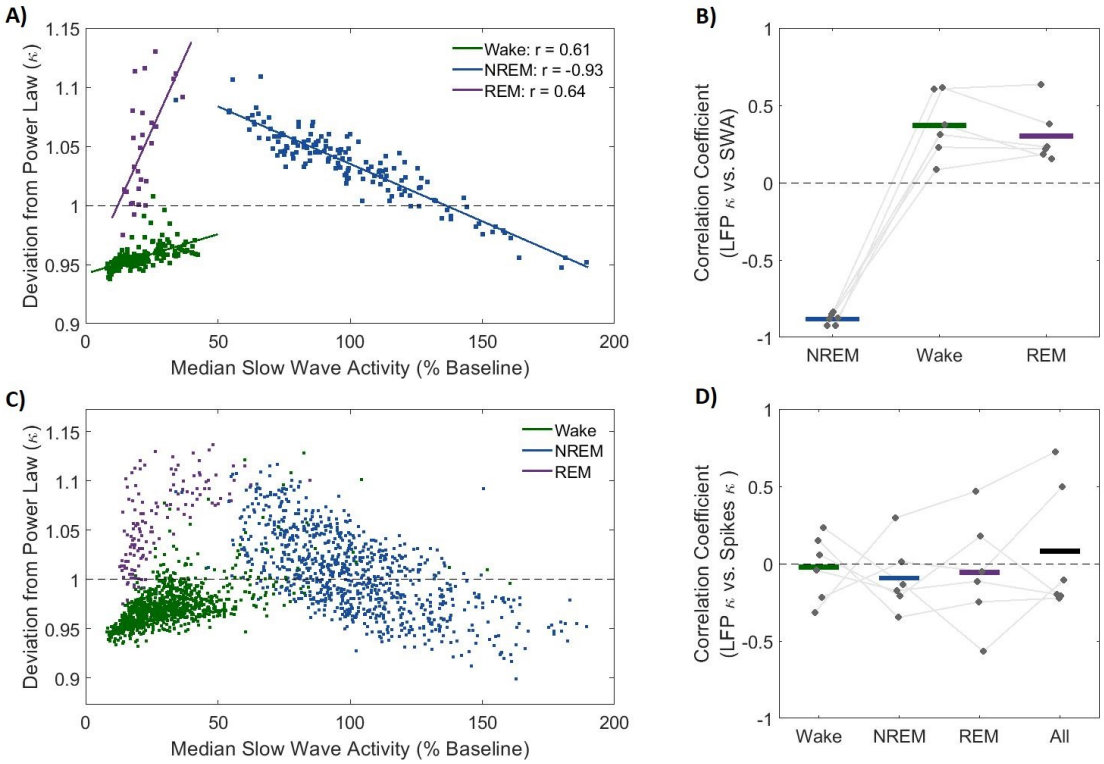


Figure 4.12: A) The correlation in one representative animal between the power law fit deviation measure κ and median slow wave activity averaged over pairwise LFP difference signals, in continuous episodes of of wake (green), NREM (blue) and REM sleep (purple). **B)** Correlation coefficients obtained over all animals. **C)** A scatter plot of κ against average slow wave activity over all time periods in all animals pooled together. **D)** The (Spearman rank) correlation between κ derived from LFP against κ derived from spiking activity for all animals, both separately for vigilance states and overall. Grey lines link values derived from the same animal and coloured lines denote the group mean.

4.4 Discussion

The aim of this analysis was to determine whether critical dynamics could be measured in this dataset of chronic *in vivo* recordings from the mouse motor cortex, and thereby discover whether criticality might vary across the sleep-wake cycle, both between vigilance states and in association with the sleep homeostatic process (Process S). Neuronal avalanche analysis was applied to LFP and spiking data and power laws were fit over selected value ranges of the resulting avalanche size distributions. A deviation from criticality metric was applied which sensitively detects deviations from the power law in the distribution

tail. The results were generally suggestive of subcritical dynamics in wakefulness and variable near-critical dynamics in NREM sleep. A deviation into the supercritical regime in REM sleep was evidenced from LFP data, but generally not in spiking avalanches. A strong association with Process S and slow wave activity was demonstrated in criticality measures derived from the LFP, finding positive correlations in wake and REM sleep, but negative correlations in NREM sleep. There was weak and inconsistent evidence for a drift from subcritical to critical dynamics over extended wakefulness.

The deviation of size distributions from a power law between LFP-derived and spike-derived avalanches was not clearly positively correlated, and compared to LFP-derived κ, the spike data showed increased variation between animals and over time, resulting in a reduced separation between wake, NREM and REM sleep states. One explanation may be that these differences are simply due to limitations of the method. The power law deviation metric κ is highly sensitive to the choice of the best fit exponent, which is more prone to error in spike-derived distributions due to the need to avoid the deviation from a power law over small avalanche values. However, it is plausible that LFP-based and spikes-based avalanches reflect criticality with respect to different system properties. Indeed, criticality describes a dynamic regime on the boundary of a continuous phase transition, yet the identity of the parameter space within which this boundary lies remains unclear. Avalanches in large amplitude negative LFP deflections imply that critical activity reflects a balance of oscillatory synchronisation, whereas spike-derived avalanches likely more directly correspond to the balanced spread of excitation vs. inhibition. This interpretation would imply that the tendency of activity to spread vs. decay remains relatively stable around the critical point across sleep and wake, although is closer to criticality in sleep, whereas deviation from critical properties manifest more strongly in oscillations.

Importantly, a crucial unresolved issue is the relationship between phase transitions in neuronal dynamics which are critical, and the ability of neuronal dynamics to alternate between the different states of wake, NREM and REM sleep, which clearly constitutes

a form of phase transition. Phase transitions which are not critical are described as discontinuous, and correspond to parameter settings compatible with multiple possible dynamical phases, such that the system switches between these when perturbed by external or stochastic influences. Similarly, multi-stability has been applied to describe the regular alternation of neuronal up and down states of the slow oscillation, and variation of parameters related to excitability adjusts their dynamics (Sanchez-Vives et al. 2017), which might account for the differing levels of slow wave activity in natural wake and sleep. A relationship was found between deviation from criticality measures and levels of slow wave activity. It suggests that dynamics are subcritical when SWA is very low and tends towards criticality with increasing SWA. Speculatively this might be due to increasing synchrony, as spikes are initiated at the down-to-up state transition, which could facilitate larger avalanches. However, at some point increasing SWA causes avalanche size to reach a maximum level (possibly in the supercritical regime), and subsequently dynamics return towards subcriticality. This could plausibly be due to an increased tendency for down states to cut short developing avalanches. Although the precise relationship remains uncertain, this result provides some evidence that the neural mechanisms which control the degree to which cortical networks undergo slow oscillatory vs. irregular asynchronous activity could be used tune dynamics across vigilance states towards or away from the critical point.

A limitation of these results is that power laws are necessary but not strictly sufficient to prove the presence of criticality. Indeed, stronger evidence for criticality can be obtained by demonstrating scaling relationships between different critical exponents (Beggs and Timme 2012; Friedman et al. 2012; Ma et al. 2019). For example, the mean size of avalanches may vary as a function of their duration according to a power law relationship with exponent β. At criticality, this exponent obeys the scaling law:

$$\beta = \frac{\tau - 1}{\alpha - 1}$$

Preliminary work has been performed searching for evidence of this scaling relationship,

finding that the value of β suggested by empirical α and τ more closely matches empirically-derived β in data derived from NREM sleep, compared to wake and REM sleep. This result is in agreement with the LFP-derived results, particularly with respect to a deviation from criticality in REM sleep which was not evident in the spike avalanche κ metric. More work is required to confirm that this holds over all animals. Notably, this scaling relation will not hold for LFP-derived avalanches because $0 > \alpha > -1$ in all cases, and so is only applicable to spike-derived avalanches.

Other methods for exploring critical dynamics in neural systems test for the presence of long-range temporal correlations, such as detrended fluctuation analysis (Hardstone et al. 2012), and multi-regressive autocorrelation (Wilting and Priesemann 2018). Both these methods were tested, drawing conflicting results. Detrended fluctuation analysis estimates the Hurst parameter, a measure of self-affinity over multiple scales, such as that which characterises fractal systems. Application of this analysis to the LFP yielded values that were different between wake, NREM and REM sleep, but none were consistent with true fractal statistics indicative of criticality. In addition, the results do not inform as to whether dynamics are more subcritical vs. supercritical. Similarly, auto-regression was applied to multi-unit spike data to estimate the rate of temporal decay, which is higher in systems approaching criticality. Consistent with a prior study (Meisel et al. 2017b), the decay in autocorrelation was lower in wake than NREM sleep, indicative of dynamics closer to the critical point. This result apparently contradicts the evidence from avalanches and more theoretical work will be needed to understand the functional implications of this difference.

5

The Effects of Psilocin on Sleep & Cortical Neuronal Activity

Contents

5.1 Introduction 114

5.2 Methods 116

5.3 Results 124

5.4 Discussion 148

5.1 Introduction

Agonists of the serotonin 5-HT_{2A} receptor are an exceptional class of drugs which induce profound alterations to perception, cognition and behaviour, commonly characterised as the psychedelic state. In addition to these unusual acute effects, a growing body of preclinical and clinical evidence suggests that, under appropriate controlled conditions, psychedelics can promote lasting positive effects on psychological well-being, offering a promising new treatment method for depression, anxiety and related mental illnesses (Carhart-Harris et al. 2016; Carhart-Harris and Goodwin 2017; Hibicke et al. 2020). However, a great deal remains unknown about the basic neurophysiological mechanisms which underlie both the acute psychedelic response and its putative long-term consequences.

It is well established that the psychedelic effect depends fundamentally on activation of the 5-HT_{2A} receptor. While this receptor is expressed throughout the brain, labelling studies identify that expression is highest in the cortex, where receptors are most densely located on both layer 5 pyramidal neurones and inhibitory interneurones (Burnet et al. 1995; Xu and Pandey 2000; Weber and Andrade 2010). Activation of 5-HT_{2A} receptors has a predominantly excitatory effect, which includes direct depolarisation of cortical neurones (Beique et al., 2007) as well as a facilitation of glutamate transmission both locally and long range (Lambe and Aghajanian 2006; Marek 2018). Since both excitatory and inhibitory neurones are excited by 5-HT_{2A} receptor agonists, the overall effects on neuronal firing and network activation are variable and dose dependent (Puig et al. 2003; Celada et al. 2008; Wood et al. 2012. The network level dynamic effects appear to include a breakdown in cortical neuronal synchrony and an increase in the entropy of activity patterns (Celada et al. 2008; Muthukumaraswamy et al. 2013; Carhart-Harris et al. 2014; Tagliazucchi et al. 2016). 5-HT_{2A} receptor agonists have been shown to both promote a downscaling of existing synapses (Berthoux et al. 2019) and the formation of new ones (Ly et al. 2018).

The most robust acute behavioural effects of administration of psychedelic substances

in mice is the induction of the head twitch response, comprising irregular paroxysmal rotational movements of the head. The head twitch response is a popular behavioural model of psychedelic activity in animals, due to its strong correlation with the psychotropic effects of different substances (Corne and Pickering 1967; Marek 2018; Halberstadt et al. 2020) and apparent overlapping mechanisms requiring cortical 5-HT_{2A} receptor activation (González-Maeso et al. 2007; Fox et al. 2010; Halberstadt et al. 2011).

Based on human functional neuroimaging studies, a possible mechanism for the clinically relevant benefits of the psychedelic state has been identified, which involves a facilitation of the breakdown and reformation of functional associations between higher cortical areas, such as medial prefrontal cortex, and the rest of the brain (Carhart-Harris et al. 2017). However, fundamental questions remain as to the precise nature of 5-HT_{2A}-receptor-agonist-induced neuroplasticity and how this relates to the well-characterised homeostatic processes which regulate synapses, neuronal activity and global brain dynamics. In particular, sleep is known to play an essential role in all of these processes (Rasch and Born 2013; Vyazovskiy and Harris 2013; Tononi and Cirelli 2014), and yet there is currently a striking absence of literature exploring the possibility that many of the enduring beneficial effects of serotonergic psychedelics are dependent on sleep (Froese et al. 2018).

Conversely, psychedelics might provide a novel approach to study the basic science underpinning sleep regulation. The psychedelic state provides a means to manipulate the content of wakefulness, such that certain properties of brain dynamics can be altered, without inducing sleep-like brain activity. Indeed, the psychedelic state has been characterised as one with enhanced dynamical complexity (Carhart-Harris 2018; Scott and Carhart-Harris 2019) and so is, by some measures, an exaggerated version of wakefulness. Psychedelic stimulation offers important advantages compared to other manipulations of waking brain activity. Compared to, for example, optogenetic activation of cortical neurones, a 5-HT_{2A}-receptor-dependent perturbation of brain dynamics is simpler, more physiologically realistic, feasibly translatable to humans, and more comprehensible

in terms of the associated conscious experience.

To advance understanding of the links between psychedelics and sleep, chronic *in vivo* electrophysiological recordings were obtained from the prefrontal cortex of mice administered with psilocin (the psychoactive form of the prodrug psilocybin) and a vehicle control, in both an undisturbed and a sleep deprivation condition. The aims were to identify the effects of psilocin on:

- Spontaneous behaviour, particularly the head twitch response, to validate drug efficacy and enable comparison with the existing literature on responses to psychedelics in mice.
- Sleep-wake architecture, both while the drug is active and over the subsequent day.
- Neuronal dynamics, such as EEG and LFP spectra and multi-unit firing rates, while the drug is active and during subsequent sleep.
- The accumulation and dissipation of Process S, as reflected in the dynamics of slow wave activity at both EEG and LFP levels.

5.2 Methods

5.2.1 Preparation of Psilocin

The dose of psilocin used for this study was chosen by comparison with the existing animal behaviour literature. A dose of 2 mg/kg is standard, and consistent with the range of doses over which the reported psilocin-induced HTR is greatest (Halberstadt et al. 2011).

The psilocin was obtained from two suppliers. An initial behaviour-only pilot study was conducted using psilocin sourced from Tocris (Bristol, UK). This supply was then

depleted and, since this supplier had discontinued the sale of psilocin, additional drug was sourced from LGC Standards for the electrophysiological experiments.

A number of methods for dissolving crystalline psilocin have been reported in existing studies. Psilocin has limited solubility in aqueous solution but can be dissolved by a weak acid, with 50 mM tartaric acid being a common choice (Halberstadt et al. 2011). Psilocin was then diluted in saline (containing 5% glucose) up to a concentration of 0.25 mg/ml. It was confirmed with a pH meter that this preparation has approximately pH 5.5 and so has tolerable acidity for injection. Alternatively, it is possible to dissolve psilocin in an organic solvent, such as dimethyl sulfoxide (DMSO). This method was trialled for three behaviour-only injection experiments. Although the DMSO was easier to use, this option was less favourable for the implanted animals due to concerns over its aversive quality, particularly as multiple injections were required and the pilot study animals displayed substantially increased licking or scratching of the injection site, indicative of pain or irritation.

The psilocin was stored in a locked freezer at -20°C. Psilocin is not stable in solution for more than 24 hours, and so it was necessary to make fresh preparations before each injection. Before each batch of experiments, the psilocin was weighed out using an analytical balance into separate samples, ranging 0.4 – 1.2 mg, aiming to take as little as possible while remaining in the measurable range of the balance. This was done since, even with the smallest measurable amounts, there would be substantial wastage of the drug. Additionally, tartaric acid samples were similarly weighed out, each 10 – 13 mg.

The drug was always administered by intraperitoneal injection as this delivery route was the most convenient for awake mice and allows for precise control over the timing and dosage.

A few injection experiments, one behaviour-only and one on implanted animals, were performed using DOI (2,5-dimethoxy-4-iodoamphetamine), another 5-HT_{2A} receptor agonist which has been more commonly studied than psilocin, particularly with respect

to the head twitch response. A small supply was obtained (from another research group) comprising two 0.9 mg samples. These were dissolved in saline on the day of injection to produce a concentration of 0.25 mg/ml, identical to psilocin. In contrast to psilocin, DOI has high solubility and stability in solution.

5.2.2 Preliminary Behavioural Observation Studies

A behavioural pilot study was conceived in order to confirm the efficacy of the drug preparation and to obtain an estimate for the duration of its effects on natural wake and sleep. This experiment was conducted using six adult male C57BL/6J mice. The conditions were chosen to mimic those that would be experienced by the implanted animals. The mice were housed individually in plexiglass cages under a standard 12 - 12 hour light-dark cycle and placed into ventilated sound-attenuated Faraday chambers (Campden instruments). They were provided with bedding and *ad libitum* food and water. The mice were left to habituate to their home cage for 3 days before injection. Four mice were given psilocin (2 mg/kg) and two mice were injected only with the tartaric acid vehicle. The injections began at 12 pm and were given to the mice in pairs, separated by intervals of approximately 1 hour. During this time, the most recently injected animal's behaviour was carefully observed both manually and with video recording (Dericam HD 1080p webcam). Passive infrared sensors were setup to individually record the activity of all animals from 12 hours before to 12 hours after injection. One such sensor (Panasonic, Model EW AMN32111) was taped near a top corner of each cage, approximately 35 cm from the cage floor, and carefully positioned so as to respond to motion in as great a fraction of the cage floor as possible. The PIR sensor output was collated by an Arduino Uno (Rev3) and transmitted to a Raspberry Pi, sampling activity every 10 seconds. Sleep was estimated to correspond to periods of at least 5 minutes of undetected movement.

Further experiments were run with altered parameters, aiming to identify possible

factors explaining the low frequency of head twitches (see Results). In all these experiments the mice were removed from their home cage immediately prior to injection and then transferred to an unfamiliar sparse cage. As before, video was recorded for at least 30 minutes post injection to capture the head twitch response. Notably, these injections were performed using a fresh source of psilocin, obtained from a different supplier. The first four injections reused animals from the initial behavioural study but took place 3 weeks later. Two of these animals received psilocin at 2 mg/kg and two at 5 mg/kg (achieved with a 2.5 fold increase in injection volume). Before and in between experiments, these mice were individually housed as in the original behavioural experiment. Subsequent experiments were performed using 3 naïve mice. These were first injected with 2 mg/kg psilocin prepared instead using a DMSO vehicle. After 2 weeks, they were injected again with 2 mg/kg DOI. Before and in between injections these three mice were kept in a group housing facility and shared a cage together. All animals used in these behavioural observation experiments were eventually culled by CO_2 inhalation.

5.2.3 Experimental Design for Electrophysiological Recording

The electrophysiological recordings were performed in two batches, each comprising four mice. Briefly, these mice were surgically implanted with frontal and occipital EEG screws, nuchal EMG electrodes, and either a microwire array or laminar probe in the medial prefrontal cortex. A complete description of the animal husbandry, surgical procedures and electrophysiological data acquisition process is given in chapter 2.

Once fully recovered from surgery, each batch of animals underwent four injection experiments. The injections were counterbalanced such that, during each experiment, two animals received psilocin and two received the vehicle. In one condition, mice were immediately returned to their home cage after injection and left undisturbed. In another condition, a sleep deprivation protocol was enforced for four hours after injection. During

this time, the mice were kept awake using a combination of presentation of novel materials and gentle physical stimulation. After four hours of enforced wakefulness, the mice were left to sleep undisturbed. The design was repeated measures, as each mouse experienced all combinations of psilocin vs. vehicle and undisturbed vs. sleep deprivation exactly once. Each injection experiment was separated by three days, following a pattern of baseline day, then injection day, then recovery day. The final recovery day was not recorded. The injections were given as soon as possible after light onset at 9 am. The longest delay to starting after 9 am was 45 minutes. Injections were performed as quickly as possible, with a maximum delay of 10.5 minutes between first and last injection. The second batch of mice experienced a fifth experimental treatment, 4 weeks after the prior recordings finished, in which all were injected with DOI and then left undisturbed.

5.2.4 The Head Twitch Response

The head twitch response was scored for all behavioural experiments and the undisturbed condition of the electrophysiology experiments using the video footage. Cameras were rigged to record mice individually or in pairs. Head twitch events were counted over the 30 minutes following injection and expressed as a rate of number of head twitches per minute. If the animal fell asleep during the 30 minute period after injection (which happened only 3 times in total, exclusively in the vehicle condition) the head twitch rate was calculated only from time spent awake.

5.2.5 Time Windows for Analysis

To carefully characterise the effects of psilocin on neuronal activity during wake, NREM and REM sleep, analyses were performed on data segments in several specifically defined windows. Each window was checked visually to confirm its correspondence to the intended section of time. In the vehicle condition:

- Initial wake: From the time of injection to the first epoch scored as NREM sleep (Duration: 18.6 ± 17.2 min).
- Initial sleep: From the first epoch of the first episode of continuous NREM sleep lasting at least 1 minute after injection to the first epoch of the next episode of continuous wakefulness lasting at least 5 minutes (Duration: 86.8 ± 24.9 min). Both NREM and REM sleep are separately analysed here.

In the psilocin condition:

- Initial wake: From the time of injection to the first epoch scored as NREM sleep (Duration: 26.3 ± 12.7 min).
- Transitional period: From the end of initial wake to the first epoch of the next episode of continuous NREM sleep lasting at least 1 minute. Both wake and NREM sleep are separately analysed here (Duration: 17.1 ± 10.0 min).
- Initial sleep: From the end of the transitional period to the first epoch of the next episode of continuous wakefulness lasting at least 5 minutes (Duration: 74.2 ± 30.0 min). Both NREM and REM sleep are separately analysed here.
- Second wake: From the end of initial sleep to the first epoch of the next episode of continuous NREM sleep lasting at least 1 minute (Duration: 16.0 ± 6.8 min).
- Second sleep: From the end of second wake to the first epoch of the next episode of continuous wakefulness lasting at least 5 minutes (Duration: 72.5 ± 35.2 min). Both NREM and REM sleep are separately analysed here.

In the sleep deprivation condition (whether psilocin or vehicle):

- Start SD: From the time of injection until 30 minutes after.

- End SD: From 3.5 hours into sleep deprivation until the 4^{th} hour (end of sleep deprivation).
- Initial NREM: NREM sleep only from the start of the first episode of NREM sleep lasting at least 1 minute, after 4 hours of sleep deprivation, until the next episode of wakefulness lasting at least 5 minutes (Vehicle duration: 1.47 ± 0.7 hrs; Psilocin duration: 1.24 ± 0.4 hrs).
- Second NREM: NREM sleep only from the start of the first episode of NREM sleep lasting at least 1 minute occurring after the episode of wakefulness which terminates initial NREM, until the end of the light period (Vehicle duration: 6.45 ± 0.5 hrs; Psilocin duration: 6.12 ± 0.8 hrs).

5.2.6 Spectral Analysis

The spectral properties of EEG and LFP signals were analysed by applying a discrete fast Fourier transform (FFT), using the Matlab function `fft`, to segments of 4-second duration. Before applying the FFT, signals were multiplied by a Hann window (H) in order to reduce edge artefacts: $H(x) = \frac{1}{2}(1 - \cos(2\pi x/L))$, where $x = \{0, 1, \ldots, N-1\}$, $L = N - 1$, and $N = 1024$ samples per 4-second epoch.

The amplitude was extracted by taking the absolute value of the resulting complex FFT output. The amplitude was then squared to obtain the power. The power values were averaged over epochs scored as the same vigilance state within the time window of interest separately for each animal. An average power for each discrete frequency value in wake, NREM and REM sleep was calculated for each animal from the whole 24 hour baseline day before psilocin injection. In different analyses, as described, values were then averaged between animals or within animals over specific frequency bands. For plotting spectra, values between 45 - 55 Hz were interpolated for ease of visualisation, but in actuality power in this frequency range was removed by a notch filter targeting

50 Hz line noise. When comparing changes in band power, power values obtained from experimental days ($P_{f,v,t}$) were normalised to the power within the same vigilance state at the same frequency in the corresponding baseline day ($Q_{f,v}$) by calculating the power change in decibels: $10\log_{10}(P_{f,v,t}/Q_{f,v})$, for each discrete frequency, f, vigilance state, v, and analysed time window, t, (see above).

When specifically testing for changes in Process S at the end of sleep deprivation, the delta power was obtained for each epoch by summing over frequencies from 0.5 to 4 Hz from the FFT. The median value was taken over each continuous NREM sleep episode at least 1 minute duration and finally the maximum of these values was used to represent peak Process S after sleep deprivation. These were compared between vehicle and psilocin conditions using the decibel log ratio transform.

5.2.7 Firing Rates Analysis

The multi-unit spike rate was calculated in 4-second epochs separately for each channel on each day. Spike rates were averaged within epochs scored as the same vigilance state within the time windows described. These were expressed as a percentage of the mean spike rate in the same channel and same vigilance state on the baseline day before psilocin injection in the relevant condition. Spike rates normalised to baseline were then averaged across channels.

5.2.8 Process S Modelling

The significance and details of the modelling approach are presented in chapter 3. Briefly, the equations of the classic Process S model which predicts slow wave activity levels

as a function of sleep-wake history are:

$$\text{WAKE/REM:} \qquad \frac{dS}{dt} = \alpha(S_{max} - S(t))$$

$$\text{NREM :} \qquad \frac{dS}{dt} = -\beta(S(t) - S_{min})$$

This model was fit to SWA derived from the frontal EEG over 48 hours, comprising the baseline and sleep deprivation days, in both vehicle and psilocin conditions. This was done by calculating the median SWA for each NREM sleep episode at least 1 minute duration and choosing parameters to minimise the deviation of modelled Process S from these empirical values. The parameters S_{max} and S_{min}, and initial value S_0, were selected manually based on visual inspection, then α and β only were subsequently optimised using the Matlab function `fminsearch`. For a fair comparison, S_{max} and S_{min} were constrained to be the same for both vehicle and psilocin conditions within the same animal.

5.3 Results

5.3.1 Head twitches & transiently disturbed sleep are seen in response to psilocin

Some behavioural observation experiments were conducted, involving administration of vehicle solution, psilocin, and DOI to non-implanted mice. The first experiment was performed before electrophysiological recording began. It aimed 1) to confirm the efficacy of the psilocin preparation and delivery method, 2) to provide a preliminary characterisation of the typical behavioural response (importantly including head twitches), and 3) to establish the approximate nature and duration of the effects of psilocin on natural sleep and wake.

For this, six mice were given injections, four with psilocin and two with vehicle solution, and their immediate behaviour was observed. Overall, in comparison to controls, the

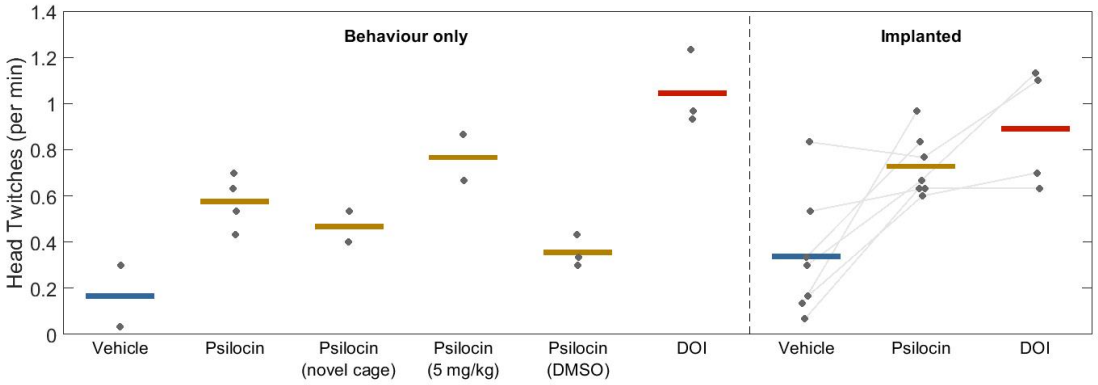


Figure 5.1: The head twitch response (number of twitches per minute averaged over 30 minutes after injection) for each mouse. Left: the behavioural observation conditions. Right: the electrophyiologically implanted animals in the spontaneous wake-sleep condtion. Coloured lines (vehicle is blue, psilocin yellow, and DOI red) correspond to the group mean. Grey lines link results from the same animal (for the implanted animals only).

psilocin-injected mice appeared to be more active; they walked around their cage more, spent more time out of their nest, and showed visibly elevated muscular tremor and breathing rate. All four of these mice were observed to remain awake for at least an hour after injection. Notably, whenever these mice occupied their nest and adopted a sleep-like posture, their eyes remained open and their rest was frequently interrupted by small body movements. In contrast, both vehicle-injected mice initiated sleep relatively soon after injection (11 min and 38 min).

Data from passive infrared sensors, which recorded each animal's motion for 12 hours post injection, suggested that the psilocin-injected mice remained awake for 64 - 108 min. However, passive infrared sensor data suggested that over the following hours these mice exhibited typical patterns of activity and quiescence, which resembled controls. The psilocin-injected animals appeared to sleep between 38 - 75% (mean 56%) of the subsequent 12 hrs, compared to 47% and 65% (mean 56%) in controls. These results were suggestive that the arousing effects of psilocin were short lasting (on the order of a few hours) and that any long-term effects on sleep homeostasis would be subtle.

Head twitches were difficult to detect during the initial live observation of the mice

following psilocin administration. However, through a more careful inspection of the recorded video footage it was possible to identify several subtle forms of head movement which were sudden, unusual and lacking behavioural relevance (and therefore might fit the definition of the head twitch response). Such behaviours were less frequent in the vehicle-injected controls, even when accounting for their increased time spent asleep (Figure 5.1, leftmost two conditions).

Despite this observed difference between psilocin and control conditions, many of the detected head motions were unlike the commonly reported description of the head twitch as a lateral rotational shake. For example, around half of the identified twitch-like head movements comprised a single forward jerk of the neck, often also involving movement in the shoulder area. Furthermore, the rate of detected head twitches, even when including the unusual head movements, resulted in an approximately three-fold lower head twitch rate compared to existing reports (Halberstadt et al. 2011).

Further behavioural observation experiments were performed under slight variations in conditions, aiming to identify possible factors that might be limiting the efficacy of the drug, as measured through the head twitch response. Owing to the large possible parameter space, just a few animals were tested in each condition. The aim was not to thoroughly characterise factors that might affect the psilocin-induced HTR, but rather to establish that there was no likely methodological choice or environmental condition drastically attenuating the action of psilocin in the electrophysiological experiments.

It was observed that the more traditional head shakes typically occurred while the animal was ambulating, whereas atypical neck extension twitches occurred while the animal was adopting a resting position. Therefore, one possible explanation for the observed atypical head twitch response might arise from the tendency of these animals to spend most of their time post injection curled up inside their nest; the altered posture leading to an unusual movement. Indeed, previous studies which reported the head twitch response did so with mice placed in a testing cage, a novel environment which stimulates

wakefulness and exploration, rather than the home cage.

Two mice were administered psilocin at 2 mg/kg as before and observed outside their home cage. The overall frequency of head twitches was not clearly changed (Figure 5.1) and neither was the contribution of the two types of head twitch. An additional two mice were administered psilocin at a higher dose of 5 mg/kg, resulting in only a modest increase in the HTR (Figure 5.1) which included both types of twitch.

It was additionally hypothesised that the low HTR might occur due to incomplete dissolving of the psilocin in the tartaric acid vehicle. Instead, a psilocin solution was prepared using DMSO as an alternative solvent. Indeed, the psilocin dissolved more quickly in DMSO, without requiring physical vortexing. In a subsequent experiment, three mice were injected with psilocin (2 mg/kg) prepared using the DMSO vehicle. There was a small reduction in the observed HTR (Figure 5.1). Interestingly however, all of these twitches were of the classic lateral rotational type. Speculatively, this could be because these animals were more active, possibly owing to the pain or discomfort that DMSO injection is known to cause rodents and which was visible in their behaviour.

Finally, the head twitch response was tested in response to DOI, a 5-HT_{2A} receptor agonist whose behavioural effects are more thoroughly characterised in comparison with psilocin and which is known to evoke archetypical head twitches in rodents. Indeed, DOI evoked head twitches were more easily identifiable and a higher HTR rate was observed (Figure 5.1) which were exclusively of the traditional lateral type.

5.3.2 Electrophysiological recordings were obtained under psilocin

Stable high quality electrophysiological recordings were obtained from 8 mice over a recording period of 11 days. Of these 8 animals, EEG recordings were successfully obtained from 7, multi-unit spiking activity from 7, and local field potentials from 6. All signals were obtained simultaneously from 5 animals.

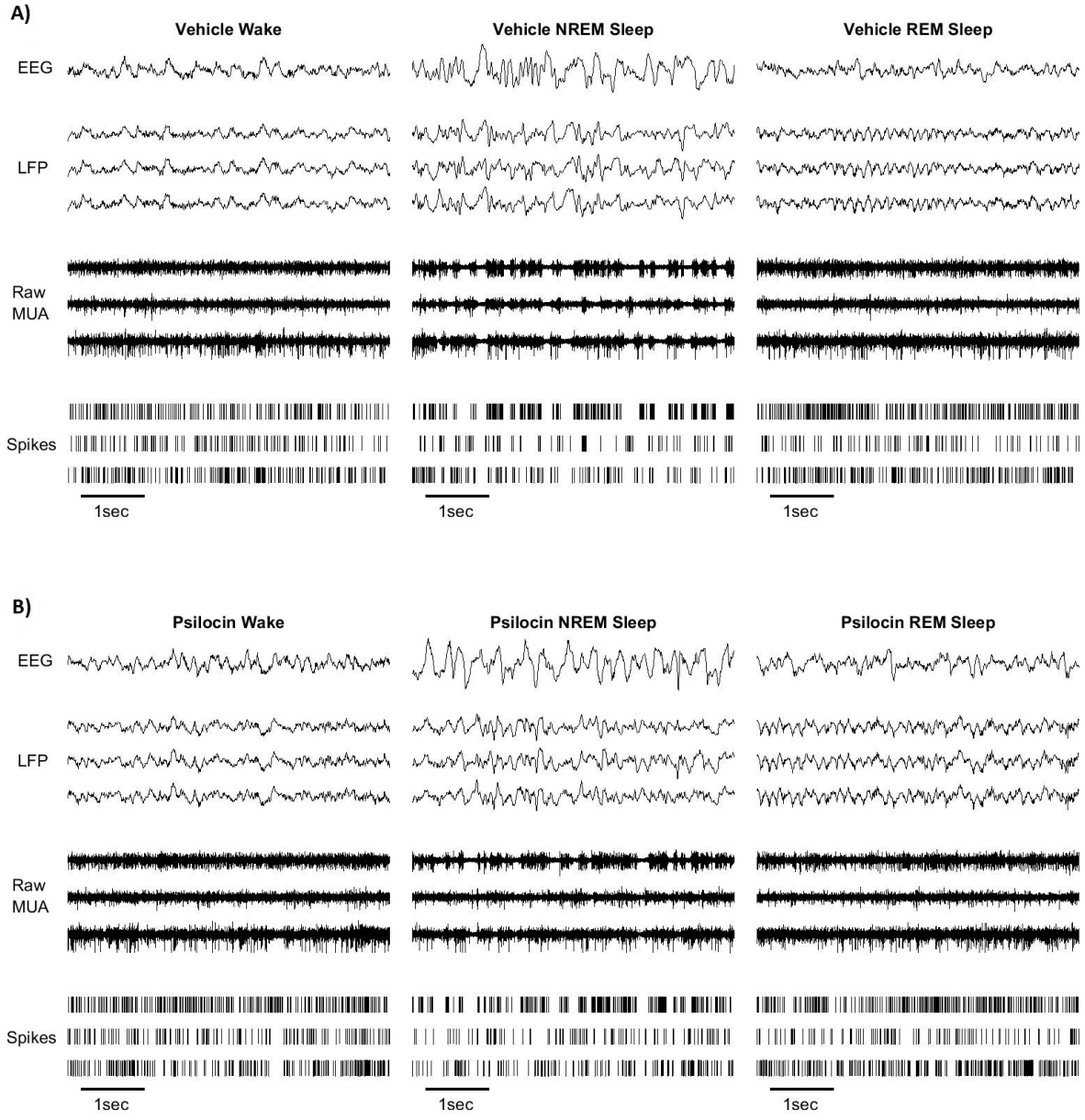


Figure 5.2: An example of frontal electroencephalogram (EEG), 3 medial prefrontal cortical (mPFC) local field potentials (LFP), corresponding raw signal with multi-unit activity (MUA) and detected spikes in representative segments of waking, NREM and REM sleep, soon after **A)** injection with vehicle solution, **B)** injection with psilocin.

Sleep-wake related electrophysiological activity was as expected. Wake was characterised by low amplitude irregular EEG and LFP signals alongside asynchronous high frequency multi-unit spiking. In contrast, NREM sleep was identifiable by the presence of high amplitude EEG and LFP slow waves coincident with synchronous spiking multi-unit off periods. REM sleep periods were identifiable by a reduced slow wave activity, increased theta power and readily distinguishable from waking by low EMG levels and sleep-wake context. Psilocin injection did not change the essential features of electrophysiological signals in wake, NREM or REM sleep in a way that was immediately visually identifiable (Figure 5.2).

5.3.3 Sleep is acutely destabilised & fragmented after psilocin

In one experimental condition, the mice were left undisturbed immediately after injection with either a 2 mg/kg dose of psilocin or the tartaric acid vehicle, in order to study spontaneous sleep-wake architecture. The animals were, of course, necessarily awakened by the intraperitoneal injection procedure. The most behaviourally striking effect of the psilocin was to disrupt the animals' first attempts at initiating sleep. When affected by the drug, as in the pilot experiments, the mice spent a significant amount of time in their nests, adopting a posture compatible with sleep, but while apparently awake according to electrophysiological criteria. Rest in these psilocin-affected animals was frequently disturbed by small body movements, such as stretches and readjustments of posture, and often the eyes remained open even while motionless. Analysis of this period using electrophysiological criteria for sleep-wake definition suggested that the animals were rapidly alternating between short wake and shallow NREM sleep bouts (Figure 5.3).

The average latency from the time of injection to the first epoch scored as NREM sleep, based on electrophysiological criteria, was 18.6 $\pm$ 6.1 minutes in the vehicle condition and 26.3 $\pm$ 4.5 minutes in the psilocin animals, which was not significantly different between

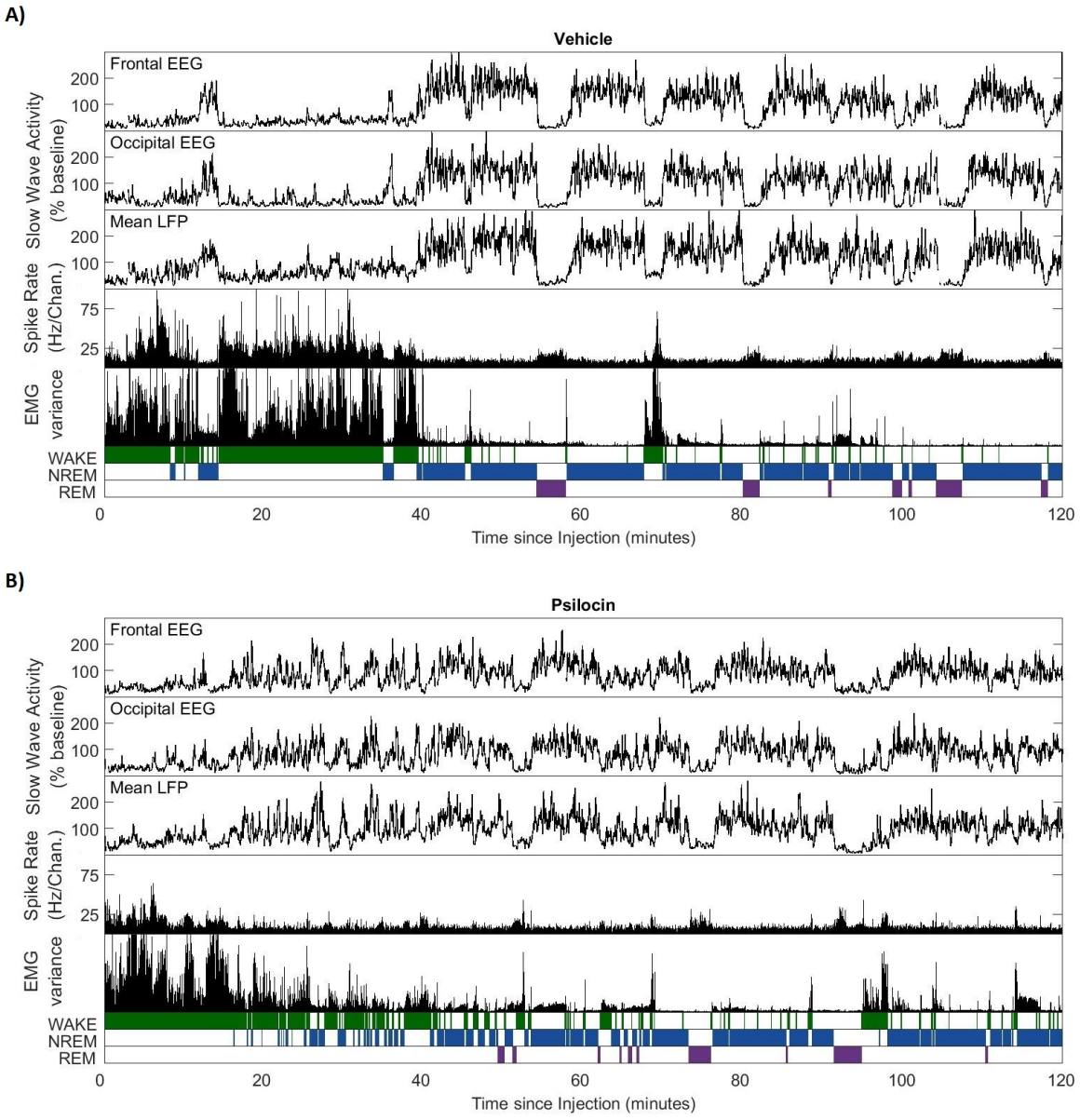


Figure 5.3: Slow wave activity (0.5 - 4 Hz power) derived from frontal electroencephalogram (EEG), occipital EEG, and averaged local field potential (LFP), alongside the total recorded spike firing rate (spikes per second per channel), variance of the electromyogram (EMG) and scored vigilance states, all with a resolution of 4 seconds over a period of 2 hours after **A)** injection with vehicle solution, **B)** injection with psilocin in the undisturbed condition.

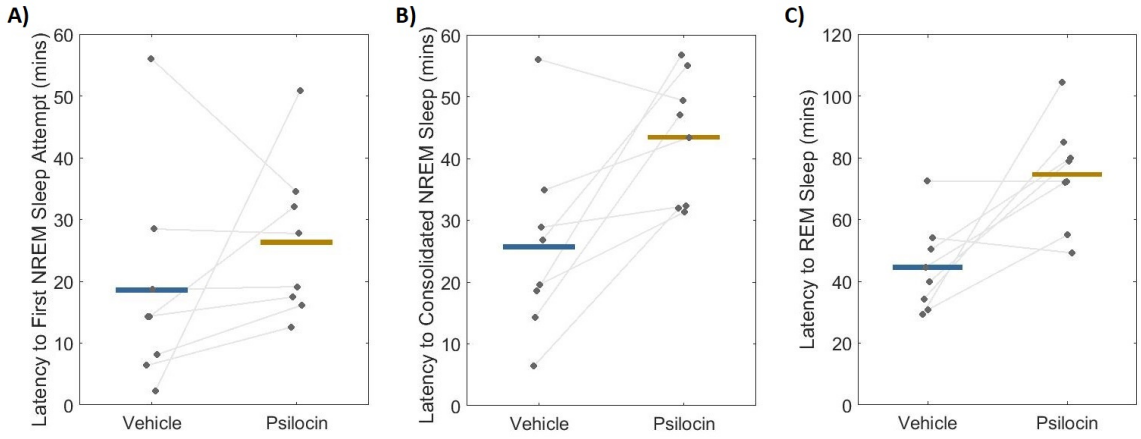


Figure 5.4: Latency in minutes from the time of injection until **A)** the first 4-second epoch scored as NREM sleep, **B)** the start of the first episode of NREM sleep at least 1-minute duration, and **C)** the first 4-second epoch scored as REM sleep, in each animal after injection with vehicle (blue) and with psilocin (yellow). Grey lines link values derived from the same animal and coloured lines denote the group mean.

conditions ($p = 0.30$, $n = 8$, paired t-test) (Figure 5.4A). However, the mean latency to the first NREM sleep episode, defined as continuous NREM sleep of at least 1 minute duration, was 25.7 ± 5.4 minutes in vehicle animals compared to 43.4 ± 3.7 minutes in animals affected by psilocin, a significant difference ($p = 0.015$, $n = 8$, paired t-test) (Figure 5.4B). Similarly, the latency to the initiation of any REM sleep was increased by psilocin also, from an average of 44.5 ± 5.1 minutes in vehicle condition to 74.6 ± 6.1 minutes in the psilocin condition ($p = 0.013$, $n = 8$, paired t-test) (Figure 5.4C).

In the three hours following injection, psilocin significantly increased the average proportion of time spent awake (Vehicle: 30.8 ± 2.0%, Psilocin: 44.3 ± 3.4%, $p = 6.8 \times 10^{-4}$, $n = 8$, paired t-test), and correspondingly significantly decreased the time spent in NREM (Vehicle: 59.7 ± 1.7%, Psilocin: 50.6 ± 2.9%, $p = 0.0011$, $n = 8$, paired t-test), and REM sleep (Vehicle: 9.4 ± 0.5%, Psilocin: 5.1 ± 0.8%, $p = 0.0012$, $n = 8$, paired t-test) (Figure 5.5A). Interestingly, from the first sleep attempt until 3 hours after injection, the average duration of wake episodes was unchanged (Vehicle: 28.8 ± 4.5 secs, Psilocin: 29.8 ± 3.1 secs, $p = 0.89$, paired t-test), whereas episode duration was significantly reduced in both NREM (Vehicle: 93.6 ± 12.9 seconds, Psilocin: 50.0 ± 2.6

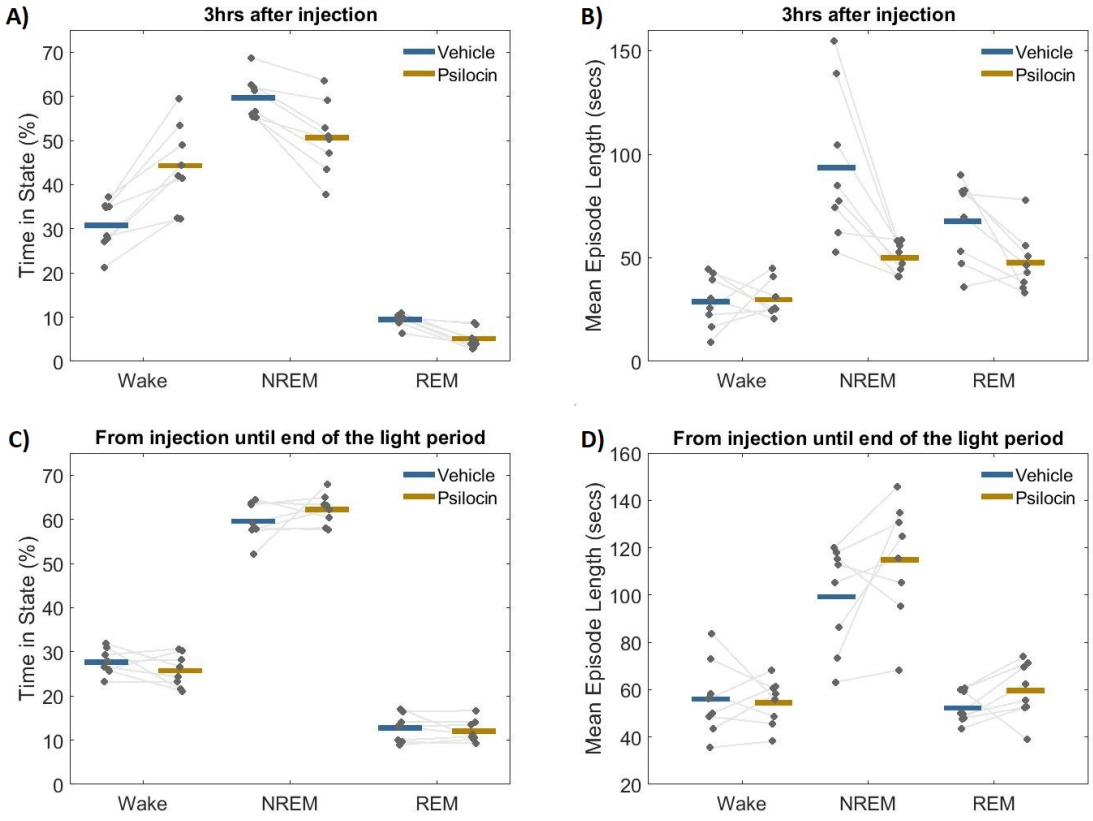


Figure 5.5: A) Total percentage of time and **B)** mean duration of continuous episodes of wake, NREM and REM sleep in the three hours following injection with vehicle (blue) and with psilocin (yellow). **C)** Total percentage of time and **D)** mean duration of continuous episodes of wake, NREM and REM sleep following injection with vehicle (blue) and with psilocin (yellow) until the end of the light period. Grey lines link values derived from the same animal and coloured lines denote the group mean.

seconds, p = 0.0070 paired t-test) and REM sleep (Vehicle: 67.7 ± 7.0 secs, Psilocin: 47.6 ± 5.1 seconds, p = 0.019) (Figure 5.5B). This suggests that the increased wakefulness resulting from the psilocin is due to an increased drive to awaken from NREM sleep, corresponding to an impairment of NREM sleep maintenance rather than an enhanced stability of wakefulness. Interestingly, there was no significant change in the percentage of REM episodes in this time period that transitioned to wakefulness, rather than NREM sleep (Vehicle: 32.8 ± 4.6%, Psilocin: 45.9 ± 6.4%, p = 0.19, n = 8, paired t-test).

5.3.4 Long-term sleep-wake architecture is unaffected by psilocin

From three hours after injection until the end of the light period, the total fraction of time spent in each vigilance state was not significantly different between psilocin and vehicle conditions (Wake: $p = 0.25$, NREM: $p = 0.24$, REM: $p = 0.42$, $n = 8$, paired t-test) (Figure 5.5C) and the average duration of wake, NREM and REM sleep episodes was unchanged (Wake: $p = 0.79$, NREM: $p = 0.13$, REM: $p = 0.13$, $n = 8$, paired t-test) (Figure 5.5D). Similarly, the quantity of wake, NREM and REM sleep was not different in the dark period after injection (Wake: $p = 0.50$, NREM: $p = 0.92$, REM: $p = 0.07$, $n = 4$, paired t-test).

The hour-by-hour distribution of wake, NREM and REM sleep averaged over animals for 24 hours after injection is shown in Figure 5.6A-C. A clear light-dark cycle is evident, in which animals are awake more throughout the dark phase, particularly during its first half (beginning between 11 and 12 hours after injection). Overall, there is no striking change in sleep-wake architecture due to psilocin, except for the increase in wake and suppression of NREM and REM sleep in the first few hours. Importantly, there is no specific time point following the acute suppression of sleep at which a rebound in NREM or REM sleep is evident. The cumulative time courses of the proportion of time spent in wake, NREM and REM sleep (Figure 5.6D-F) do suggest, however, that homeostasis of vigilance state quantity is restored within one day.

To investigate potential enduring effects of psilocin on sleep-wake architecture, REM sleep was compared between the baseline day before and recovery day after all psilocin injections. There were no differences between the undisturbed and sleep deprivation conditions and so these two populations were pooled for statistical analysis (Figure 5.7). No changes were found in total REM sleep amount ($p = 0.78$, $n = 12$, paired t-test), number of REM sleep episodes ($p = 0.69$, $n = 12$, paired t-test) nor mean duration of REM sleep episodes ($p = 0.93$, $n = 12$, paired t-test).

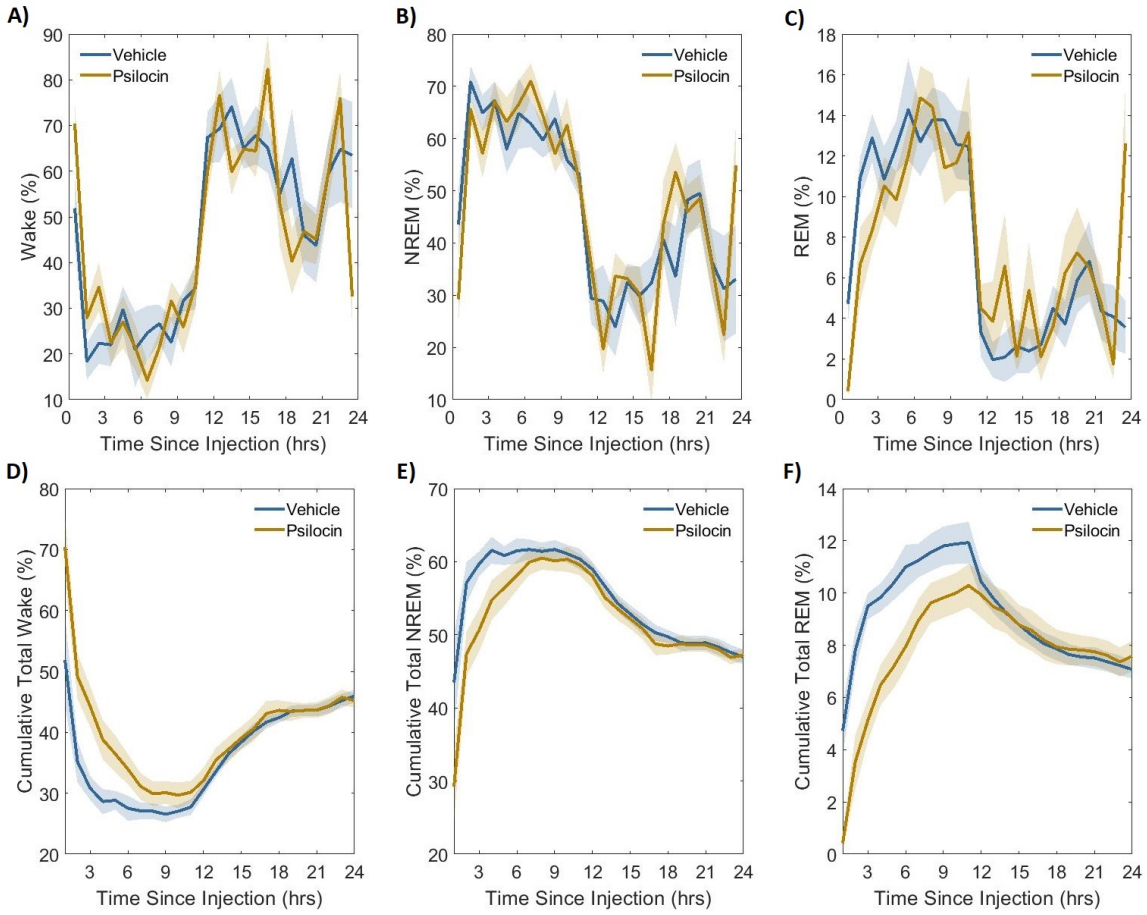


Figure 5.6: Percentage of time scored as **A)** wake, **B)** NREM sleep and **C)** REM sleep in successive non-overlapping windows of one hour up to 24 hours after injection with vehicle (blue) and with psilocin (yellow). The total percentage of time scored as **D)** wake, **E)** NREM sleep and **F)** REM sleep from injection until up to 24 hours after injection with vehicle (blue) and with psilocin (yellow) as a function of time since injection. Lines denote the mean and coloured sections the standard deviation over all animals.

5.3.5 Psilocin acutely enhances 3 - 5 Hz field potential power

The neuronal activity in wake, NREM and REM sleep after psilocin was investigated by first looking at averaged power in EEG and LFP signals within specific time windows after psilocin and vehicle injection (see Methods).

Figure 5.8A shows the averaged power spectra obtained from frontal EEG in baseline wake, the initial wake period after vehicle injection, the initial wake after psilocin injection, the subsequent wake periods after psilocin while the animal is attempting to sleep (termed

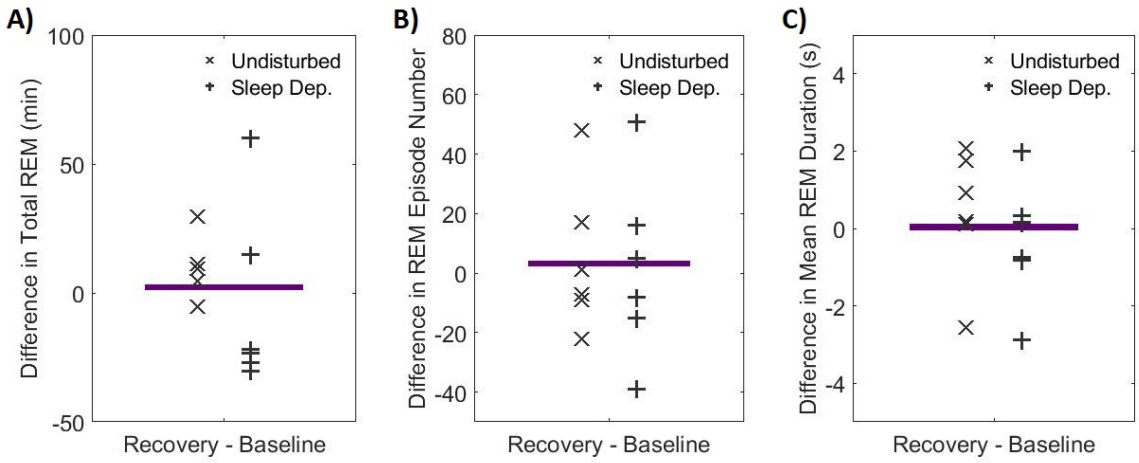


Figure 5.7: The difference in **A)** the total quantity of time scored as REM sleep in minutes, **B)** the number of REM sleep episodes, and **C)** the mean duration of REM sleep episodes in seconds, calculated over 24 hours between the day following and the day preceding injection with psilocin (recovery day minus baseline day). Crosses correspond to days around the undisturbed injection condition and pluses to days before vs. after the sleep deprivation condition. The coloured line denotes the group mean.

transitional wake), and the wake after the first extended sleep episode after psilocin. Figure 5.8B shows the same for the LFP. In all cases, wake spectra were characterised by a peak around 4 Hz, and corresponding band power around 3 - 5 Hz, which is noticeably increased after psilocin injection. Changes in average spectral power relative to baseline were statistically compared across time windows within four specific frequency bands, which were chosen based on the average spectra. Time period had a significant effect in both EEG and LFP on power in the 3 - 5 Hz range (EEG: $F_{3,18} = 28.9$, p = 4.2×10^{-7}; LFP: $F_{3,15} = 18.6$, p = 2.5×10^{-5}; two-way ANOVA), on lower delta frequencies 1 - 3 Hz (EEG: $F_{3,18} = 4.7$, p = 0.013; LFP: $F_{3,15} = 5.3$, p = 0.011), on theta frequencies 5 - 9 Hz (EEG: $F_{3,18} = 7.4$, p = 0.0019; LFP: $F_{3,15} = 4.6$, p = 0.019; two-way ANOVA), and on gamma frequencies 30 - 70 Hz (EEG: $F_{3,18} = 24.2$, p = 1.6e-6; LFP: $F_{3,15} = 25.3$, p = 4.1×10^{-6}; two-way ANOVA).

Post-hoc tests identified that, in the period of initial wake immediately after psilocin, it is only 3 - 5 Hz band power in frontal EEG that is significantly higher compared to vehicle controls (Figure 5.8A). Most significant differences were found during the transitional

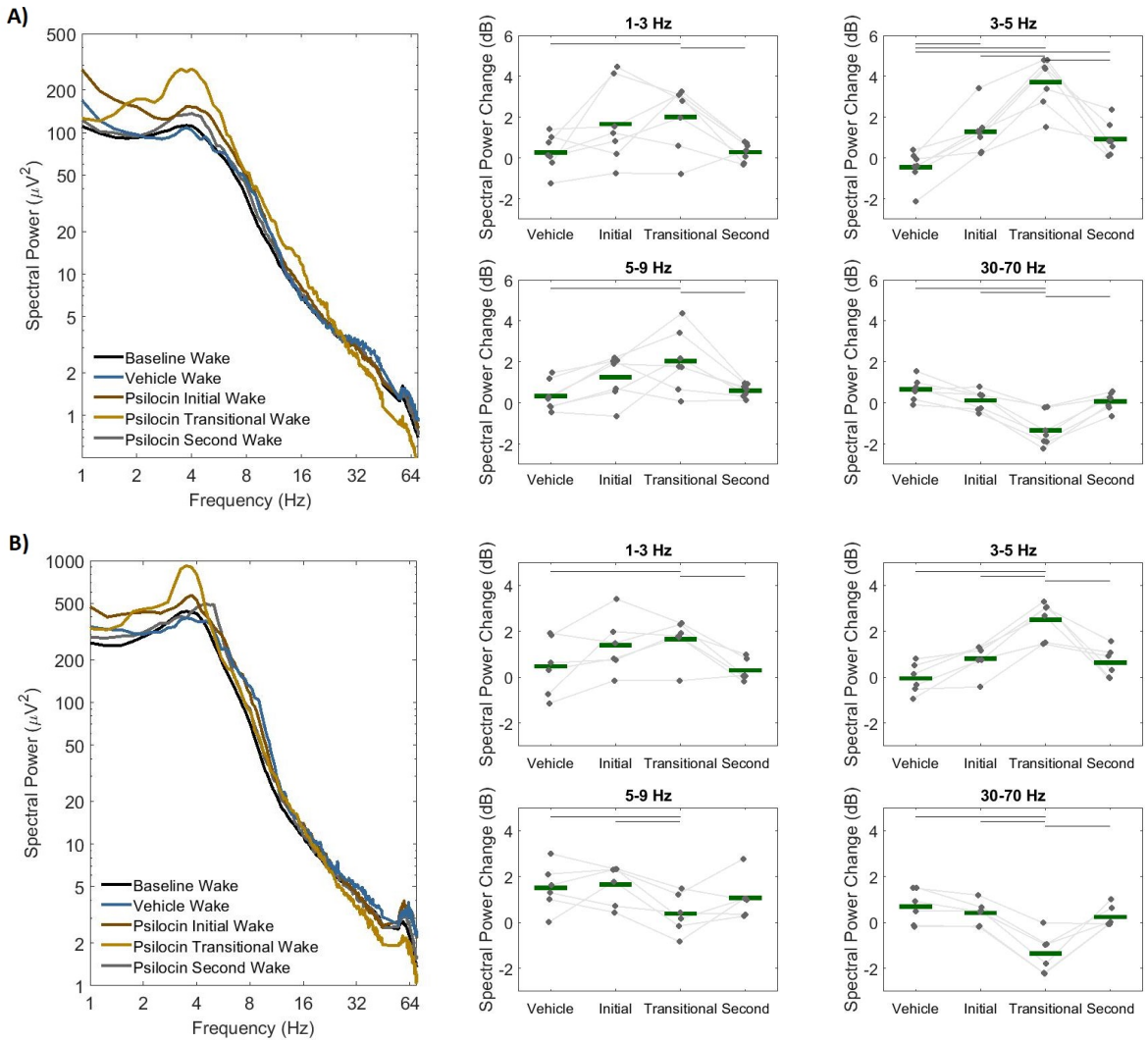


Figure 5.8: Left: Average spectral power in the **A)** frontal EEG and **B)** mean LFP during wakefulness in the baseline day (black), after vehicle injection until first NREM sleep (blue), after psilocin injection until first NREM sleep (brown), from the first NREM sleep after psilocin injection until the first NREM sleep episode at least 1 minute duration (yellow), from the first wakefulness after the initial sleep period after psilocin until the second period of consolidated sleep (grey). Spectra correspond to the mean averaged over animals. Right: Change in spectral power in decibels relative to baseline within specified frequency bands for the aforementioned conditions. Grey lines link values derived from the same animal and coloured lines denote the group mean. Black lines link conditions which are significantly different according to a Tukey post-hoc test.

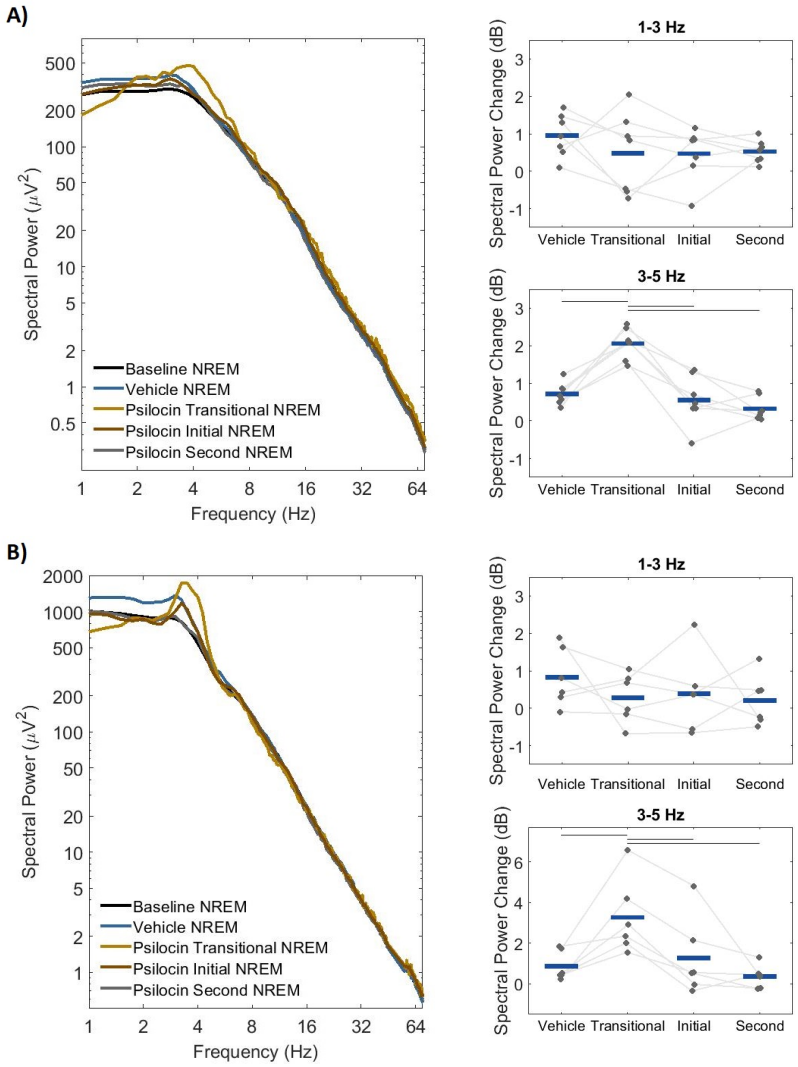


Figure 5.9: Left: Average spectral power in the **A)** frontal EEG and **B)** mean LFP during NREM sleep in the baseline day (black), after vehicle injection (blue), between the first NREM sleep attempt and the first NREM sleep episode at least 1 minute duration after psilocin injection (yellow), from the first episode of NREM sleep at least 1 minute duration after psilocin injection until subsequent wakefulness (brown), from the end of the second wake period after psilocin until subsequent wakefulness (grey). Spectra correspond to the mean averaged over animals. Right: Change in spectral power in decibels relative to baseline within specified frequency bands for the aforementioned conditions. Grey lines link values derived from the same animal and coloured lines denote the group mean. Black lines link conditions which are significantly different according to a Tukey post-hoc test.

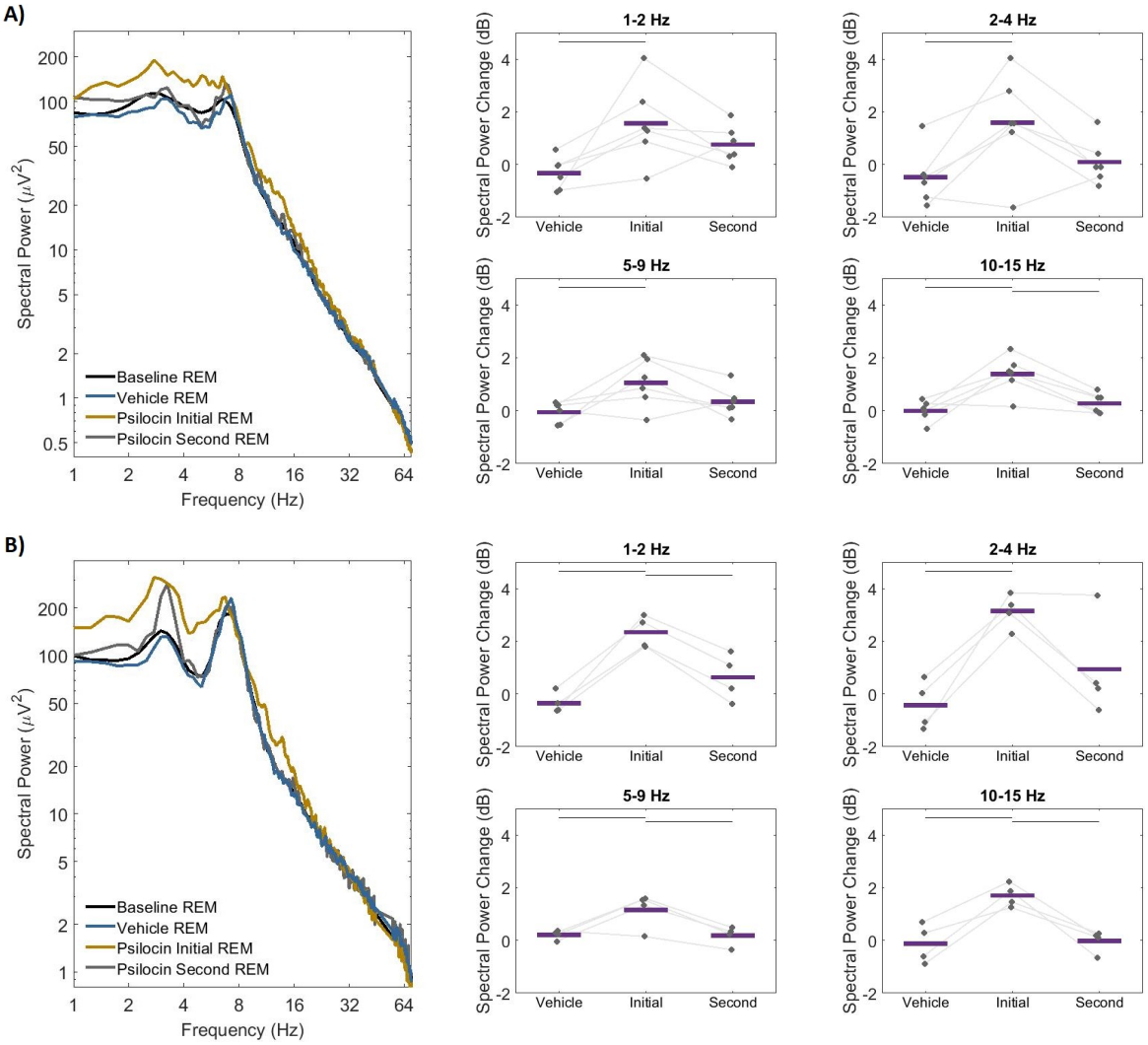


Figure 5.10: Left: Average spectral power in the **A)** frontal EEG and **B)** mean LFP during REM sleep in the baseline day (black), after vehicle injection (blue), in the first period of consolidated sleep after psilocin injection (yellow), in the second period of consolidated sleep after psilocin injection (grey). Spectra correspond to the mean averaged over animals. Right: Change in spectral power in decibels relative to baseline within specified frequency bands for the aforementioned conditions. Grey lines link values derived from the same animal and coloured lines denote the group mean. Black lines link conditions which are significantly different according to a Tukey post-hoc test.

period, while the animal was attempting to sleep but making frequent awakenings. Again, 3 - 5 Hz power is further enhanced, and now is significantly different from vehicle in the LFP also. Furthermore, gamma band power is significantly suppressed. There is some evidence of increased delta power in both signals, increased theta in the EEG and decreased theta in the LFP. During the second wake period, after sustained sleep is achieved, the signals return to more closely resemble vehicle and baseline conditions; only the EEG 3 - 5 Hz power remains significantly higher than vehicle.

Figure 5.9 shows the power spectra obtained during NREM sleep in EEG and LFP signals. There was again evidence of a 3 - 5 Hz peak, which was significantly affected by time period (EEG: $F_{3,18} = 29.4$, p = 3.8×10^{-7}; LFP: $F_{3,15} = 8.3$, p = 0.0018; two-way ANOVA), but this was only pronounced, and statistically significant according to post-hoc analysis, during the transitional period where NREM sleep is shallow and fragmentary, not during subsequent consolidated sleep (Figure 5.9A). This was equally true at EEG and LFP levels. Delta power in the 1 - 3 Hz range during NREM sleep was not significantly different between time periods (EEG: $F_{3,18} = 1.1$, p = 0.38; LFP: $F_{3,15} = 0.7$, p = 0.55; two-way ANOVA).

Figure 5.10 shows the power spectra obtained during REM sleep. Baseline REM spectra were characterised by clear peaks in the upper delta (2 - 4 Hz) and theta (5 - 9 Hz) range. Time period had a significant effect in both EEG and LFP on power in the lower delta 1 - 2 Hz (EEG: $F_{2,10} = 5.5$, p = 0.024; LFP: $F_{2,6} = 34.1$, p = 5.3×10^{-4}; two-way ANOVA), upper delta 2 - 4 Hz (EEG: $F_{2,10} = 6.3$, p = 0.017; LFP: $F_{2,6} = 8.2$, p = 0.019; two-way ANOVA), theta 5 - 9 Hz (EEG: $F_{2,10} = 5.1$, p = 0.029; LFP: $F_{2,6} = 7.7$, p = 0.022; two-way ANOVA). Notably also, a possible difference was apparent in the spindle frequency range 10 - 15 Hz, which was significant (EEG: $F_{2,10} = 13.3$, p = 0.0015; LFP: $F_{2,6} = 17.2$, p = 0.0033; two-way ANOVA). Post-hoc tests revealed that these differences were significantly different from vehicle during REM in the initial sleep period after psilocin, not the second sleep episode. Spindles and delta frequencies are characteristic of NREM sleep, suggesting a blending of NREM activities into REM sleep.

5.3.6 Multi-unit firing rates are acutely reduced by psilocin during undisturbed wakefulness

Changes in multi-unit firing rates, relative to baseline and averaged over channels, were obtained for the different time windows of analysis in wake, NREM and REM sleep. There was a significant effect of wake time window on firing rate ($F_{3,15} = 14.5$, p = 1.1×10^{-4}; two-way ANOVA). Firing rate was overall reduced compared to vehicle during the initial wake period after psilocin injection, and also during wake in the transitional period, then returned to baseline during the second wake period (Figure 5.11). There was no significant effect of psilocin found on multi-unit spike rates during NREM sleep ($F_{3,15} = 2.9$, p = 0.073; two-way ANOVA) or REM sleep ($F_{2,8} = 1.0$, p = 0.41; two-way ANOVA) (Figure 5.11). To determine whether this change was robust, firing rates were also examined in the sleep deprivation condition, finding no significant difference in the 30 minutes after injection in vehicle and psilocin conditions ($F_{3,15} = 0.9$; p = 0.46; two-way ANOVA).

5.3.7 Psilocin does not influence the sleep homeostatic process

The effects of psilocin on Process S in the spontaneous condition are not straightforward to assess; the acute effects on arousal and neuronal oscillations complicate the interpretation of NREM slow wave activity, and hence Process S was explored after sleep deprivation. In this second experimental condition, mice were injected as before at light onset with either 2 mg/kg psilocin or the tartaric acid vehicle, and then kept awake for 4 hours, through a combination of gentle handling and novel object presentation. The aim was to investigate how psilocin might alter neuronal activity during a period of active wakefulness in which behaviour was similar between drug and control conditions, and crucially to determine whether the sleep homeostatic process was in any way changed by exposure to a 5-HT_{2A} receptor agonist. Indeed, behaviour was not strikingly different, and based on subjective observation, psilocin-affected mice were judged to engage with novel objects approximately

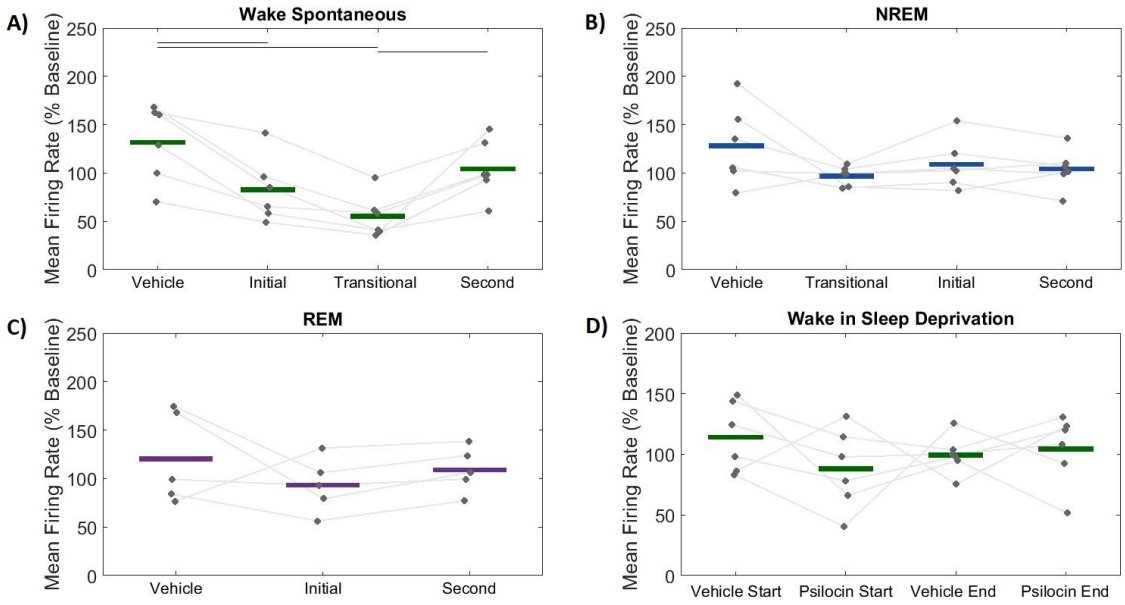


Figure 5.11: Mean firing rate (normalised by expression as a percentage of mean firing rate over baseline) in the period **A)** after vehicle injection until first NREM sleep (Vehicle), after psilocin injection until first NREM sleep (Initial), from the first NREM sleep after psilocin injection until the first NREM sleep episode at least 1 minute duration (Transitional), from the first wakefulness after consolidated sleep after psilocin until the second period of consolidated sleep (Second), **B)** after vehicle injection (Vehicle), between first NREM sleep attempt and first NREM sleep episode at least 1 minute duration after psilocin injection (Transitional), from the first episode of NREM sleep at least 1 minute duration after psilocin injection until subsequent wakefulness (Initial), from the end of the second wake period after psilocin injection until subsequent wakefulness (Second), **C)** after vehicle injection (Vehicle), in the first period of consolidated sleep after psilocin injection (Initial), in the second period of consolidated sleep after psilocin injection (Second), **D)** in the 30 minutes of sleep deprivation after injection with vehicle (Vehicle Start) and psilocin (Psilocin Start), and in the last 30 minutes of sleep deprivation with vehicle (Vehicle End) and psilocin (Psilocin End). Grey lines link values derived from the same animal and coloured lines denote the group mean. Black lines link conditions which are significantly different according to a Tukey post-hoc test.

as much as vehicle injected controls. The time course of EEG and average LFP slow wave activity alongside neuronal spiking and EMG activity under both injection types is shown for one representative example animal in Figure 5.12. Increased SWA is clear in the initial NREM period following the 4 hours of sleep deprivation, particularly in the EEG, and there is no obvious difference in the psilocin condition.

Figure 5.13 shows frontal EEG and mean LFP power spectra obtained by averaging

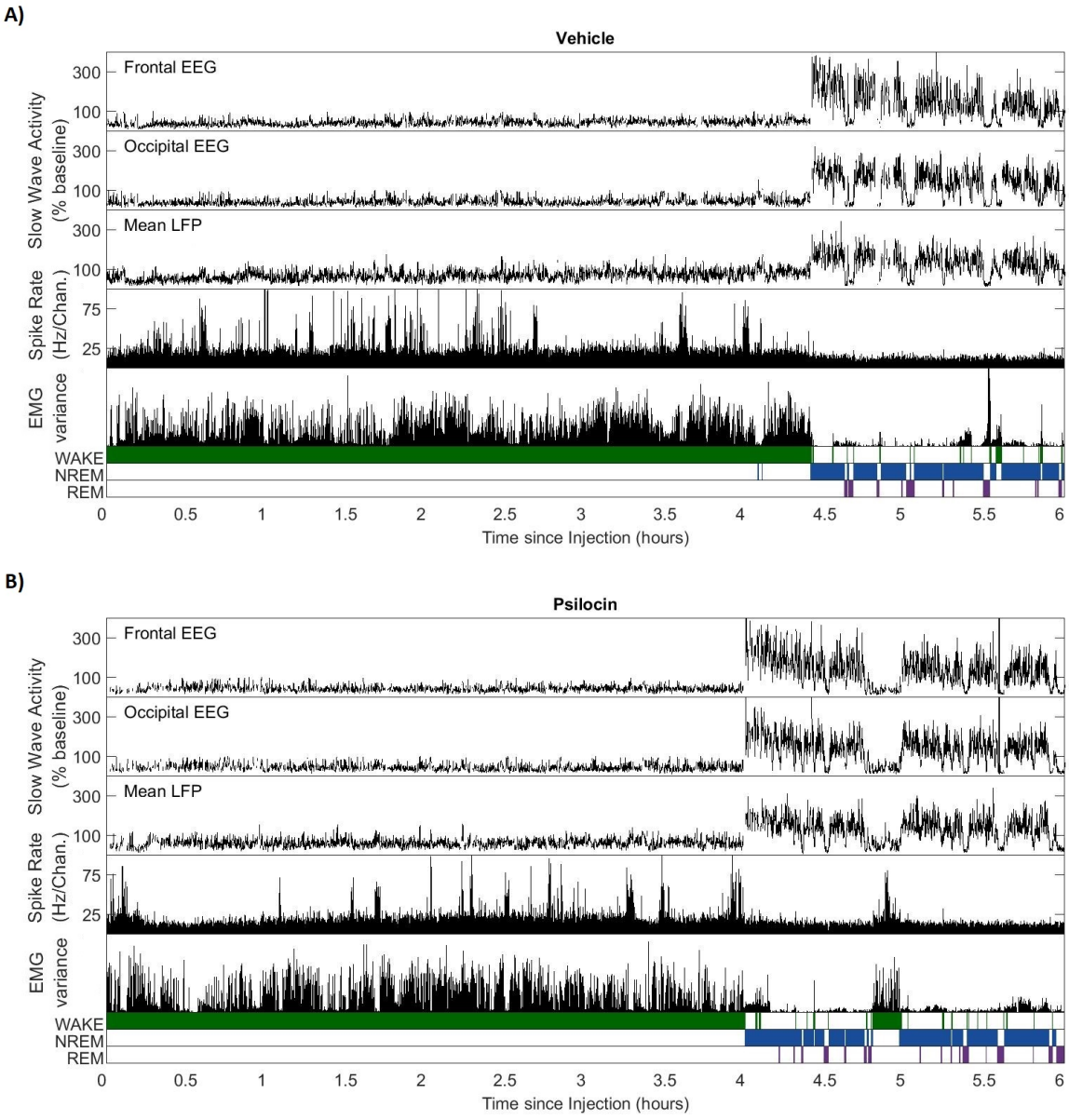


Figure 5.12: Slow wave activity (0.5-4 Hz power) derived from frontal electroencephalogram (EEG), occipital EEG, and averaged local field potential (LFP), alongside the total recorded spike firing rate (spikes per second per channel), variance of the electromyogram (EMG) and scored vigilance states, all with a resolution of 4 seconds over a period of 6 hours after **A)** injection with vehicle solution, **B)** injection with psilocin in the sleep deprivation condition.

over the 30 minutes following injection (start of sleep deprivation) and 30 minutes prior to sleep (end of sleep deprivation) in both vehicle and psilocin conditions alongside spectra derived from wake in the baseline day. The 3 - 5 Hz peak found previously was less pronounced, except in the frontal EEG during the psilocin condition at the start of sleep deprivation. Time period had a significant effect on 3 - 5 Hz power (EEG: $F_{3,15} = 3.6$, $p = 0.037$; LFP: $F_{3,15} = 18.8$, $p = 2.4 \times 10^{-5}$; two-way ANOVA) and also on lower delta 1 - 3 Hz power (EEG: $F_{3,15} = 5.1$, $p = 0.013$; LFP: $F_{3,15} = 5.9$, $p = 0.0073$; two-way ANOVA) in both signals. Post-hoc comparison suggests that this is due to power increases from start to the end of sleep deprivation, in both conditions in the LFP and only with vehicle in the EEG, but not differences as a result of the drug. There was no effect of time window on theta frequencies 5 - 9 Hz (EEG: $F_{3,15} = 3.5$, $p = 0.042$; LFP: $F_{3,15} = 2.4$, $p = 0.10$; two-way ANOVA), or gamma frequencies 30 - 70 Hz in the EEG ($F_{3,15} = 0.4$, $p = 0.73$). A weakly significant effect was obtained for gamma in the LFP (LFP: $F_{3,15} = 14.4$, $p = 1.1 \times 10^{-4}$; two-way ANOVA), however this was only evident in post-hoc tests between early sleep deprivation after psilocin and late sleep deprivation in the vehicle condition, so is not clearly interpretable.

Figure 5.14 show spectra derived from both frontal EEG and mean LFP during the initial NREM sleep after sleep deprivation, and in the subsequent second episode of NREM sleep (separated by the first by at least 5 minutes of spontaneous wake). Delta power 1 - 4 Hz was clearly higher in initial sleep than baseline or in later second sleep (EEG: $F_{3,15} = 92.9$, $p = 6.5 \times 10^{-10}$; LFP: $F_{3,15} = 47.7$, $p = 6.6 \times 10^{-8}$; two-way ANOVA). Post-hoc differences identified only increases in delta power due to sleep deprivation, with no differences in this effect between psilocin and vehicle conditions.

Despite an absence of evidence for gross spectral changes during NREM sleep after sleep deprivation between vehicle and psilocin conditions, a weak trend was present for higher slow frequencies after psilocin, at least in the EEG. To investigate the sleep homeostatic process more specifically, the maximum SWA after sleep deprivation was

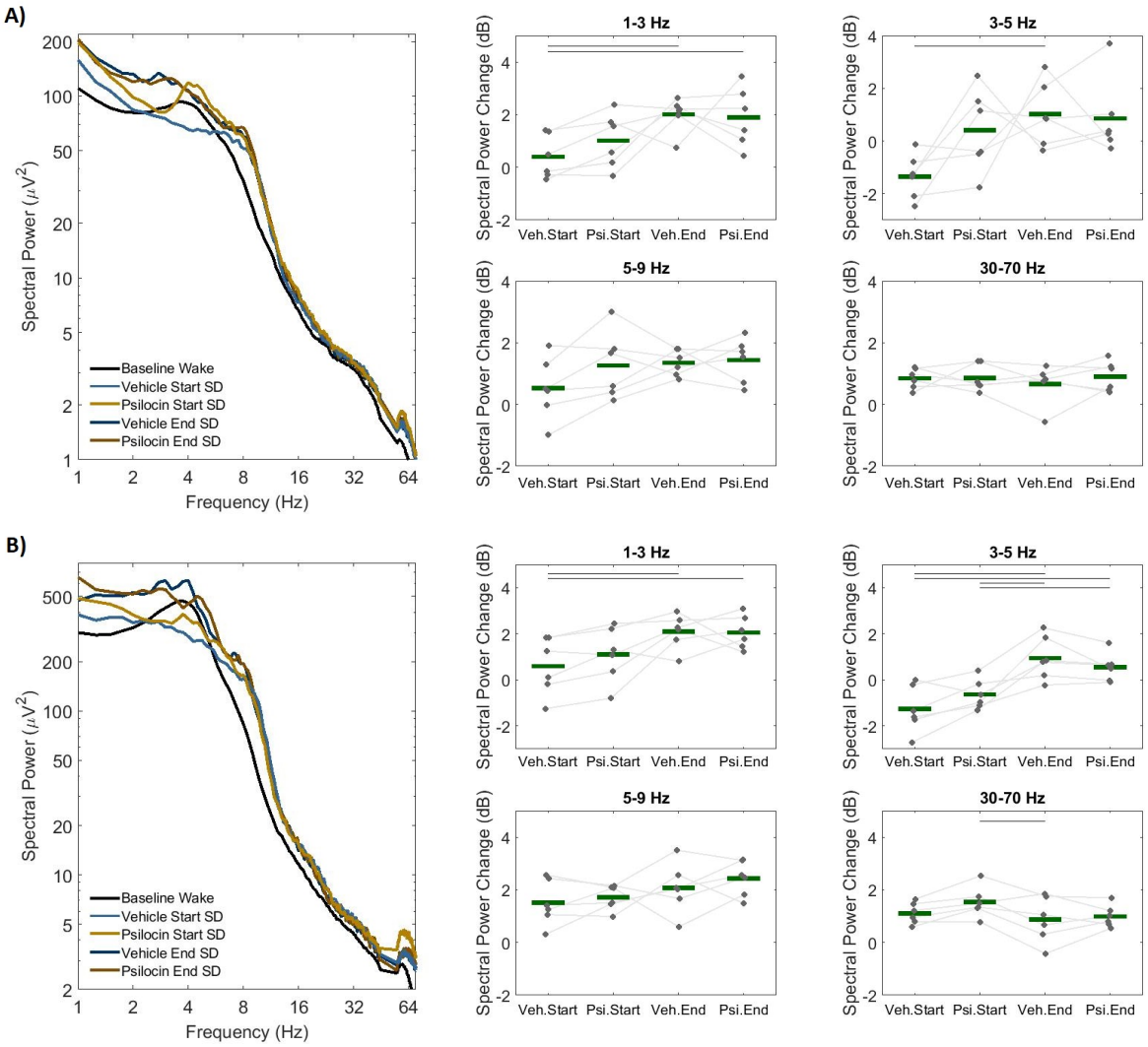


Figure 5.13: Left: Average spectral power in the **A)** frontal EEG and **B)** mean LFP during wakefulness in the baseline day (black), for 30 minutes after vehicle injection (light blue), for 30 minutes after psilocin injection (yellow), in the 30 minutes before the end of sleep deprivation after vehicle injection (dark blue), in the 30 minutes before the end of sleep deprivation after psilocin injection (brown). Spectra correspond to the mean averaged over animals. Right: Change in spectral power in decibels relative to baseline within specified frequency bands for the aforementioned conditions. Grey lines link values derived from the same animal and coloured lines denote the group mean. Black lines link conditions which are significantly different according to a Tukey post-hoc test.

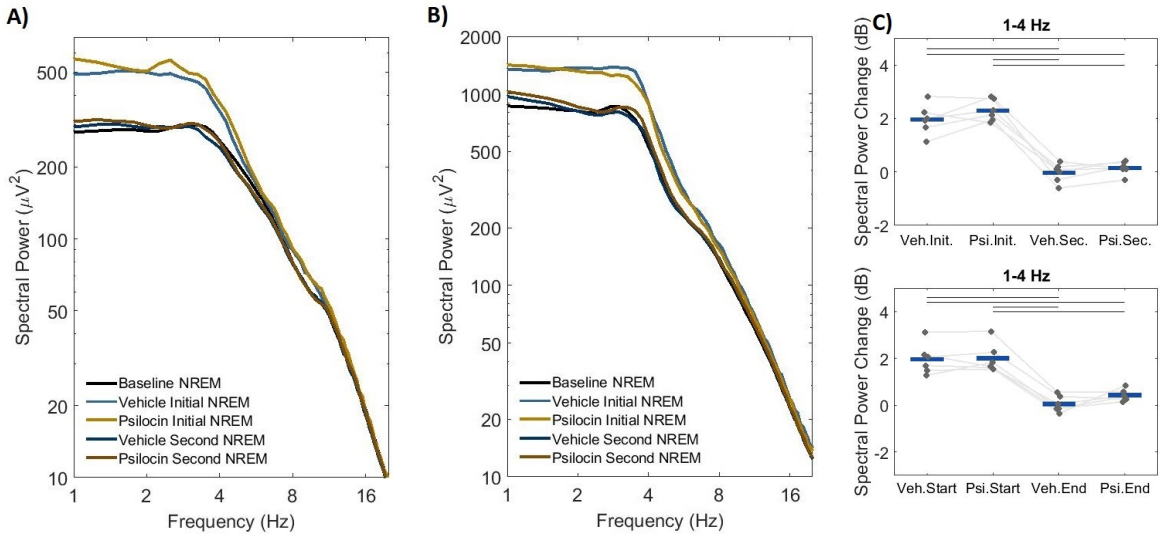


Figure 5.14: Average spectral power in the **A)** frontal EEG and **B)** mean LFP during NREM sleep in the baseline day (black), in the first period of sleep after vehicle injection (light blue), in the first period of sleep after psilocin injection (yellow), in the second period of sleep after vehicle injection (dark blue), in the second period of sleep after psilocin injection (brown). Spectra correspond to the mean averaged over animals. **C)** Change in spectral power in decibels relative to baseline within specified frequency bands for the aforementioned conditions (EEG above, LFP below). Grey lines link values derived from the same animal and coloured lines denote the group mean. Black lines link conditions which are significantly different according to a Tukey post-hoc test.

obtained in both conditions and compared, expressed as a change in decibels for the EEG and each LFP individual channel (Figure 5.15A). Within the same animal, SWA changes across LFP channels were very similar. The average of these values across mice was not significantly different from zero ($p = 0.90$, $n = 6$, t-test) and neither were values obtained from the frontal EEG ($p = 0.18$, $n = 6$, t-test). Furthermore, the total quantity of sleep (both NREM and REM) in the remainder of the light period after sleep deprivation (8 hours) was not different between vehicle and psilocin conditions ($p = 0.61$, $n = 8$, t-test), further supporting that psilocin did not systematically affect the accumulation of homeostatic sleep pressure (Figure 5.15B).

To further explore possible changes to sleep homeostasis related to psilocin, a simple Process S model was fit to SWA values derived from frontal EEG over the baseline and injection day in both vehicle and psilocin conditions. This model assumes that Process S increases towards an upper asymptote during wakefulness and REM sleep, and decreases

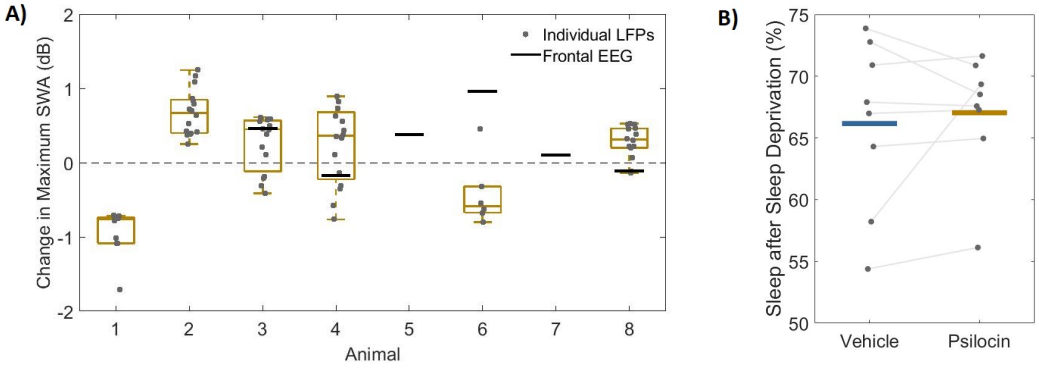


Figure 5.15: A) The change in decibels between vehicle and psilocin conditions in the maximum median level of SWA (0.5-4 Hz power) obtained from a continuous episode of NREM sleep during a 1-hour period after the end of sleep deprivation (positive number is higher in psilocin condition). Points denote single LFP channels from individual animals and their distribution are described by boxplots. Black lines correspond to frontal EEG. **B)** The percentage of time scored as sleep after sleep deprivation until the end of the light period after injection with vehicle (blue) and with psilocin (yellow). Grey lines link values derived from the same animal and coloured lines denote the group mean.

towards a lower asymptote during NREM sleep, where the rates of changes are proportional to the difference between the level of S and the asymptotic value (see chapter 3 for a more detailed description). Here Process S is measured as the median SWA in frontal EEG during an episode of NREM sleep at least 1 minute duration. An example of the fit of such a model to an experiment involving psilocin injection with sleep deprivation is shown in Figure 5.16A, illustrating a high level of agreement. The fit quality of the model, quantified as the median percent absolute difference between empirical SWA and the model, was not different between psilocin and vehicle conditions (Figure 5.16B, $p = 0.75$, $n = 6$, t-test) and neither were median raw error values, suggesting no consistent change in the tendency of the model to over-estimate or under-estimate SWA (Figure 5.16C, $p = 0.25$, $n = 6$, t-test). Similarly, neither the rate of increase parameter α (Figure 5.16D, $p = 0.13$, $n = 6$, t-test), nor the rate of decrease parameter β (Figure 5.16E, $p = 0.25$, $n = 6$, t-test) were significantly different between psilocin and vehicle conditions.

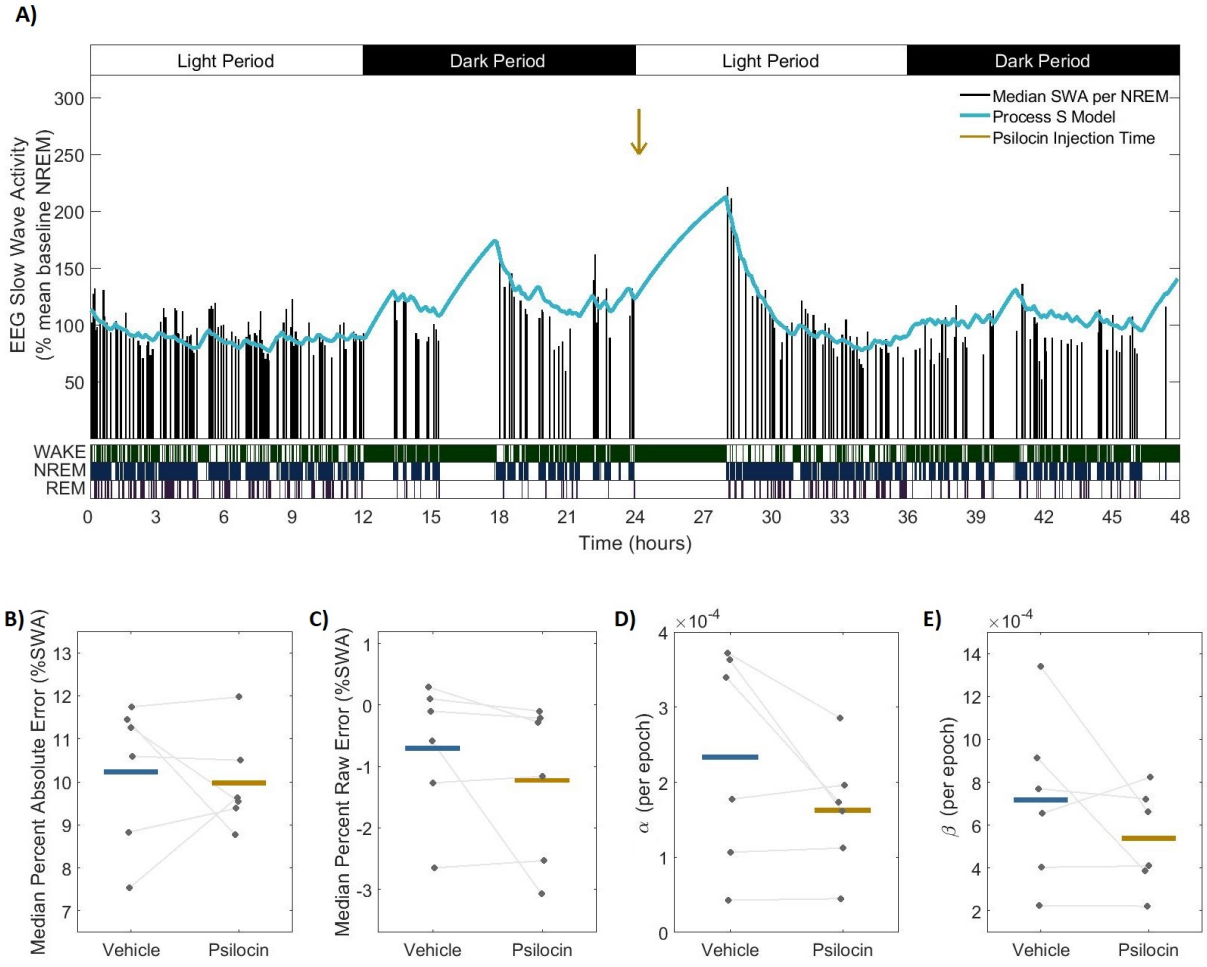


Figure 5.16: **A)** An example of the classic Process S model (blue) describing the dynamics of frontal EEG SWA (median per NREM sleep episode, black bars) over 48 hours in one representative animal. Sleep deprivation occurred as indicated at light onset of the second day and lasted 4 hours. Scored vigilance states are also shown. Yellow arrow marks the time of psilocin injection. **B)** The median value of the absolute error, between empirical SWA and modelled Process S, as a percentage of empirical SWA. **C)** The median value of the error, between empirical SWA and modelled Process S, as a percentage of empirical SWA. **D)** The optimised value of the parameter α and **E)** β in Process S model fit to psilocin sleep deprivation data. Grey lines link values derived from the same animal and coloured lines denote the group mean.

5.4 Discussion

The aim of this work was to explore possible effects of psilocin (4-hydroxy-dimethyl-tryptamine), a classical psychedelic and potent agonist of the 5-HT_{2A} receptor, on sleep-wake regulation and associated neuronal activity. This was performed in both an undisturbed condition in which sleep is preferential and a condition of enforced prolonged wakefulness. Psilocin was observed to acutely disrupt sleep, suppressing the maintenance of both NREM and REM sleep, resulting in a pattern of fragmented sleep attempts which lasted up to approximately 3 hours. However, no enduring effects of psilocin were observed, and notably the sleep homeostatic process was not found to be disrupted by exposure to the drug. These results have important value as preclinical data on the acute effects of psychedelics in rodents but also reveal an unexpected robustness of the sleep homeostatic mechanism despite substantially altered brain activity.

Before attempting electrophysiological recording experiments, it was necessary to perform pilot studies in order to gain an approximate understanding of the effect of the drug, and indeed to confirm its efficacy. The most widely reported behavioural effect of serotonergic psychedelic drugs in animals is the head twitch response (Canal and Morgan 2012; Halberstadt and Geyer 2018), which indeed was present. However, in addition to the classically described twitch, a lateral rotation of the head, another type of paroxysmal head movement was observed, consisting of a rapid forward neck extension. This latter type of head movement was common when the animals were adopting a resting posture, lying in their nests. Perhaps more significantly, the total rate of head twitches, of both types combined, in the 30 minutes following psilocin injection was lower than expected. The observed head twitch responses fell in the range of 0.3 – 0.97 per minute (including behavioural and implanted electrophysiology animals), lower than previously reported values using 2 mg/kg psilocin, such as 1.7 per min (Halberstadt et al. 2011) and 1.5 per min (Zhuk et al. 2015).

Through a series of additional behavioural pilot studies, it was shown that this reduced rate of head twitches was likely not because the psilocin dose was too low, nor that the drug incompletely dissolved, nor that the product quality was poor. Neither did the low HTR seem to be a consequence of observing the animals in their home cage, rather than a novel environment. One possibility is that these differences are due to mouse strain (Canal and Morgan 2012), however a recent study using C57BL/6J mice reported a mean HTR of 2.2 per min after 3 mg/kg dimethyltryptamine, so this is perhaps a less likely explanation (Halberstadt et al. 2020). Notably, also, this study automated head twitch counting using head-mounted magnets and magnetometer detection coil, rather than relying on manual observation, an approach which has been validated (Halberstadt and Geyer 2013), but against observation using a higher speed camera than was used in this study, which suggests that some twitches could have been missed. A further relevant factor might be the age of the mice, as the DOI-induced HTR has been shown to be reduced in older animals (Weiss et al. 2003) and the animals used in this study were older; 14 - 20 weeks compared to 6 - 8 weeks (Halberstadt et al. 2020). Animal age was unfortunately unreported in the other psilocin head twitch studies. Importantly it was concluded that the HTR data are not so unusual as to doubt the efficacy of the psilocin injection, although for future studies it may be valuable to consider that different strains or ages of mice could possibly show stronger psilocin-induced effects.

In addition to head twitches, the acute observed behavioural effects of psilocin included increased respiration, increased muscular tremor, increased locomotion and a decreased ability to maintain a resting posture or initiate sleep. These effects lasted up to an hour before sleep was initiated. The quality and architecture of subsequent sleep was then explored in animals implanted for electrophysiological recording. These results revealed that sleep after psilocin was highly fragmented, with a reduction of both NREM and REM sleep. This acute sleep suppression has been previously described in rodents in response to various 5-HT_{2A} agonists (Colasanti and Khazan 1975; Kay and Martin 1978; Monti and

Jantos 2006). Mechanistically, this effect might be explained by the direct activation of serotonin signalling, since serotonin is a classically wake-promoting transmitter. However, activation of prefrontal cortical 5-HT_{2A} receptors has been associated with increased acetylcholine (Nair and Gudelsky 2004) and dopamine (Bortolozzi et al. 2005) signalling, so the underlying mechanism might be much more complex and remains unclear.

The acute disruption of REM sleep might be particularly interesting, since REM sleep suppression is a common side-effect of antidepressants (Wichniak et al. 2017), and REM sleep is strongly associated with the regulation of emotional memory (Perogamvros and Schwartz 2015). However, the observed suppression of REM sleep lasted only on the order of hours, and no differences were found in REM sleep properties between the day before and the day after psilocin exposure, suggesting that long-term modulation of REM sleep does not occur. Notably, injection experiments were performed with three-day intervals, and it was therefore not possible to track long-term changes in sleep. However, the differences in wake, NREM and REM sleep amount seen after psilocin disappeared within 12 hours and no evidence was found for effects which persisted into the following dark period or subsequent day. It is therefore concluded that exposure to psilocin does not necessarily lead to changes in sleep-wake architecture in the long-term in mice.

Analysis of EEG and LFP spectra in these recordings identified a prominent 3 - 5 Hz peak amplified by psilocin. This peak was present in baseline wakefulness in both conditions in both EEG and LFP, so does not likely correspond to novel dynamics, but an enhancement of a particular form of existing activity. Such an increase in upper delta frequencies might be linked to increased local sleep and the presence of off periods indicating increased homeostatic sleep pressure. However, comparing wake spectra before and after sleep deprivation suggests that increased sleep pressure actually manifests as a much wider low frequency spectral power increase, including also frequencies 1 - 3 Hz. Oscillatory activity in this frequency range has been previously reported during wakefulness in mice in prefrontal cortex (Biskamp et al. 2017), as well as other areas (Jessberger et al.

2016; Chi et al. 2016), and has been associated with breathing. This activity emerges during wake immobility, synchronises with nasal respiration and modulates ongoing gamma activity and spiking (Biskamp et al. 2017). The respiratory rhythm has also been linked with neocortical-hippocampal communication, plasticity and memory (Liu et al. 2017). Indeed, both the rate and intensity of breathing was often noticed to increase in the mice after psilocin injection. However, that this rhythm is related to respiration remains to be directly tested, and moreover its functional significance within the context of both endogenous 5-HT_{2A} receptor activation and the psychedelic phenomenon is unclear.

Cortical neuronal firing rates were lower during wakefulness immediately after injection with psilocin compared to the vehicle in the spontaneous condition. However, no firing rate changes were found during waking in the 30 minutes post injection in the sleep deprivation condition, suggesting that the effect is behaviour dependent, rather than a direct consequence of 5-HT_{2A} receptor activation. Note that the mean duration of spontaneous wake after psilocin was 26.3 minutes, so these are comparable time windows. The firing rate difference appears more compatible with an increase in firing in the vehicle condition, since post-psilocin firing rates are closer to baseline levels, so this effect is not likely to be functionally relevant (Figure 5.11A). Previous studies on cortical firing rates have reported both increases and decreases in net cortical activity in different conditions, different brain regions and with different drug doses (Ashby et al. 1989; Puig et al. 2003; Celada et al. 2008; Wood et al. 2012). Overall, the existing evidence suggests that modulation of global total activity levels is not a fundamental effect of serotonergic psychedelics.

The primary aim of this study was to determine effects of psilocin on Process S. The highly disordered acute state appears to enable large scale functional reorganisation in the human brain (Carhart-Harris et al. 2014; Tagliazucchi et al. 2014; Carhart-Harris et al. 2017), a process which likely requires plasticity of glutamatergic synaptic transmission (Vollenweider and Kometer 2010). Indeed, rodent studies *in vivo* indicate that psychedelics can promote synaptogenesis and increase excitatory synaptic transmission (Ly et al. 2018).

Furthermore, successful antidepressant therapies were associated with increased cortical excitability, suggestive of increased synaptic strengths (Canali et al., 2014). Therefore, the effects of psilocin might be predicted to include a net increase in synaptic strengths, which, according to the synaptic homeostasis hypothesis, is identical to an increase in Process S (Tononi and Cirelli 2003). However, it has been alternatively argued that the neuroplastic influence of psychedelics might actually complement or even substitute the effects of sleep, therefore reducing Process S, since both involve a temporary relaxation of typical neuronal constraints followed by self-organised functional re-optimisation (Froese et al. 2018). In this study, no effect of psilocin on Process S was found. The lack of any discernible effect on the sleep homeostatic process is surprising, considering the disruption to normal wakefulness, neuronal activity, and plasticity that is presumed to occur. This result suggests that Process S is extremely robust in its ability to estimate prior wake duration despite perturbation of brain dynamics and subjective waking quality.

6

Conclusions

Contents

6.1 Overview 154

6.2 Homeostasis of Sleep & Neuronal Activity 156

6.3 Limitations & Future Work 161

6.4 Summary 165

6.1 Overview

Sleep is essential to life and occurs in some form in all living organisms. Far from being just a resting behaviour, sleep as it relates to mammalian physiology constitutes a complex adaptive state. Sleep involves myriad physiological systems and processes, ultimately serving many beneficial bodily functions which prefer disconnection from the environment, such as organism development, regeneration and repair, and reflective processing of information. Sleep is homeostatically regulated, a phenomenon which manifests as a relative constancy of sleep's daily amount and intensity within individuals. Universally, the need for sleep accumulates during wakefulness and dissipates during subsequent sleep. Despite substantial scientific characterisation of many sleep-dependent functions over the last few decades, it is still uncertain precisely which biological variables form the substrate of homeostatic sleep need, how information about these variables are integrated to regulate sleep globally, how sleep mediates the restoration of homeostasis, and how completion of this process promotes subsequent wakefulness.

The neuronal activities associated with sleep, the slow oscillation and corresponding alternating up and down activity states, occur non-uniformly across the cortex and, importantly, are modulated by both prior behaviour and local cortical activity history. Furthermore, the proposed substrates of the sleep homeostatic process relate to functional properties of single neurones, such as synaptic strength and cellular maintenance and energetics, leading to the widespread idea that sleep has a local and activity-dependent origin. This thesis aimed to apply electrophysiological recording and mathematical modelling techniques to better characterise bidirectional relationships between the sleep homeostatic process and cortical neuronal dynamics.

Classical theoretical descriptions of homeostatic sleep regulation define "Process S", a variable with dynamics dependent only on sleep-wake history, whose levels are reflected in the slow wave activity of field potentials during NREM sleep. In chapter 3, novel

mathematical models of Process S were described which first assume that its dynamics are a function of the deviation of cortical neuronal firing rates from a locally defined set-point, crucially without explicit knowledge of sleep-wake state. An alternative measure for Process S with more local origins than SWA was then introduced, based on the total time that locally recorded spiking populations spent in putative off periods. Using this measure, it was subsequently shown how Process S dynamics may be described in terms of two opponent processes, dependent on spiking rate and off period occurrence. Importantly, these results demonstrate that Process S dynamics can be derived entirely from local multi-unit neuronal spiking activity, without reference to global sleep-wake states. Beyond this, the results also suggested that Process S at the global level attains the ability to track sleep-wake history through an integration of local cortical neuronal activity levels over time and across spatially distributed networks.

Given this view of sleep homeostasis, it is feasible that the cellular level functional properties of neurones which change as function of sleep-wake history might translate into changes in the properties of global network dynamics with implications for brain function and behaviour. One prominent theory of global brain dynamics linked to sleep and wake is that cortical networks operate at, or near, a critical point. Changes in different hallmarks of critical dynamics in neural activity have previously been associated with extended wakefulness, and yet the maintenance of brain activity near criticality has been shown to offer many advantages to neural computation, implicating a possible role for sleep-wake-dependent homeostatic regulation. In chapter 4, neuronal avalanche analysis was applied to both LFP and spiking data, aiming to determine to what extent critical dynamics differ between and within vigilance states and whether changes in criticality across the sleep-wake cycle could be linked to Process S. Indeed, in agreement with previous experimental and theoretical studies, wakefulness was generally found to correspond to a slightly subcritical regime, with critical or supercritical behaviour typically associated with both NREM and REM sleep. The evidence for changes in critical dynamics as a function of

Process S was weak in wakefulness, yet strong in NREM sleep. Furthermore, deviation from criticality was found to correlate significantly with LFP slow wave activity in all vigilance states, suggesting that control of brain critical dynamics might occur through mechanisms which regulate the degree to which cortical dynamics are governed by the slow oscillation.

Finally, it was sought to determine whether physiologically realistic perturbations to the quality of wakefulness, and associated altered cortical dynamics, would translate into variation in the sleep homeostatic process. In chapter 5, this aim was addressed by exposing mice to a psychotropic 5-HT_{2A} receptor agonist, psilocin, which is a classical psychedelic drug. In humans this class of drugs exerts powerful acute alterations to perception and cognition, and its use under controlled conditions has been associated with long-lasting positive changes in psychological well-being, an effect with possible clinical applications to the treatment of depressive mood disorders. Given the general lack of understanding as to the mechanism of action of this class of drugs, and their striking effects on the waking brain, it was hypothesised that psilocin might influence the dynamics of Process S or lead to enduring changes in sleep-wake architecture. While an acute sleep-inhibiting effect of psilocin was robustly found, this effect appeared to be short-lived, and no enduring changes in sleep-wake architecture were observed. Similarly, there was no effect of administering psilocin vs. a control during a period of extended wake of equal duration on subsequent NREM sleep slow wave activity levels in the frontal EEG or prefrontal LFP. This result has important relevance for efforts to understand the therapeutic mechanisms of psychedelics and also implies a surprising robustness in the ability of Process S to track sleep-wake history, despite substantial perturbation of neuronal activity.

6.2 Homeostasis of Sleep & Neuronal Activity

The notion of homeostasis is central in the field of neuroscience, yet much confusion remains as to precisely which variables are homeostatically regulated in the brain and

what are the underlying mechanisms. An implicit assumption in much of the discussion of the fundamental nature of homeostatic sleep regulation is that it corresponds to an active process which dynamically shapes daily sleep-wake architecture in response to a physiological need for the homeostatic regulation of specific cellular variables. Although numerous molecular and cellular substrates have been proposed, none have been conclusively demonstrated to be equivalent to Process S or to unambiguously underpin its dynamics, yet all are in some way related to neuronal activity. On a single neurone level, *in vitro*, neuronal firing rates are maintained around a cell-specific set point, yet *in vivo*, this occurs alongside regular dramatic changes in brain activity resulting from cognition and behaviour, but importantly also from the sleep-wake cycle. A role for sleep and wake in the regulation of firing rates is well established, and state-dependent changes in synaptic plasticity rules are identified as the key mechanism, however the magnitude and direction of state-dependent firing rate modulations vary in different studies. Despite major efforts, the evidence supporting an association between neuronal activity or synaptic weights with sleep need is inconsistent or indirect.

In this thesis, in was found that prior wake duration was not a strong predictor of changes in global brain dynamics measured in the form of critical neuronal avalanches, although some striking changes to criticality were occasionally observable in individual cases during the final hour of sleep deprivation. Furthermore, substantially perturbing ongoing wakefulness and neuronal activity with the classical serotonergic psychedelic psilocin did not consistently alter measured Process S dynamics. Through the development of novel mathematical models it was found that Process S could be described entirely in terms of local neuronal activities, however, at higher scales the local variability in Process S appeared to be discarded through an averaging across spatially distributed networks.

Overall, these results are consistent with an alternative view of the nature of sleep homeostasis; that it corresponds fundamentally to a time-keeping process, which ensures only that a certain daily duration of sleep is obtained. In this scenario, physiological signals

which are generated preferentially in association with wakefulness might be integrated over time in order to estimate total time spent awake. Importantly, this means that the variables which change as a function of time spent awake or asleep, such as synaptic strengths, cellular stresses or deviation from critical set points, do not themselves necessarily need to regulate sleep directly. Conversely, variables which remain stable during continuous wake or sleep, such as firing rates, could still make essential contributions to the time-keeping mechanism. The resulting signal would thereby enable the brain to enforce a particular quota of sleep, whose duration is ecologically and physiologically appropriate. Therefore, Process S need not be faithfully reflected in the dynamics of any one specific regulated variable, nor would such a variable be solely responsible for controlling sleep drive.

Specifically, it is concluded that the integration of cortical firing rates constitutes a key element of this time-keeping mechanism. The models presented in chapter 3 show how the levels of neuronal activity themselves need not be directly proportional to the levels of Process S, but through their temporal integration, firing rates are nonetheless able to predict Process S dynamics. The approximately equivalent overall accuracy of both firing-rate-based and vigilance-state-based models supports this proposed mechanism, as does the evidence that homeostatically regulated cellular variables can actually be stable during extended wakefulness, and that maintenance processes in sleep may be ultimately prophylactic (Vyazovskiy and Harris 2013). Similarly, it was found that measures of population critical dynamics were inconsistently associated with Process S in wakefulness, dependent on other factors, such as circadian phase and individual differences. While there may be an important role for sleep in regulating critical dynamics, it is concluded that sleep need is not robustly signalled by a deviation from criticality. The results of the experiment with psilocin also demonstrate the sleep homeostatic process is dissociable from alterations in global neuronal dynamics. Of relevance here is whether firing rates were decreased in response to psilocin, and yet Process S was unchanged. Such an effect on firing rates was present in the undisturbed condition, but was not observed in the

sleep deprivation condition, so unfortunately this remains unclear.

Mechanistically, firing rates are associated with the local accumulation of sleep-promoting signalling molecules, such as adenosine and cytokines (Krueger et al. 2008; Clinton et al. 2011). These are amplified and integrated over local networks through intercellular signalling pathways, for example involving astrocytes (Fellin et al. 2012), and ultimately modulate neuronal electrophysiological properties, such as the local tendency to generate down states. Synaptic coupling and the slow oscillation similarly enables an intrinsic local spatial integration. This process would produce a global sleep propensity signal that reflects the total time spent awake with great accuracy and translates into a particular average amplitude of slow wave activity measurable in field potentials. This mechanism is conceptually very similar to that which enables robust time-keeping by the circadian master clock; circadian periods and phases represented by the activity of individual clock cells in the SCN are highly variable, but the SCN output signals time accurately through an averaging of the activity of many neurones (Liu et al. 1997).

Once sleep is initiated, local cellular homeostatic processes likely unfold according to their specific need, and such processes might be enabled during the down states of the slow oscillation. Importantly, through this mechanism, the target quantity of sleep a brain enforces may be longer than is absolutely necessary for essential homeostatic processes to occur. This then leaves time for non-essential sleep processes, such as those related to offline information processing and the associated consolidation and integration of memories (Rasch and Born 2013; Tononi and Cirelli 2014). Furthermore, conservation of energy was one of the earliest proposed functions of sleep (Berger, 1995; Schmidt, 2014), and excess sleep might become adaptive dependent on certain ecological factors, such as the timing of the availability of food. While a trend does exists between sleep-wake ratio and brain metabolic rate (Savage and West 2007), which likely accounts for the time course of cellular homeostatic processes, there are notable outliers and exceptions; for example, can the >18 hours a day of sleep in some animals really be necessary for cellular homeostasis

resulting from just a few hours of wakefulness? If the sleep homeostasis is primarily a time-keeping mechanism, homeostatic, mnemonic and ecological factors can all influence the sleep quota, which is likely ultimately genetically encoded (Cirelli 2009). This explains why daily sleep amount varies greatly across the animal kingdom, and yet individuals generally perform a relatively constant and species-specific amount of sleep each day.

Another conceptual advantage of the proposed view of sleep homeostasis is that it reconciles the apparently local origins of the accumulation of homeostatic sleep pressure with the preferentially global level of its dissipation. If regulation of the sleep homeostatic process can occur entirely at the local level, why then is global sleep preferred over a hypothetical state including asynchronous local off periods, which presumably could be used to sustain longer periods of behavioural wakefulness? It has been argued previously that it is optimal to synchronise off periods and undergo dedicated periods of total behavioural shutdown, because local off periods during waking impair behaviour (Lima and Rattenborg 2007; Vyazovskiy et al. 2011). Mechanistically, the occurrence of local off periods might be obstructed by strong synaptic coupling and shared neuromodulatory tone. Indeed, it has been observed that the degree of coupling between an individual neurone's firing and the population firing rate, is variable between cells but characteristic to an individual neurone and likely reflects total synaptic strength with its neighbours (Okun et al. 2015). Some neurones may therefore be less able to express asynchronous off periods than others. By enforcing a sleep quota, global sleep can be achieved, and by estimating sleep time based on neuronal activity, mechanistic links to the local origins of sleep need are retained. This view also has implications for the regulation of firing rates. In order to maximise the efficiency of global sleep, single neuronal activities may be modulated such that sleep pressure accumulates, on average, as uniformly as possible. This is consistent with recent reports that sleep regulates the distribution of firing rates at the population level by reducing its variance (Watson et al. 2016; Levenstein et al. 2017; Miyawaki et al. 2019).

6.3 Limitations & Future Work

Perhaps the most important limitation of the presented results is that they derive only from recordings in a single brain region and only from 16 simultaneous sites. Considering that the cellular anatomy, composition, connectivity and functional properties of neurones are heterogeneous across the cortex, it is unknown to what extent these results can be generalised. The motor cortex was chosen because of the striking characteristic differences in neuronal activity between wake and sleep, and because the response to sleep deprivation is well characterised (Vyazovskiy et al. 2006, McKillop et al. 2018). It is noteworthy that, even within motor cortex, individual recorded channels and neurones display significant variability in their activity as a function of behaviour (Fisher et al. 2016).

For the modelling study, the important property that firing rates are higher in wake than sleep has been reported in other brain areas in rodents, such as somatosensory barrel cortex (Vyazovskiy et al. 2009b), and global wide-field calcium imaging in mice (Niethard et al. 2016) supports that this is generally true over the whole cortex. Interestingly, an absence of a difference between firing rates in wake and sleep has been reported for the primary visual cortex (Hengen et al. 2013). However, this is likely an interesting exception, especially considering that homeostatic changes in SWA are lower in posterior cortex (Huber et al. 2000b) and that slow waves typically have a frontal site of generation (Massimini et al. 2004; Vyazovskiy et al. 2009a). Importantly, it should be emphasised that universally higher spiking in wakefulness is not necessary for this conclusion to hold, owing to the proposed process of spatial integration across the brain. Notably it was shown within a population of prefrontal units that the neurones with a higher firing rate in NREM sleep are those which typically have the lowest waking firing rates, and therefore might experience a weaker homeostatic challenge during wakefulness compared with the majority of neurones whose activity is higher in wake. These neurones might therefore express Process S such that it is not reflecting their own level of sleep need per se, but to

a degree that follows the need of the wider network in which they are embedded.

In order to demonstrate that the modelling results are not limited to a single brain region, preliminary work was performed on the medial prefrontal data, finding that the firing-rate dependent model captures SWA-derived Process S with comparable accuracy. A more thorough analysis might be revealing, if parameters and fit quality do vary significantly across cortical regions, however it is not deemed likely that the fundamental conclusions will be challenged by data from other cortical areas.

It is important to acknowledge that the evidence presented in the modelling study is correlational, and that establishing causality was outside the scope of the project. To directly test the conclusion that global Process S reflects integrated cortical activity would require both the simultaneous recording and manipulation of neuronal activity across many brain regions, possibly including also subcortical areas. Unfortunately such a study is not current feasible. Furthermore, it is not entirely clear on what scale perturbations would need to be enacted, since highly localised neuronal activity manipulations would be predicted to be averaged out from measurable Process S, as has been found previously (Rodriguez et al. 2016). Going forward, it may be more useful to develop experimental approaches that would provide better insights into which variables are merely correlated with Process S, vs. which are causally responsible for the homeostatic control of sleep's duration and depth, for example by studying sleep homeostasis in genetic knockouts of key proteins involved in metabolic or synaptic regulation.

Another important factor which was neglected in the modelling analysis is the influence of the circadian rhythm on Process S and also on neuronal activity. It may be possible, for example, that the time-keeping mechanism derives information also from circadian signals, possibly running faster or slower at different phases of the light-dark cycle. Such a possibility is testable using the models developed here, if data is obtained comprising spiking and LFP SWA over many days which includes circadian or light-dark manipulations.

With regard to criticality, the crucial limitation for convincingly measuring neuronal avalanches is the number and spatial distribution of sites which can be simultaneously recorded. The ongoing development of new electrophysiological probe technologies capable of large scale multi-site recording provides an opportunity to investigate the temporal dynamics of criticality across the sleep-wake cycle with improved accuracy and precision. Furthermore, the relationship between concepts in critical theory, such as avalanches and deviation from the critical point, and other neuronal metrics, such as synchrony or complexity, could be explored within the same dataset in order to better validate the extent to which this theory extends our understanding of brain dynamics.

Related to this, one important challenge for future work will be to better integrate criticality within the theoretical framework of Process S. For instance, there may not just be a role for Process S in regulating critical dynamics, but also a role for criticality in explaining the how Process S is integrated over many spatiotemporal scales. A theoretical modelling approach might be most useful here, to understand how critical avalanches are altered in spiking networks capable of displaying variable degrees of asynchronous irregular vs. synchronous up-down state alternation, which replicates the range of slow wave activity seen *in vivo* between and also within vigilance states. Alternatively, using a similar approach to Process S modelling as in chapter 3, it could be tested whether measures of the proximity to critical dynamics, derived from the population activity, offer similar predictive power as firing rates for describing Process S dynamics. However, it is not clear how subcritical and supercritical dynamics might be linked mechanistically to sleep homeostatic functions. Indeed, any mechanism would likely depend on firing patterns, probably changes in firing rates, since homeostasis of firing rate allows for homeostasis of criticality (Hsu and Beggs 2006).

The main aim of the experiment using the 5-HT_{2A} agonist psilocin was to determine whether perturbation of neuronal dynamics by serotonergic psychedelics might affect sleep homeostasis, and surprisingly no effect was found. One possible limitation in this study

may be that the duration of sleep deprivation was too long, and as such a ceiling effect on SWA reduced the ability to discriminate Process S between psilocin and vehicle conditions. However, using a shorter sleep deprivation duration comes with the risk that the acute arousing effects of psilocin remain active or that insufficient sleep pressure has built up to guarantee that the mice will initiate sleep once experimentally enforced sleep deprivation is terminated. To circumvent this issue would require a very large sample size of mice and then selecting for analysis only those animals which slept immediately after sleep deprivation, for example of only two or three hours duration.

The discovery of neuronal oscillatory changes at both the frontal EEG and mPFC level as a result of psilocin requires more work to interpret. In particular, separating out which effects are due to the direct influence of the drug, rather than an indirect consequence of behavioural change would require more carefully controlled experiments. The 3 - 5 Hz oscillation, which may be linked to respiration and quiescent inactivity, particularly deserves further attention, with respect to ongoing neuronal activity, ideally with well-isolated single unit data.

It still remains possible that the therapeutic benefits of psilocybin in depressed humans do depend on sleep-related processes. Indeed, neuroplasticity facilitated by 5-HT_{2A} receptor agonists likely depends on specific experiential cognitive processes, analogous to the way in which the psychological benefits to humans occur under controlled conditions requiring the intervention of a therapist. It is further possible that these processes might require a higher cognitive function than is possible in rodents, or the presence of a depressive disorder with associated sleep dysregulation. Future work should aim to characterise the effects of psilocin on Process S in rodent models of depression and also in healthy and clinically relevant human populations. The possible contributions of REM sleep also require further study which should not be overlooked.

6.4 Summary

Sleep is a complex and multi-faceted neurophysiological phenomenon, and the mechanisms by which sleep is regulated within neural circuits allude to fundamental processes governing the control of activity in the brain in general. Although much progress has been made in recent years in identifying the physiological substrate and mechanisms of the sleep homeostatic process, many essential questions remain.

In this thesis, it is argued that Process S reflects a spatiotemporal integration of the levels of cortical neuronal activity. Evidence is then presented that Process S may indirectly, in association with the sleep slow oscillation, regulate the statistical properties of neuronal activity across many spatiotemporal scales, through modulation of criticality. Furthermore, it shown how Process S is remarkably robust to perturbation of waking neuronal dynamics by a serotonergic psychedelic drug. Finally, it is concluded that regulation of neuronal functional homeostasis by sleep is achieved by a Process S whose primary purpose is to track time spent in different vigilance states in the absence of external time cues, ultimately ensuring that individuals obtain a species-specific quota of sleep each day.

Bibliography

Abasolo, D., S. Simons, R. M. d. Silva, G. Tononi, and V. V. Vyazovskiy (2015). **Lempel-Ziv complexity of cortical activity during sleep and waking in rats**. In: *Journal of Neurophysiology*, jn.00575.2014. DOI: 10.1152/jn.00575.2014.

Achermann, P., D.-J. Dijk, D. P. Brunner, and A. A. Borbély (1993). **A model of human sleep homeostasis based on EEG slow-wave activity: Quantitative comparison of data and simulations**. In: *Brain Research Bulletin* 31.1, pp. 97–113. DOI: 10.1016/0361-9230(93)90016-5.

Aghajanian, G. K and G. J Marek (1997). **Serotonin Induces Excitatory Postsynaptic Potentials in Apical Dendrites of Neocortical Pyramidal Cells**. In: *Neuropharmacology* 36.4, pp. 589–599. DOI: 10.1016/S0028-3908(97)00051-8.

Aghajanian, G. K. and G. J. Marek (1999). **Serotonin, via 5-HT2A receptors, increases EPSCs in layer V pyramidal cells of prefrontal cortex by an asynchronous mode of glutamate release**. In: *Brain Research* 825.1, pp. 161–171. DOI: 10.1016/s0006-8993(99)01224-x.

Aghajanian, G. K. (2009). **Modeling "psychosis" in vitro by inducing disordered neuronal network activity in cortical brain slices**. In: *Psychopharmacology* 206.4, pp. 575–585. DOI: 10.1007/s00213-009-1484-9.

Amsterdam, J. van, A. Opperhuizen, and W. van den Brink (2011). **Harm potential of magic mushroom use: a review**. In: *Regulatory Toxicology and Pharmacology* 59.3, pp. 423–429. DOI: 10.1016/j.yrtph.2011.01.006.

Amzica, F. and M. Steriade (1995). **Short- and long-range neuronal synchronization of the slow (< 1 Hz) cortical oscillation**. In: *Journal of Neurophysiology* 73.1, pp. 20–38. DOI: 10.1152/jn.1995.73.1.20.

Amzica, F. and M. Steriade (1998). **Electrophysiological correlates of sleep delta waves**. In: *Electroencephalography and Clinical Neurophysiology* 107.2, pp. 69–83. DOI: 10.1016/s0013-4694(98)00051-0.

Appel, J. B., F. J. White, and A. M. Holohean (1982). **Analyzing mechanism(s) of hallucinogenic drug action with drug discrimination procedures**. In: *Neuroscience and Biobehavioral Reviews* 6.4. Place: Netherlands Publisher: Elsevier Science, pp. 529–536. DOI: 10.1016/0149-7634(82)90036-7.

Arvanov, V. L., X. Liang, P. Magro, R. Roberts, and R. Y. Wang (1999). **A pre- and postsynaptic modulatory action of 5-HT and the 5-HT2A, 2C receptor**

agonist DOB on NMDA-evoked responses in the rat medial prefrontal cortex. In: *The European Journal of Neuroscience* 11.8, pp. 2917–2934. DOI: 10.1046/j.1460-9568.1999.00708.x.

Ashby, C. R., E. Edwards, K. Harkins, and R. Y. Wang (1989). **Effects of (±)-DOI on medial prefrontal cortical cells: a microiontophoretic study**. In: *Brain Research* 498.2, pp. 393–396. DOI: 10.1016/0006-8993(89)91124-4.

Atasoy, S., L. Roseman, M. Kaelen, M. L. Kringelbach, G. Deco, and R. L. Carhart-Harris (2017). **Connectome-harmonic decomposition of human brain activity reveals dynamical repertoire re-organization under LSD**. In: *Scientific Reports* 7.1. Number: 1 Publisher: Nature Publishing Group, pp. 1–18. DOI: 10.1038/s41598-017-17546-0.

Attwell, D. and S. B. Laughlin (2001). **An energy budget for signaling in the grey matter of the brain**. In: *Journal of Cerebral Blood Flow and Metabolism* 21.10, pp. 1133–1145. DOI: 10.1097/00004647-200110000-00001.

Avesar, D. and A. T. Gulledge (2012). **Selective serotonergic excitation of callosal projection neurons**. In: *Frontiers in Neural Circuits* 6, p. 12. DOI: 10.3389/fncir.2012.00012.

Baglioni, C., G. Battagliese, B. Feige, K. Spiegelhalder, C. Nissen, U. Voderholzer, C. Lombardo, and D. Riemann (2011). **Insomnia as a predictor of depression: a meta-analytic evaluation of longitudinal epidemiological studies**. In: *Journal of Affective Disorders* 135.1, pp. 10–19. DOI: 10.1016/j.jad.2011.01.011.

Bak, P., C. Tang, and K. Wiesenfeld (1987). **Self-organized criticality: An explanation of the 1/f noise**. In: *Physical Review Letters* 59.4, pp. 381–384. DOI: 10.1103/PhysRevLett.59.381.

Barbanoj, M. J., J. Riba, S. Clos, S. Giménez, E. Grasa, and S. Romero (2008). **Daytime Ayahuasca administration modulates REM and slow-wave sleep in healthy volunteers**. In: *Psychopharmacology* 196.2, pp. 315–326. DOI: 10.1007/s00213-007-0963-0.

Barre, A., C. Berthoux, D. De Bundel, E. Valjent, J. Bockaert, P. Marin, and C. Bécamel (2016). **Presynaptic serotonin 2A receptors modulate thalamocortical plasticity and associative learning**. In: *Proceedings of the National Academy of Sciences of the United States of America* 113.10, E1382–1391. DOI: 10.1073/pnas.1525586113.

Beggs, J. M. and D. Plenz (2003). **Neuronal Avalanches in Neocortical Circuits**. In: *The Journal of Neuroscience* 23.35, pp. 11167–11177.

Beggs, J. M. and N. Timme (2012). **Being Critical of Criticality in the Brain**. In: *Frontiers in Physiology*. DOI: 10.3389/fphys.2012.00163.

Bell-Pedersen, D., V. M. Cassone, D. J. Earnest, S. S. Golden, P. E. Hardin, T. L. Thomas, and M. J. Zoran (2005). **Circadian rhythms from multiple oscillators: lessons from diverse organisms**. In: *Nature Reviews Genetics* 6.7, pp. 544–556. DOI: 10.1038/nrg1633.

Bellesi, M., D. Bushey, M. Chini, G. Tononi, and C. Cirelli (2016). **Contribution of sleep to the repair of neuronal DNA double-strand breaks: evidence from flies and mice**. In: *Scientific Reports* 6, p. 36804. DOI: 10.1038/srep36804.

Belouin, S. J. and J. E. Henningfield (2018). **Psychedelics: Where we are now, why we got here, what we must do**. In: *Neuropharmacology*. Psychedelics: New Doors, Altered Perceptions 142, pp. 7–19. DOI: 10.1016/j.neuropharm.2018.02.018.

Berthoux, C., A. Barre, J. Bockaert, P. Marin, and C. Bécamel (2019). **Sustained Activation of Postsynaptic 5-HT2A Receptors Gates Plasticity at Prefrontal Cortex Synapses**. In: *Cerebral Cortex* 29.4, pp. 1659–1669. DOI: 10.1093/cercor/bhy064.

Bertschinger, N. and T. Natschlager (2004). **Real-time computation at the edge of chaos in recurrent neural networks**. In: *Neural Computation* 16.7, pp. 1413–1436. DOI: 10.1162/089976604323057443.

Biskamp, J., M. Bartos, and J.-F. Sauer (2017). **Organization of prefrontal network activity by respiration-related oscillations**. In: *Scientific Reports* 7, p. 45508. DOI: 10.1038/srep45508.

Bjorness, T. E., C. L. Kelly, T. Gao, V. Poffenberger, and R. W. Greene (2009). **Control and Function of the Homeostatic Sleep Response by Adenosine A1 Receptors**. In: *Journal of Neuroscience* 29.5. Publisher: Society for Neuroscience Section: Articles, pp. 1267–1276. DOI: 10.1523/JNEUROSCI.2942-08.2009.

Blumberg, M. S., J. A. Lesku, P.-A. Libourel, M. H. Schmidt, and N. C. Rattenborg (2020). **What Is REM Sleep?** In: *Current Biology* 30.1. Publisher: Elsevier, R38–R49. DOI: 10.1016/j.cub.2019.11.045.

Bogenschutz, M. P., A. A. Forcehimes, J. A. Pommy, C. E. Wilcox, P. C. R. Barbosa, and R. J. Strassman (2015). **Psilocybin-assisted treatment for alcohol dependence: a proof-of-concept study**. In: *Journal of Psychopharmacology* 29.3, pp. 289–299. DOI: 10.1177/0269881114565144.

Borbély, A. A. (1982). **A two process model of sleep regulation**. In: *Human Neurobiology* 1.3, pp. 195–204.

Borbély, A. A. and P. Achermann (1999). **Sleep homeostasis and models of sleep regulation**. In: *Journal of Biological Rhythms* 14.6, pp. 557–568.

Borbély, A. A. and A. Wirz-Justice (1982). **Sleep, sleep deprivation and depression. A hypothesis derived from a model of sleep regulation**. In: *Human Neurobiology* 1.3, pp. 205–210.

Borbély, A. A., S. Daan, A. Wirz-Justice, and T. Deboer (2016). **The two-process model of sleep regulation: a reappraisal**. In: *Journal of Sleep Research* 25.2, pp. 131–143. DOI: 10.1111/jsr.12371.

Bortolozzi, A., L. Díaz-Mataix, M. C. Scorza, P. Celada, and F. Artigas (2005). **The activation of 5-HT2A receptors in prefrontal cortex enhances dopaminergic**

activity. In: *Journal of Neurochemistry* 95.6, pp. 1597–1607. DOI: 10.1111/j.1471-4159.2005.03485.x.

Béïque, J.-C., M. Imad, L. Mladenovic, J. A. Gingrich, and R. Andrade (2007). **Mechanism of the 5-hydroxytryptamine 2A receptor-mediated facilitation of synaptic activity in prefrontal cortex**. In: *Proceedings of the National Academy of Sciences of the United States of America* 104.23, pp. 9870–9875. DOI: 10.1073/pnas.0700436104.

Brown, R. E., R. Basheer, J. T. McKenna, R. E. Strecker, and R. W. McCarley (2012). **Control of sleep and wakefulness**. In: *Physiological Reviews* 92.3, pp. 1087–1187. DOI: 10.1152/physrev.00032.2011.

Bukhtiyarova, O., S. Soltani, S. Chauvette, and I. Timofeev (2019). **Slow wave detection in sleeping mice: Comparison of traditional and machine learning methods**. In: *Journal of Neuroscience Methods*. Methods and models in sleep research: A Tribute to Vincenzo Crunelli 316, pp. 35–45. DOI: 10.1016/j.jneumeth.2018.08.016.

Bunney, B. G. and W. E. Bunney (2013). **Mechanisms of rapid antidepressant effects of sleep deprivation therapy: clock genes and circadian rhythms**. In: *Biological Psychiatry* 73.12, pp. 1164–1171. DOI: 10.1016/j.biopsych.2012.07.020.

Burnet, P. W., S. L. Eastwood, K. Lacey, and P. J. Harrison (1995). **The distribution of 5-HT1A and 5-HT2A receptor mRNA in human brain**. In: *Brain Research* 676.1, pp. 157–168. DOI: 10.1016/0006-8993(95)00104-x.

Buzsáki, G., C. A. Anastassiou, and C. Koch (2012). **The origin of extracellular fields and currents — EEG, ECoG, LFP and spikes**. In: *Nature Reviews Neuroscience* 13.6, pp. 407–420. DOI: 10.1038/nrn3241.

Cajochen, C., R. Foy, and D. J. Dijk (1999). **Frontal predominance of a relative increase in sleep delta and theta EEG activity after sleep loss in humans**. In: *Sleep Research Online* 2.3, pp. 65–69.

Cameron, L. P., C. J. Benson, L. E. Dunlap, and D. E. Olson (2018). **Effects of N, N-Dimethyltryptamine on Rat Behaviors Relevant to Anxiety and Depression**. In: *ACS Chemical neuroscience* 9.7, pp. 1582–1590. DOI: 10.1021/acschemneuro.8b00134.

Canal, C. E. and D. Morgan (2012). **Head-twitch response in rodents induced by the hallucinogen 2,5-dimethoxy-4-iodoamphetamine: a comprehensive history, a re-evaluation of mechanisms, and its utility as a model**. In: *Drug Testing and Analysis* 4.0, pp. 556–576. DOI: 10.1002/dta.1333.

Canal, C. E., R. G. Booth, and D. Morgan (2013). **Support for 5-HT2C receptor functional selectivity in vivo utilizing structurally diverse, selective 5-HT2C receptor ligands and the 2,5-dimethoxy-4-iodoamphetamine elicited head-twitch response model**. In: *Neuropharmacology* 70, pp. 112–121. DOI: 10.1016/j.neuropharm.2013.01.007.

Canal, C. E., U. B. Olaghere da Silva, P. J. Gresch, E. E. Watt, E. Sanders-Bush, and D. C. Airey (2010). **The serotonin 2C receptor potently modulates the**

head-twitch response in mice induced by a phenethylamine hallucinogen. In: *Psychopharmacology* 209.2, pp. 163–174. DOI: 10.1007/s00213-010-1784-0.

Carhart-Harris, R. L. (2018). **The entropic brain - revisited**. In: *Neuropharmacology*. Psychedelics: New Doors, Altered Perceptions 142, pp. 167–178. DOI: 10.1016/j.neuropharm.2018.03.010.

Carhart-Harris, R. L., M. Bolstridge, J. Rucker, C. M. J. Day, D. Erritzoe, M. Kaelen, M. Bloomfield, J. A. Rickard, B. Forbes, A. Feilding, D. Taylor, S. Pilling, V. H. Curran, and D. J. Nutt (2016). **Psilocybin with psychological support for treatment-resistant depression: an open-label feasibility study**. In: *The Lancet Psychiatry* 3.7, pp. 619–627. DOI: 10.1016/S2215-0366(16)30065-7.

Carhart-Harris, R. L., D. Erritzoe, T. Williams, J. M. Stone, L. J. Reed, A. Colasanti, R. J. Tyacke, R. Leech, A. L. Malizia, K. Murphy, P. Hobden, J. Evans, A. Feilding, R. G. Wise, and D. J. Nutt (2012). **Neural correlates of the psychedelic state as determined by fMRI studies with psilocybin**. In: *Proceedings of the National Academy of Sciences of the United States of America* 109.6, pp. 2138–2143. DOI: 10.1073/pnas.1119598109.

Carhart-Harris, R. L. and G. M. Goodwin (2017). **The Therapeutic Potential of Psychedelic Drugs: Past, Present, and Future**. In: *Neuropsychopharmacology* 42.11, pp. 2105–2113. DOI: 10.1038/npp.2017.84.

Carhart-Harris, R. L., L. Roseman, M. Bolstridge, L. Demetriou, J. N. Pannekoek, M. B. Wall, M. Tanner, M. Kaelen, J. McGonigle, K. Murphy, R. Leech, H. V. Curran, and D. J. Nutt (2017). **Psilocybin for treatment-resistant depression: fMRI-measured brain mechanisms**. In: *Scientific Reports* 7.1, p. 13187. DOI: 10.1038/s41598-017-13282-7.

Carhart-Harris, R. L., R. Leech, P. J. Hellyer, M. Shanahan, A. Feilding, E. Tagliazucchi, D. R. Chialvo, and D. Nutt (2014). **The entropic brain: a theory of conscious states informed by neuroimaging research with psychedelic drugs**. In: *Frontiers in Human Neuroscience* 8. DOI: 10.3389/fnhum.2014.00020.

Casali, A. G., O. Gosseries, M. Rosanova, M. Boly, S. Sarasso, K. R. Casali, S. Casarotto, M.-A. Bruno, S. Laureys, G. Tononi, and M. Massimini (2013). **A Theoretically Based Index of Consciousness Independent of Sensory Processing and Behavior**. In: *Science Translational Medicine* 5.198. DOI: 10.1126/scitranslmed.3006294.

Catlow, B. J., S. Song, D. A. Paredes, C. L. Kirstein, and J. Sanchez-Ramos (2013). **Effects of psilocybin on hippocampal neurogenesis and extinction of trace fear conditioning**. In: *Experimental Brain Research* 228.4, pp. 481–491. DOI: 10.1007/s00221-013-3579-0.

Celada, P., M. V. Puig, L. Díaz-Mataix, and F. Artigas (2008). **The Hallucinogen DOI Reduces Low-Frequency Oscillations in Rat Prefrontal Cortex: Reversal by Antipsychotic Drugs**. In: *Biological Psychiatry*. Glutamatergic Mechanisms

of Schizophrenia Vulnerability and Treatment 64.5, pp. 392–400. DOI: 10.1016/j.biopsych.2008.03.013.

Charton, J. P., M. Herkert, C. M. Becker, and H. Schröder (1999). **Cellular and subcellular localization of the 2B-subunit of the NMDA receptor in the adult rat telencephalon**. In: *Brain Research* 816.2, pp. 609–617. DOI: 10.1016/s0006-8993(98)01243-8.

Chauvette, S., M. Volgushev, and I. Timofeev (2010). **Origin of Active States in Local Neocortical Networks during Slow Sleep Oscillation**. In: *Cerebral Cortex* 20.11, pp. 2660–2674. DOI: 10.1093/cercor/bhq009.

Chen, A., C. J. Hough, and H. Li (2003). **Serotonin type II receptor activation facilitates synaptic plasticity via N-methyl-D-aspartate-mediated mechanism in the rat basolateral amygdala**. In: *Neuroscience* 119.1, pp. 53–63. DOI: 10.1016/s0306-4522(03)00076-9.

Chi, V. N., C. Müller, T. Wolfenstetter, Y. Yanovsky, A. Draguhn, A. B. L. Tort, and J. Brankačk (2016). **Hippocampal Respiration-Driven Rhythm Distinct from Theta Oscillations in Awake Mice**. In: *Journal of Neuroscience* 36.1, pp. 162–177. DOI: 10.1523/JNEUROSCI.2848-15.2016.

Cirelli, C. and G. Tononi (2000). **Gene expression in the brain across the sleep-waking cycle**. In: *Brain Research* 885.2, pp. 303–321. DOI: 10.1016/s0006-8993(00)03008-0.

Cirelli, C. (2009). **The genetic and molecular regulation of sleep: from fruit flies to humans**. In: *Nature Reviews Neuroscience* 10.8, pp. 549–560. DOI: 10.1038/nrn2683.

Cirelli, C., U. Faraguna, and G. Tononi (2006). **Changes in brain gene expression after long-term sleep deprivation**. In: *Journal of Neurochemistry* 98.5, pp. 1632–1645. DOI: 10.1111/j.1471-4159.2006.04058.x.

Cirelli, C., P. J. Shaw, A. Rechtschaffen, and G. Tononi (1999). **No evidence of brain cell degeneration after long-term sleep deprivation in rats1Published on the World Wide Web on 8 July 1999.1**. In: *Brain Research* 840.1, pp. 184–193. DOI: 10.1016/S0006-8993(99)01768-0.

Cirelli, C. and G. Tononi (2008). **Is Sleep Essential?** In: *PLOS Biology* 6.8, e216. DOI: 10.1371/journal.pbio.0060216.

Clinton, J. M., C. J. Davis, M. R. Zielinski, K. A. Jewett, and J. M. Krueger (2011). **Biochemical regulation of sleep and sleep biomarkers.** In: *Journal of Clinical Sleep Medicine* 7.5, S38–42. DOI: 10.5664/JCSM.1360.

Cobley, J. N., M. L. Fiorello, and D. M. Bailey (2018). **13 reasons why the brain is susceptible to oxidative stress**. In: *Redox Biology* 15, pp. 490–503. DOI: 10.1016/j.redox.2018.01.008.

Cocchi, L., L. L. Gollo, A. Zalesky, and M. Breakspear (2017). **Criticality in the brain: A synthesis of neurobiology, models and cognition**. In: *Progress in Neurobiology* 158, pp. 132–152. DOI: 10.1016/j.pneurobio.2017.07.002.

Colasanti, B. and N. Khazan (1975). **Electroencephalographic studies on the development of tolerance and cross tolerance to mescaline in the rat**. In: *Psychopharmacologia* 43.3, pp. 201–205. DOI: 10.1007/bf00429251.

Corne, S. J. and R. W. Pickering (1967). **A possible correlation between drug-induced hallucinations in man and a behavioural response in mice**. In: *Psychopharmacologia* 11.1, pp. 65–78.

Cornea-Hébert, V., M. Riad, C. Wu, S. K. Singh, and L. Descarries (1999). **Cellular and subcellular distribution of the serotonin 5-HT2A receptor in the central nervous system of adult rat**. In: *Journal of Comparative Neurology* 409.2, pp. 187–209. DOI: 10.1002/(SICI)1096-9861(19990628)409:2<187::AID-CNE2>3.0.CO;2-P.

Daan, S., D. G. Beersma, and A. A. Borbély (1984). **Timing of human sleep: recovery process gated by a circadian pacemaker**. In: *The American Journal of Physiology* 246.2, R161–183. DOI: 10.1152/ajpregu.1984.246.2.R161.

Dallaspezia, S. and F. Benedetti (2015). **Sleep deprivation therapy for depression**. In: *Current Topics in Behavioral Neurosciences* 25, pp. 483–502. DOI: 10.1007/7854_2014_363.

Darmani, N. A., B. R. Martin, U. Pandey, and R. A. Glennon (1990). **Do functional relationships exist between 5-HT1A and 5-HT2 receptors?** In: *Pharmacology, Biochemistry, and Behavior* 36.4, pp. 901–906. DOI: 10.1016/0091-3057(90)90098-3.

Darmani, N. A., O. B. Mock, L. C. Towns, and C. F. Gerdes (1994). **The head-twitch response in the least shrew (Cryptotis parva) is a 5-HT2- and not a 5-HT1C-mediated phenomenon**. In: *Pharmacology, Biochemistry, and Behavior* 48.2, pp. 383–396. DOI: 10.1016/0091-3057(94)90542-8.

Dauvilliers, Y. (2007). **Insomnia in patients with neurodegenerative conditions**. In: *Sleep Medicine* 8 Suppl 4, S27–34. DOI: 10.1016/S1389-9457(08)70006-6.

Dave, K. D., J. A. Harvey, and V. J. Aloyo (2002). **A novel behavioral model that discriminates between 5-HT2A and 5-HT2C receptor activation**. In: *Pharmacology, Biochemistry, and Behavior* 72.1, pp. 371–378. DOI: 10.1016/s0091-3057(01)00767-5.

David, F., J. T. Schmiedt, H. L. Taylor, G. Orban, G. Di Giovanni, V. N. Uebele, J. J. Renger, R. C. Lambert, N. Leresche, and V. Crunelli (2013). **Essential thalamic contribution to slow waves of natural sleep**. In: *The Journal of Neuroscience* 33.50, pp. 19599–19610. DOI: 10.1523/JNEUROSCI.3169-13.2013.

de Arcangelis, L., C. Perrone-Capano, and H. J. Herrmann (2006). **Self-Organized Criticality Model for Brain Plasticity**. In: *Physical Review Letters* 96.2, p. 028107. DOI: 10.1103/PhysRevLett.96.028107.

Dehghani, N., N. G. Hatsopoulos, Z. D. Haga, R. Parker, B. Greger, E. Halgren, S. S. Cash, and A. Destexhe (2012). **Avalanche Analysis from Multielectrode Ensemble Recordings in Cat, Monkey, and Human Cerebral Cortex during Wakefulness and Sleep**. In: *Frontiers in Physiology* 3. DOI: 10.3389/fphys.2012.00302.

Dibner, C., U. Schibler, and U. Albrecht (2010). **The mammalian circadian timing system: organization and coordination of central and peripheral clocks**. In: *Annual Review of Physiology* 72, pp. 517–549. DOI: 10.1146/annurev-physiol-021909-135821.

Dijk, D. J., D. G. Beersma, and S. Daan (1987a). **EEG power density during nap sleep: reflection of an hourglass measuring the duration of prior wakefulness**. In: *Journal of Biological Rhythms* 2.3, pp. 207–219. DOI: 10.1177/074873048700200304.

Dijk, D. J., D. G. Beersma, S. Daan, G. M. Bloem, and R. H. Van den Hoofdakker (1987b). **Quantitative analysis of the effects of slow wave sleep deprivation during the first 3 h of sleep on subsequent EEG power density**. In: *European Archives of Psychiatry and Neurological Sciences* 236.6, pp. 323–328. DOI: 10.1007/bf00377420.

Edgar, R. S., E. W. Green, Y. Zhao, G. v. Ooijen, M. Olmedo, X. Qin, Y. Xu, M. Pan, U. K. Valekunja, K. A. Feeney, E. S. Maywood, M. H. Hastings, N. S. Baliga, M. Merrow, A. J. Millar, C. H. Johnson, C. P. Kyriacou, J. S. O'Neill, and A. B. Reddy (2012). **Peroxiredoxins are conserved markers of circadian rhythms**. In: *Nature* 485.7399. Number: 7399 Publisher: Nature Publishing Group, pp. 459–464. DOI: 10.1038/nature11088.

Elmenhorst, D., R. Basheer, R. W. McCarley, and A. Bauer (2009). **Sleep deprivation increases A(1) adenosine receptor density in the rat brain**. In: *Brain Research* 1258, pp. 53–58. DOI: 10.1016/j.brainres.2008.12.056.

Erritzoe, D., V. G. Frokjaer, S. Haugbol, L. Marner, C. Svarer, K. Holst, W. F. C. Baaré, P. M. Rasmussen, J. Madsen, O. B. Paulson, and G. M. Knudsen (2009). **Brain serotonin 2A receptor binding: relations to body mass index, tobacco and alcohol use**. In: *NeuroImage* 46.1, pp. 23–30. DOI: 10.1016/j.neuroimage.2009.01.050.

Esser, S. K., S. L. Hill, and G. Tononi (2007). **Sleep Homeostasis and Cortical Synchronization: I. Modeling the Effects of Synaptic Strength on Sleep Slow Waves**. In: *Sleep* 30.12, pp. 1617–1630.

Fantegrossi, W. E., J. Simoneau, M. S. Cohen, S. M. Zimmerman, C. M. Henson, K. C. Rice, and J. H. Woods (2010). **Interaction of 5-HT2A and 5-HT2C Receptors in R(-)-2,5-Dimethoxy-4-iodoamphetamine-Elicited Head Twitch Behavior in Mice**. In: *The Journal of Pharmacology and Experimental Therapeutics* 335.3, pp. 728–734. DOI: 10.1124/jpet.110.172247.

Fantegrossi, W. E., B. W. Gray, J. M. Bailey, D. A. Smith, M. Hansen, and J. L. Kristensen (2015). **Hallucinogen-like effects of 2-([2-(4-cyano-2,5-dimethoxyphenyl) ethylamino]methyl)phenol (25CN-NBOH), a novel N-benzylphenethylamine with**

100-fold selectivity for 5-HT2A receptors, in mice. In: *Psychopharmacology* 232.6, pp. 1039–1047. DOI: 10.1007/s00213-014-3739-3.

Fellin, T., J. M. Ellenbogen, M. De Pittà, E. Ben-Jacob, and M. M. Halassa (2012). **Astrocyte regulation of sleep circuits: experimental and modeling perspectives**. In: *Frontiers in Computational Neuroscience* 6. DOI: 10.3389/fncom.2012.00065.

Fisher, S. P., N. Cui, L. E. McKillop, J. Gemignani, D. M. Bannerman, P. L. Oliver, S. N. Peirson, and V. V. Vyazovskiy (2016). **Stereotypic wheel running decreases cortical activity in mice**. In: *Nature Communications* 7, ncomms13138. DOI: 10.1038/ncomms13138.

Fox, M. A., H. T. French, J. L. LaPorte, A. R. Blackler, and D. L. Murphy (2010). **The serotonin 5-HT2A receptor agonist TCB-2: a behavioral and neurophysiological analysis**. In: *Psychopharmacology* 212.1, pp. 13–23. DOI: 10.1007/s00213-009-1694-1.

Frank, M. G. and H. C. Heller (2019). **The Function(s) of Sleep**. In: *Handbook of Experimental Pharmacology*. DOI: 10.1007/164_2018_140.

Franken, P., D. J. Dijk, I. Tobler, and A. A. Borbely (1991a). **Sleep deprivation in rats: effects on EEG power spectra, vigilance states, and cortical temperature**. In: *American Journal of Physiology-Regulatory, Integrative and Comparative Physiology* 261.1, R198–R208. DOI: 10.1152/ajpregu.1991.261.1.R198.

Franken, P., I. Tobler, and A. A. Borbély (1991b). **Sleep homeostasis in the rat: simulation of the time course of EEG slow-wave activity**. In: *Neuroscience Letters* 130.2, pp. 141–144.

Friedman, N., S. Ito, B. A. W. Brinkman, M. Shimono, R. E. L. DeVille, K. A. Dahmen, J. M. Beggs, and T. C. Butler (2012). **Universal Critical Dynamics in High Resolution Neuronal Avalanche Data**. In: *Physical Review Letters* 108.20, p. 208102. DOI: 10.1103/PhysRevLett.108.208102.

Froese, T., I. Leenen, and T. Palenicek (2018). **A role for enhanced functions of sleep in psychedelic therapy?** In: *Adaptive Behavior* 26.3, pp. 129–135. DOI: 10.1177/1059712318762735.

Funk, C. M., S. Honjoh, A. V. Rodriguez, C. Cirelli, and G. Tononi (2016). **Local Slow Waves in Superficial Layers of Primary Cortical Areas during REM Sleep**. In: *Current Biology* 26.3, pp. 396–403. DOI: 10.1016/j.cub.2015.11.062.

Gautam, S. H., T. T. Hoang, K. McClanahan, S. K. Grady, and W. L. Shew (2015). **Maximizing Sensory Dynamic Range by Tuning the Cortical State to Criticality**. In: *PLOS Computational Biology* 11.12, e1004576. DOI: 10.1371/journal.pcbi.1004576.

Gireesh, E. D. and D. Plenz (2008). **Neuronal avalanches organize as nested theta- and beta/gamma-oscillations during development of cortical layer 2/3**. In: *Proceedings of the National Academy of Sciences* 105.21, pp. 7576–7581. DOI: 10.1073/pnas.0800537105.

Glebov, K., M. Löchner, R. Jabs, T. Lau, O. Merkel, P. Schloss, C. Steinhäuser, and J. Walter (2015). **Serotonin stimulates secretion of exosomes from microglia cells**. In: *Glia* 63.4, pp. 626–634. DOI: 10.1002/glia.22772.

Glennon, R. A., M. Titeler, and J. D. McKenney (1984). **Evidence for 5-HT2 involvement in the mechanism of action of hallucinogenic agents**. In: *Life Sciences* 35.25, pp. 2505–2511. DOI: 10.1016/0024-3205(84)90436-3.

González-Maeso, J., N. V. Weisstaub, M. Zhou, P. Chan, L. Ivic, R. Ang, A. Lira, M. Bradley-Moore, Y. Ge, Q. Zhou, S. C. Sealfon, and J. A. Gingrich (2007). **Hallucinogens Recruit Specific Cortical 5-HT2A Receptor-Mediated Signaling Pathways to Affect Behavior**. In: *Neuron* 53.3, pp. 439–452. DOI: 10.1016/j.neuron.2007.01.008.

González-Rueda, A., V. Pedrosa, R. C. Feord, C. Clopath, and O. Paulsen (2018). **Activity-Dependent Downscaling of Subthreshold Synaptic Inputs during Slow-Wave-Sleep-like Activity In Vivo**. In: *Neuron* 97.6, 1244–1252.e5. DOI: 10.1016/j.neuron.2018.01.047.

Gooley, J. J., J. Lu, T. C. Chou, T. E. Scammell, and C. B. Saper (2001). **Melanopsin in cells of origin of the retinohypothalamic tract**. In: *Nature Neuroscience* 4.12, p. 1165. DOI: 10.1038/nn768.

Graupner, M., P. Wallisch, and S. Ostojic (2016). **Natural Firing Patterns Imply Low Sensitivity of Synaptic Plasticity to Spike Timing Compared with Firing Rate**. In: *The Journal of Neuroscience* 36.44, pp. 11238–11258. DOI: 10.1523/JNEUROSCI.0104-16.2016.

Griffiths, R. R., M. W. Johnson, M. A. Carducci, A. Umbricht, W. A. Richards, B. D. Richards, M. P. Cosimano, and M. A. Klinedinst (2016). **Psilocybin produces substantial and sustained decreases in depression and anxiety in patients with life-threatening cancer: A randomized double-blind trial**. In: *Journal of Psychopharmacology* 30.12, pp. 1181–1197. DOI: 10.1177/0269881116675513.

Grob, C. S., A. L. Danforth, G. S. Chopra, M. Hagerty, C. R. McKay, A. L. Halberstadt, and G. R. Greer (2011). **Pilot Study of Psilocybin Treatment for Anxiety in Patients With Advanced-Stage Cancer**. In: *Archives of General Psychiatry* 68.1, pp. 71–78. DOI: 10.1001/archgenpsychiatry.2010.116.

Grosmark, A. D., K. Mizuseki, E. Pastalkova, K. Diba, and G. Buzsáki (2012). **REM Sleep Reorganizes Hippocampal Excitability**. In: *Neuron* 75.6, pp. 1001–1007. DOI: 10.1016/j.neuron.2012.08.015.

Guillaumin, M. C. C., L. E. McKillop, N. Cui, S. P. Fisher, R. G. Foster, M. de Vos, S. N. Peirson, P. Achermann, and V. V. Vyazovskiy (2018). **Cortical region specific sleep homeostasis in mice: effects of time of day and waking experience**. In: *Sleep*. DOI: 10.1093/sleep/zsy079.

Hahn, G., T. Petermann, M. N. Havenith, S. Yu, W. Singer, D. Plenz, and D. Nikolic (2010). **Neuronal avalanches in spontaneous activity in vivo**. In: *Journal of Neurophysiology*, jn.00953.2009. DOI: 10.1152/jn.00953.2009.

Haimovici, A., E. Tagliazucchi, P. Balenzuela, and D. R. Chialvo (2013). **Brain Organization into Resting State Networks Emerges at Criticality on a Model of the Human Connectome**. In: *Physical Review Letters* 110.17, p. 178101. DOI: 10.1103/PhysRevLett.110.178101.

Halberstadt, A. L., M. Chatha, A. K. Klein, J. Wallach, and S. D. Brandt (2020). **Correlation between the potency of hallucinogens in the mouse head-twitch response assay and their behavioral and subjective effects in other species**. In: *Neuropharmacology*, p. 107933. DOI: 10.1016/j.neuropharm.2019.107933.

Halberstadt, A. L. and M. A. Geyer (2013). **Characterization of the head-twitch response induced by hallucinogens in mice: detection of the behavior based on the dynamics of head movement**. In: *Psychopharmacology* 227.4. DOI: 10.1007/s00213-013-3006-z.

Halberstadt, A. L. and M. A. Geyer (2018). **Effect of Hallucinogens on Unconditioned Behavior**. In: *Current Topics in Behavioral Neurosciences* 36, pp. 159–199. DOI: 10.1007/7854_2016_466.

Halberstadt, A. L., L. Koedood, S. B. Powell, and M. A. Geyer (2011). **Differential contributions of serotonin receptors to the behavioral effects of indoleamine hallucinogens in mice**. In: *Journal of Psychopharmacology* 25.11, pp. 1548–1561. DOI: 10.1177/0269881110388326.

Haldeman, C. and J. M. Beggs (2005). **Critical Branching Captures Activity in Living Neural Networks and Maximizes the Number of Metastable States**. In: *Physical Review Letters* 94.5, p. 058101. DOI: 10.1103/PhysRevLett.94.058101.

Hardstone, R., S.-S. Poil, G. Schiavone, R. Jansen, V. V. Nikulin, H. D. Mansvelder, and K. Linkenkaer-Hansen (2012). **Detrended Fluctuation Analysis: A Scale-Free View on Neuronal Oscillations**. In: *Frontiers in Physiology* 3. DOI: 10.3389/fphys.2012.00450.

Hastings, M. H., M. Brancaccio, and E. S. Maywood (2014). **Circadian pacemaking in cells and circuits of the suprachiasmatic nucleus**. In: *Journal of Neuroendocrinology* 26.1, pp. 2–10. DOI: 10.1111/jne.12125.

Hendricks, P. S., C. B. Thorne, C. B. Clark, D. W. Coombs, and M. W. Johnson (2015). **Classic psychedelic use is associated with reduced psychological distress and suicidality in the United States adult population**. In: *Journal of Psychopharmacology* 29.3, pp. 280–288. DOI: 10.1177/0269881114565653.

Hengen, K. B., A. T. Pacheco, J. N. McGregor, S. D. Van Hooser, and G. G. Turrigiano (2016). **Neuronal Firing Rate Homeostasis is Inhibited by Sleep and Promoted by Wake**. In: *Cell* 165.1, pp. 180–191. DOI: 10.1016/j.cell.2016.01.046.

Hengen, K., M. Lambo, S. Van Hooser, D. Katz, and G. Turrigiano (2013). **Firing Rate Homeostasis in Visual Cortex of Freely Behaving Rodents**. In: *Neuron* 80.2, pp. 335–342. DOI: 10.1016/j.neuron.2013.08.038.

Hibicke, M., A. N. Landry, H. M. Kramer, Z. K. Talman, and C. D. Nichols (2020). **Psychedelics, but Not Ketamine, Produce Persistent Antidepressant-like Effects in a Rodent Experimental System for the Study of Depression**. In: *ACS Chemical Neuroscience*. Publisher: American Chemical Society. DOI: 10.1021/acschemneuro.9b00493.

Hsu, D. and J. M. Beggs (2006). **Neuronal avalanches and criticality: A dynamical model for homeostasis**. In: *Neurocomputing*. Computational Neuroscience: Trends in Research 2006Computational Neuroscience 2005 69.10, pp. 1134–1136. DOI: 10.1016/j.neucom.2005.12.060.

Huber, R., T. Deboer, and I. Tobler (2000a). **Effects of sleep deprivation on sleep and sleep EEG in three mouse strains: empirical data and simulations**. In: *Brain Research* 857.1, pp. 8–19. DOI: 10.1016/s0006-8993(99)02248-9.

Huber, R., T. Deboer, and I. Tobler (2000b). **Topography of EEG dynamics after sleep deprivation in mice**. In: *Journal of Neurophysiology* 84.4, pp. 1888–1893. DOI: 10.1152/jn.2000.84.4.1888.

Huber, R., M. F. Ghilardi, M. Massimini, and G. Tononi (2004). **Local sleep and learning**. In: *Nature* 430.6995, pp. 78–81. DOI: 10.1038/nature02663.

Huber, R., H. Mäki, M. Rosanova, S. Casarotto, P. Canali, A. G. Casali, G. Tononi, and M. Massimini (2013). **Human cortical excitability increases with time awake**. In: *Cerebral Cortex* 23.2, pp. 332–338. DOI: 10.1093/cercor/bhs014.

Hughes, S., A. Jagannath, M. W. Hankins, R. G. Foster, and S. N. Peirson (2015). **Photic regulation of clock systems**. In: *Methods in Enzymology* 552, pp. 125–143. DOI: 10.1016/bs.mie.2014.10.018.

Jacobs, B. L., M. E. Trulson, and W. C. Stern (1976). **An animal behavior model for studying the actions of LSD and related hallucinogens**. In: *Science* 194.4266, pp. 741–743. DOI: 10.1126/science.982043.

Jajoo, S., D. Mukherjea, S. Pingle, Y. Sekino, and V. Ramkumar (2006). **Induction of adenosine A1 receptor expression by pertussis toxin via an adenosine 5'-diphosphate ribosylation-independent pathway**. In: *The Journal of Pharmacology and Experimental Therapeutics* 317.1, pp. 1–10. DOI: 10.1124/jpet.105.096255.

Jakab, R. L. and P. S. Goldman-Rakic (1998). **5-Hydroxytryptamine2A serotonin receptors in the primate cerebral cortex: possible site of action of hallucinogenic and antipsychotic drugs in pyramidal cell apical dendrites**. In: *Proceedings of the National Academy of Sciences of the United States of America* 95.2, pp. 735–740.

Jessberger, J., W. Zhong, J. Brankačk, and A. Draguhn (2016). **Olfactory Bulb Field Potentials and Respiration in Sleep-Wake States of Mice**. In: *Neural Plasticity*.

Johnson, M. W., A. Garcia-Romeu, M. P. Cosimano, and R. R. Griffiths (2014). **Pilot study of the 5-HT2AR agonist psilocybin in the treatment of tobacco addiction**. In: *Journal of Psychopharmacology* 28.11, pp. 983–992. DOI: 10.1177/0269881114548296.

Kajikawa, Y. and C. E. Schroeder (2011). **How local is the local field potential?** In: *Neuron* 72.5, pp. 847–858. DOI: 10.1016/j.neuron.2011.09.029.

Kattler, H, D. J. Dijk, and A. A. Borbély (1994). **Effect of unilateral somatosensory stimulation prior to sleep on the sleep EEG in humans**. In: *Journal of Sleep Research* 3.3, pp. 159–164. DOI: 10.1111/j.1365-2869.1994.tb00123.x.

Kay, D. C. and W. R. Martin (1978). **LSD and tryptamine effects on sleep/wakefulness and electrocorticogram patterns in intact cats**. In: *Psychopharmacology* 58.3, pp. 223–228. DOI: 10.1007/bf00427383.

Keller, D. L. and W. W. Umbreit (1956). **Permanent alteration of behavior in mice by chemical and psychological means**. In: *Science* 124.3225, pp. 723–724. DOI: 10.1126/science.124.3225.723.

Kempf, A., S. M. Song, C. B. Talbot, and G. Miesenböck (2019). **A potassium channel Beta-subunit couples mitochondrial electron transport to sleep**. In: *Nature* 568.7751, pp. 230–234. DOI: 10.1038/s41586-019-1034-5.

Kessenich, L. M. v., L. d. Arcangelis, and H. J. Herrmann (2016). **Synaptic plasticity and neuronal refractory time cause scaling behaviour of neuronal avalanches**. In: *Scientific Reports* 6.1, pp. 1–7. DOI: 10.1038/srep32071.

Kilman, V., M. C. W. van Rossum, and G. G. Turrigiano (2002). **Activity deprivation reduces miniature IPSC amplitude by decreasing the number of postsynaptic GABA(A) receptors clustered at neocortical synapses**. In: *The Journal of Neuroscience* 22.4, pp. 1328–1337.

Kinouchi, O. and M. Copelli (2006). **Optimal dynamical range of excitable networks at criticality**. In: *Nature Physics* 2.5, pp. 348–351. DOI: 10.1038/nphys289.

Kültz, D. (2005). **Molecular and Evolutionary Basis of the Cellular Stress Response**. In: *Annual Review of Physiology* 67.1, pp. 225–257. DOI: 10.1146/annurev.physiol.67.040403.103635.

Kometer, M., A. Schmidt, L. Jäncke, and F. X. Vollenweider (2013). **Activation of Serotonin 2A Receptors Underlies the Psilocybin-Induced Effects on Alpha Oscillations, N170 Visual-Evoked Potentials, and Visual Hallucinations**. In: *Journal of Neuroscience* 33.25, pp. 10544–10551. DOI: 10.1523/JNEUROSCI.3007-12.2013.

Krueger, J. M., D. M. Rector, S. Roy, H. P. A. V. Dongen, G. Belenky, and J. Panksepp (2008). **Sleep as a fundamental property of neuronal assemblies**. In: *Nature Reviews Neuroscience* 9.12, p. 910. DOI: 10.1038/nrn2521.

Krueger, J. M. and G. Tononi (2011). **Local Use-Dependent Sleep; Synthesis of the New Paradigm**. In: *Current topics in medicinal chemistry* 11.19, pp. 2490–2492.

Lagarias, J., J. Reeds, M. Wright, and P. Wright (1998). **Convergence Properties of the Nelder–Mead Simplex Method in Low Dimensions**. In: *SIAM Journal on Optimization* 9.1, pp. 112–147. DOI: 10.1137/S1052623496303470.

Lambe, E. K. and G. K. Aghajanian (2007). **Prefrontal cortical network activity: Opposite effects of psychedelic hallucinogens and D1/D5 dopamine receptor activation**. In: *Neuroscience* 145.3, pp. 900–910. DOI: 10.1016/j.neuroscience.2006.12.048.

Lambe, E. K. and G. K. Aghajanian (2006). **Hallucinogen-induced UP states in the brain slice of rat prefrontal cortex: role of glutamate spillover and NR2B-NMDA receptors**. In: *Neuropsychopharmacology* 31.8, pp. 1682–1689. DOI: 10.1038/sj.npp.1300944.

Lappalainen, J., J. Herpich, and C. Tetzlaff (2019). **A Theoretical Framework to Derive Simple, Firing-Rate-Dependent Mathematical Models of Synaptic Plasticity**. In: *Frontiers in Computational Neuroscience* 13. DOI: 10.3389/fncom.2019.00026.

Lebedev, A., M. Kaelen, M. Lövdén, J. Nilsson, A. Feilding, D. Nutt, and R. Carhart-Harris (2016). **LSD-induced entropic brain activity predicts subsequent personality change**. In: *Human Brain Mapping* 37.9, pp. 3203–3213. DOI: 10.1002/hbm.23234.

Lee, S.-H. and Y. Dan (2012). **Neuromodulation of Brain States**. In: *Neuron* 76.1, pp. 209–222. DOI: 10.1016/j.neuron.2012.09.012.

Levenstein, D., B. O. Watson, J. Rinzel, and G. Buzsáki (2017). **Sleep regulation of the distribution of cortical firing rates**. In: *Current Opinion in Neurobiology*. Neurobiology of Sleep 44, pp. 34–42. DOI: 10.1016/j.conb.2017.02.013.

Lewis, P. A. and S. J. Durrant (2011). **Overlapping memory replay during sleep builds cognitive schemata**. In: *Trends in Cognitive Sciences* 15.8, pp. 343–351. DOI: 10.1016/j.tics.2011.06.004.

Leysen, J. E., C. J. Niemegeers, J. M. V. Nueten, and P. M. Laduron (1982). **[3H]Ketanserin (R 41 468), a selective 3H-ligand for serotonin2 receptor binding sites. Binding properties, brain distribution, and functional role.** In: *Molecular Pharmacology* 21.2, pp. 301–314.

Lima, S. L. and N. C. Rattenborg (2007). **A behavioural shutdown can make sleeping safer: a strategic perspective on the function of sleep**. In: *Animal Behaviour* 74.2, pp. 189–197. DOI: 10.1016/j.anbehav.2006.12.007.

Liu, C., D. R. Weaver, S. H. Strogatz, and S. M. Reppert (1997). **Cellular construction of a circadian clock: period determination in the suprachiasmatic nuclei**. In: *Cell* 91.6, pp. 855–860. DOI: 10.1016/s0092-8674(00)80473-0.

Liu, D. and Y. Dan (2019). **A Motor Theory of Sleep-Wake Control: Arousal-Action Circuit**. In: *Annual Review of Neuroscience* 42.1. Publisher: Annual Reviews, pp. 27–46. DOI: 10.1146/annurev-neuro-080317-061813.

Liu, Y., S. S. McAfee, and D. H. Heck (2017). **Hippocampal sharp-wave ripples in awake mice are entrained by respiration**. In: *Scientific Reports* 7.1. Number: 1 Publisher: Nature Publishing Group, pp. 1–9. DOI: 10.1038/s41598-017-09511-8.

Liu, Z.-W., U. Faraguna, C. Cirelli, G. Tononi, and X.-B. Gao (2010). **Direct evidence for wake-related increases and sleep-related decreases in synaptic strength in rodent cortex**. In: *The Journal of Neuroscience* 30.25, pp. 8671–8675. DOI: 10.1523/JNEUROSCI.1409-10.2010.

Lord, L.-D., P. Expert, S. Atasoy, L. Roseman, K. Rapuano, R. Lambiotte, D. J. Nutt, G. Deco, R. L. Carhart-Harris, M. L. Kringelbach, and J. Cabral (2019). **Dynamical exploration of the repertoire of brain networks at rest is modulated by psilocybin**. In: *NeuroImage* 199, pp. 127–142. DOI: 10.1016/j.neuroimage.2019.05.060.

Lowrey, P. L. and J. S. Takahashi (2011). **Genetics of circadian rhythms in Mammalian model organisms**. In: *Advances in Genetics* 74, pp. 175–230. DOI: 10.1016/B978-0-12-387690-4.00006-4.

Lucas, R. J., M. S. Freedman, D. Lupi, M. Munoz, Z. K. David-Gray, and R. G. Foster (2001). **Identifying the photoreceptive inputs to the mammalian circadian system using transgenic and retinally degenerate mice**. In: *Behavioural Brain Research* 125.1, pp. 97–102. DOI: 10.1016/s0166-4328(01)00274-1.

Ly, C., A. C. Greb, L. P. Cameron, J. M. Wong, E. V. Barragan, P. C. Wilson, K. F. Burbach, S. S. Zarandi, A. Sood, M. R. Paddy, W. C. Duim, M. Y. Dennis, A. K. McAllister, K. M. Ori-McKenney, J. A. Gray, and D. E. Olson (2018). **Psychedelics Promote Structural and Functional Neural Plasticity**. In: *Cell Reports* 23.11, pp. 3170–3182. DOI: 10.1016/j.celrep.2018.05.022.

Ma, Z., G. G. Turrigiano, R. Wessel, and K. B. Hengen (2019). **Cortical Circuit Dynamics Are Homeostatically Tuned to Criticality In Vivo**. In: *Neuron* 104.4, 655–664.e4. DOI: 10.1016/j.neuron.2019.08.031.

Mackiewicz, M., K. R. Shockley, M. A. Romer, R. J. Galante, J. E. Zimmerman, N. Naidoo, D. A. Baldwin, S. T. Jensen, G. A. Churchill, and A. I. Pack (2007). **Macromolecule biosynthesis: a key function of sleep**. In: *Physiological Genomics* 31.3, pp. 441–457. DOI: 10.1152/physiolgenomics.00275.2006.

Mahowald, M. W. and C. H. Schenck (2005). **Insights from studying human sleep disorders**. In: *Nature*. DOI: 10.1038/nature04287.

Marek, G. J., R. A. Wright, J. C. Gewirtz, and D. D. Schoepp (2001). **A major role for thalamocortical afferents in serotonergic hallucinogen receptor function in the rat neocortex**. In: *Neuroscience* 105.2, pp. 379–392. DOI: 10.1016/s0306-4522(01)00199-3.

Marek, G. J. (2018). **Interactions of Hallucinogens with the Glutamatergic System: Permissive Network Effects Mediated Through Cortical Layer V Pyramidal Neurons**. In: *Behavioral Neurobiology of Psychedelic Drugs*. Current Topics in Behavioral Neurosciences. Ed. by A. L. Halberstadt, F. X. Vollenweider, and D. E. Nichols, pp. 107–135. DOI: 10.1007/7854_2017_480.

Mascetti, G. G. (2016). **Unihemispheric sleep and asymmetrical sleep: behavioral, neurophysiological, and functional perspectives**. In: *Nature and Science of Sleep*. DOI: 10.2147/NSS.S71970.

Massimini, M., R. Huber, F. Ferrarelli, S. Hill, and G. Tononi (2004). **The sleep slow oscillation as a traveling wave**. In: *The Journal of Neuroscience* 24.31, pp. 6862–6870. DOI: 10.1523/JNEUROSCI.1318-04.2004.

Mattia, M. and M. V. Sanchez-Vives (2012). **Exploring the spectrum of dynamical regimes and timescales in spontaneous cortical activity**. In: *Cognitive Neurodynamics* 6.3, pp. 239–250. DOI: 10.1007/s11571-011-9179-4.

McKillop, L. E., S. P. Fisher, N. Cui, S. N. Peirson, R. G. Foster, K. A. Wafford, and V. V. Vyazovskiy (2018). **Effects of Aging on Cortical Neural Dynamics and Local Sleep Homeostasis in Mice**. In: *Journal of Neuroscience* 38.16, pp. 3911–3928. DOI: 10.1523/JNEUROSCI.2513-17.2018.

Meerlo, P., R. Havekes, and A. Steiger (2015). **Chronically restricted or disrupted sleep as a causal factor in the development of depression**. In: *Current Topics in Behavioral Neurosciences* 25, pp. 459–481. DOI: 10.1007/7854_2015_367.

Meerlo, P., A. Sgoifo, and D. Suchecki (2008). **Restricted and disrupted sleep: effects on autonomic function, neuroendocrine stress systems and stress responsivity**. In: *Sleep Medicine Reviews* 12.3, pp. 197–210. DOI: 10.1016/j.smrv.2007.07.007.

Meisel, C., K. Bailey, P. Achermann, and D. Plenz (2017a). **Decline of long-range temporal correlations in the human brain during sustained wakefulness**. In: *Scientific Reports* 7. DOI: 10.1038/s41598-017-12140-w.

Meisel, C., A. Klaus, V. V. Vyazovskiy, and D. Plenz (2017b). **The Interplay between Long- and Short-Range Temporal Correlations Shapes Cortex Dynamics across Vigilance States**. In: *Journal of Neuroscience* 37.42, pp. 10114–10124. DOI: 10.1523/JNEUROSCI.0448-17.2017.

Meisel, C., E. Olbrich, O. Shriki, and P. Achermann (2013). **Fading Signatures of Critical Brain Dynamics during Sustained Wakefulness in Humans**. In: *The Journal of Neuroscience* 33.44, pp. 17363–17372. DOI: 10.1523/JNEUROSCI.1516-13.2013.

Meisel, C., A. Storch, S. Hallmeyer-Elgner, E. Bullmore, and T. Gross (2012). **Failure of Adaptive Self-Organized Criticality during Epileptic Seizure Attacks**. In: *PLOS Computational Biology* 8.1, e1002312. DOI: 10.1371/journal.pcbi.1002312.

Miner, L. a. H., J. R. Backstrom, E. Sanders-Bush, and S. R. Sesack (2003). **Ultrastructural localization of serotonin2A receptors in the middle layers of the rat prelimbic prefrontal cortex**. In: *Neuroscience* 116.1, pp. 107–117. DOI: 10.1016/s0306-4522(02)00580-8.

Miyawaki, H. and K. Diba (2016). **Regulation of hippocampal firing by network oscillations during sleep**. In: *Current Biology* 26.7, pp. 893–902. DOI: 10.1016/j.cub.2016.02.024.

Miyawaki, H., B. O. Watson, and K. Diba (2019). **Neuronal firing rates diverge during REM and homogenize during non-REM**. In: *Scientific Reports* 9.1, p. 689. DOI: 10.1038/s41598-018-36710-8.

Mohawk, J. A., C. B. Green, and J. S. Takahashi (2012). **Central and Peripheral Circadian Clocks in Mammals**. In: *Annual Review of Neuroscience* 35, pp. 445–462. DOI: 10.1146/annurev-neuro-060909-153128.

Monti, J. M. and H. Jantos (2006). **Effects of the serotonin 5-HT2A/2C receptor agonist DOI and of the selective 5-HT2A or 5-HT2C receptor antagonists EMD 281014 and SB-243213, respectively, on sleep and waking in the rat**. In: *European Journal of Pharmacology* 553.1, pp. 163–170. DOI: 10.1016/j.ejphar.2006.09.027.

Moreno, F. A., C. B. Wiegand, E. K. Taitano, and P. L. Delgado (2006). **Safety, tolerability, and efficacy of psilocybin in 9 patients with obsessive-compulsive disorder**. In: *The Journal of Clinical Psychiatry* 67.11, pp. 1735–1740. DOI: 10.4088/jcp.v67n1110.

Moretti, P. and M. A. Munoz (2013). **Griffiths phases and the stretching of criticality in brain networks**. In: *Nature Communications* 4, p. 2521. DOI: 10.1038/ncomms3521.

Morin, L. P. (2013). **Neuroanatomy of the extended circadian rhythm system**. In: *Experimental Neurology* 243, pp. 4–20. DOI: 10.1016/j.expneurol.2012.06.026.

Mukhametov, L. M., A. Y. Supin, and I. G. Polyakova (1977). **Interhemispheric asymmetry of the electroencephalographic sleep patterns in dolphins**. In: *Brain Research* 134.3, pp. 581–584. DOI: 10.1016/0006-8993(77)90835-6.

Murphy, M., R. Huber, S. Esser, B. A. Riedner, M. Massimini, F. Ferrarelli, M. F. Ghilardi, and G. Tononi (2011). **The cortical topography of local sleep**. In: *Current Topics in Medicinal Chemistry* 11.19, pp. 2438–2446.

Muthukumaraswamy, S. D., R. L. Carhart-Harris, R. J. Moran, M. J. Brookes, T. M. Williams, D. Errtizoe, B. Sessa, A. Papadopoulos, M. Bolstridge, K. D. Singh, A. Feilding, K. J. Friston, and D. J. Nutt (2013). **Broadband Cortical Desynchronization Underlies the Human Psychedelic State**. In: *Journal of Neuroscience* 33.38, pp. 15171–15183. DOI: 10.1523/JNEUROSCI.2063-13.2013.

Naidoo, N., W. Giang, R. J. Galante, and A. I. Pack (2005). **Sleep deprivation induces the unfolded protein response in mouse cerebral cortex**. In: *Journal of*

Neurochemistry 92.5. _eprint: https://onlinelibrary.wiley.com/doi/pdf/10.1111/j.1471-4159.2004.02952.x, pp. 1150–1157. DOI: 10.1111/j.1471-4159.2004.02952.x.

Nair, S. G. and G. A. Gudelsky (2004). **Activation of 5-HT2 receptors enhances the release of acetylcholine in the prefrontal cortex and hippocampus of the rat**. In: *Synapse* 53.4, pp. 202–207. DOI: 10.1002/syn.20054.

Ness, T. V., M. W. H. Remme, and G. T. Einevoll (2016). **Active subthreshold dendritic conductances shape the local field potential**. In: *The Journal of Physiology* 594.13, pp. 3809–3825. DOI: 10.1113/JP272022.

Niethard, N., M. Hasegawa, T. Itokazu, C. Oyanedel, J. Born, and T. Sato (2016). **Sleep-Stage-Specific Regulation of Cortical Excitation and Inhibition**. In: *Current Biology* 26.20, pp. 2739–2749. DOI: 10.1016/j.cub.2016.08.035.

Nir, Y., R. J. Staba, T. Andrillon, V. V. Vyazovskiy, C. Cirelli, I. Fried, and G. Tononi (2011). **Regional slow waves and spindles in human sleep**. In: *Neuron* 70.1, pp. 153–169. DOI: 10.1016/j.neuron.2011.02.043.

Nobili, L., M. Ferrara, F. Moroni, L. De Gennaro, G. Lo Russo, C. Campus, F. Cardinale, and F. De Carli (2011). **Dissociated wake-like and sleep-like electro-cortical activity during sleep**. In: *NeuroImage* 58, pp. 612–9. DOI: 10.1016/j.neuroimage.2011.06.032.

Obal, F. and J. M. Krueger (2003). **Biochemical regulation of non-rapid-eye-movement sleep**. In: *Frontiers in Bioscience* 8, pp. d520–550. DOI: 10.2741/1033.

Okun, M., N. A. Steinmetz, L. Cossell, M. F. Iacaruso, H. Ko, P. Barthó, T. Moore, S. B. Hofer, T. D. Mrsic-Flogel, M. Carandini, and K. D. Harris (2015). **Diverse coupling of neurons to populations in sensory cortex**. In: *Nature* 521.7553, pp. 511–515. DOI: 10.1038/nature14273.

O'Leary, T., A. H. Williams, A. Franci, and E. Marder (2014). **Cell types, network homeostasis, and pathological compensation from a biologically plausible ion channel expression model**. In: *Neuron* 82.4, pp. 809–821. DOI: 10.1016/j.neuron.2014.04.002.

Palhano-Fontes, F., K. C. Andrade, L. F. Tofoli, A. C. Santos, J. A. S. Crippa, J. E. C. Hallak, S. Ribeiro, and D. B. de Araujo (2015). **The psychedelic state induced by ayahuasca modulates the activity and connectivity of the default mode network**. In: *PLOS ONE* 10.2, e0118143. DOI: 10.1371/journal.pone.0118143.

Palva, J. M., A. Zhigalov, J. Hirvonen, O. Korhonen, K. Linkenkaer-Hansen, and S. Palva (2013). **Neuronal long-range temporal correlations and avalanche dynamics are correlated with behavioral scaling laws**. In: *Proceedings of the National Academy of Sciences of the United States of America* 110.9, pp. 3585–3590. DOI: 10.1073/pnas.1216855110.

Pasquale, V., P. Massobrio, L. L. Bologna, M. Chiappalone, and S. Martinoia (2008). **Self-organization and neuronal avalanches in networks of dissociated cortical**

neurons. In: *Neuroscience* 153.4, pp. 1354–1369. DOI: 10.1016/j.neuroscience.2008.03.050.

Passie, T., J. Seifert, U. Schneider, and H. M. Emrich (2002). **The pharmacology of psilocybin**. In: *Addiction Biology* 7.4, pp. 357–364. DOI: 10.1080/1355621021000005937.

Paxinos, G. and K. Franklin (2013). **The Rat Brain in Stereotaxic Coordinates - 7th Edition**.

Pazos, A., A. Probst, and J. M. Palacios (1987). **Serotonin receptors in the human brain–IV. Autoradiographic mapping of serotonin-2 receptors**. In: *Neuroscience* 21.1, pp. 123–139. DOI: 10.1016/0306-4522(87)90327-7.

Pearlmutter, B. A. and C. J. Houghton (2009). **A new hypothesis for sleep: tuning for criticality**. In: *Neural Computation* 21.6, pp. 1622–1641. DOI: 10.1162/neco.2009.05-08-787.

Perogamvros, L. and S. Schwartz (2015). **Sleep and emotional functions**. In: *Current Topics in Behavioral Neurosciences* 25, pp. 411–431. DOI: 10.1007/7854_2013_271.

Petermann, T., T. C. Thiagarajan, M. A. Lebedev, M. A. L. Nicolelis, D. R. Chialvo, and D. Plenz (2009). **Spontaneous cortical activity in awake monkeys composed of neuronal avalanches**. In: *Proceedings of the National Academy of Sciences* 106.37, pp. 15921–15926. DOI: 10.1073/pnas.0904089106.

Pigarev, I. N., H. C. Nothdurft, and S. Kastner (1997). **Evidence for asynchronous development of sleep in cortical areas**. In: *Neuroreport* 8.11, pp. 2557–2560.

Plenz, D. and T. C. Thiagarajan (2007). **The organizing principles of neuronal avalanches: cell assemblies in the cortex?** In: *Trends in Neurosciences* 30.3, pp. 101–110. DOI: 10.1016/j.tins.2007.01.005.

Priesemann, V., M. H. Munk, and M. Wibral (2009). **Subsampling effects in neuronal avalanche distributions recorded in vivo**. In: *BMC Neuroscience* 10, p. 40. DOI: 10.1186/1471-2202-10-40.

Priesemann, V., M. Valderrama, M. Wibral, and M. Le Van Quyen (2013). **Neuronal Avalanches Differ from Wakefulness to Deep Sleep – Evidence from Intracranial Depth Recordings in Humans**. In: *PLOS Computational Biology* 9.3, e1002985. DOI: 10.1371/journal.pcbi.1002985.

Priesemann, V., M. Wibral, M. Valderrama, R. Pröpper, M. Le Van Quyen, T. Geisel, J. Triesch, D. Nikolić, and M. H. J. Munk (2014). **Spike avalanches in vivo suggest a driven, slightly subcritical brain state**. In: *Frontiers in Systems Neuroscience* 8. DOI: 10.3389/fnsys.2014.00108.

Puig, M. V., P. Celada, L. Díaz-Mataix, and F. Artigas (2003). **In vivo modulation of the activity of pyramidal neurons in the rat medial prefrontal cortex by 5-HT2A receptors: relationship to thalamocortical afferents**. In: *Cerebral Cortex* 13.8, pp. 870–882. DOI: 10.1093/cercor/13.8.870.

Qiu, M.-H., M. C. Chen, and J. Lu (2015). **Cortical neuronal activity does not regulate sleep homeostasis**. In: *Neuroscience* 297, pp. 211–218. DOI: 10.1016/j.neuroscience.2015.03.070.

Quiroga, R. Q., Z. Nadasdy, and Y. Ben-Shaul (2004). **Unsupervised spike detection and sorting with wavelets and superparamagnetic clustering**. In: *Neural Computation* 16.8, pp. 1661–1687. DOI: 10.1162/089976604774201631.

Raizen, D. M., J. E. Zimmerman, M. H. Maycock, U. D. Ta, Y.-j. You, M. V. Sundaram, and A. I. Pack (2008). **Lethargus is a Caenorhabditis elegans sleep-like state**. In: *Nature* 451.7178, pp. 569–572. DOI: 10.1038/nature06535.

Ralph, M., R. Foster, F. Davis, and M Menaker (1990). **Transplanted Suprachiasmatic Nucleus Determines Circadian Period**. In: *Science* 247, pp. 975–8. DOI: 10.1126/science.2305266.

Rambousek, L., T. Palenicek, K. Vales, and A. Stuchlik (2014). **The Effect of Psilocin on Memory Acquisition, Retrieval, and Consolidation in the Rat**. In: *Frontiers in Behavioral Neuroscience* 8. DOI: 10.3389/fnbeh.2014.00180.

Rasch, B. and J. Born (2013). **About Sleep's Role in Memory**. In: *Physiological Reviews* 93.2, pp. 681–766. DOI: 10.1152/physrev.00032.2012.

Rattenborg, N. C., S. L. Lima, and J. A. Lesku (2012). **Sleep Locally, Act Globally**. In: *The Neuroscientist* 18.5, pp. 533–546. DOI: 10.1177/1073858412441086.

Rattenborg, N. C., D. Martinez-Gonzalez, and J. A. Lesku (2009). **Avian sleep homeostasis: convergent evolution of complex brains, cognition and sleep functions in mammals and birds**. In: *Neuroscience and Biobehavioral Reviews* 33.3, pp. 253–270. DOI: 10.1016/j.neubiorev.2008.08.010.

Rector, D. M., J. L. Schei, H. P. A. Van Dongen, G. Belenky, and J. M. Krueger (2009). **Physiological Markers of Local Sleep**. In: *The European Journal of Neuroscience* 29.9, pp. 1771–1778. DOI: 10.1111/j.1460-9568.2009.06717.x.

Reed, W. J. and B. D. Hughes (2002). **From gene families and genera to incomes and internet file sizes: Why power laws are so common in nature**. In: *Physical Review E* 66.6, p. 067103. DOI: 10.1103/PhysRevE.66.067103.

Reig, R. and M. V. Sanchez-Vives (2007). **Synaptic Transmission and Plasticity in an Active Cortical Network**. In: *PLOS ONE* 2.8, e670. DOI: 10.1371/journal.pone.0000670.

Reimund, E. (1994). **The free radical flux theory of sleep**. In: *Medical Hypotheses* 43.4, pp. 231–233. DOI: 10.1016/0306-9877(94)90071-X.

Reppert, S. M. and D. R. Weaver (2002). **Coordination of circadian timing in mammals**. In: *Nature* 418.6901, pp. 935–941. DOI: 10.1038/nature00965.

Riba, J., P. Anderer, F. Jané, B. Saletu, and M. J. Barbanoj (2004). **Effects of the South American psychoactive beverage ayahuasca on regional brain electrical activity in humans: a functional neuroimaging study using low-resolution**

electromagnetic tomography. In: *Neuropsychobiology* 50.1, pp. 89–101. DOI: 10.1159/000077946.

Ribeiro, T. L., M. Copelli, F. Caixeta, H. Belchior, D. R. Chialvo, M. A. L. Nicolelis, and S. Ribeiro (2010). **Spike Avalanches Exhibit Universal Dynamics across the Sleep-Wake Cycle**. In: *PLOS ONE* 5.11, e14129. DOI: 10.1371/journal.pone.0014129.

Riedner, B. A., B. K. Hulse, M. J. Murphy, F. Ferrarelli, and G. Tononi (2011). **Temporal dynamics of cortical sources underlying spontaneous and peripherally evoked slow waves**. In: *Progress in Brain Research* 193, pp. 201–218. DOI: 10.1016/B978-0-444-53839-0.00013-2.

Riedner, B. A., V. V. Vyazovskiy, R. Huber, M. Massimini, S. Esser, M. Murphy, and G. Tononi (2007). **Sleep homeostasis and cortical synchronization: III. A high-density EEG study of sleep slow waves in humans**. In: *Sleep* 30.12, pp. 1643–1657. DOI: 10.1093/sleep/30.12.1643.

Rodriguez, A. V., C. M. Funk, V. V. Vyazovskiy, Y. Nir, G. Tononi, and C. Cirelli (2016). **Why Does Sleep Slow-Wave Activity Increase After Extended Wake? Assessing the Effects of Increased Cortical Firing During Wake and Sleep**. In: *Journal of Neuroscience* 36.49, pp. 12436–12447. DOI: 10.1523/JNEUROSCI.1614-16.2016.

Ross, S., A. Bossis, J. Guss, G. Agin-Liebes, T. Malone, B. Cohen, S. E. Mennenga, A. Belser, K. Kalliontzi, J. Babb, Z. Su, P. Corby, and B. L. Schmidt (2016). **Rapid and sustained symptom reduction following psilocybin treatment for anxiety and depression in patients with life-threatening cancer: a randomized controlled trial**. In: *Journal of Psychopharmacology* 30.12, pp. 1165–1180. DOI: 10.1177/0269881116675512.

Rubinov, M., O. Sporns, J.-P. Thivierge, and M. Breakspear (2011). **Neurobiologically Realistic Determinants of Self-Organized Criticality in Networks of Spiking Neurons**. In: *PLOS Computational Biology* 7.6, e1002038. DOI: 10.1371/journal.pcbi.1002038.

Rusterholz, T. and P. Achermann (2011). **Topographical aspects in the dynamics of sleep homeostasis in young men: individual patterns**. In: *BMC Neuroscience* 12, p. 84. DOI: 10.1186/1471-2202-12-84.

Saberi-Moghadam, S., A. Simi, H. Setareh, C. Mikhail, and M. Tafti (2018). **In vitro Cortical Network Firing is Homeostatically Regulated: A Model for Sleep Regulation**. In: *Scientific Reports* 8.1, p. 6297. DOI: 10.1038/s41598-018-24339-6.

Sanchez-Vives, M. V. and D. A. McCormick (2000). **Cellular and network mechanisms of rhythmic recurrent activity in neocortex**. In: *Nature Neuroscience* 3.10, pp. 1027–1034. DOI: 10.1038/79848.

Sanchez-Vives, M. and M. Mattia (2014). **Slow wave activity as the default mode of the cerebral cortex**. In: *Archives Italiennes de Biologie* 152, pp. 147–55. DOI: 10.12871/000298292014239.

Sanchez-Vives, M. V., M. Massimini, and M. Mattia (2017). **Shaping the Default Activity Pattern of the Cortical Network**. In: *Neuron* 94.5, pp. 993–1001. DOI: 10.1016/j.neuron.2017.05.015.

Santana, N., A. Bortolozzi, J. Serrats, G. Mengod, and F. Artigas (2004). **Expression of Serotonin1A and Serotonin2A Receptors in Pyramidal and GABAergic Neurons of the Rat Prefrontal Cortex**. In: *Cerebral Cortex* 14.10, pp. 1100–1109. DOI: 10.1093/cercor/bhh070.

Santos, R. G. dos, F. L. Osório, J. A. S. Crippa, J. Riba, A. W. Zuardi, and J. E. C. Hallak (2016). **Antidepressive, anxiolytic, and antiaddictive effects of ayahuasca, psilocybin and lysergic acid diethylamide (LSD): a systematic review of clinical trials published in the last 25 years**. In: *Therapeutic Advances in Psychopharmacology* 6.3, pp. 193–213. DOI: 10.1177/2045125316638008.

Saper, C. B., P. M. Fuller, N. P. Pedersen, J. Lu, and T. E. Scammell (2010). **Sleep state switching**. In: *Neuron* 68.6, pp. 1023–1042. DOI: 10.1016/j.neuron.2010.11.032.

Savage, V. M. and G. B. West (2007). **A quantitative, theoretical framework for understanding mammalian sleep**. In: *Proceedings of the National Academy of Sciences* 104.3, pp. 1051–1056. DOI: 10.1073/pnas.0610080104.

Scharf, M. T., N. Naidoo, J. E. Zimmerman, and A. I. Pack (2008). **The energy hypothesis of sleep revisited**. In: *Progress in Neurobiology* 86.3, pp. 264–280. DOI: 10.1016/j.pneurobio.2008.08.003.

Schartner, M. M., R. L. Carhart-Harris, A. B. Barrett, A. K. Seth, and S. D. Muthukumaraswamy (2017). **Increased spontaneous MEG signal diversity for psychoactive doses of ketamine, LSD and psilocybin**. In: *Scientific Reports* 7, p. 46421. DOI: 10.1038/srep46421.

Schlemmer, R. F. and J. M. Davis (1986). **A primate model for the study of hallucinogens**. In: *Pharmacology, Biochemistry, and Behavior* 24.2, pp. 381–392. DOI: 10.1016/0091-3057(86)90368-0.

Schreiber, R., M. Brocco, V. Audinot, A. Gobert, S. Veiga, and M. J. Millan (1995). **(1-(2,5-dimethoxy-4 iodophenyl)-2-aminopropane)-induced head-twitches in the rat are mediated by 5-hydroxytryptamine (5-HT) 2A receptors: modulation by novel 5-HT2A/2C antagonists, D1 antagonists and 5-HT1A agonists**. In: *The Journal of Pharmacology and Experimental Therapeutics* 273.1, pp. 101–112.

Scott, G. and R. L. Carhart-Harris (2019). **Psychedelics as a treatment for disorders of consciousness**. In: *Neuroscience of Consciousness* 2019.1. DOI: 10.1093/nc/niz003.

Scruggs, J. L., D. Schmidt, and A. Y. Deutch (2003). **The hallucinogen 1-[2,5-dimethoxy-4-iodophenyl]-2-aminopropane (DOI) increases cortical extracellular gluta-**

mate levels in rats. In: *Neuroscience Letters* 346.3, pp. 137–140. DOI: 10.1016/S0304-3940(03)00547-0.

Seibt, J. and M. G. Frank (2019). **Primed to Sleep: The Dynamics of Synaptic Plasticity Across Brain States**. In: *Frontiers in Systems Neuroscience* 13, p. 2. DOI: 10.3389/fnsys.2019.00002.

Shaw, P. J., C. Cirelli, R. J. Greenspan, and G. Tononi (2000). **Correlates of Sleep and Waking in Drosophila melanogaster**. In: *Science* 287.5459, pp. 1834–1837. DOI: 10.1126/science.287.5459.1834.

Shaw, P. J., G. Tononi, R. J. Greenspan, and D. F. Robinson (2002). **Stress response genes protect against lethal effects of sleep deprivation in Drosophila**. In: *Nature* 417.6886, pp. 287–291. DOI: 10.1038/417287a.

Shew, W. L. and D. Plenz (2013). **The functional benefits of criticality in the cortex**. In: *The Neuroscientist* 19.1, pp. 88–100. DOI: 10.1177/1073858412445487.

Shew, W. L., H. Yang, T. Petermann, R. Roy, and D. Plenz (2009). **Neuronal Avalanches Imply Maximum Dynamic Range in Cortical Networks at Criticality**. In: *The Journal of Neuroscience* 29.49, pp. 15595–15600. DOI: 10.1523/JNEUROSCI.3864-09.2009.

Shew, W. L., H. Yang, S. Yu, R. Roy, and D. Plenz (2011). **Information capacity and transmission are maximized in balanced cortical networks with neuronal avalanches**. In: *The Journal of Neuroscience* 31.1, pp. 55–63. DOI: 10.1523/JNEUROSCI.4637-10.2011.

Shriki, O., J. Alstott, F. Carver, T. Holroyd, R. N. Henson, M. L. Smith, R. Coppola, E. Bullmore, and D. Plenz (2013). **Neuronal Avalanches in the Resting MEG of the Human Brain**. In: *The Journal of Neuroscience* 33.16, pp. 7079–7090. DOI: 10.1523/JNEUROSCI.4286-12.2013.

Slomowitz, E., B. Styr, I. Vertkin, H. Milshtein-Parush, I. Nelken, M. Slutsky, and I. Slutsky (2015). **Interplay between population firing stability and single neuron dynamics in hippocampal networks**. In: *eLife* 4. DOI: 10.7554/eLife.04378.

Stepp, N., D. Plenz, and N. Srinivasa (2015). **Synaptic Plasticity Enables Adaptive Self-Tuning Critical Networks**. In: *PLOS Computational Biology* 11.1, e1004043. DOI: 10.1371/journal.pcbi.1004043.

Steriade, M., D. A. McCormick, and T. J. Sejnowski (1993a). **Thalamocortical oscillations in the sleeping and aroused brain**. In: *Science* 262.5134, pp. 679–685.

Steriade, M., A. Nuñez, and F. Amzica (1993b). **A novel slow (< 1 Hz) oscillation of neocortical neurons in vivo: depolarizing and hyperpolarizing components**. In: *The Journal of Neuroscience* 13.8, pp. 3252–3265.

Steriade, M., A. Nuñez, and F. Amzica (1993c). **Intracellular analysis of relations between the slow (< 1 Hz) neocortical oscillation and other sleep rhythms of the electroencephalogram**. In: *The Journal of Neuroscience* 13.8, pp. 3266–3283.

Steriade, M., I. Timofeev, and F. Grenier (2001). **Natural waking and sleep states: a view from inside neocortical neurons**. In: *Journal of Neurophysiology* 85.5, pp. 1969–1985. DOI: 10.1152/jn.2001.85.5.1969.

Steriade, M. (2003). **The corticothalamic system in sleep**. In: *Frontiers in Bioscience* 8, pp. d878–899.

Styr, B., N. Gonen, D. Zarhin, A. Ruggiero, R. Atsmon, N. Gazit, G. Braun, S. Frere, I. Vertkin, I. Shapira, M. Harel, L. R. Heim, M. Katsenelson, O. Rechnitz, S. Fadila, D. Derdikman, M. Rubinstein, T. Geiger, E. Ruppin, and I. Slutsky (2019). **Mitochondrial Regulation of the Hippocampal Firing Rate Set Point and Seizure Susceptibility**. In: *Neuron* 102.5, 1009–1024.e8. DOI: 10.1016/j.neuron.2019.03.045.

Tagliazucchi, E., P. Balenzuela, D. Fraiman, and D. R. Chialvo (2012). **Criticality in Large-Scale Brain fMRI Dynamics Unveiled by a Novel Point Process Analysis**. In: *Frontiers in Physiology* 3. DOI: 10.3389/fphys.2012.00015.

Tagliazucchi, E., R. Carhart-Harris, R. Leech, D. Nutt, and D. R. Chialvo (2014). **Enhanced repertoire of brain dynamical states during the psychedelic experience**. In: *Human Brain Mapping* 35.11, pp. 5442–5456. DOI: 10.1002/hbm.22562. arXiv: 1405.6466.

Tagliazucchi, E., L. Roseman, M. Kaelen, C. Orban, S. Muthukumaraswamy, K. Murphy, H. Laufs, R. Leech, J. McGonigle, N. Crossley, E. Bullmore, T. Williams, M. Bolstridge, A. Feilding, D. Nutt, and R. Carhart-Harris (2016). **Increased Global Functional Connectivity Correlates with LSD-Induced Ego Dissolution**. In: *Current Biology* 26.8, pp. 1043–1050. DOI: 10.1016/j.cub.2016.02.010.

Tanaka, T., T. Kaneko, and T. Aoyagi (2008). **Recurrent Infomax Generates Cell Assemblies, Neuronal Avalanches, and Simple Cell-Like Selectivity**. In: *Neural Computation* 21.4, pp. 1038–1067. DOI: 10.1162/neco.2008.03-08-727.

Terao, A., T. L. Steininger, K. Hyder, A. Apte-Deshpande, J. Ding, D. Rishipathak, R. W. Davis, H. C. Heller, and T. S. Kilduff (2003). **Differential increase in the expression of heat shock protein family members during sleep deprivation and during sleep**. In: *Neuroscience* 116.1, pp. 187–200. DOI: 10.1016/s0306-4522(02)00695-4.

Timofeev, I., F. Grenier, M. Bazhenov, T. J. Sejnowski, and M. Steriade (2000). **Origin of slow cortical oscillations in deafferented cortical slabs**. In: *Cerebral Cortex* 10.12, pp. 1185–1199.

Timofeev, I. and M. Steriade (1996). **Low-frequency rhythms in the thalamus of intact-cortex and decorticated cats**. In: *Journal of Neurophysiology* 76.6, pp. 4152–4168. DOI: 10.1152/jn.1996.76.6.4152.

Timofeev, I. and S. Chauvette (2017). **Sleep slow oscillation and plasticity**. In: *Current Opinion in Neurobiology* 44, pp. 116–126. DOI: 10.1016/j.conb.2017.03.019.

Tobler, I., T. Deboer, and M. Fischer (1997). **Sleep and sleep regulation in normal and prion protein-deficient mice**. In: *The Journal of Neuroscience* 17.5, pp. 1869–1879.

Tobler, I. (1995). **Is sleep fundamentally different between mammalian species?** In: *Behavioural Brain Research*. The Function of Sleep 69.1, pp. 35–41. DOI: 10.1016/0166-4328(95)00025-O.

Todorova, R. and M. Zugaro (2019). **Isolated cortical computations during delta waves support memory consolidation**. In: *Science* 366.6463, pp. 377–381. DOI: 10.1126/science.aay0616.

Tononi, G. and C. Cirelli (2003). **Sleep and synaptic homeostasis: a hypothesis**. In: *Brain Research Bulletin* 62.2, pp. 143–150. DOI: 10.1016/j.brainresbull.2003.09.004.

Tononi, G. and C. Cirelli (2014). **Sleep and the Price of Plasticity: From Synaptic and Cellular Homeostasis to Memory Consolidation and Integration**. In: *Neuron* 81.1, pp. 12–34. DOI: 10.1016/j.neuron.2013.12.025.

Touboul, J. and A. Destexhe (2010). **Can Power-Law Scaling and Neuronal Avalanches Arise from Stochastic Dynamics?** In: *PLOS ONE* 5.2, e8982. DOI: 10.1371/journal.pone.0008982.

Tovote, P., J. P. Fadok, and A. Lüthi (2015). **Neuronal circuits for fear and anxiety**. In: *Nature Reviews Neuroscience* 16.6, pp. 317–331. DOI: 10.1038/nrn3945.

Turrigiano, G. (2011). **Too Many Cooks? Intrinsic and Synaptic Homeostatic Mechanisms in Cortical Circuit Refinement**. In: *Annual Review of Neuroscience* 34.1, pp. 89–103. DOI: 10.1146/annurev-neuro-060909-153238.

Van Dongen, H. P. A., G. Belenky, and J. M. Krueger (2011). **A local, bottom-up perspective on sleep deprivation and neurobehavioral performance**. In: *Current Topics in Medicinal Chemistry* 11.19, pp. 2414–2422. DOI: 10.2174/156802611797470286.

Vergara, R. C., S. Jaramillo-Riveri, A. Luarte, C. Moënne-Loccoz, R. Fuentes, A. Couve, and P. E. Maldonado (2019). **The Energy Homeostasis Principle: Neuronal Energy Regulation Drives Local Network Dynamics Generating Behavior**. In: *Frontiers in Computational Neuroscience* 13, p. 49. DOI: 10.3389/fncom.2019.00049.

Vickers, S. P., N. Easton, C. S. Malcolm, N. H. Allen, R. H. Porter, M. J. Bickerdike, and G. A. Kennett (2001). **Modulation of 5-HT(2A) receptor-mediated head-twitch behaviour in the rat by 5-HT(2C) receptor agonists**. In: *Pharmacology, Biochemistry, and Behavior* 69.3, pp. 643–652. DOI: 10.1016/s0091-3057(01)00552-4.

Viol, A., F. Palhano-Fontes, H. Onias, D. B. d. Araujo, and G. M. Viswanathan (2017). **Shannon entropy of brain functional complex networks under the influence**

of the psychedelic Ayahuasca. In: *Scientific Reports* 7.1, pp. 1–13. DOI: 10.1038/s41598-017-06854-0.

Vivo, L. de, M. Bellesi, W. Marshall, E. A. Bushong, M. H. Ellisman, G. Tononi, and C. Cirelli (2017). **Ultrastructural Evidence for Synaptic Scaling Across the Wake/sleep Cycle**. In: *Science* 355.6324, pp. 507–510. DOI: 10.1126/science.aah5982.

Vollenweider, F. X., M. F. Vollenweider-Scherpenhuyzen, A. Bäbler, H. Vogel, and D. Hell (1998). **Psilocybin induces schizophrenia-like psychosis in humans via a serotonin-2 agonist action**. In: *Neuroreport* 9.17, pp. 3897–3902. DOI: 10.1097/00001756-199812010-00024.

Vollenweider, F. X. and M. Kometer (2010). **The neurobiology of psychedelic drugs: implications for the treatment of mood disorders**. In: *Nature Reviews Neuroscience* 11.9. Number: 9 Publisher: Nature Publishing Group, pp. 642–651. DOI: 10.1038/nrn2884.

Vyazovskiy, V. V., P. Achermann, and I. Tobler (2007). **Sleep homeostasis in the rat in the light and dark period**. In: *Brain Research Bulletin* 74.1, pp. 37–44. DOI: 10.1016/j.brainresbull.2007.05.001.

Vyazovskiy, V. V. and I. Tobler (2008). **Handedness leads to interhemispheric EEG asymmetry during sleep in the rat**. In: *Journal of Neurophysiology* 99.2, pp. 969–975. DOI: 10.1152/jn.01154.2007.

Vyazovskiy, V. V., C. Cirelli, M. Pfister-Genskow, U. Faraguna, and G. Tononi (2008). **Molecular and electrophysiological evidence for net synaptic potentiation in wake and depression in sleep**. In: *Nature Neuroscience* 11.2, pp. 200–208. DOI: 10.1038/nn2035.

Vyazovskiy, V. V., N. Cui, A. V. Rodriguez, C. Funk, C. Cirelli, and G. Tononi (2014). **The dynamics of cortical neuronal activity in the first minutes after spontaneous awakening in rats and mice**. In: *Sleep* 37.8, pp. 1337–1347. DOI: 10.5665/sleep.3926.

Vyazovskiy, V. V. and A. Delogu (2014). **NREM and REM Sleep: Complementary Roles in Recovery after Wakefulness**. In: *The Neuroscientist* 20.3, pp. 203–219. DOI: 10.1177/1073858413518152.

Vyazovskiy, V. V., U. Faraguna, C. Cirelli, and G. Tononi (2009a). **Triggering slow waves during NREM sleep in the rat by intracortical electrical stimulation: effects of sleep/wake history and background activity**. In: *Journal of Neurophysiology* 101.4, pp. 1921–1931. DOI: 10.1152/jn.91157.2008.

Vyazovskiy, V. V. and K. D. Harris (2013). **Sleep and the single neuron: the role of global slow oscillations in individual cell rest**. In: *Nature Reviews Neuroscience* 14.6, pp. 443–451. DOI: 10.1038/nrn3494.

Vyazovskiy, V. V., U. Olcese, E. C. Hanlon, Y. Nir, C. Cirelli, and G. Tononi (2011). **Local sleep in awake rats**. In: *Nature* 472.7344, pp. 443–447. DOI: 10.1038/nature10009.

Vyazovskiy, V. V., U. Olcese, Y. M. Lazimy, U. Faraguna, S. K. Esser, J. C. Williams, C. Cirelli, and G. Tononi (2009b). **Cortical firing and sleep homeostasis**. In: *Neuron* 63.6, pp. 865–878. DOI: 10.1016/j.neuron.2009.08.024.

Vyazovskiy, V. V., G. Ruijgrok, T. Deboer, and I. Tobler (2006). **Running wheel accessibility affects the regional electroencephalogram during sleep in mice**. In: *Cerebral Cortex* 16.3, pp. 328–336. DOI: 10.1093/cercor/bhi110.

Wang, X. and E. K. Michaelis (2010). **Selective neuronal vulnerability to oxidative stress in the brain**. In: *Frontiers in Aging Neuroscience* 2. DOI: 10.3389/fnagi.2010.00012.

Watson, B. O., D. Levenstein, J. P. Greene, J. N. Gelinas, and G. Buzsáki (2016). **Network Homeostasis and State Dynamics of Neocortical Sleep**. In: *ResearchGate*. DOI: 10.1016/j.neuron.2016.03.036.

Weber, E. T. and R. Andrade (2010). **Htr2a Gene and 5-HT(2A) Receptor Expression in the Cerebral Cortex Studied Using Genetically Modified Mice**. In: *Frontiers in Neuroscience* 4. DOI: 10.3389/fnins.2010.00036.

Weiss, K. C., D. Y. Kim, C. T. Pawson, and S. P. Cordes (2003). **A genetic screen for mouse mutations with defects in serotonin responsiveness**. In: *Brain Research. Molecular Brain Research* 115.2, pp. 162–172. DOI: 10.1016/s0169-328x(03)00205-5.

Welsh, D. K., J. S. Takahashi, and S. A. Kay (2010). **Suprachiasmatic nucleus: cell autonomy and network properties**. In: *Annual Review of Physiology* 72, pp. 551–577. DOI: 10.1146/annurev-physiol-021909-135919.

Werth, E., P. Achermann, and A. A. Borbély (1996a). **Brain topography of the human sleep EEG: antero-posterior shifts of spectral power**. In: *Neuroreport* 8.1, pp. 123–127. DOI: 10.1097/00001756-199612200-00025.

Werth, E., D. J. Dijk, P. Achermann, and A. A. Borbély (1996b). **Dynamics of the sleep EEG after an early evening nap: experimental data and simulations**. In: *The American Journal of Physiology* 271.3, R501–510. DOI: 10.1152/ajpregu.1996.271.3.R501.

Wichniak, A., A. Wierzbicka, M. Walęcka, and W. Jernajczyk (2017). **Effects of Antidepressants on Sleep**. In: *Current Psychiatry Reports* 19.9. DOI: 10.1007/s11920-017-0816-4.

Willins, D. L., A. Y. Deutch, and B. L. Roth (1997). **Serotonin 5-HT2A receptors are expressed on pyramidal cells and interneurons in the rat cortex**. In: *Synapse* 27.1, pp. 79–82. DOI: 10.1002/(SICI)1098-2396(199709)27:1<79::AID-SYN8>3.0.CO;2-A.

Wilting, J. and V. Priesemann (2019). **Between Perfectly Critical and Fully Irregular: A Reverberating Model Captures and Predicts Cortical Spike Propagation**. In: *Cerebral Cortex* 29.6, pp. 2759–2770. DOI: 10.1093/cercor/bhz049.

Wilting, J. and V. Priesemann (2018). **Inferring collective dynamical states from widely unobserved systems**. In: *Nature Communications* 9.1, pp. 1–7. DOI: 10.1038/s41467-018-04725-4.

Winter, C. A. and L. Flataker (1956). **Effects of lysergic acid diethylamide upon performance of trained rats**. In: *Proceedings of the Society for Experimental Biology and Medicine. Society for Experimental Biology and Medicine (New York, N.Y.)* 92.2, pp. 285–289. DOI: 10.3181/00379727-92-22453.

Wirz-Justice, A. and R. H. Van den Hoofdakker (1999). **Sleep deprivation in depression: what do we know, where do we go?** In: *Biological Psychiatry* 46.4, pp. 445–453. DOI: 10.1016/s0006-3223(99)00125-0.

Wirz-Justice, A., F. Benedetti, M. Berger, R. W. Lam, K. Martiny, M. Terman, and J. C. Wu (2005). **Chronotherapeutics (light and wake therapy) in affective disorders**. In: *Psychological Medicine* 35.7, pp. 939–944. DOI: 10.1017/s003329170500437x.

Wood, J., Y. Kim, and B. Moghaddam (2012). **Disruption of Prefrontal Cortex Large Scale Neuronal Activity by Different Classes of Psychotomimetic Drugs**. In: *The Journal of Neuroscience* 32.9, pp. 3022–3031. DOI: 10.1523/JNEUROSCI.6377-11.2012.

Xie, L., H. Kang, Q. Xu, M. J. Chen, Y. Liao, M. Thiyagarajan, J. O'Donnell, D. J. Christensen, C. Nicholson, J. J. Iliff, T. Takano, R. Deane, and M. Nedergaard (2013). **Sleep Drives Metabolite Clearance from the Adult Brain**. In: *Science* 342.6156, pp. 373–377. DOI: 10.1126/science.1241224.

Xu, T. and S. C. Pandey (2000). **Cellular localization of serotonin(2A) (5HT(2A)) receptors in the rat brain**. In: *Brain Research Bulletin* 51.6, pp. 499–505. DOI: 10.1016/s0361-9230(99)00278-6.

Yang, H., W. L. Shew, R. Roy, and D. Plenz (2012). **Maximal Variability of Phase Synchrony in Cortical Networks with Neuronal Avalanches**. In: *The Journal of Neuroscience* 32.3, pp. 1061–1072. DOI: 10.1523/JNEUROSCI.2771-11.2012.

Zavada, A., A. M. Strijkstra, A. S. Boerema, S. Daan, and D. G. M. Beersma (2009). **Evidence for differential human slow-wave activity regulation across the brain**. In: *Journal of Sleep Research* 18.1, pp. 3–10. DOI: 10.1111/j.1365-2869.2008.00696.x.

Zepelin, H., J. M. Siegel, and I. Tobler (1989). **Mammalian Sleep. In M. H. Kryger, T. Roth, & W. C. Dement (Eds.), Principles And Practices Of Sleep Medicine (pp. 81-92).**

Zhang, G., H. N. Asgeirsdottir, S. J. Cohen, A. H. Munchow, M. P. Barrera, and R. W. Stackman (2013). **Stimulation of serotonin 2A receptors facilitates consolidation and extinction of fear memory in C57BL/6J mice**. In: *Neuropharmacology* 64.1, pp. 403–413. DOI: 10.1016/j.neuropharm.2012.06.007.

Zhang, G. and R. W. J. Stackman (2015). **The role of serotonin 5-HT2A receptors in memory and cognition**. In: *Frontiers in Pharmacology* 6. DOI: 10.3389/fphar.2015.00225.

Zhou, F.-M. and J. J. Hablitz (1999). **Activation of Serotonin Receptors Modulates Synaptic Transmission in Rat Cerebral Cortex**. In: *Journal of Neurophysiology* 82.6, pp. 2989–2999. DOI: 10.1152/jn.1999.82.6.2989.

Zhuk, O., I. Jasicka-Misiak, A. Poliwoda, A. Kazakova, V. V. Godovan, M. Halama, and P. P. Wieczorek (2015). **Research on Acute Toxicity and the Behavioral Effects of Methanolic Extract from Psilocybin Mushrooms and Psilocin in Mice**. In: *Toxins* 7.4, pp. 1018–1029. DOI: 10.3390/toxins7041018.

Zucca, S., V. Pasquale, P. Lagomarsino de Leon Roig, S. Panzeri, and T. Fellin (2019). **Thalamic Drive of Cortical Parvalbumin-Positive Interneurons during Down States in Anesthetized Mice**. In: *Current Biology* 29.9, 1481–1490.e6. DOI: 10.1016/j.cub.2019.04.007.

Zylka, M. J., L. P. Shearman, D. R. Weaver, and S. M. Reppert (1998). **Three period Homologs in Mammals: Differential Light Responses in the Suprachiasmatic Circadian Clock and Oscillating Transcripts Outside of Brain**. In: *Neuron* 20.6, pp. 1103–1110. DOI: 10.1016/S0896-6273(00)80492-4.